Development of Novel Demountable Shear Connectors for Precast Steel-Concrete Composite Bridges

By

Ahmed S. H. Suwaed

Thesis Submitted to the University of Warwick for the degree of

Doctor of Philosophy

Structural Engineering Group, Civil and Environmental Discipline Stream

School of engineering, University of Warwick

Feb 2017

Abstract:

Two novel demountable shear connectors for precast steel-concrete composite bridges are presented. The connectors use high-strength steel bolts, which are fastened to the steel beam with the aid of a special locking configuration that prevents slip of bolts within their holes. Moreover, the connectors promote accelerated construction and overcome typical construction tolerances issues of precast structures. Most importantly, the connectors allow bridge disassembly, and therefore, can address different bridge deterioration scenarios with minimum disturbance to traffic flow, i.e. (1) precast deck panels can be rapidly uplifted and replaced; (2) connectors can be rapidly removed and replaced; and (3) steel beams can be replaced, while precast decks and shear connectors can be reused. A series of push-out tests and a beam test were conducted to assess the behavior of the connectors and quantify the effect of important parameters. The experimental results showed that shear resistance and slip capacity can reach 2.5 and 2.7 times respectively of those of welded shear studs along with superior stiffness and strength against slab uplift. Additionally, shear stiffness of M16 mm LNSC was equal to that of M19 mm welded studs. Identical tests reveal negligible scatter in the shear load – slip displacement behavior. Design equations are proposed to predict the shear resistance with minimum deviations.

Table of Contents

List of Tables

List of Figures

List of Symbols and Abbreviations

Δ	Mid-span deflection of composite beam
Δ_{th}	Elastic deflection at mid-span of composite beam
μ	Coefficient of friction between concrete and steel
a	Distance from point load to support in 4 point-loads beam test
A_s	Area of steel section in composite beam test
b	Slab width in composite beam test
BT1-4	References for pushout tests in (Pavlović 2013)
c	Depth of compression part of concrete section in composite beam test
d	Diameter of bolt
DBLNB	Double-nut bolt shear connector
DTI	Direct tension indicator washer
E_{cm}	Secant modulus of elasticity of the concrete
E_s	Modulus of elasticity of steel
F	Applied load on one slab of pushout test
F_1	Applied one point load
FBSC	friction based shear connector
f_{ck}	Characteristic compressive cylinder strength of concrete
f_{cu}	Concrete mean experimental cube test strength in N/mm^2
f_u	Tensile strength of steel (ultimate).
f_y	Yield strength of steel
H	Horizontal compression force on slab in pushout test
h_1	Distance from the centre of shear connector to the floor in pushout test, or thickness of concrete slab in composite beam test
h_2	Half thickness of the slab in pushout test, or depth of steel beam in composite beam test
HASAA	adhesive anchor
HTFGB	high-tension friction grip bolt
I	Moment of inertia
L	Effective length of beam (i.e. length between supports in simply supported beams)
LNSC	locking nut shear connector
LVDT	linear variable displacement transducer
M	Mid-span bending moment of composite beam test

N.A. Neutral axis in composite beam test

N.A.1 Neutral axis of concrete in composite beam test

N.A.2 Neutral axis of steel in composite beam test

P Shear resistance of shear connector

P_{1st} Shear load at which first slip

P_i Shear force in connector i

P_{Rk} Characteristic resistance of shear connector according to Eurocode 4

P_s shear strength of a bolt

PT1-8 Reference for pushout test in (Lam et. al. 2013)

S Interface slip between concrete slab and steel beam

T Tensile force in the bolts

TCB Tension Control Bolts

t_w Web thickness of steel beam

β Angle of the deflected shape of the bolt from the vertical at the level of the shear failure plane

ε Strain

σ Stress

S_{ult} Slip at ultimate load (in mm)

f_c Compressive cylinder strength of concrete (in N/mm^2)

d_{sh} Shank diameter of the stud

P_R Shear resistance of welded suds according to Eurocode 4

F_c Total compression force in concrete in composite beam test

F_s Total tensile force in steel in composite beam test

M_{fp} Full plastic moment capacity with 100% degree of shear connection

M_{FBSC} Shear force of all shear connectors in one shear span

c_1 Depth of N.A.1 from the top fibre of composite section

c_2 Depth of N.A.2 from the steel-concrete interface

F_{s1} Compression force in top flange of steel element in composite section

F_{s2} Compression force in top part of web of steel element in composite section

F_{s3} Tensile force of whole steel element in composite section

$M_{p70\%}$ Partial plastic moment capacity with 70% degree of shear connection

Acknowledgements

Grateful appreciations to my supervisor and advisor, Professor Theodore L. Karavasilis, for his endless support at both academic and personal level. Sincere thanks to the 2nd supervisor Dr Stana Zivanovic for her valuable and fruitful scientific support. Emeritus Professor Roger P. Johnson of the University of Warwick kindly reviewed interim technical reports and offered comments and advices of significant value. This work was financially supported by the Iraqi Ministry of Higher Education and Scientific Research (PhD scholarship to the author) and from the University of Warwick through their Strategic EPSRC Impact Fund (PI: Professor Karavasilis). Hanson Cement & Packed Products Ltd and Grace Construction Products Ltd donated raw materials for the fabrication of the test specimens. Technical staff of the University of Warwick provided valuable help with the experimental setup. The authors acknowledge with thanks the aforementioned support. Any opinions, findings, and conclusions expressed in this dissertation are those of the author and do not necessarily reflect the views of the sponsors and supporters.

Dedication

During the period of the last four years, it is the author's family who invariably suffer most. Their patience, support and understanding has been most valuable to me. Thanks then are due to my wife Ola and my children Hayder, Zainab, Mohammed, and Narjis. This dissertation is dedicated to them.

Declaration

This thesis is submitted to the University of Warwick in support of my application for the degree of Doctor of Philosophy. It has been composed by myself and has not been submitted in any previous application for any degree.

The work presented was carried out by the author.

Parts of this thesis have been published as following:

Suwaed, A., Karavasilis, T.L., and Zivanovic, S. (2016). “Steel-Concrete Composite Structure.” International WIPO Patent No. WO2016/135512A1, Geneva, Switzerland.

Suwaed, A., and Karavasilis, T.L. (2017). “Novel Demountable Shear Connector for Accelerated Disassembly, Repair or Replacement of Precast Steel-Concrete Composite Bridges.” Journal of Bridge Engineering, ASCE, DOI: 10.1061/(ASCE)BE.1943-5592.0001080.

Chapter 1: Introduction

1.1 Introduction

During the last two decades, rapid deterioration of bridges has become a major issue due to various reasons including increase in traffic flow, increase in the allowable weight of vehicles compared to those considered in the initial design (Hanswille 2011), harsh environmental conditions, use of de-icing salts especially in countries with cold climates, poor quality of construction materials, and limited maintenance (Ramey and Oliver 1998). Many bridges in Europe suffer from the aforementioned factors (PANTURA 2011), while the same is true for the USA where one third of the 607,380 bridges need maintenance (ASCE 2014). Bridge maintenance ensures serviceability along with safety for users and typically involves inspection, repair, strengthening or replacement of the whole or part of a bridge. Such operations result in direct economic losses (e.g. material and labour costs) as well as in indirect socio-economic losses due to disruption of traffic flow such as travel delays, longer travel distances, insufficient move of goods, and business interruption. Depending on the type of bridge and scale of the maintenance operations, indirect losses might be several times higher than direct losses and constitute one of the major challenges for bridge owners, decision makers, and bridge engineers (PANTURA 2011). For instant, it is suggested that bridges in Japan should be designed for fatigue life of 300 years because of the rapidly increasing maintenance costs (Oehlers et al. 2000). Thus, sustainable methods for bridge repair, strengthening or replacement that minimize direct costs and traffic flow disturbance are urgently needed.

Bridge decks typically deteriorate faster than other bridge components (Ramey and Oliver 1998, and Hanswille 2011), e.g. the decks of 33% of the bridges in America are in the need of repair or replacement after an average service life of 40 years (ASCE 2014). Similar trends in deterioration of bridges have been noticed in the UK (Long et al. 2008). It is important to note that deck replacement is the typical maintenance decision as repair methods such as deck overlay are not sufficient for long extension of the bridge lifespan (Deng et al. 2016, Hanswille 2011). In the case of steel-concrete composite bridges, removing and replacing their deteriorating deck is a challenging process due to the connection among the deck and the steel beams. Such connection is traditionally achieved with the aid of shear studs, which are welded on the top flange of the steel beams and are fully embedded within the concrete deck. Therefore, removing the deck involves drilling and crushing the concrete around the shear studs and then breaking the deck into manageable sections (Tadros and Baishya 1998).

Such processes are costly, time-consuming, involve the use of hazardous equipment, and cause congestion in traffic flow during construction time. For example, a replacement of one bridge (Tinsley Viaduct bridge in UK) was estimated to cost £200m however the associated cost of congestion over a period of 2-3 years of construction was assessed to be around £1400m (Long et al. 2008). Other bridge deterioration mechanisms include fatigue or corrosion in the steel beam or in the shear studs. Repair in these cases is again challenging and often questionable in terms of the post-repair structural integrity, while replacement of a deteriorating steel beam or shear stud is costly and time consuming due to the aforementioned monolithic connection between the steel beam, shear connectors, and concrete deck.

Apart from repairing or strengthening existing bridges, bridge engineers should adopt reparability and easy maintenance as major goals for new bridge design projects. This can be achieved not only by designing bridges based on a life-cycle cost approach that will assess repair costs and losses during their lifespan, but also by changing the paradigm in structural detailing so that bridge structural systems have the inherent potential to be easily repaired, strengthened or replaced. A possible way to meet this challenging goal is the development and design of novel bridge structural systems that allow bridge disassembly without compromising their structural integrity and efficiency. Rapid bridge disassembly will offer the unique advantage of easy replacement of deteriorating structural components, and therefore, will result in extension of bridge lifespan with minimum cost and traffic disturbance. In the case of steel-concrete composite bridges, bridge disassembly calls for a demountable shear connector that would allow easy separation of the deck from the steel beam without compromising composite action. The potential for bridge disassembly can be further facilitated by using precast concrete panels that are connected to each other with dry joints, such as those proposed by Hallmark (2012).

1.2 Objective

In line with the challenging task of developing bridges that allow disassembly (see discussion in the last paragraph of the previous section), this thesis presents two novel demountable shear connectors for precast steel-concrete composite bridges. The connectors use high-strength steel bolts, which are fastened to the steel beam with the aid of a special locking nut/washer configuration that prevents slip of bolts within their holes. Additional structural details ensure that the connectors overcome typical construction tolerance issues of precast structures. The connectors allow full bridge disassembly, and therefore, can address

different bridge deterioration scenarios with minimum disturbance to traffic flow, i.e. (i) precast deck panels can be rapidly uplifted and replaced; (ii) connectors can be rapidly removed and replaced; and (iii) steel beams can be easily replaced, while precast decks and shear connectors can be reused. A series of push-out tests and a composite beam test are conducted to assess the behaviour of the connectors and quantify the effect of important parameters. The experimental results show shear resistance, stiffness, and slip capacity higher than those of welded shear studs along with superior stiffness and strength against slab uplift. Identical tests reveal negligible scatter in the shear load – slip displacement behaviour. Design equations are proposed to predict the shear resistance with absolute minimum errors. The suitability of the new shear connectors in developing plastic moment capacity in composite beams was also confirmed by testing a beam with 70% partial shear connection. This feature is important in designing long composite beams (spans exceeding 20 m) with partial connection method.

1.3 Scope of the Dissertation

This dissertation focuses on the development and assessment of the behaviour of two new shear connectors. The thesis is based on experimental results and interpretation of these results using structural mechanics theory and its applications to steel-concrete composite structures design. The dissertation consists of eight chapters. A detailed literature review can be found in the next chapter, where various types of previously developed demountable shear connectors are described in chronological order. Their advantages and disadvantages are highlighted. Overcoming such disadvantages along with providing additional advantages was the main goal set for this PhD research. The locking nut shear connector (LNSC) and the friction based shear connector (FBSC) are explored in Chapter 3, where a detailed description of their components along with the suggested procedures for bridge assembly and disassembly are provided. Chapter 4 provides full details of the specifications of 23 pushout tests and one composite beam test. In particular, Chapter 4 describes the test setup and procedures, specimen dimensions, materials properties, and instrumentation. The results of the pushout tests on the LNSC and FBSC can be found in Chapters 5 and 6, respectively. These chapters also include the assessment of the load-slip and the load-uplift behaviours of the two shear connectors. Comparisons with welded studs and parametric studies (effects of bolt diameter, concrete compressive strength, and bolt preload) are also included. The results from a composite beam test are discussed in Chapter 7, where the FBSC was used in a 9.0m beam under four point-loading. The structural behaviour of the beam was analysed and discussed with emphasis on the load-deflection behaviour, slip displacement, concrete

and steel strains, and FBSC tensile forces. Chapter 8 summarizes the research results from the LNSC and FBSC pushout tests and the FBSC composite beam test. In addition, Chapter 8 provides the main conclusions of this PhD research.

1.4 Limitations

The current research focused on developing experimentally novel shear connectors for composite precast steel-concrete bridges. The following parameters are out of scope

- Time dependent effects like fatigue, shrinkage, creep, relaxation, and preload loss of bolts.
- The effect of longitudinal joints that liked the panels of the concrete deck of the composite bridge.
- The effect of transverse bending between adjacent steel beams in composite bridge.

Chapter 2: Literature Review

2.1 Introduction

The research described in this dissertation was conducted to develop efficient and practical demountable new shear connectors to enable bridge disassembly and replacement of deteriorating structural components. To understand and fully appreciate the concept and development of the new connectors, as well as the reasons behind the decisions taken during this research program, an extensive literature review on prior relevant research is first presented. Therefore, this chapter provides a brief review of previous types of shear connectors including the conventional welded shear studs, which are currently used in practice. Then, the chapter proceeds with an extensive review of previous research on demountable shear connectors. The advantages and disadvantages of previously developed demountable shear connectors are highlighted. The chapter concludes by describing in more detail the challenges of developing a demountable shear connector, which is suitable for practical applications (see Section 2.6).

2.2 Composite Action in Steel Concrete Bridges

If a concrete deck is supported on a group of steel beams by its weight only without interface bonding, then the slab and the beams will deflect with respect to their own neutral axes. This will result in a differential displacement (slip) developed at the concrete slab and steel beam interface. In that case, the beam is referred to as *non-composite* beam. The role of shear connectors is to prevent or minimize this slip in a way that both the concrete slab and the steel beam behave as a single monolithic structural member that deflects using a single neutral axis; having its concrete slab under compression while its steel beam under tension. Such structure is referred to as a steel-concrete *composite* beam. If the shear connectors prevent slip completely then a condition of *full interaction* exists, while if a limited slip occurred while maintaining the applied load, then a *partial interaction* condition is occurred (Oehlers and Bradford 1999). When the slip capacity is at least 6 mm, the shear connector is described as *ductile* and is assumed to be capable to redistribute the shear force among many shear connectors during plastic behaviour (BSI 2004a). If the number of shear connectors are large enough to transmit the full shear forces between the concrete slab and the steel beam at the ultimate state, then the connection is called *full shear connection*, while if the number is less than that, the connection is called as *partial shear connection*. Thus, the term 'interaction' indicates the slip state of the connection, while the 'connection' term describe its strength. According to that, it is possible in the same connection to have *partial*

interaction and *full connection* or *full interaction* and *partial connection,* as will be seen in Chapter 7.

2.3 Welded Stud Shear Connectors

Among many types of shear connectors, Eurocode 4 (BSI 2004a) provides detailed design rules for welded studs. These connectors are commercially manufactured and offered in several diameters. Eurocode 4 limits the diameters to a range of 16 mm to 25 mm. The former limit of 16 mm can be explained by knowing that Eurocode 4 (BSI 2004a) has a requirement for a minimum slip capacity of 6 mm for ductile shear connectors. Studs having slip capacity equal or higher than 6 mm can help a composite beam to achieve inelastic redistribution of shear forces (BSI 2004a). Furthermore, ductile connectors can be distributed uniformly over a length between adjacent critical cross-sections (BSI 2004a). A ductile connector is a requirement of Eurocode 4 (BSI 2004a) to use partial shear connection design. On the other hand, it was proved that there is no constant slip capacity for all connector with different diameters. Oehlers and Bradford (1999) suggest that slip capacity at fracture normally equal to 0.3 times the connector diameter. Furthermore, they gave a detailed relationship as follows

$$S_{\mathrm{ult}} = (0.48 - 0.0042 f_{\mathrm{c}}) d_{\mathrm{sh}} \qquad (2.1)$$

where S_{ult} is the slip at ultimate (in mm), f_{c} is compressive cylinder strength of concrete (in N/mm^2), and d_{sh} is the shank diameter of the stud (in mm). Therefore, for a stud of $d_{\mathrm{sh}} = 16\ \mathrm{mm}$ diameter, and normal concrete of $f_{\mathrm{c}} = 25\ \mathrm{N/mm^2}$, then $S_{\mathrm{ult}} = 6\ \mathrm{mm}$. Thus, studs with diameter less than 16 mm, will not have the minimum requirement of slip capacity. Eurocode 4 (BSI 2004a) sets an upper bound of 25 mm for diameter of a stud. Johnson (2004) gave two reasons for this limitation. First, there are difficulties in the welding process for large diameter studs, and moreover, it is related to the thickness of the top flange of the composite beam. Different heights can be used for welded studs. Eurocode 4 limits the height to not less than 4 times the diameter. Oehlers and Bradford (1995) explained this as to avoid a concrete pullout failure as shown in Fig. 2.1. Studs are welded to the steel beam, by means of an electric arch, causing a total continuity between the two elements.

The success of the stud connector is due to several characteristics: the stud welding is fast; they anchor well in concrete and it is easy to dispose the reinforcement through the slab and between the studs; it can easily resist the slab uplift because of the existence of the stud head (Johnson 2004, Oehlers and Bradford 1995); Lastly, they are equally strong and stiff in

shear in all directions normal to the axis of the stud (El-lobody 2002) as compare to 'L' and 'T' shaped shear connectors.

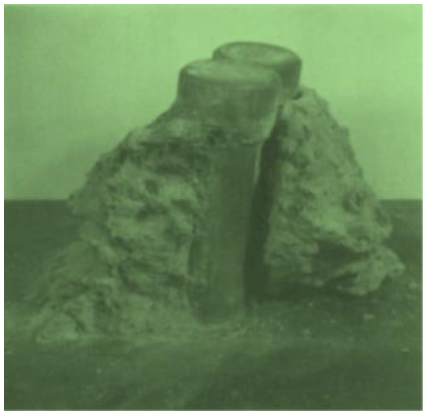

Fig. 2.1. Pullout concrete failure of welded studs (Oehlers and Bradford 1995)

The main problems related to welded studs can be listed as follows. Because the installation technique depends on welding, getting specific welding devices and/or high power generator on site in remote locations is expected to be difficult or expensive. The welding procedure is severely affected by bad weather (moisture and rain), which may represent a problem in countries where the rain is likely to fall all around the year.

On the structural behaviour of the studs, and in addition to the aforementioned pullout failure of Fig. 2.1, it has been found that the welded studs as they act as steel dowels embedded in the concrete slab, they represent concentrated loads that induces lateral tensile forces in the slab, which may cause the slab to split (as shown in Fig. 2.2). Oehlers (1989) found that splitting can reduce the resistance of the shear connector to less than 20%. Furthermore, he found that using transverse reinforcement in the concrete slab as recommended by Clause (6.6.5.3.2) of the Eurocode 4 (BSI 2004a) did not avoid the failure mode of slab splitting, but it did change it from brittle failure to more ductile one, by controlling the propagation of cracks.

One of the major problems of welded studs is that the results of pushout tests are highly affected by the degree of compaction of the concrete, and even by the local arrangement of particles of aggregate. The effect is concentrated in very small but critical area in-front of the base of the stud (Johnson 2004), which results in diversity and variations in the results of identical tests. A typical example of such scatter in results can be seen in Fig. 2.3. The load-slip relationships for six different groups are shown in Fig. 2.3. Each group has three identical pushout tests, however very obvious scatter can be identified between the three curves of each group in both load and slip.

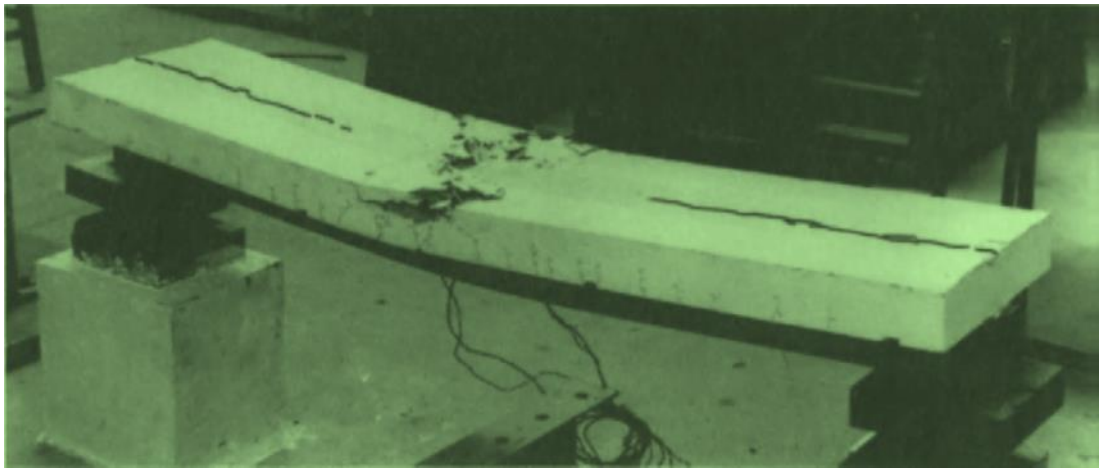

Fig. 2.2. Splitting and crushing failures of composite beam (Oehlers and Bradford 1995)

It should be noted that Clause (B.2.5) of Eurocode 4 accept most of the scatter in pushout results by applying reduction factors, as long as the difference between any result from the average does not exceeds 10%; The characteristic shear resistance of three identical pushout tests, is said to be equal to the smallest among them reduced by 10%. If we take the graph of STUD1-3 of Fig. 2.3 for example, assuming that the shear resistance *P* = 120, 130, and 140 kN, then the characteristic shear resistance would be = 0.9x120 = 108 kN, which represent 23% reduction of the 140 kN curve.

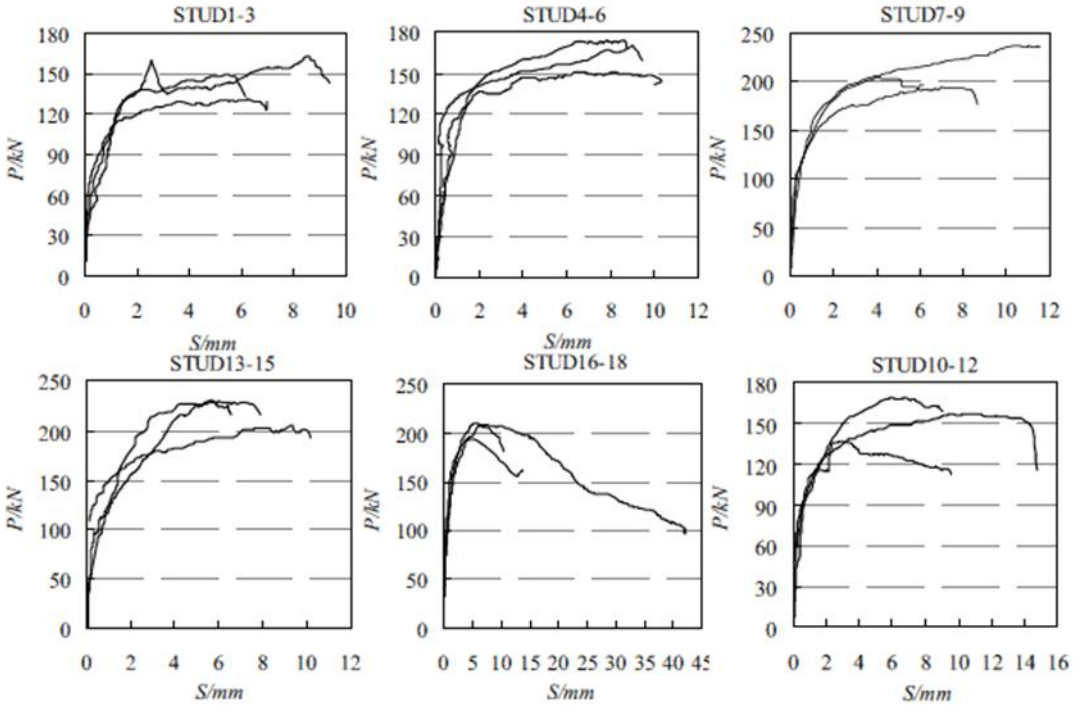

Fig. 2.3. Scatter in identical pushout tests (Xue et. al. 2008)

2.4 Combined Shear and Tension

In composite bridges, certain patterns of loading (e.g. near transverse braces) tend to cause separation of slab from steel beam, so the shear connectors must prevent uplift as well as slip (Johnson and Buckby 1986). One may argues that by applying tensile force to the connector, its shear strength will be reduced (e.g. Oehlers (1980) suggested 11% reduction). In contrast, Steve and Wingate (2012) proved experimentally with preloaded 'aerospace' bolts to 47% of tensile strength that the preloading has no effect on either the ultimate tensile or shear capacities. Steve and Wingate (2012) referred these mechanisms to the "joint separation prior to bolt failure under tensile loading and relaxation of preload due to plastic deformations under shear loading." Furthermore, Pavlović (2013) stated that with preload up to 100% of proof load, no influence on shear connector behaviour was noticed; a statement had been previously proved experimentally by Wallaert and Fisher (1964). The later explained it as follows: "when a bolt is torqued to a certain preload, most of the inelastic deformations develops in the threaded portion of the bolt and not in the shank, and all failure planes in these bolts were through the bolt shanks." At the same time, Chesson *et al.* (1965) proved more than that by stating that the tensile strength of high strength bolts under combined tension-shear forces is larger than that under tension alone. Chesson *et al.* (1965) referred this to the effect of shear in developing an inclined failure plane rather than a failure plane through a necking reduced section. It should be mentioned that Eurocode 4 (BSI 2004a) allows for the existence of an external tensile force in studs less than 10% of their shear strengths. However, such a restriction might be because the uplift resistance of studs is based on the anchorage of the head of the stud in the concrete; Because of the small area provided by a stud's head, high concentrated stresses can develop on the bearing concrete, with the possibility of a concrete cone pull-out failure (BSI 1994) (see Fig. 2.1). Pull-out failure occurred when the whole stud rotates and pulls out of the slab, carrying with it a wedge shaped or pyramidal portion of concrete (Johnson and Yuan 1998), especially if pull-out force is higher than 10% of stud shear strength. In summary, the conservative recommendations of Oehlers (1980) and Eurocode 4 (BSI 2004a) are based on stud behaviour due to its geometry and more specifically as related to the strength of the surrounded concrete in creating a failure of pullout of concrete cone, and away from that there is no notable effect of tension on the shear strength of bolts.

2.5 Demountable Shear Connectors

When searching for an option alternative to welding connections to achieve demountability, the straight and obvious solution would be bolted connection. Although, in 1925, J. C.

Lathrop suggested using bolts in roof and floor construction in a patent published in 1928, it can be considered that the work of (Dallam 1968, and Dallam and Harpster 1968) is the first 'standard' experimental attempt to replace the welded studs by high-strength friction-grip bolts.

Dallam (1968) and Dallam and Harpster (1968) carried out several push-out and beam tests. Their idea is based on temporarily erecting the bolts over the steel beams using spring chairs while pouring the concrete over the steel beam, and after the concrete hardening, the nuts are tightened from below the slab. Dallam's shear connector is limited to in-situ construction and cannot be used in precast construction since very tight tolerances would need to be overcome to coincide the pre-embedded bolts in the slab with their corresponding holes on the steel beam. Moreover, this shear connector demands the installer to work underneath the bridge, which is a time consuming and an unfavourable construction practice. The replaceability is only possible if the whole slab (including the bolts) is lifted-up and replaced, and there is no solution when only the shear connector need to be changed (e.g. due to corrosion). Another drawback in Dallam's connector is that pretension is concentrated within a very small length (approximately 20 mm) in each bolt and that pretension will not extend at the same level to the rest of the bolt length because of the hardened concrete. Dallam did not publish the readings of the strain gauges attached to the bolts during pretension process and he described the results as 'negative'. It should be noted that all tensile forces in bolts will be transferred into the slab, and if a gap between the slab and the beam exists, flexural tensile stresses will be developed at the bottom face of the concrete slab, which increase the possibility of crack initiation around the bolt. Six of Dallam's specimens failed due to split cracking after bolt pretension. The magnitude of the pretension pressure applied to the bolts was based on what is called a "snug tight" condition, which can be accomplished by the full effort of a man using an ordinary spud wrench (Kulak *et al.* 2001). It should be noted that 'full effort of a man' is a vague value. In practice, it can be changed between the bolts, causing different frictional forces (and hence different slips) at each bolt, and consequently, it will affect the vertical alignment of the pushout specimen and the eccentricity of the applied point load. Possibly this was the cause of the 'misalignment' mentioned in one of his specimen that enforced him to exclude its results from his paper. Thus, the shear capacity of his tests may not represent the 'mean' value of the four bolts, but the capacity of the 'weakest' one, which is always less than the expected average value that can be achieved when all the bolts failed at the same time. Long-term effect in the bolt pretension pressure was also examined by allowing some of the specimens to set for a long period (138 days)

before testing. He concluded, by comparison, that the critical load was about the same. As compared to welded studs, the average critical load (Serviceability Limit State, SLS, 50% of maximum load) for the bolts was considerably greater (about twice) than that of studs, but the average slip was smaller. The ultimate load was also higher. He explained this by the differences in material properties of the bolts and the studs. The tensile strength of the studs was 493 MPa, while the strength of the bolts was 969 MPa. A specific behaviour was observed during Dallam's push-out specimens. At a certain point in the test a loud sound occurred, simultaneously with a sudden decrease in load and a jump in slip. He explained this behaviour by friction force overcome. Unfortunately, he did not include any graph to present the shear force - slip displacement of this behaviour. Dallam added that: 'surprisingly… the load at which friction was overcome increased in the successive loading cycles'. This observation can only be explained if the residual slip increased after each cycle, and hence, the tensile force inside each bolt increased; therefore, the frictional force increased. It can be concluded from the previous statement that there is a direct correlation between slip and tensile bolt force, as it will be proved through testing during this research. For all the reasons mentioned before, Dallam's work was not adopted or disseminate around the world despite his good results.

Sattlar (1960) used HS (High Strength) bolts in composite beam but his specimens were 'non-standard' in that he used one slab connected to two steel channels. Fortunately, Marshall et. al. (1971) repeated Sattlar's work using standard push-out tests (Fig. 2.4(a)), and he also examined additional parameters like: pretension force, concrete strength, and casting methods (Fig. 2.4(b)). All the bolts were provided with hardened square washers (51×51×13 mm) and nuts from both sides. Also, the concrete around the bolts holes was reinforced with helical reinforcement. A main disadvantage of their shear connector is that threading of the bolts into the concrete slab after hardening represents an extremely difficult and time consuming task to be carried out on site. Additionally, the accuracy required to coincide the hole of the concrete to that of the steel beam is very critical. Because of the existence of the upper nut and thick plate above the concrete level, there should be an additional overall layer to be cast in-site to cover these details which represent additional cost and delay. Marshall et. al. (1971) suggested using the shearing strength of a bolt as the ultimate capacity of the connection. However, Eurocode 4 (BSI 2004a) adopts two equations: one for steel strength and one for concrete strength, and the ultimate capacity is the lowest value of the two. In terms of the SLS capacity, Marshall et. al. (1971) suggested using the frictional resistance. However, due to the sudden major slip when frictional resistance is overcome,

his suggestion should be taken as unreliable. Marshall et. al. (1971) noticed that individual readings of slip for each bolt were affected by the uneven breaking of bond and unequal distribution of load between the slab and the beam.

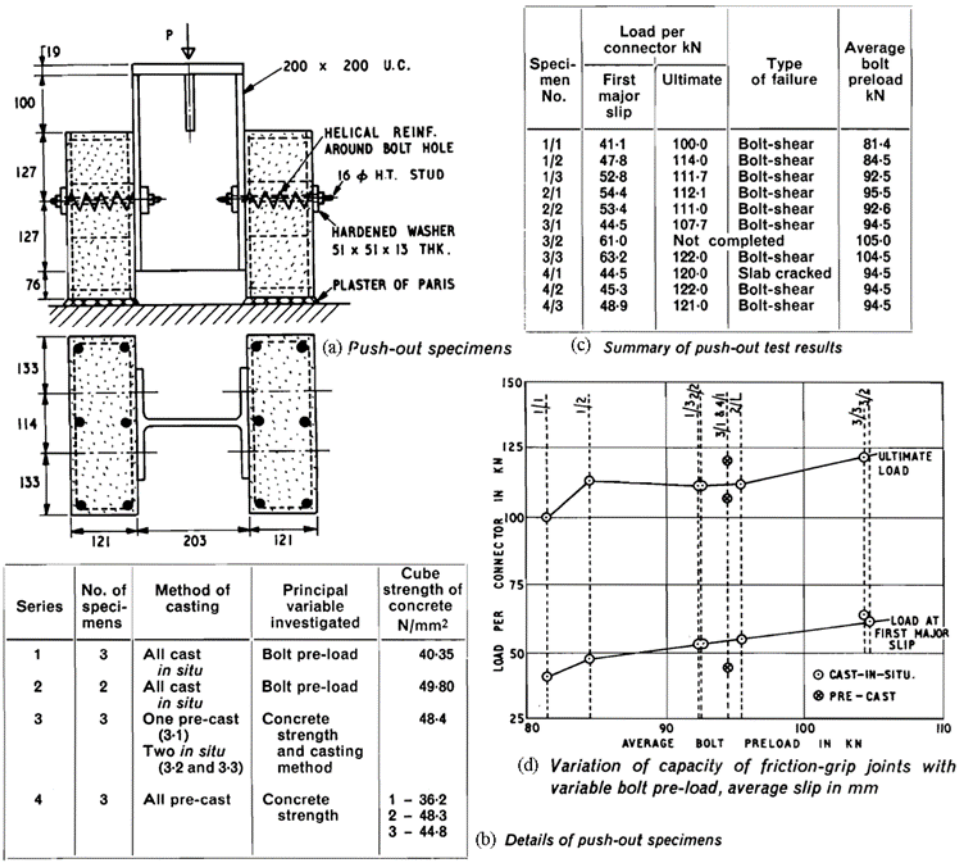

Specimen No.	Load per connector kN: First major slip	Load per connector kN: Ultimate	Type of failure	Average bolt preload kN
1/1	41·1	100·0	Bolt-shear	81·4
1/2	47·8	114·0	Bolt-shear	84·5
1/3	52·8	111·7	Bolt-shear	92·5
2/1	54·4	112·1	Bolt-shear	95·5
2/2	53·4	111·0	Bolt-shear	92·6
3/1	44·5	107·7	Bolt-shear	94·5
3/2	61·0	Not completed		105·0
3/3	63·2	122·0	Bolt-shear	104·5
4/1	44·5	120·0	Slab cracked	94·5
4/2	45·3	122·0	Bolt-shear	94·5
4/3	48·9	121·0	Bolt-shear	94·5

Series	No. of specimens	Method of casting	Principal variable investigated	Cube strength of concrete N/mm²
1	3	All cast *in situ*	Bolt pre-load	40·35
2	2	All cast *in situ*	Bolt pre-load	49·80
3	3	One pre-cast (3·1) Two *in situ* (3·2 and 3·3)	Concrete strength and casting method	48·4
4	3	All pre-cast	Concrete strength	1 – 36·2 2 – 48·3 3 – 44·8

Fig. 2.4. Marshall et. al. (1971) pushout tests specifications and results

Marshall et. al. (1971) conducted 11 push-out tests but 'the only measurements taken were for the slip between the I-beam and the slab which was measured for each bolt'. Unfortunately, no measurements were made for the slab uplift separation, which is also important for steel-concrete composite beams (Clause B.2.4(4) of BSI 2004a). Vertical separation between the steel and concrete slab is usually induced by flexural distortion of composite beams (Oehlers and Bradford 1995). All specimens of Marshall et. al. (1971) failed by shearing of bolts, except for one specimen that failed by crushing of concrete (Fig. 2.4c). The crushed slab had a cube strength of 36 MPa, while the strength of other specimens was in the range of 40 to 50 MPa. Thus, concrete strength controls the mode of failure, despite what they concluded that the strength of concrete did not affect the behaviour of shear connector. Their results are shown in Fig. 2.4(c and d). It can be seen from the first five specimens that there is obvious correlation between the preload and first slip but no clear trend at ultimate load. The average ultimate load of the five tests is 110 kN and the difference

between any individual test and the average is less than 10%. Recalling that this is exactly the definition of identical pushout tests according to Eurocode 4 (BSI 2004a), these tests are identical.

Dedic and Klaiber (1984) examined the use of high-strength bolts as shear connectors in rehabilitation of bridges and other structures. Two types of shear connectors, as shown in Fig. 2.5, were examined. Shear failure of the bolts above the beam flange along with tensile cracking in the slab were observed in all specimens. Fig. 2.6 shows a comparison of the load-slip behaviour of the two new shear connectors with that of welded studs. In general, higher shear resistance and slip capacity were achieved. The welded stud failed at displacement less than 4 mm. For loads up to 89 kN, the bolts provided a slightly higher stiffness against slip than that of welded studs. From 89 to 200 kN, the slip resistance of the bolts was lower. It was explained that this behaviour was due to the deformations of the bolt threads inside the bolt hole until complete bearing could be achieved. Referring to Fig. 2.5(a), excessive labour work is needed to drill the holes on the concrete slab and on the steel flange as well as to install the bolts and to grout the slab hole.

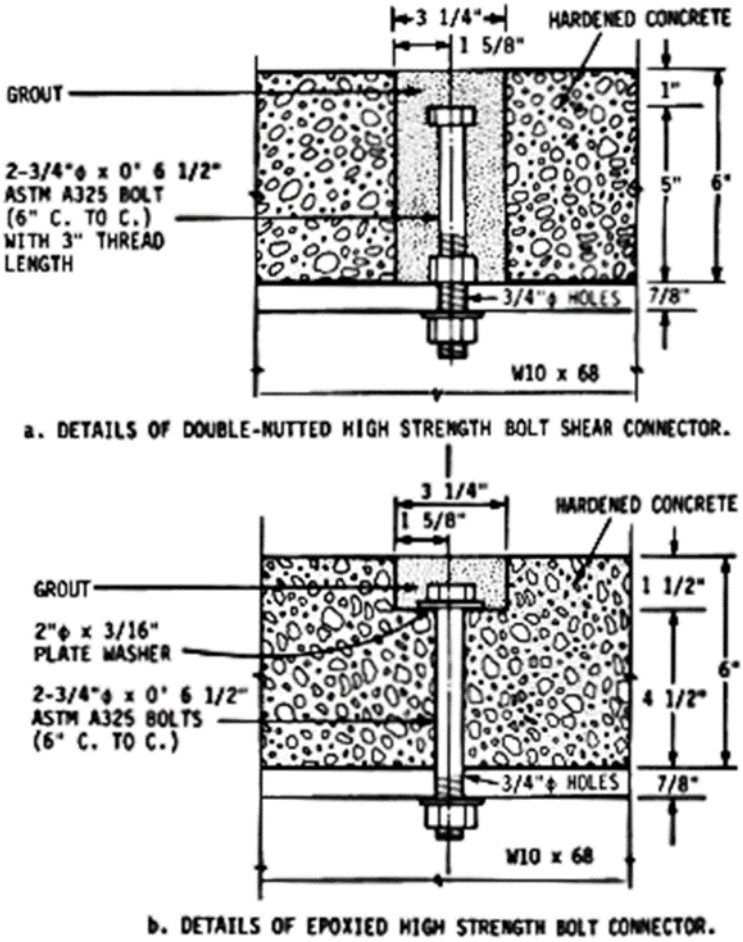

Fig. 2.5. Dedic and Klaiber (1984) shear connectors

Installing the bolts requires working underneath the bridge which is considered as unfavourable practice. Grouting the hole has the potential to create cracking due to shrinkage and variation in properties between the grout and the concrete slab. Fig. 2.5(b) shows that there is full contact between the concrete slab and the steel beam. In reality, gaps exist within this interface. In this case, if the bolt is tightened, cracks will be developed in the concrete slab. Fig. 2.6 shows that the two connectors do not have significant shear resistance as compared to welded studs. Given their excessive construction method, such connectors are likely to be expensive.

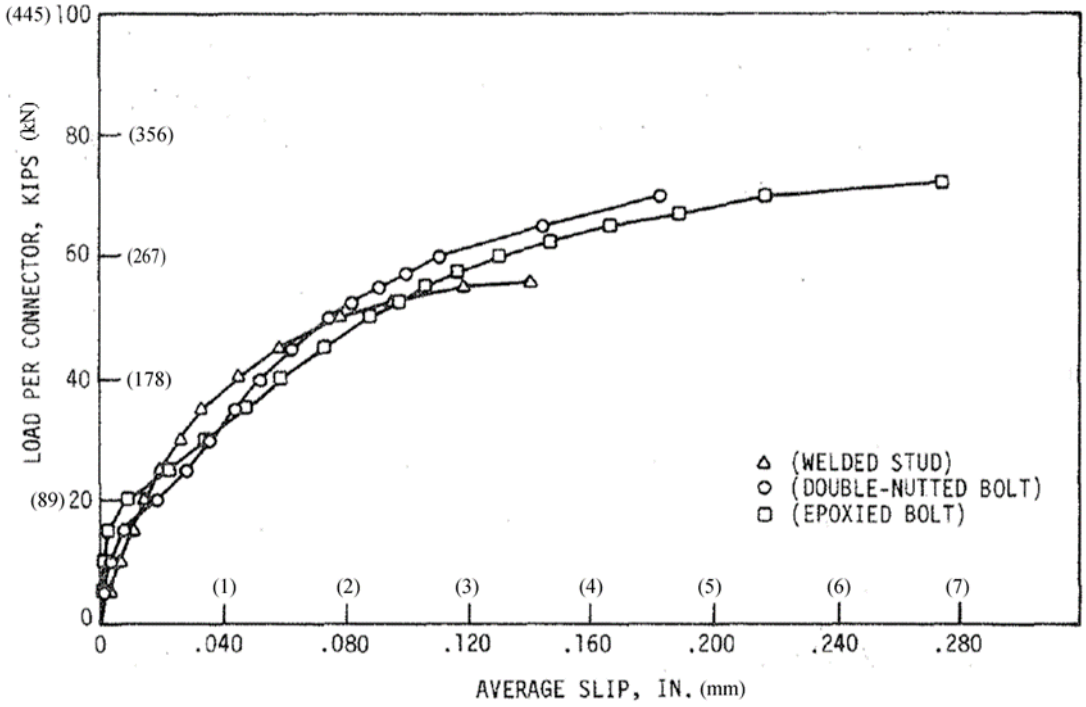

Fig. 2.6. Dedic and Klaiber (1984) pushout tests results

Eleven new shear connectors were examined by Kwon et. al. (2007), Kwon (2008), and Kwon et. al. (2010). Finally, three types of shear connectors were proposed by Kwon et. al. (2011), which are shown in Fig. 2.7. These connectors were referred to as the double-nut bolt (DBLNB), the high-tension friction grip bolt (HTFGB), and the adhesive anchor connector (HASAA). The work consists of 26 (single) push-out tests (i.e. in the horizontal direction) for static and fatigue loading using 19 mm and 22 mm bolts. In general, all shear connectors failed by fracture. The DBLNB specimens showed less concrete crushing than the other types due to the large bearing area of nuts embedded in the concrete block. The HTFGB showed the highest initial stiffness because it transfers shear at the steel-concrete interface by friction. Therefore, a full composite action without any slip can be achieved before friction is overcome.

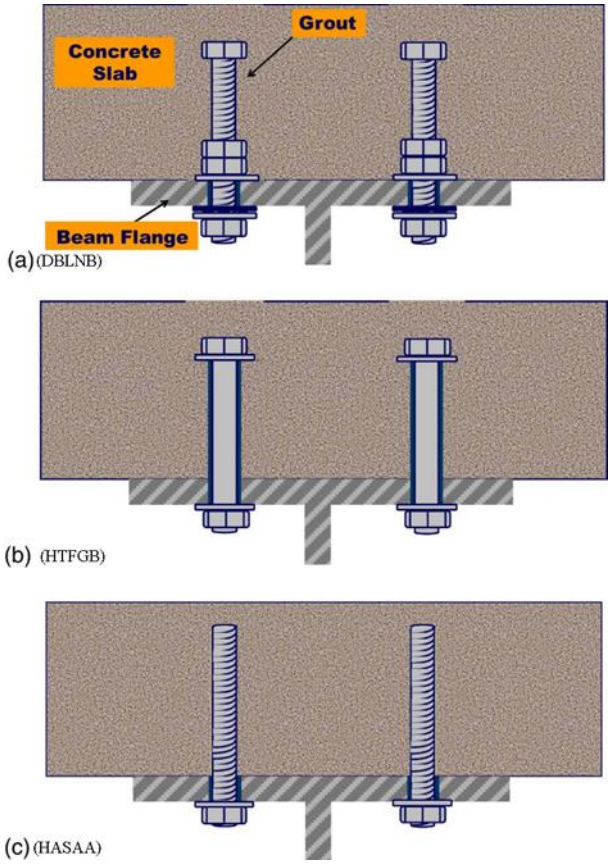

Fig. 2.7. Three shear connectors from Kwon et. al. (2011)

The researchers also performed full-scale tests on beams of 11.6 m span to evaluate the structural performance of their shear connectors, and the results are shown in Fig. 2.8. It was estimated that with only 30% of shear connection (i.e. partially composite beam), a 40% increase in the ultimate load-carrying capacity is achieved as compared to non-composite beams. Composite beams of DBLNB and HASAA showed a sudden strength drop at approximately 115-mm vertical deflection because of the sudden failure of multiple shear connectors at the steel-concrete interface. Fig. 2.7(a) shows that the bolt has two nuts and washer at the steel-concrete interface where the shear force is maximum. The two nuts will increase the concrete bearing area in comparison to using a bare shank. The maximum width of a M16 nut, for example, is 30 mm. This will decrease the compressive stress in the concrete close to the bolt. The cross-sectional area at the interface is for the bolt threaded part only. For most commonly used bolts, the net area is about 70% of the shank area (Kulak *et al.* 2001). Hence, less shear resistance as compared to a bare bolt was achieved. In Fig. 2.7(b), full contact between the concrete and steel is assumed, which may not be a realistic assumption due to imperfections in the steel beam and concrete slab such as lack of straightness, lack of flatness, lack of fit and other minor eccentricities (BSI 2005b). Fig. 2.7(c) shows that the main construction procedure should be carried out beneath the bridge, which

is considered as unfavourable practice. In addition, the geometry does not show any potential for slab separation. Fig. 2.8 shows several sudden slips at the end of the elastic behaviour of the DBLNB and HASAA. This raises questions relevant to their suitability to satisfy the SLS criterion. In general, the shear resistances (e.g. 137 kN of 19 mm DBLNB) are close to those of welded studs (i.e. 100 kN of 19 mm 450 MPa studs), which means that no appreciable reduction in the number of shear connectors can be achieved.

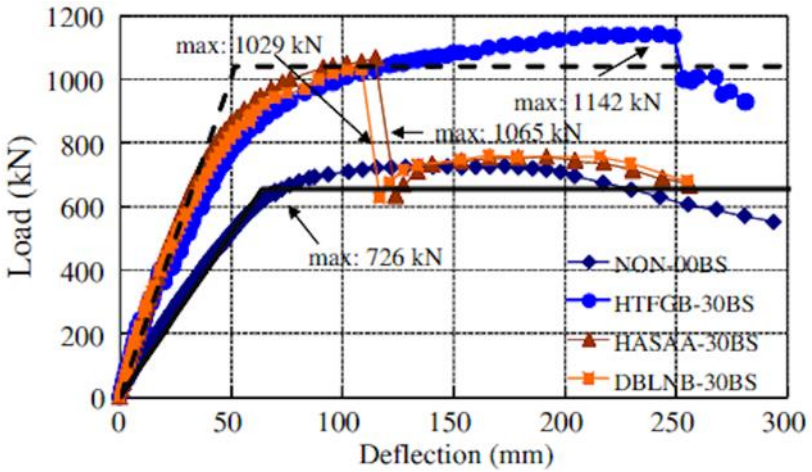

Fig. 2.8. Composite beam results of three shear connectors (Kwon et. al. 2011)

Blind bolts were tested by Mirza et. al. (2010) to be used as shear connectors for demountable purposes including portable construction and material reuse. The numerical model developed by Pathirana et. al. (2013) was compared with experimental beam tests. Blind bolts were also used for retrofitting existing composite beams by Pathirana et. al. (2015) and Pathirana et. al. (2016a). The bending behaviour was examined by Pathirana et. al. (2016b), while dynamic load effects by Henderson et. al. (2017). A typical blind bolt is shown in Fig. 2.9.

Fig. 2.9. Two types of blind bolts (Pathirana et. al. 2016a)

The results of pushout tests are shown in Fig. 2.10. It should be noted that the Y-axis in Fig. 2.10 represents the load for 8 connectors. In general, the results showed comparable shear resistance but less slip capacity as compared to welded studs. Fig. 2.9 (top photo) shows that due to the inherent blind bolting mechanism, the collar (2 in top-left photo) had to expand radially (2 in top-right photo) inside the hardened concrete, when the nut 1 is tighten. In order for this expansion to be realized in practice, the surrounding concrete has to be crushed or at least to be under radial compressive and circumferential tensile stresses. Fig. 2.9 (bottom photo) reveals the same disadvantages of having an increased bearing area due to nut 4 and washer 3, and a reduced cross-sectional area through the threaded part of bolt 1 at the interface.

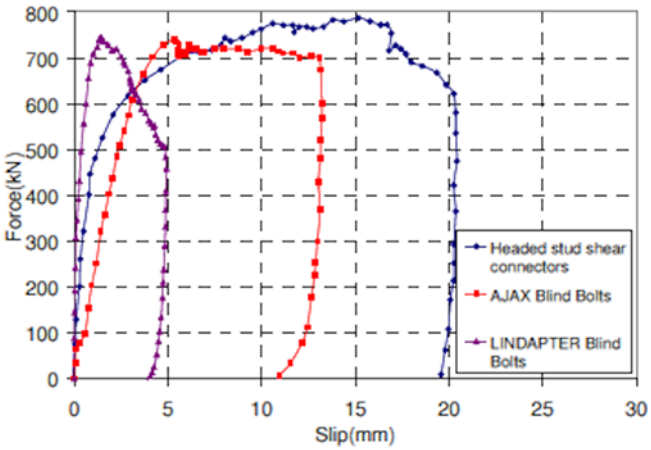

Fig. 2.10. Comparison in pushout results between blind bolts and stud (Mirza et. al. 2010)

A new demountable shear connector was presented and verified by pushout tests by Lam and Saveri (2012), confirmed using nonlinear FEM model by Lam et. al (2013), tested in beam tests with profiled slabs by Moynihan and Allwood (2014), used in parametric studies by Dai et. al. (2015), and extended to profiled slabs in pushout tests by Rehman et. al. (2016). This shear connector differs from previous types in that it did not use high strength preloaded bolts, but it was machined from standard welded studs (16 and 19 mm), as shown in Fig. 2.11.

Fig. 2.11. New connectors machined from studs (Lam and Saveri 2012)

Obviously, the new connector, as a material (mild steel) and geometry (headed stud), inherent the characteristics of studs like ductility, uplift resistance, and shear resistance. In addition, most of the equations in international standards would be available for its assessment. The only difference between the two is that the stud has a welded collar (increase in diameter), while the new type has a collar shaft (decrease in diameter) and a nut. The welded collar of a stud is believed to be responsible for 70% of the stud's shear resistance (Johnson 2012, and Oehlers 1980). A sample of pushout tests results is shown in Fig. 2.12. It is interesting to note that, although a reduction in diameter is present in the connector, no significant reduction in shear resistance was noticed by comparing PT2 and PT8 in Fig. 2.12(a). It seems that the role of collar shaft is for construction purposes, i.e. to secure the connectors in position prior to concrete casting. It can be seen from Fig. 2.12(b) that all the specimens share a slip capacity exceeds the Eurocode 4 (BSI 2004a) limit of 6 mm. This behaviour makes the connector suitable for partial shear connection in steel-concrete composite beams. It is also noted that the maximum slip of welded studs in PT7 is a representative example of the scatter expected in the results of pushout tests on welded studs as explained before.

(a) Push test program and results

Ref.	Concrete Cube Strength, f_{cu} (MPa)	Stud Type	Max. Load per stud (kN)	Slip at Max. Load (mm)	Mode of Failure
PT 1	19.85	16mm	75.0	8.75	Stud fracture
PT 2	21.45	17mm collar	93.5	7.94	Stud fracture
PT 3	20.10	18mm collar	71.9	22.03	Concrete crushing
PT 4	25.20	18mm collar	81.5	18.22	Concrete crushing
PT 5	29.90	18mm collar	90.0	21.25	Concrete crushing
PT 6	61.38	18mm collar	107.5	22.03	Stud fracture
PT 7	20.10	19mm welded	71.6	5.20	Concrete crushing
PT 8	29.90	19mm welded	92.7	9.00	Concrete crushing

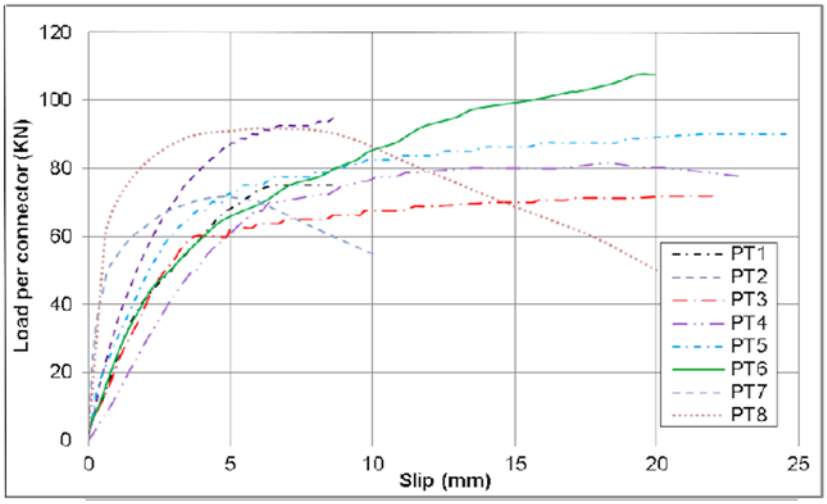

(b) Load – slip curves

Fig. 2.12. Pushout results of demountable shear connector (Lam et. al. 2013)

Deconstructable shear connector using high strength bolts was also suggested by Lee and Bradford (2013), confirmed by analytical models by Rowe and Bradford (2013) and Bradford and Pi (2012), supported by numerical FEM models by Ataei and Bradford (2014), studied independently by Chen et. al. (2014), followed by detailed ABAQUS analysis by Liu et. al. (2014), and finally, tested under beam action by Ataei et. al. (2016). The new type is shown in Fig. 2.13, where the bolts are not embedded into the concrete slab, but located in empty through-holes. These holes are intended not to be grouted, to make it possible for future demountability. It is clear from Fig. 2.13 that this type is different from the previous ones in that, it has the potential to replace the bolts only without replacing the concrete slab.

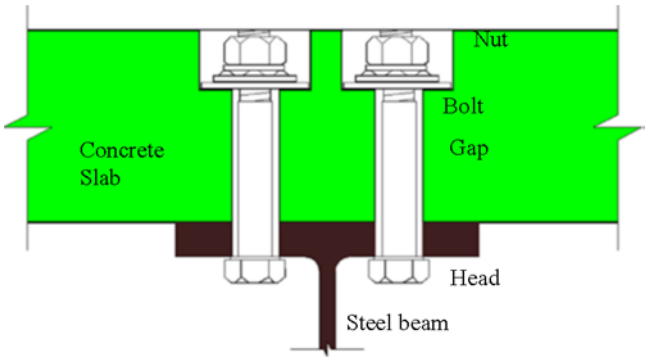

Fig. 2.13. Deconstructable shear connectors (Ataei et. al. 2016)

However, a drawback relevant to this feature has been identified, and can be explained with reference to Fig. 2.14. The bolt has an initial pretension, which creates friction resistance. When the shear force overcomes the frictional resistance, there is no additional shear resistance. Therefore, a sudden slip occurs until the bearing resistance is activated, i.e., the slab will continue to slip until the gap clearance is closed (about 4 mm). During this slip, the connection has no resistance at all. This can be confirmed by checking some of their pushout tests shown in Fig. 2.15.

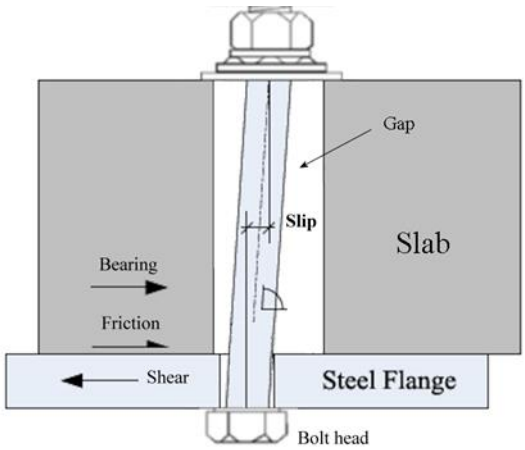

Fig. 2.14. First slip mechanism of deconstructable shear connectors

Fig. 2.15 shows the load-slip behaviour of four different specimens of deconstructable shear connectors. The sudden slip, and zero resistance can be seen in all specimens described as 'First slip'. It is interesting to know that this problem was recognized by (Johnson and Buckby 1986). These researchers suggested as a solution that 'the bolt should be grouted after tightening' or that the ultimate shear resistance to be considered equal to the frictional resistance only. Furthermore, the gap around the bolt has a major effect. Rowe and Bradford (2013) suggested that this gap is approximately the same for all bolts. In practice, matching the holes of the precast slab to those on the steel beam will definitely generate variations in the gap of each bolt. At SLS loading, minimum slip displacements are expected, e.g. welded studs slip in fractions of millimetre. Test results in Fig. 2.15, however, show slip displacement up to 12 mm, which is expected to have an effect on the vertical deflection in composite beams. Nevertheless, the deconstructable connectors have a unique performance in terms of ultimate shear resistance and slip capacity, which are the highest among those of all the shear connectors discussed in this literature review (taking into account variations in bolt diameter and concrete compressive strength). It should be noted that the Y-axis, in Fig. 2.15, represents the total load, and the shear resistance can be found by dividing the load by 4, except in case (d) where it should be divided by 8.

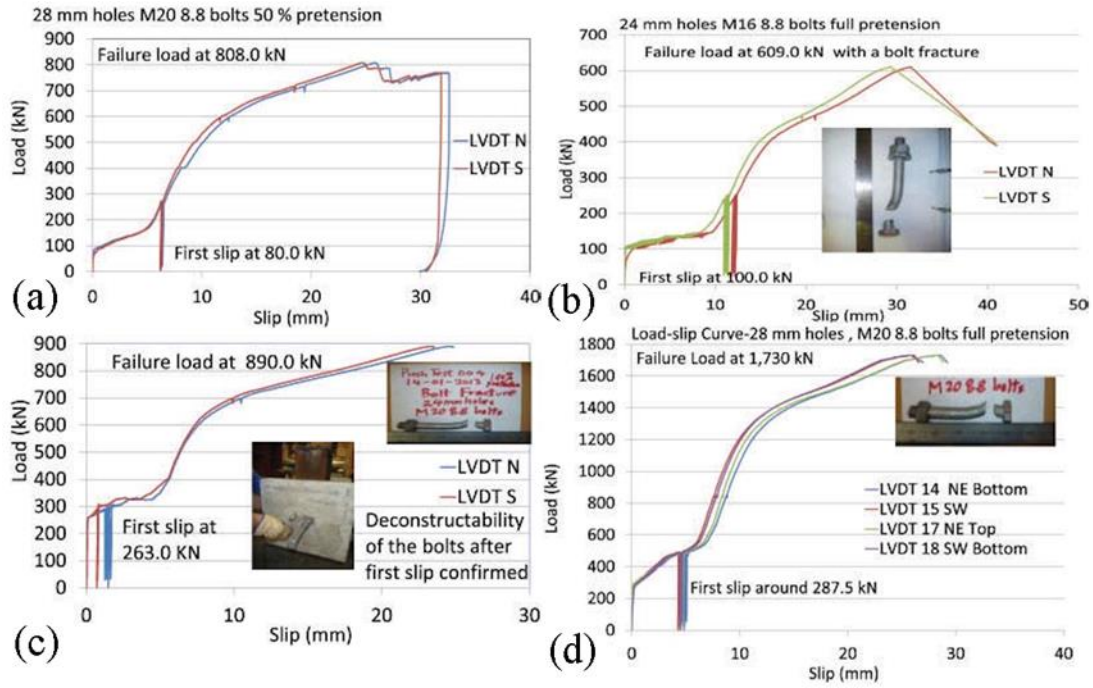

Fig. 2.15. Load-slip behaviour of deconstructable shear connectors (Lee and Bradford 2013)

Pavlović (2013) and Pavlović et. al. (2013) also used high strength bolts as shear connectors. The bolt is embedded in concrete and supplied with a single nut. Fig. 2.16 shows the shear connector with several results from pushout tests. Similar details are observed in Figs. 2.16 and 2.5a. The load-slip figure also includes a comparison with welded studs. Fig. 2.16 shows that the single nut shear connector has very limited slip capacity, i.e. below the 6 mm limit of Eurocode 4 (BSI 2004a). The inclusion of a single nut limits the pretension inside the bolt between the two nuts (Fig. 2.16). The effect of friction resistance is, therefore, minor. It is obvious that the single nut has a bearing area larger than the shank; therefore, it decreases stress concentration in the surrounding concrete. The threaded part of the bolt is located exactly at the interface where the shear force is maximum. Since the threaded part of the bolt has a reduced cross-sectional area to resist shear forces, the connector becomes more vulnerable to bolt shearing rather than to concrete crushing (assuming normal strength concrete and M16 high strength bolts). The single nut represents a stiff element, which concentrates bending of bolt to the interface and prevents the smooth deflected shape that is usually observed in welded studs. Thus, less slip capacity is achieved.

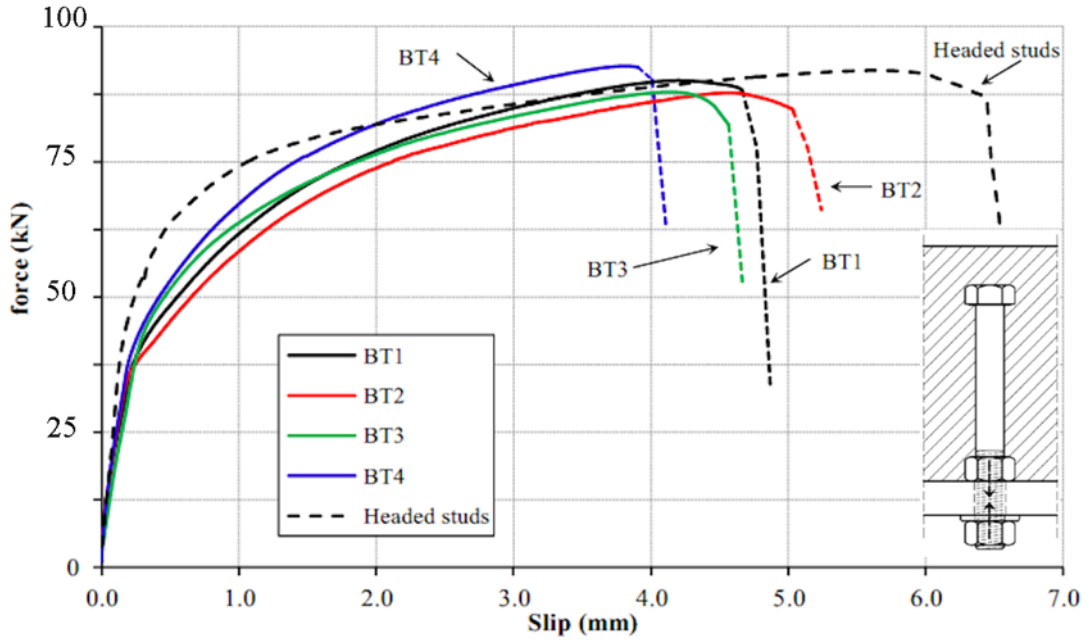

Fig. 2.16. Load-slip behaviour of single nut shear connector (Pavlović 2013)

2.6 The Problem

All the previous tests on friction-grip bolts as shear connectors revealed an undesirable large slip displacement due to bolts sliding inside the bolt holes when friction resistance in the steel beam-concrete slab interface was exceeded. It should be noted that the pre-standard of Eurocode 4 (BSI 1994) included friction-grip bolts as shear connectors but with major

restrictions in the exploitation of their full shear resistance. In particular, the BSI (1994) pre-standard allowed the summation of two horizontal shear force resisting mechanisms (i.e. friction in the steel beam-concrete slab interface and shear force resisted by the bolt only) provided that the shear force-slip displacement behavior has been verified by testing. Moreover, Johnson and Buckby (1986) discuss the use of friction-bolts as shear connectors within the framework of the BS5400-5 (BSI 1979) standard for bridges. They mention that the shear resistance of friction-bolts should be assumed equal to friction resistance only when all the gaps among the bolts and the precast slabs holes are grouted after bolt tightening. This is to ensure that bearing of the bolt onto the precast slab will take place immediately after the initiation of slip in the friction interface. It is interesting to know that BS EN 1993-2 support Johnson and Buckby (1986) opinion but in steel bridges as follows 'where holding down bolts or other similar devices are used to provide some of the resistance to horizontal movement, it should be demonstrated that this resistance is provided before any movement can take place. If bolts are provided in holes with normal tolerances, movement will inevitably take place before the full resistance to movement is achieved. This is unacceptable in service conditions.' (BSI 2006)

Apart from the bolt sliding issue discussed in the previous paragraph, all the previously proposed bolted shear connectors may not be suitable for precast construction due to different practical reasons. In the case of shear connectors that are pre-embedded in the concrete slab, precast construction tolerances make their alignment with the pre-drilled bolt holes on the top flange of the steel beam extremely difficult, if not impractical. In the case of shear connectors that are fastened underneath the steel beam after positioning of the precast slab on the top of the steel beam, gaps in the concrete slab - steel flange interface may prevent adequate bolt fastening and cause slab cracking (Biswas 1986). Moreover, working underneath the bridge to fasten the bolts is time consuming and is generally considered as substandard unfavourable practice. It is also noted that connectors that are fully embedded within the concrete slab allow uplift and replacement of the slab as a whole, but not full disassembly of the composite beam, i.e. replacement of the shear connectors, in case of damage due to fatigue or corrosion, is not practical.

In all the previous types of demountable connectors, no suggestion was made for the longitudinal connection of the concrete panels. The current construction procedure uses transverse joints between the panels, where their reinforcements are overlapped and then the joints are filled with a non-shrinkage grout that is allowed to reach the required

compressive strength. However, this method (which was used in the 1970s) was proved to have serious problems due to cracking in the grouted transverse joints. Another method using dry joints has been successfully used in Sweden in the last 15 years (Hallmark 2012). The precast panels are connected through a shear key. It is true that the Sweden method has the advantage of quick construction time. However, it has one disadvantage, which is the tight tolerance in matching the adjacent panels. This may prove to be a significant challenge, especially for long bridges.

2.7 Summary

This chapter provided important definitions usually used in composite beam theory and a detail description of welded studs and their advantages and disadvantages related to construction and structural behaviour. Then, various types of previously developed demountable shear connectors are described in chronological order. A detailed discussion of each of these connectors is provided. The chapter ended with important common findings in relation to previous demountable shear connectors. In particular, their disadvantages were identified. Such disadvantages actually constitute (or define) the research question or problem. Overcoming such disadvantages along with providing additional advantages is the main initial goal set for this PhD research.

Chapter 3: Specification of Shear Connectors

3.1 Introduction

The proposed shear connectors, namely the locking nut shear connector (LNSC) and the friction based shear connector (FBSC), were invented by Suwaed *et al.* (2016) (Appendix A). They were designed by fully considering the conclusions of the previous chapter, i.e. the main goal was to overcome the disadvantages of previous demountable shear connectors. The common feature of the new connectors is demountability to enable rapid replacement of concrete slabs or shear connectors of precast composite bridges. In addition, they exhibit advantageous structural characteristics compared to conventional welded studs like shear strength, stiffness, slip capacity, and slab uplift resistance capacity. The following sections will outline the design of the new shear connectors.

3.2 Locking Nut Shear Connector (LNSC) Details

Fig. 3.1 shows a steel-concrete composite bridge, which consists of precast concrete panels connected to steel beams with the aid of the LNSC. The concrete panels have several holes (pockets) to accommodate the shear connectors. Fig. 3. 2 shows a 3D disassembly along with an inside 3D view of the shear connector where all its components are indicated. Moreover, Fig. 3.3 shows the cross-section of a steel-concrete composite beam with the shear connector. The following paragraphs describe in detail the components of the LNSC and the associated methods of fabrication and construction.

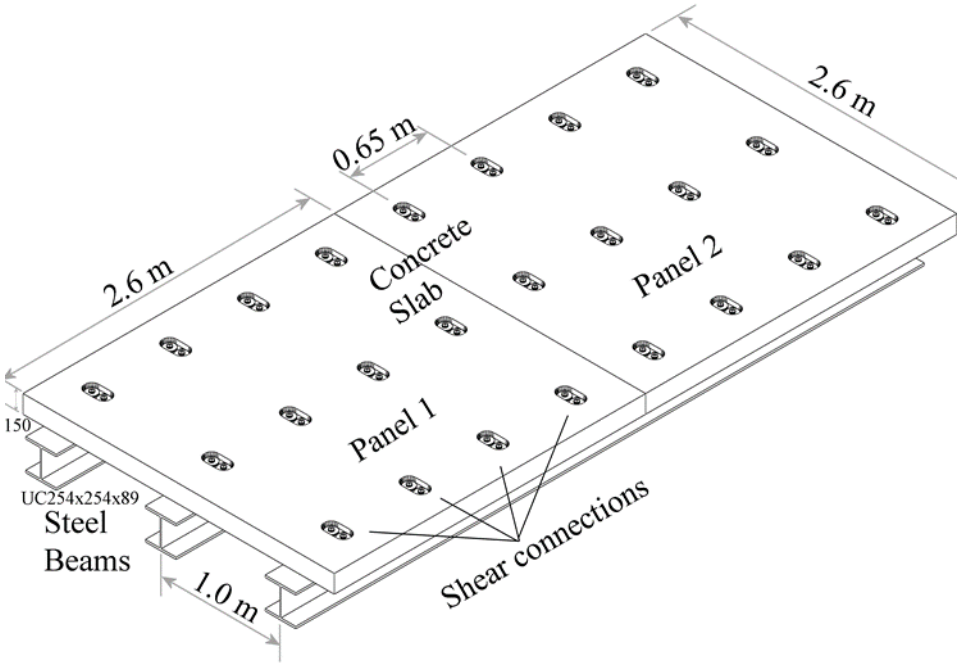

Fig. 3.1. Precast steel-concrete composite bridge using the novel shear connector

The LNSC consists of a pair of high strength steel bolts per BS EN 14399-3 (BSI 2005c) (e.g. Grade 8.8 or higher) with standard diameter (e.g. M16). The bolts were threaded to 20 mm at one end and 50 mm at the other end, while their middle part is smooth, as shown in Fig. 3.3. These bolts are fastened to the upper flange of the beam using a double nut configuration which consists of a standard lower hexagonal nut per BS EN 14399-3 (BSI 2005c) (nut 1 in Fig. 3.3) and an upper conical nut (nut 2 in Fig. 3.3). The upper part of the bolt hole is a countersunk seat with chamfered sides following an angle of 60 degrees as shown in Fig. 3.4(c). The upper conical nut (see Figs. 3.4(a) and 3.4(b)) is a standard type nut (BSI 1970) threaded over the bolt and has geometry that follows the same 60-degrees angle so that it can perfectly fit within the countersunk seat. The upper conical nut provides a mechanical stop within the countersunk seat, and in this way, prevents slip of the bolt within the bolt hole. Using locking conical nuts will ensure uniform distribution of shear force in composite beams among all bolts. On the other hand, if ordinary flat nuts used instead, and because in actual construction situation, the clearance gap between a bolt and its hole will not be the same among all bolts, the shear force would tend to be resisted by the first bolt that hits the side of its hole while other bolts are not contributing to the shear resistance yet. In addition, the conical 60-degrees tapered shape of the locking nuts will increase the contact bearing area between the nut and bolt hole in the steel beam as compare to shank bearing only, and therefore reduce the compressive stresses in the bolt hole. Similarly, the conical 60-degrees tapered shape of the locking nuts will reduce the bearing pressure on the countersunk hole by decomposing the shear force into two components: one perpendicular to the tapered surface of the countersunk hole with magnitude equal to 87% of the shear force (i.e. $\sin 60^{\circ}$) and one parallel to the tapered surface of the countersunk hole with magnitude equal to 50% of the shear force (i.e. $\cos 60^{\circ}$). It should be noted, however, that the conical nut is part of a double nut connection, and therefore, both nuts will resist the shear force; the lower nut by friction (then bearing), while the conical nut by friction and bearing simultaneously. The parallel component (50% of shear force) will try to slide the conical nut over the tapered side of the flange hole. The sliding force will be resisted by a component of the tensile force inside the double nuts (i.e. sin 60^{o}), as well as friction resistance resulted from the second components of each shear and tensile forces. By equating the aforementioned forces together, assuming the shear force is as high as 1.1 of tensile resistance, the whole force transmitted to the conical nut, and the friction coefficient of steel-steel interface is 0.2, the minimum tensile force inside the double nut would be 37% of tensile resistance. The 37% of tensile resistance for M16 bolts (Table 4.5) equals 66 kN;

therefore, the net tensile force between nuts 1 and 2 (Fig. 3.3) should be higher than 66 kN. The net tensile force equals the design tensile force between nuts 1 and 2 minus the design tensile force between nuts 2 and 3. Few millimetres of the total height of the upper conical nut appear above the top surface of the beam flange (see Fig. 3.3) to represent the optimum height of the collar of welded shear studs which is 0.35 times the stud diameter (where 70-75% of load is believed to be carried by the collar (Johnson 2012, and Oehlers 1980)). In this way, the LNSC increases the contact bearing area of the bolt with the surrounding concrete, reduces concrete stress concentrations, and therefore, delays concrete crushing. It is believed that the load profile inside the concrete slab due to embedded dowel has a hydrostatic shape with a maximum value at the dowel toe and decrease to zero or even to negative value at the other end of the dowel. Bearing this in mind, the role of the conical locking nut is to provide stiff support for the bolt in the region of the maximum bearing pressure. Higher shear force is, therefore, needed to fracture the bolt as compare to bolt without a conical locking nut. Moreover, Fig. 3.4(b) shows the M16 conical nut after removing five millimetres of its internal threading. In this way, the bolt is partially hidden inside the conical nut and shear failure within its weaken threaded length (as seen in other types of bolt shear connectors) is prevented. It has been shown from double shear tests that about 30% increase can be gain if failure occurred through the shank part of bolt as compare to that occurred through its threads (Pavlović 2013, and Chesson *et al.* 1965).

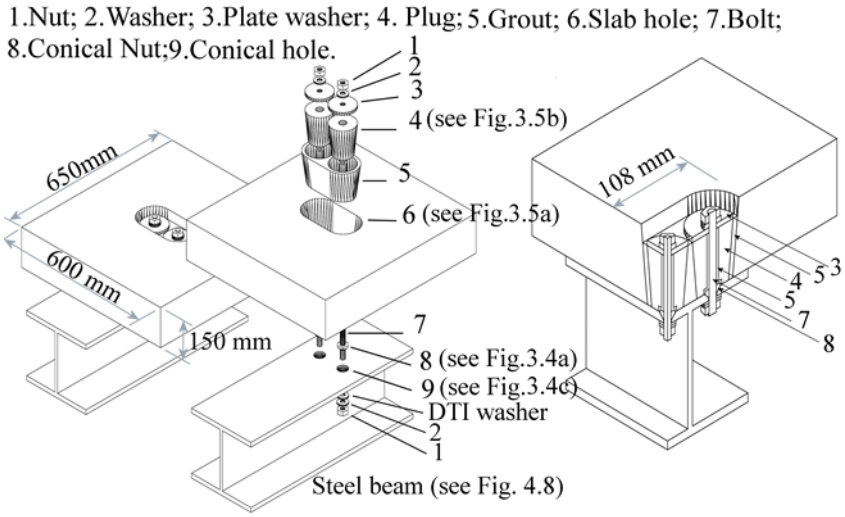

Fig. 3.2. 3D disassembly and inside view of the LNSC

Fig. 3.2 shows that the lower part of the double nut connection consists of a DTI washer, a washer and a nut. The DTI washer was per BS EN 14399-9 (BSI 2009a), the washer was a hardened chamfered washer per BS EN 14399-6 (BSI 2005d), and the nut was a hexagonal

nut per BS EN 14399-3 (BSI 2005c). It should be noted that the standard DTI washer cannot guarantee an exact proof load but loading within a specific range. A proof load (e.g. in the range 88-106 kN for an M16 bolt, which represents 70% of its ultimate capacity per BSI (2009a)) is applied between the lower nut and the conical nut to ensure a robust locking configuration that prevents slip of the bolt within its hole. The setup procedure including bolts fitting is outlined in Section 3.4 and Appendix A.

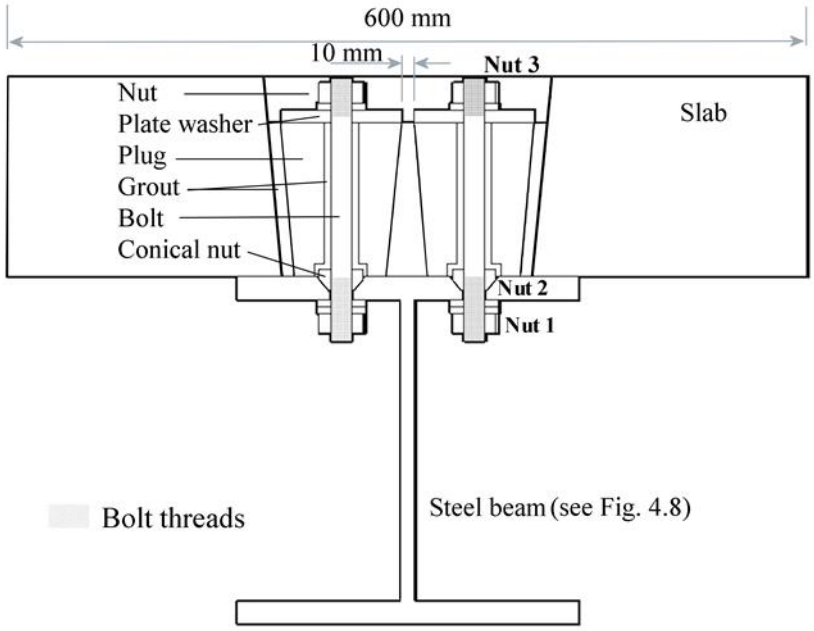

Fig. 3.3. Cross-section of a steel-concrete composite beam using LNSC

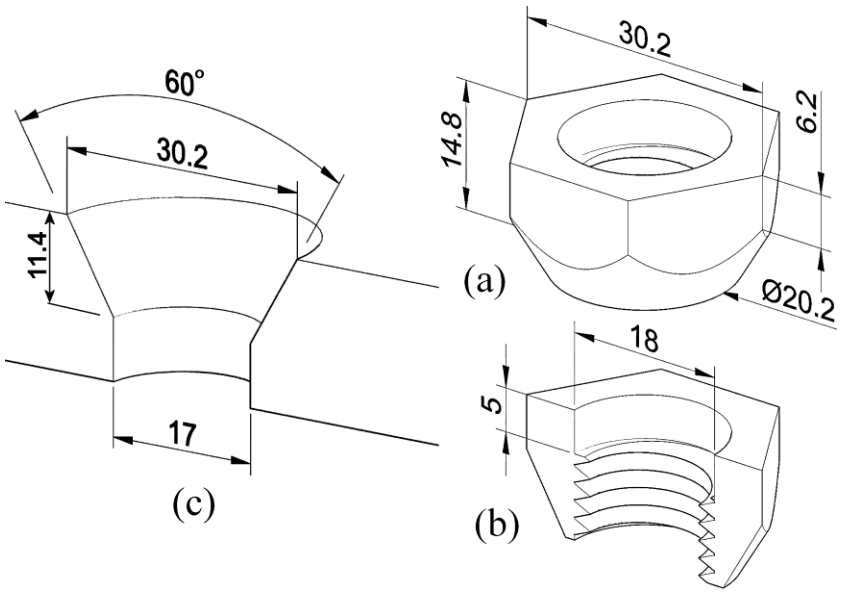

Fig. 3.4. Geometry of the locking connection. (a) full nut (b) half nut (c) half countersunk hole

The slab pocket is a countersunk hole with an inclination of 5 degrees following the recommendations of Vayas and Iliopoulos (2014). A typical geometry of a slab pocket, relevant to the test specimens presented later, is shown in Fig. 3.5(a). Inside each slab pocket there are two inverted conical precast concrete plugs (see Figs. 3.2 and 3.3) with geometry following the inclination angle of the slab pocket. A typical geometry of a plug, relevant to the test specimens presented later, is shown in Fig. 3.5(b). Each plug has a central circular hole with a 26-mm diameter that accommodates an M16 bolt with 10 mm clearance. The diameter of the central circular hole increases from 26 to 40 mm at the base of the plug to accommodate an M16 conical nut with 10 mm clearance as shown in Fig. 3.5(b). The 10-mm clearance is planned to help in creating adequate slip capacity; more than that, it should be checked against bolt fracture due to excessive slip (Oehlers and Bradford 1999). One of the fundamental disadvantages of conventional welded studs that they impose highly-concentrated loads into the concrete slab (Oehlers and Bradford 1995); therefore, the dimensions of the plug ensure that shear forces are transmitted from the LNSC into the concrete slab without the risk of premature longitudinal shear failure and/or splitting in the concrete mass. On the other hand, a gap filled with ordinary strength grout (less than 50 MPa cubic compressive strength) between the steel bolt and its concrete plug will ensure development of dowel action (i.e. resistance of shear by bending (Oehlers and Bradford 1995)) before bolt fracture. Thus, the grouted gap will permit the formation of bolt deflected shape through bending and shear, as well as, working as a cushion to distribute the bolt concentrated force both radially and longitudinally into the stronger concrete plug. Moreover, the diameters of the plugs are small enough compared to the diameters of the slab pocket to overcome construction tolerance issues typically encountered during precast bridge construction (Hallmark 2012). It has been proved by Oehlers (1980) that the strength of a stud depends on the concrete strength in the vicinity of the welded collar. The plug is, therefore, designed with high strength concrete (preferably 80-100 MPa cubic compressive strength), while the slab is kept as normal strength concrete (less than 50 MPa cubic compressive strength). Grout is used to fill the gaps between the bolt and the hole of the plug as well as the gaps between the plugs and the slab pocket (see Figs. 2 and 3). Rapid hardening grout of ordinary strength (as will be designed later – Section 4.4.5) that flows into gaps without bleeding or segregation is recommended for the LNSC. The height of the plug is 115mm (i.e. less than the 150-mm height of the slab) to allow for additional cover or waterproof grout.

A hardened plate washer (shown in Fig. 3.3) is used to uniformly distribute the bolt thrust on the upper face of the concrete plug without premature failure. The plate washer has a diameter of 90 mm, a hole of 18 mm diameter, and 10 mm thickness. More detailed specifications can be found in Section 4.4.1 including hardness condition and tensile strength. Usually, gaps exist between the steel beam and concrete slab (Badie and Tadros 2008). Thus, bolt tightening results in cracking of the concrete slab (Biswas 1986). Tightening of nut 3 (shown in Fig. 3.3) is carried before hardening of the grout. In this way, internal compression stresses are developed in the plug and not in the slab. Based on experimental experience, the following observations are made (1) tightening of bolts after grout hardening has no effect on frictional resistance at the interface because of anchorage; (2) Tightening of bolts using thin plate washers (<5 mm) may result in cracking of the concrete plug; (3) Tightening of bolts while the top surface of the plug is not flat probably result in cracking of the concrete plug.

It should be mentioned that different configurations of the LNSC could be adopted by using different number of bolts. For example, one bolt in one precast concrete plug within a single slab pocket can be adopted to reduce the quantity of in-situ grout or four bolts in a single plug within a single slab pocket could be adopted to increase the total shear strength, and, to allow reduction of the shear connectors needed along the length of the bridge.

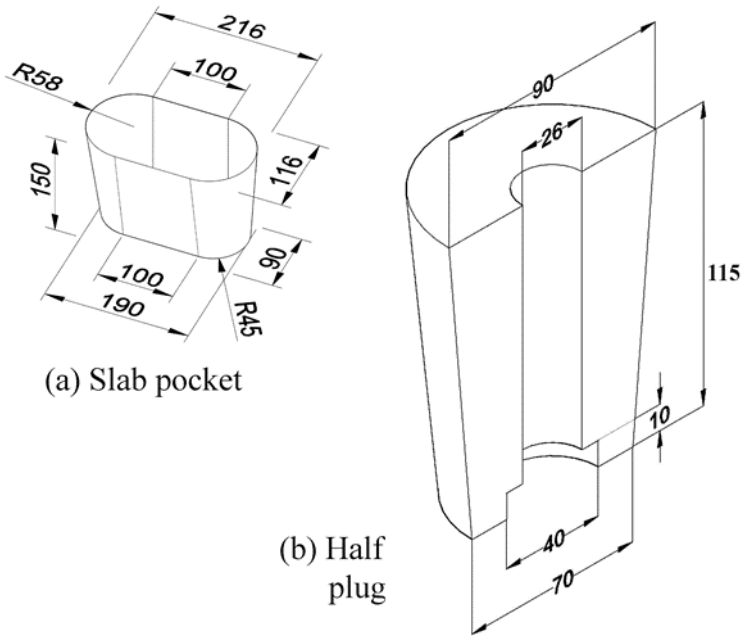

Fig. 3.5. Dimensions of (a) slab pocket and (b) half plug for LNSC

3.3 Friction Based Shear Connector (FBSC) details

The idea behind the FBSC is to resist service loading by friction resistance (hence the name) that is created at the interface between the lower face of the concrete plug and the upper face of the upper flange of the steel beam. The latter mechanism could be very beneficial in avoiding fatigue effects that occur in other shear connectors, such as welded studs due to repeated service loading.

The FBSC consists of a pair of high strength steel bolts (e.g. Grade 8.8 or higher) with standard diameter (e.g. M16) as shown in Fig. 3.6.

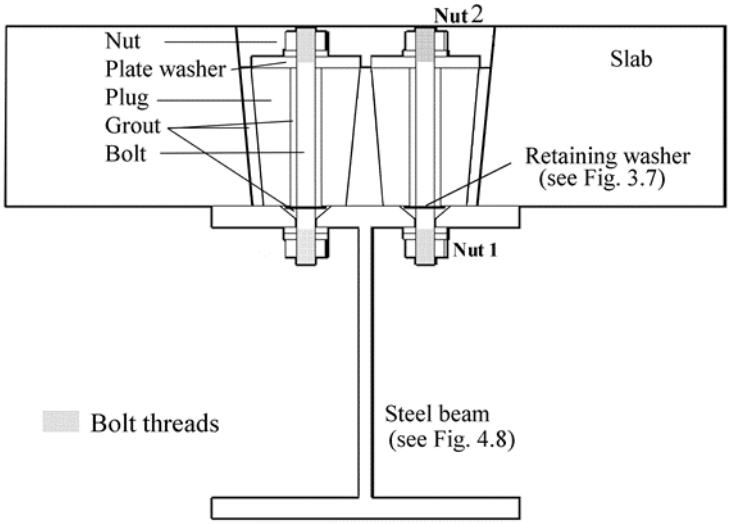

Fig. 3.6. Cross-section of a steel-concrete composite beam using the FBSC

The bolts are of smooth shank with 20 mm threaded ends. These bolts are positioned through the chamfered countersunk seat holes of the upper flange of the beam with the aid of retaining washers, designed as per BS EN 3386 (BSI 2012). The latter consists of a radial mounting shape with external diameter equal to or less than the external diameter of the chamfered countersunk seat hole; internal diameter equal to the bolt diameter minus 1mm; and several radial gaps (Fig. 3.7). The main role of these washers is to hold the bolts in position prior to grout casting, insertion of the concrete plugs, and installation of the upper nuts. In addition, the existence of radial gaps in these washers will ensure the penetration of grout into the chamfered countersunk seat holes and into the clearances gaps between the bolts and their holes in the steel beam. In this way, a complete linkage between the bolts

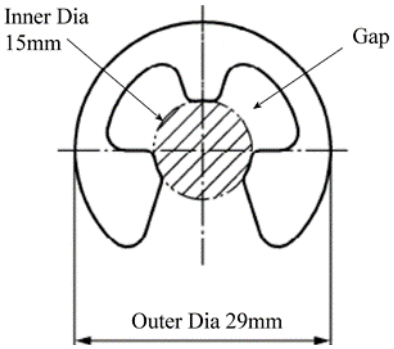

Fig. 3.7. Dimensions of retaining washer used in FBSC

and the steel beam is formed that should prevent sudden slippage observed in previous demountable shear connectors when friction resistance between the concrete plug and steel beam is overcome. The chamfered countersunk seat is similar to LNSC with geometry that follow an angle of 60 degrees, as shown in Fig. 3.4(c). It should be noted that bolt threads should be kept below the chamfered countersunk seat hole (Fig. 3.6). In this way, the bolt is partially hidden inside the upper flange of the steel beam and shear failure within its weak threaded length (as seen in other types of bolt shear connectors like Pavlović (2013), Kwon *et al.* (2011), and Dedic and Klaiber (1984)) is prevented. All other bolting assembly components are the same with those of the LNSC. The lower standard hexagonal nut (BSI 2005c) is used along with a hardened chamfered washer (BSI 2005d).

A proof load of 75-100% is applied between the lower nut (Nut 1) and the upper nut (Nut 2) to ensure a robust locking configuration that prevents slip under service loading by creating friction resistance between the lower surface of the concrete plug and the upper surface of the flange of the steel beam. Ensuring that the bolt is locked within a fully grouted countersunk seat prevents slip of the bolt within its hole.

There are no changes to the slab pocket dimensions from LNSC. While the plugs are also practically the same, there is one difference, which is the elimination of the enlargement in the lower part of the central hole that was created previously to accommodate a conical nut. A typical geometry of a plug, relevant to the FBSC test specimens in Chapter 6, is shown in Fig. 3.8.

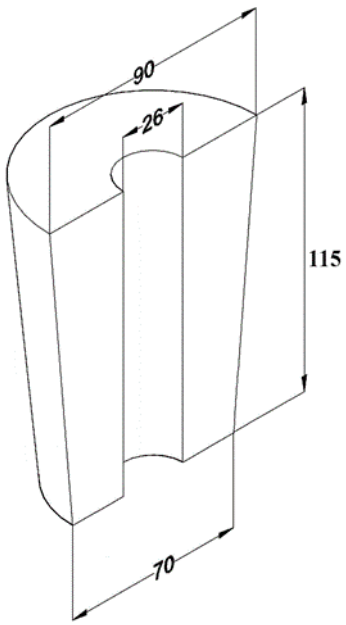

Fig. 3.8. Dimensions of half plug for FBSC

Careful attention should be made to ensure flat finish of the upper face of the plug and hence to ensure uniform stress distribution without any concentrations. It should be noted that the grout is still fresh when tightening the bolts; therefore, the strength of concrete of plugs did not benefit from the triaxial confinement yet. Adding to that, the use of a 'hardened' 'thick' plate washer is also a requirement to prevent any possible bending of the washer while tightening the bolts which may create stress concentrations at the upper face of the plug.

3.3.1 Bolt Preload Loss

FBSC is based on friction resistance between the lower face of the concrete plug and the upper face of the upper flange of the steel beam. Friction resistance is achieved with bolt axial pretension. Thus, loss of bolt pretension with time, due to plug concrete creep and bolt steel relaxation, is expected to be a technical issue. Although this PhD research does not deal with time-dependent effects, the following suggestions are offered: (1) tightening the bolts to a larger extent than the design requirement to account for the loss in tension with time (Nah *et al.* 2010) (for example designing the pretension as 60% of proof load while tightening the bolts to 100% of proof load, assuming a loss of 40%); (2) as a large percent of bolt force loss occurs during the first 24 hours after tightening (Heistermann 2011), then re-tightening may reduce this effect (BSI 1994); (3) using higher strength concrete of high aggregate/paste ratio in plugs to ensure less creep (Johnson 1967, Oehlers and Bradford 1995); (4) precast concrete eliminates/reduces the effect of shrinkage in concrete; (5) using higher strength steel (Grade 8.8, 9.8, 10.9, or 12.9) for bolts to maintain the preload; (6) using special 'spring' washers that can restore the loss in bolt force (like the commercial Bellville washers); (7) using special 'locking' nuts or washers that prevent nut loosening over time (like the commercial NordLock-washers); (8) using special tightening bolts like Tension Control Bolts (TCB) with electrical wrenches that reduces the nut self-loosening and shank torsional relaxation.

3.4 Procedure for Bridge Assembly

Prefabrication of all LNSC structural components can be carried out in the shop (i.e. machining of the conical nuts, drilling of the chamfered holes, positioning of the bolts on the steel beams by fastening the double locking nut configuration, casting of precast concrete plugs, and casting of precast slabs), while the final assembly between the precast slab and the steel beam is carried out on site. Each precast concrete panel is positioned on the top of the steel beam so that each pair of bolts is approximately aligned with the centre of the slab pocket. Quick hardening grout is then poured into the slab pocket up to a certain depth, and

then, the plugs are placed into the slab pocket so that each plug surrounds a bolt and all gaps are filled with grout. The plugs are then secured in place by tightening nut 3 in Fig. 3.3. Hardening of the grout completes the construction process of the LNSC.

A similar, yet simpler procedure can be adopted for the FBSC, which does not use a locking conical nut and does not need an enlargement gap in the plug. FBSC needs only one nut tightening operation (Nut 2 in Fig. 3.6) as compared to two nut tightening operations in the case of the LNSC (Nut 1 and Nut 3 in Fig. 3.3). It should be noted that the initial positioning of bolts before grouting is done by using 'locking' retaining washers (Fig. 3.7) which are not providing a firm locking of bolts (as compared to a locking nut in LNSC). Therefore, it is advised to keep an upper nut on bolts until the grouting stage to avoid the possibility of the bolts dropping during transportation or erecting processes. Additionally, tightening the upper nut should be carefully considered by using appropriate methods like DTI washers, calibrated wrench, etc. FBSC is based on friction resistance between the lower face of the concrete plug and the upper face of the upper flange of the steel beam. Friction resistance is achieved with bolt axial pretension. Therefore, loss of pretension with time is expected to be a technical issue. Although this PhD research does not deal with time dependent effects, the following suggestions are offered: (1) tightening the bolts to a larger extent than the design requirement to account for the loss in tension with time (Nah *et al.* 2010) (for example designing the pretension as 60% of proof load while tightening the bolts to 100% of proof load, assuming a loss of 40%); (2) as a large percent of bolt force loss occurs during the first 24 hours after tightening (Heistermann 2011), then re-tightening may reduce this effect (BSI 1994); (3) using higher strength concrete of high aggregate/paste ratio in plugs to ensure less creep (Johnson 1967, Oehlers and Bradford 1995); (4) precast concrete eliminates/reduces the effect of shrinkage in concrete; (5) using higher strength steel (Grade 8.8, 9.8, 10.9, or 12.9) for bolts to maintain the preload; (6) using special 'spring' washers that can restore the loss in bolt force (like the commercial Bellville washers); (7) using special 'locking' nuts or washers that prevent nut loosening over time (like the commercial NordLock-washers); (8) using special tightening bolts like Tension Control Bolts (TCB) with electrical wrenches that reduces the nut self-loosening and shank torsional relaxation.

3.5 Procedure for Bridge Disassembly

The LNSC allows rapid disassembly and replacement of any deteriorating structural component of a precast steel-concrete composite bridge.

In case of deterioration in a precast concrete panel, the lower nuts (nut 1 in Fig. 3.3) are removed and the precast panel along with its shear connectors can be rapidly uplifted together. If there is no access underneath the bridge, the upper nuts at the top of the plugs (nut 3 in Fig. 3.3) are removed and the precast panel can be rapidly uplifted along with its plugs by leaving the bolts in place. To achieve that easily, it is important to have bolts where their threaded lengths are not in contact with the grout.

In case of deterioration in few shear connectors, the plugs along with their surrounding grout can be rapidly extracted (pulled out) and replaced. First the lower nuts (nut 1 in Fig. 3.3) are unfastened and then the plugs and their surrounding grout are removed by applying uplift forces while using the slab as support, as can be seen from photos (a) to (d) in Fig. 3.9. Optionally, a thin layer of a release agent like a wax-based material (e.g. Pieri® Cire LM-33 from Grace Construction Products) can be applied on the surfaces of the slab pocket before casting the grout to allow easier removal of the plugs and their surrounding grout.

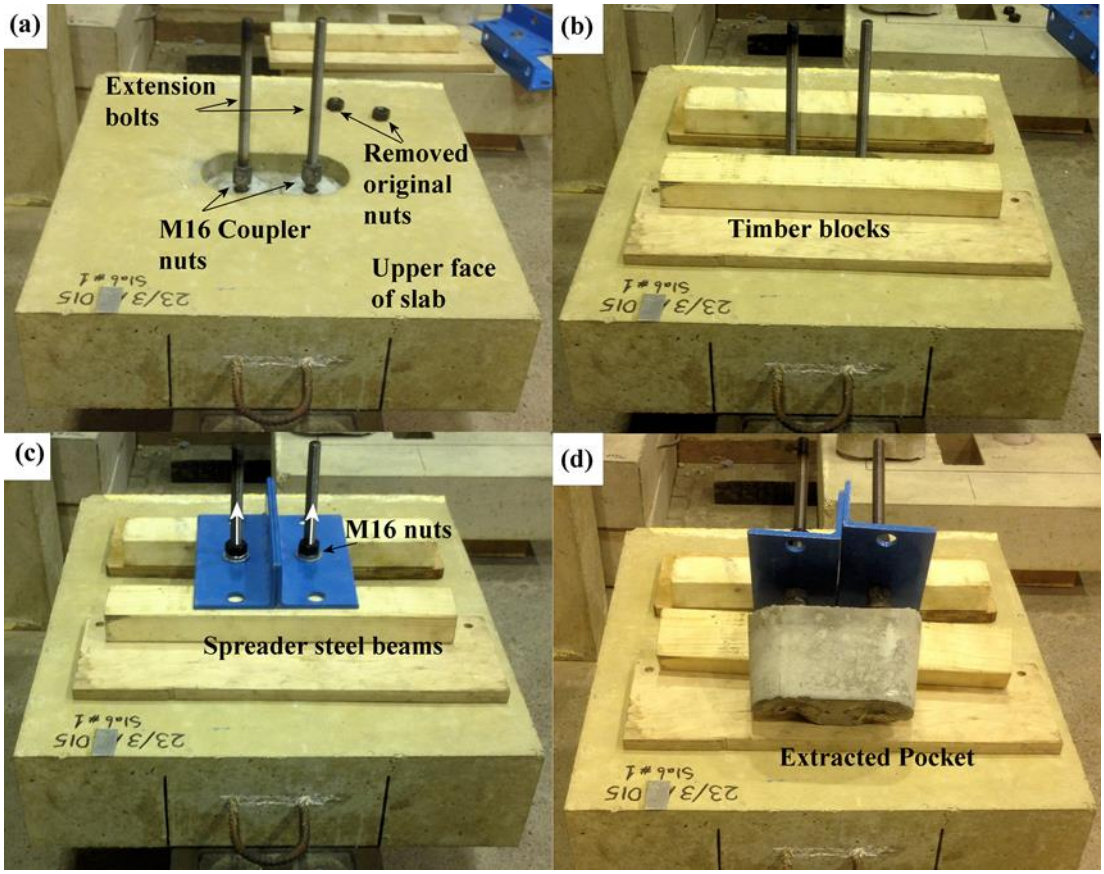

Fig. 3.9. Disassembly procedure

In case of deterioration in the steel beam, the accelerated bridge disassembly capability allows the beams to be replaced, while the precast concrete panels and shear connectors can be reused. It is emphasized that robust dry joints among the precast concrete panels,

such as those proposed by Hallmark (2012) (see Section 2.6), would further enhance bridge disassembly.

Same scenario of the LNSC can be used for the FBSC, with exception that pulling the plugs upward is not possible due to absence of middle locking conical nut. However, and for the same previous reason, pulling the bolts up, after loosening the lower nuts, is feasible. Consecutively, using some mechanical procedures (e.g. inserting screw anchor 'rawlplug' into plug hole), the plugs can be gripped and lifted up also.

3.6 Summary

Two novel demountable shear connectors, the locking nut shear connector (LNSC) and the friction based shear connector (FBSC) for precast steel-concrete composite bridges have been presented. The LNSC and FBSC use high-strength steel bolts, which are fastened to the top flange of the steel beam using a locking nut (in LNSC) or grouted countersunk seat hole (in FBSC) configurations that prevent slip of bolts inside their holes. The LNSC hides the bolt threads inside the locking nut, while the FBSC hides the bolt threads below the countersunk seat. In this way, both the LNSC and the FBSC prevent local failure within the threaded part of the bolts, and they are expected to achieve high shear resistance and ductility. The bolts are surrounded by conical precast high-strength concrete plugs, which have dimensions so that they can easily fit within the precast slab pockets. Grout is used to fill all the gaps between the bolts, the precast plugs, and the precast slab pockets, while tightening of a nut at the top of the shear connector secures the plugs in place before grout hardening. Detailed procedures of bridge assembly and disassembly were suggested.

Chapter 4: Experimental Program

4.1 Introduction

The experimental program consists of 23 pushout tests and one precast steel-concrete composite beam test. 12 pushout tests were conducted on the LNSC and 11 pushout tests were conducted on the FBSC. Each group of tests begin with six preliminary pushout tests, followed by pushout tests for evaluation of characteristic shear resistance (i.e. identical repeated tests) and investigation of the effect of different parameters (e.g. parametric tests). In the following sections (Sections 4.2 and 4.3), the final test setups, instrumentation, specimens and materials properties for the pushout tests are described in detail. It should be emphasized that these are exclusive for the final design, while the preliminary tests may have different specifications (Sections 4.4 and 4.5). The steel-concrete composite precast beam test setup, specimen specification, material properties, and instrumentation are listed in Section 4.6.

4.2 Pushout test setup and instrumentation

Push-out tests on the final design of LNSC (Section 3.2) and FBSC (Section 3.3) were conducted using the test setup shown in Fig. 4.1. The specimen consists of a pair of slabs connected to a steel beam by using the LNSC or FBSC (specimen details and materials properties will be given in Section 4.3 and Tables 4.1-4.3).

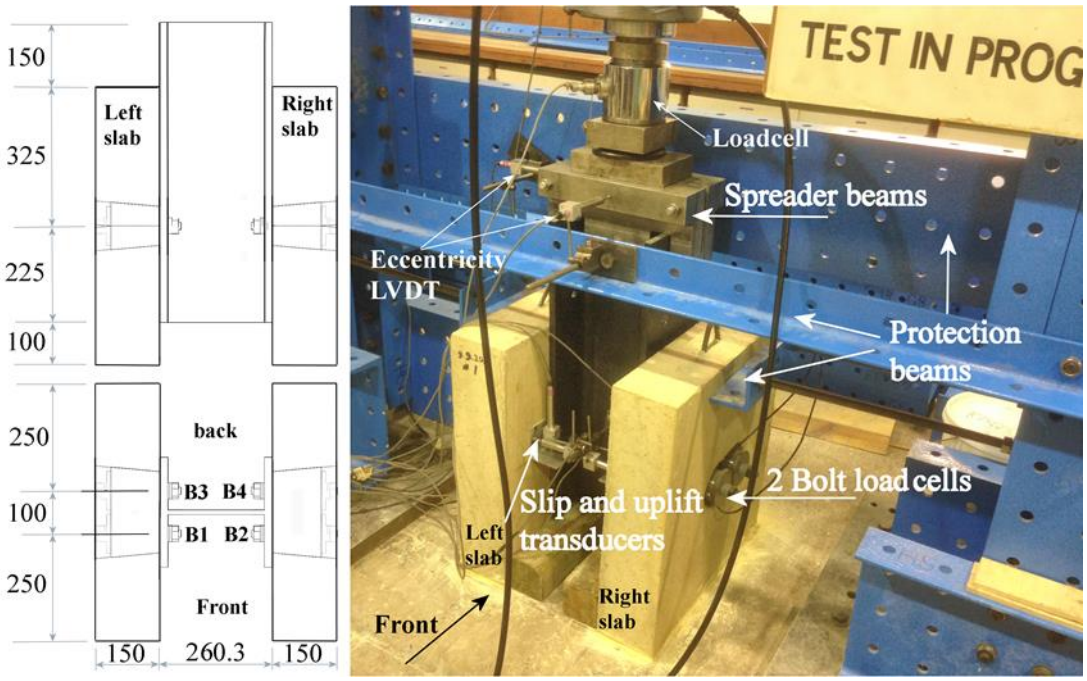

Fig. 4.1. Typical setup for push-out tests and instrumentations

Both the specimen (dimensions, reinforcement, and specifications) and the test setup follow exactly the recommendations in Annex B of Eurocode 4 (BSI 2004a) with the exception that no grease was applied at the steel-concrete interface in order to incorporate the required frictional resistance. Four linear variable displacement transducers (LVDTs) were used to measure slip between the concrete slabs and the steel beam, close to the positions of the four bolts (B1 to B4). Another pair of eccentricity LVDTs were used to measure lateral displacements at the upper tip of the specimen so that any eccentricity in the loading could be detected in advance. Moreover, four LVDTs were used to measure separation (i.e. uplift displacements) of the concrete slabs from the steel beam close to the positions of the four bolts (B1 to B4). Fig. 4.2 shows that an additional LVDT was used to monitor the jack displacement during testing. The difference in readings of the jack LVDT and the average of the four slip LVDTs represents the displacement energy stored in the testing rig during loading. A hydraulic jack with capacity of 200/100 tons was used to apply a vertical force on the specimen. A load cell (see Figs. 4.1 and 4.2) with a capacity of 100 tons was used to measure the applied load directly under the jack.

The load is transferred through a ball joint that ensures that the line of action of the load passes exactly through the centroid of the steel section without any eccentricity. This point load is uniformly distributed to the two flanges of the steel beam with the aid of two spreader beams (see Fig. 4.2), which are connected by four bolts parallel to the steel section flanges. The aforementioned test rig was originally designed at the University of Warwick, civil lab, and was successfully used by many researchers (e.g. Oehlers 1980, Mottram and Johnson 1990, Yuan 1996). The internal loads in the bolts of the LNSC were measured with the aid of washer load cells of 200 kN capacity type F313CFR0K0 from NOVATECH. Each load cell is positioned between two plate washers and then secured by a nut above each concrete plug. The push-out tests were carried out under load control of 40-

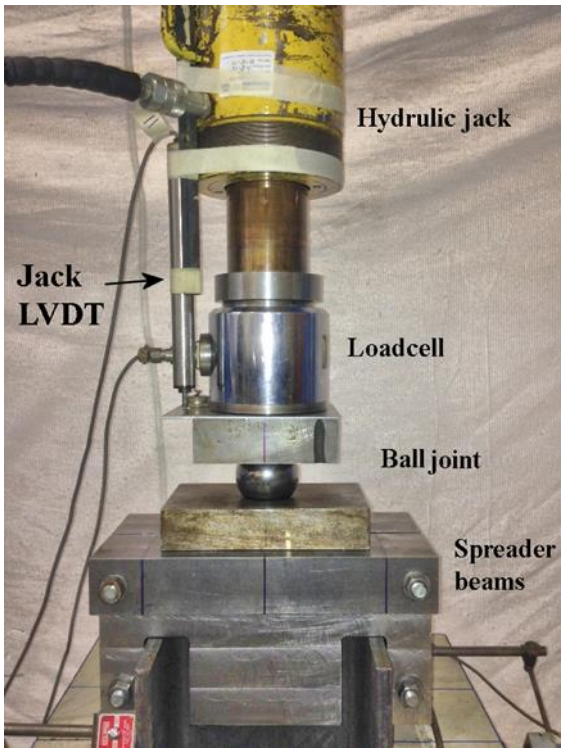

Fig. 4.2. Load transfer through ball joint in pushout tests

60 kN/min during the initial linear shear load-slip displacement behavior phase, and then under displacement control of 0.1-0.2 mm/min during the subsequent nonlinear shear load-slip displacement behavior phase. The loading (or displacement) rate was continuous and constant such that failure does not occur in less than 15 minutes, as recommended by the Eurocode 4 (BSI 2004a). This have been done to overcome the time-dependent problems associated with concrete creep and bolt relaxation (more details can be found in Section 3.3.1). The durations of pushout tests were 34, 66, 102, 49, 65, and 47 minutes for the LNSC pushout tests 7-12 (see Table 4.2), respectively, and 206, 180, 97, 61, 83 minutes for the FBSC pushout tests 6-11 (see Table 4.3), respectively. Pushout Test FBSC 6 was longer than expected due to its substantial slip and shear resistance capacities (i.e. ductile failure behaviour as will be seen later in Section 6.2.1.5), while FBSC pushout Test 7 was also delayed because of a fire alarm that caused a temporary 'drop' in load (as will be seen later in Fig. 6.43) due to the aforementioned concrete creep and bolt relaxation.

4.3 Pushout specimens and Materials Properties

The steel beam has a length equal to 80 cm, a UC254x254x89 section, and an S355 steel grade. Four holes with countersunk seat upper parts (exact dimensions for the case of M16 bolts are shown in Fig. 3.4(c)) were drilled on the beam flanges. The LNSC specimen uses four bolts Grade 8.8 per BS EN 14399-3 (BSI 2005c). Each bolt has smooth shank with threaded ends (i.e. 20 mm at one end and 50 mm at the other). Four compatible conical nuts grade 10.9 per BS EN 14399-3 (BSI 2005c) (exact dimensions for the case of M16 bolts are shown in Figs. 3.4(a) and 3.4(b)) were fabricated. In the FBSC, the bolt's threads only extend 20 mm at each end, and the conical nuts were replaced by retaining washers per BS EN 3386 (BSI 2012) (exact dimensions for the case of M16 bolts are shown in Fig. 3.7). The objective of using retaining washers is to hold the bolts in position during the construction process until grouting of the slab's pocket (more details of the retaining washers can be found in Section 3.3). The bolts along with their conical nuts/retaining washers were inserted into the countersunk seat holes of the steel beam. Then, in the LNSC, the lower nuts grade 10.9 per BS EN 14399-3 (BSI 2005c) (nut 1 in Fig. 3.3) were tightened to the proof load to securely lock the bolts within the bolt holes. The DTI washer per BS EN 14399-9 (BSI 2009a) was used to confirm the proof load limit for each bolt. Fig. 4.3 shows the bolts and the conical nuts securely locked within the chamfered countersunk seat holes of the flange of the steel beam. In FBSC, the lower nuts (nut 1 in Fig. 3.6) were tightened by hand in order to temporarily hold the bolts in position. Fig. 4.4 shows the inside of a slab's pocket where the bolts and the retaining washers are locked within the countersunk seat holes of the flange of the steel

beam. It can be seen from Figs. 4.3 and 4.4, that no enhancement of any kind was made to the roughness of the steel beam surface during all pushout tests, to simulate the actual site situation environment.

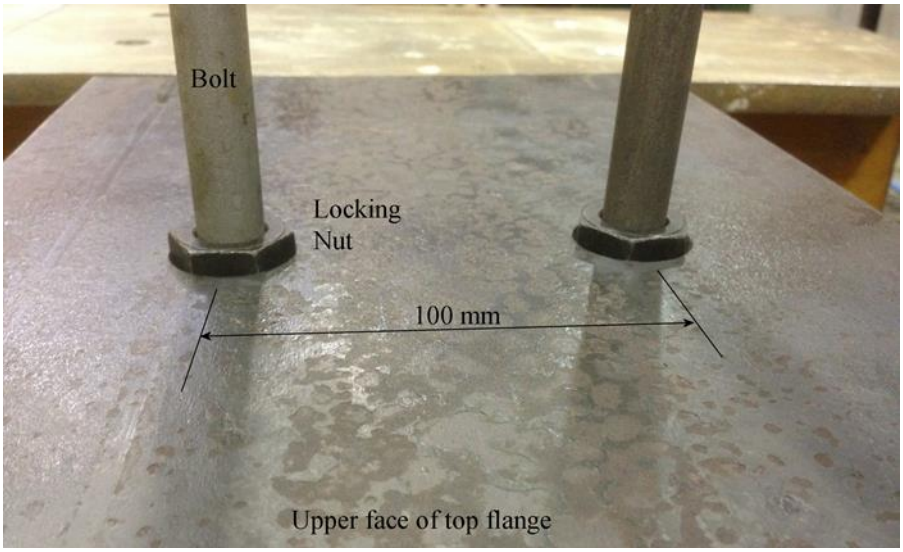

Fig. 4.3. Bolts and conical nuts securely locked within the chamfered holes of the beam flange in LNSC pushout tests

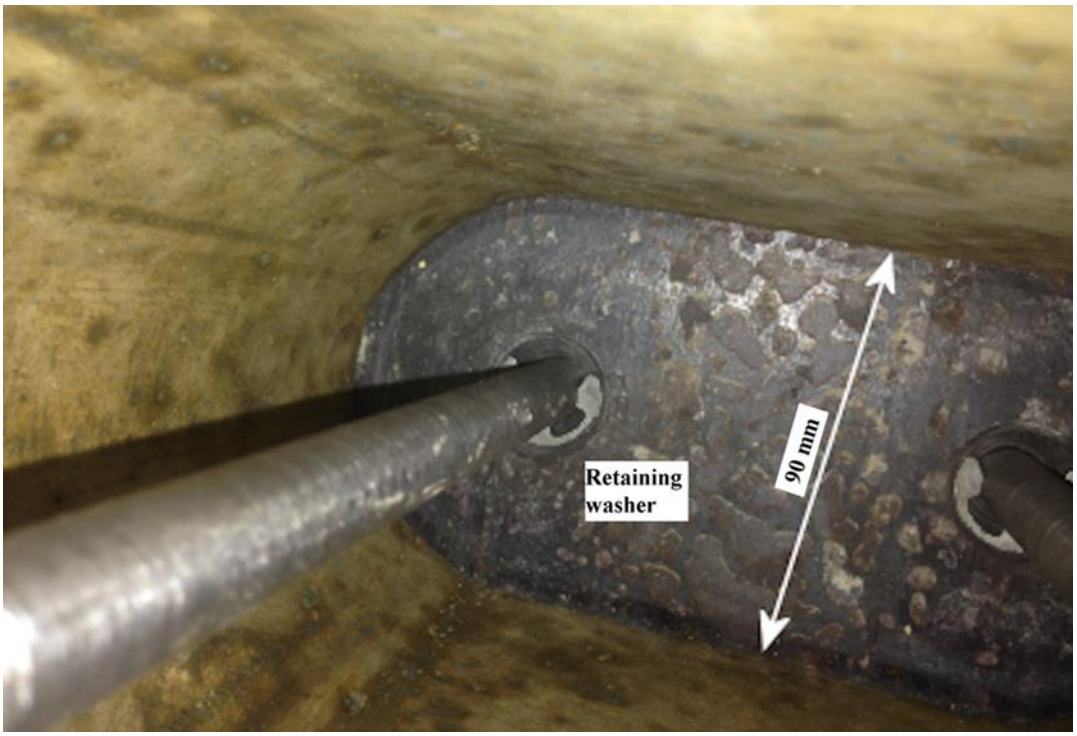

Fig. 4.4. Inside view of a slab pocket showing bolts and retaining washers in FBSC pushout tests

The precast concrete slab has a 650x600x150 mm geometry and a central countersunk conical through pocket with exact dimensions shown in Fig. 3.5(a). Slabs were casted in

horizontal position and then positioned over each flange of the steel beam as shown in Fig. 4.5(a). The slab steel reinforcement was designed per Eurocode 4 (BSI 2004a). The reinforcement details of the slab are similar to those in FBSC Test 4, as shown in Fig. 4.5(b).

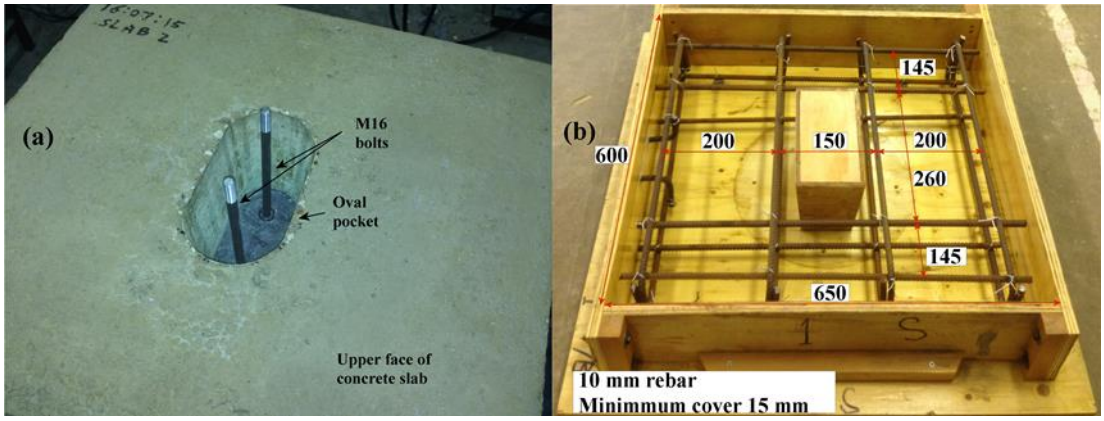

Fig. 4.5. Slab overview (a) positioned over the steel beam (b) reinforcement details

Dental paste was used to bedded the base of slabs into the floor to prevent horizontal sliding. As mentioned by Oehlers and Bradford (1995), the mechanism of standard pushout test incorporates a horizontal force at the concrete slab-steel beam connection. Supporters steel beams (Fig. 4.1) were added just 5mm away from the top of the side of each concrete slab to hold them after failure. Additional safety beams were used to hold the steel beam in case of possible tilting about the vertical, in the direction parallel to the flanges direction, due to fracture of two bolts on the same side.

The expected failure of a pushout test is by fracture of all bolts at the same time, which release a huge amount of stored strain energy into the testing rig. Packed wood blocks were positioned just 30 mm below the bottom of the steel beam (assuming the slip is always less than 30 mm) to safely absorb this energy. It is very essential to have symmetry in the test setup, i.e. the point load (lifting jack 'cylinder') to be symmetrically resisted by four reactions (shear resistances of bolts). In this case, the pushout test failure is more likely to be by fracture of the four bolts simultaneously, which means that the failure load is the mean of the four bolts. On the other hand, if eccentric loading takes place, unsymmetrical distribution of bolts positions and/or tilting of the steel beam exists. The latter will result in failure of one bolt only (the weakest one) and the corresponding failure load will represent the value of the weakest bolt. For this reason, Eurocode 4 (BSI 2004a) recommend using eight shear connectors and not four, by arranging them into two levels, i.e. four connectors in one level. By doing this, rotational stiffness is provided that prevents any tilting of the steel beam.

However, using 8 bolts would require designing and fabricating of a 200t capacity rig, which was beyond the limitation of the Civil Lab. Nevertheless, because only four shear connectors were used in all 23 pushout tests, two eccentricity LVDTs were positioned at the upper tip of the steel beam to catch any horizontal movements in two perpendicular axes during the pushout test, as shown in Fig. 4.1. Each pushout test was initially started with a load of less than 10 kN/bolt (which is below the frictional resistance of the connection), then unloaded and readjustment of positions is made and the cycle started again until the eccentricities eliminated to an acceptable amount (< 0.05 mm).

The slab pocket was treated with two layers of a release agent (Pieri® Cire LM-33 from Grace Construction Products). Grout (exact mix design will be given in Section 4.4.5 and Table 4.1) was poured into the slab pockets, and then, a precast plug (with exact dimensions shown in Fig. 3.5(b) for LNSC, and in Fig. 3.8 for FBSC) was placed around each bolt and gradually inserted into the slab pocket to ensure that all gaps are filled with grout without leaving any voids. Typical mix proportions used to cast concrete slabs, plugs and grout for final design tests are listed in Table 4.1. It should be emphasized that Table 4.1 is exclusive for final design tests and not for preliminary tests.

Table 4.1. Typical mix proportions for slabs, plugs, and grout

	Slabs (kg/m^3)	Plugs (kg/m^3)	Grout (kg/m^3)
Cement	313	500	910
Cement type	CEM II A-L 32.5 R	CEM I 52.5N	Hanson Quickcem
Water	189	182	455
Sand	825	713	910 'fine sand'
Gravel	1093 (size 10 mm)	1011 (size 10 mm)	-
Superplasticizer	0.8% of cement weight	1.2% of cement weight	-

Tables 4.2 and 4.3 list the specifications for the 23 LNSC and FBSC push-out tests, respectively. Each table starts with six preliminary tests and followed by final design tests. The preliminary tests represent six different designs with different structural details aiming to improve the structural behaviour of the shear connector in terms of shear resistance, slip capacity, and demountability.

Tests 7-12 in Table 4.2 represent two parametric studies based on the LNSC final design. In particular, Tests 7, 8, and 12 study the effect of the bolt diameter (12-16 mm), while Tests 10, 11, and 12 study the effect of the plug concrete compressive strength (50-96 MPa). Test 9 failed due to accidental loss of bolt pretension, and its measurements are not presented.

Table 4.2. Specifications of LNSC push-out tests

Test No.	Bolt Dia. (mm)	Bolt preloads (kN)		Slabs (mean)		Plugs (mean)		Grout (mean)
		Nuts 1–2*	Nuts 2-3*	Comp. str. (MPa)	Tensile str. (MPa)	Comp. str. (MPa)	Tensile str. (MPa)	Comp. str. (MPa)
1	16	88-106	88-106	31	2.5	65	4.2	122
2	16		0.0					
3	16	88-106	88-106	31	2.5	65	4.2	-
4	16	88-106	10	31	2.5	83	5.2	43
5	16	88-106	88-106	37	-	71	4.3	58
6	16	64	55-70	41	4.0	86	5.1	44
7	12	47-56	24**	50	4.0	91	4.8	28
8	14	68-81	23**	50	4.0	95	4.6	32
9	16	failed	23**	42	3.6	80	4.8	39
10	16	88-106	24**	43	3.1	50	3.7	27
11	16	88-106	26**	43	3.2	96	4.8	28
12	16	88-106	26**	42	3.5	91	4.9	28

*** See Fig. 3.3 for locations of nuts 1, 2 and 3**
**** Washer load cell actual readings, otherwise, DTI washer predictions**

Table 4.3. Specifications of FBSC push-out tests

Test No.	Bolt Dia. (mm)	Bolt preload (kN)	Slabs (mean)		Plugs (mean)		Grout (mean)
		Nuts 1–2*	Comp. str. (MPa)	Tensile str. (MPa)	Comp. str. (MPa)	Tensile str. (MPa)	Comp. str. (MPa)
1	16	88-106	31	2.5	65	4.2	83
2	16						
3	16	88-106	31	2.5	65	4.2	38
4	16	88-106	37	3.7	82	4.1	37
5	16	88-106	37	3.7	74	3.7	48
6	16	63**	50	4.0	90	4.8	41
7	14	68-81	40	3.7	72	4.0	40
8	12	47-56	40	3.7	80	4.3	51
9	14	77**	39	3.7	82	4.9	45
10	14	55**	40	3.7	85	4.7	40
11	16	59**	50	4.0	100.1	5.0	42

*** See Fig. 3.6 for locations of nuts 1 and 2**
**** Washer load cell actual readings, otherwise, DTI washer predictions**

Similarly, Tests 7-11 in Table 4.3 represent two parametric studies based on the FBSC final design. In particular, tests 6, 8, and 10 study the effect of bolt diameter (12-16 mm), while Tests 7, 9, and 10 study the effect of bolt pretension (55-77 kN). Test 11 used to evaluate the

characteristic shear resistance of the FBSC. In all parametric tests, only one variable was changed while all other variables were kept as similar as possible. The mean concrete compressive and tensile strengths in these tables were obtained on the day of each push-out test according to BS EN 12390-3 (BSI 2009c), and BS EN 12390-6 (BSI 2009d) respectively. The compressive strengths of the slabs and plugs were evaluated by using standard cubes of 100 mm sides; the compressive strength of the grout by using 75 mm cubes; and the tensile strengths of the slabs and plugs by using standard cylinders of 100 mm diameter and 200 mm height. These materials properties were evaluated using specific number of specimens. The preliminary tests will report the numbers with each test, in Sections 4.4 and 4.5. The rest of the tests used six cubes for concrete (or grout) compressive strength, and three cylinders for concrete tensile strength. It should be stated that according to Clause 3.1.1 of Eurocode 4, the strength of concrete used in the design of composite structures is between C20/25 and C60/75 (BSI 2004a).

As seen in Fig. 4.6 the washer load cell was placed between two hardened plate washers on the top surface of each plug to measure the tension load inside the bolts. Tightening the nut above each plug (nut 3 in Fig. 3.3) completed the fabrication of the LNSC specimen. All bolts had approximately the same preload to ensure a symmetrical behavior on loading.

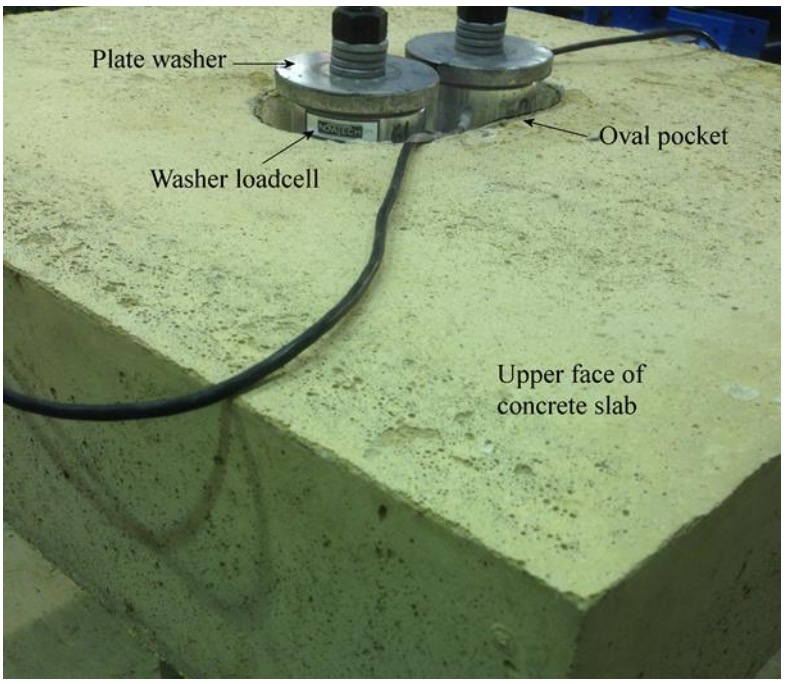

Fig. 4.6. Nut and washer load cell on the top of the concrete plugs

The bolt preloads were measured using washer load cells in Tests 7-12 of Table 4.2 and in Tests 6, 9, 10 and 11 of Table 4.3. The rest of the tests used DTI washers to estimate the

preload. The maximum size of the gravel was 10 mm. The sieve analysis (BSI 1976) for the 'fine' sand used for the grout is provided in Table 4.4. It is important to use such fine sand and not an ordinary sand to avoid possible segregation of sand particles between the lower face of the plug and the upper face of the steel flange of the steel beam.

Table 4.4. Sieve analysis of 'fine sand' used in grouts

Sieve size (mm)	Cumulative (% by weight)	Passing (% by weight)	BSI (1976), Table 1, Type B, Passing (% by weight)
0.6	0	100	55 - 100
0.3	34	66	5 - 75
0.15	58	8	0 - 20
0.063	8	0	< 5

Nine steel coupon specimens, randomly chosen and machined from bolts, were subjected to tensile tests per BS EN ISO 6892-1 (BSI 2009b). Specimen strains were measured using an axial extensometer. A typical stress-strain relationship from one coupon test is shown in Fig. 4.7, while average values of the properties of the steel bolts are listed in Table 4.5. It should be noted that yield strength, tensile strength, and bolt tensile resistance listed in Table 4.5 are calculated based on nominal diameter area and not on tensile stress area. The reasons behinds this are, first, the novel shear connectors can be classified as long thin bolts because they have a grip length-to-diameter ratio of > 9:1 (Bickford 1995); therefore, uniform stress distribution in the body of the bolts is more likely to exists. Second, when slip occurs, the shank of the bolt is anchored inside the surrounding concrete; therefore, any tensile failure should occur in the shank of the bolt and not in the threaded parts.

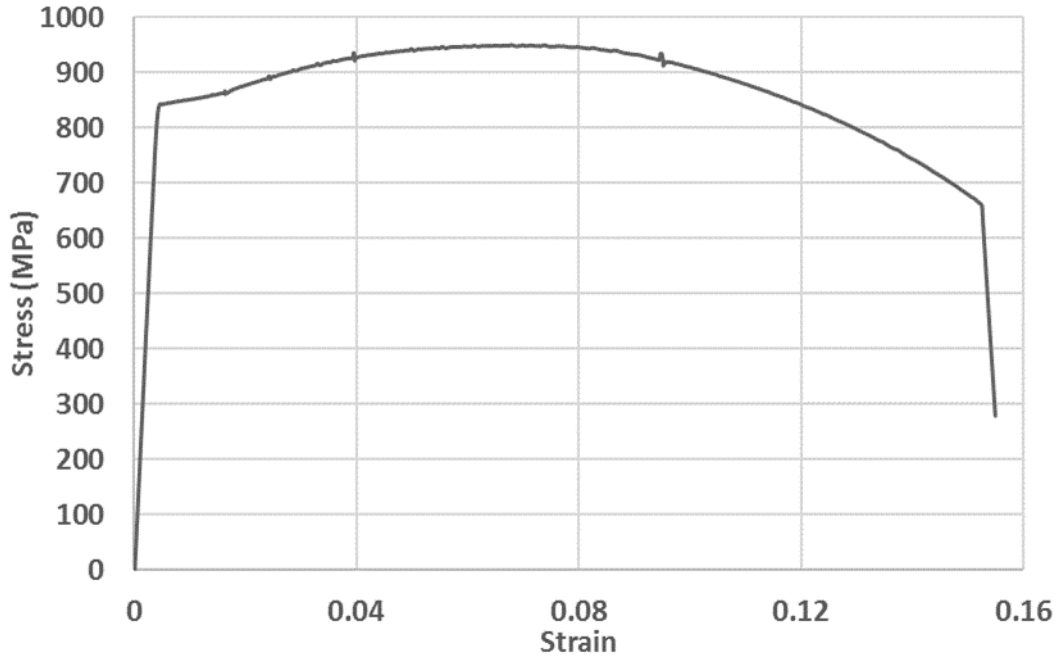

Fig. 4.7. Typical stress-strain behaviour of bolts from tensile coupon tests

Table 4.5. Mechanical properties of bolts Grade 8.8

	Modulus of elasticity (GPa)	Yield stress (MPa)	Tensile strength (MPa)	Maximum elongation %	Bolt tensile resistance (kN) (calculated)
Avg. of 9 specimens	209	787	889	8	
Min.	201	719	832	5	
Max.	215	847	950	15	
Standard deviation	5	50	41	5	
D12 mm					100.5
D14 mm					136.9
D16 mm					178.7

4.4 Preliminary pushout tests for LNSC

Six preliminary pushout tests were performed to reach the final design of the LNSC (Section 3.2). In these tests, dramatic improvements were witnessed in the design of the shear connector, testing rig, testing specimen, and testing instrumentations. Tests 1 and 2 were aimed to familiarized the author with the pushout test procedure, equipment, and safety requirements, as well as to test the concept of demountable shear connectors for steel-concrete composite precast members, inspect the testing rig and specimens, check the instrumentation and LabVIEW programming. Bearing this in mind, specimens for Tests 1 and 2 were designed with dimensions, concrete strengths, grout strength, and reinforcement to be overestimated as an early concrete failure is not favourable at this stage. The following sections will outline the six preliminary pushout tests. It should be noted that material properties and concrete mix design for slab and grout in the preliminary tests are different from what have been reported in Tables 4.1, and 4.5, as will be seen in the following subsection.

4.4.1 LNSC Pushout Preliminary Tests 1 and 2

The LNSC specimen is shown in Fig. 4.8 with all internal details shown in Fig. 4.9. The test rig is shown in Figs. 4.10 and 4.11 for Tests 1 and 2, respectively. As seen in Figs. 4.8 and 4.9, each slab has one circular conical through hole (pocket), and one plug inside each hole, holding two bolts through circular longitudinal through holes. The dimensions of the slab hole and plug were designed based on approximate calculations (assuming uniform distributed load, Fig. 4.12), which ensure that the stress in the concrete slab below the slab pocket is lower than 50% of the concrete compressive strength reported in Table 4.2. It was

found that the required force to exceed 50% of the slab concrete strength is > 2000 kN, i.e. twice the capacity of the lifting jack (maximum capacity of 100t) or the capacity of the testing rig (maximum capacity of 100t).

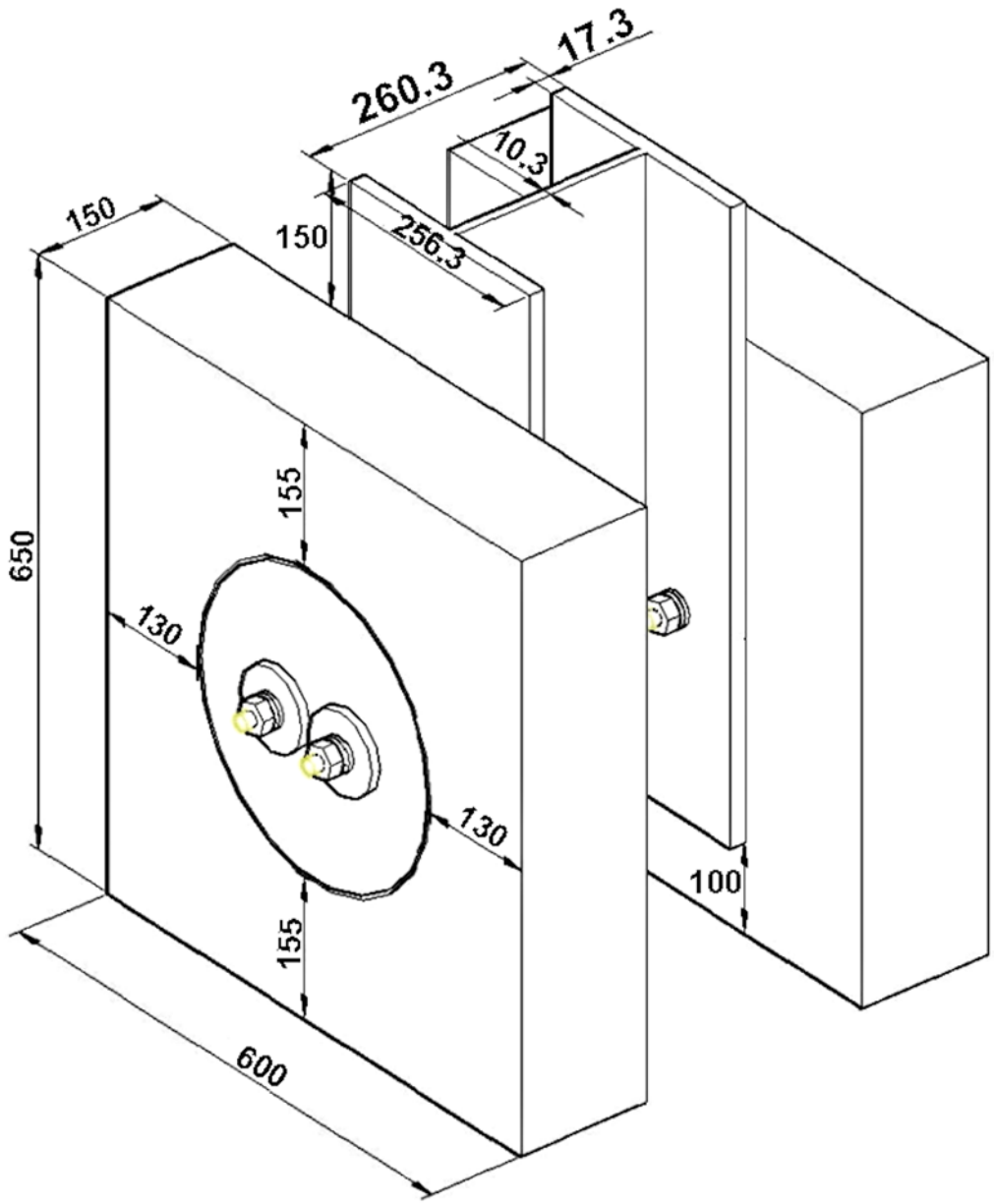

Fig. 4.8. Dimensions of LNSC pushout tests 1 and 2 specimens

Duration of Test 1 was about 3 hours while duration of Test 2 was about 2 hours including the 25 load cycles recommended by Eurocode 4 (BSI 2004a). Materials properties for Test 1 and 2 listed in Table 4.2 were evaluated as follows. Concrete compressive strength was measured using seven 100 mm cubes for slabs, three 100 mm cubes for plugs, and two 75 mm cubes for grouts, while the split tensile strength was estimated using three cylinders dia. 100 and length 200 mm for slabs and one for plugs.

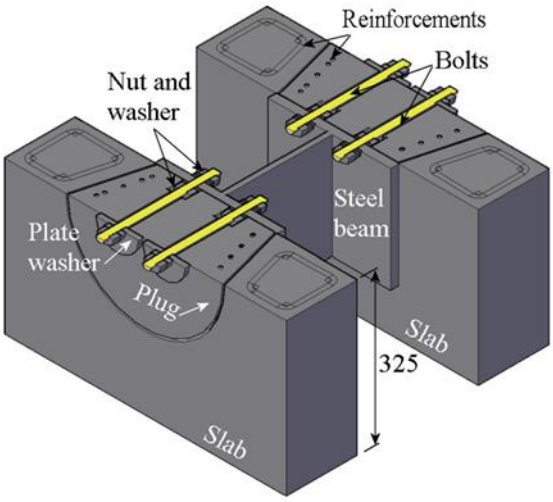

Fig. 4.9. Half pushout specimen used in LNSC pushout tests 1 and 2

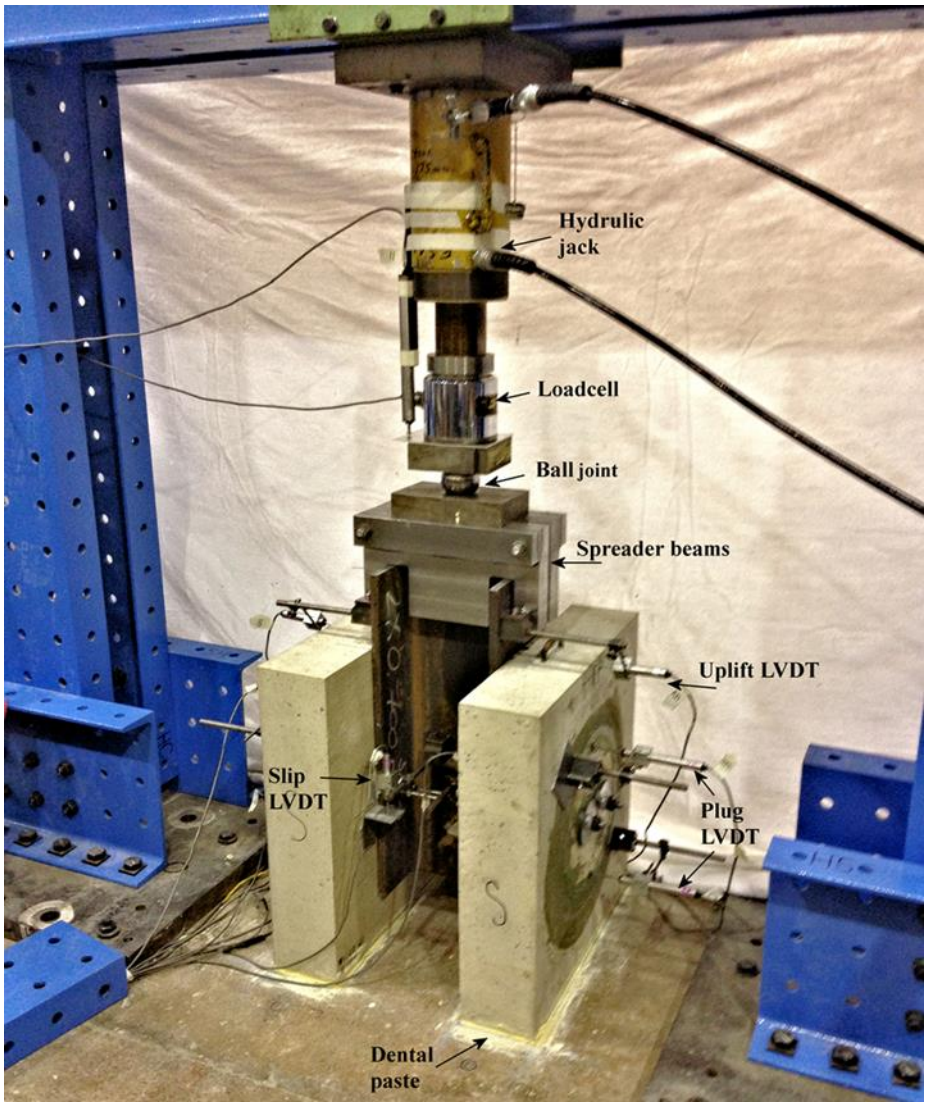

Fig. 4.10. Details of testing rig and specimen for LNSC pushout tests 1

Concrete mix design used in Tests 1 and 2 for slabs, plugs and grout are different from those of final design listed in Table 4.1. The concrete in the slab was designed to be C25/30. The

mix design quantities were: W/C = 0.65, water content = 225 kg/m^3, cement content = 243 kg/m^3, fine aggregate (sand) content = 918 kg/m^3, coarse aggregate (crushed gravel) content = 1079 kg/m^3, admixture (super-plasticizer 'TamCem 60') = 0.8% of cement weight, maximum size of coarse aggregate = 10mm, and cement type CEM II A-L 32.5 R. In the British method (BRE Building Research Establishment) for concrete mix design (Teychenné *et al.* (1997)), the total water in the concrete mix consists of the water required for the cement hydration, the water required for the workability of the fresh mix, and the water absorbed by the aggregate to bring it to a saturated surface-dry condition (SSD). In order to bring the Civil Lab's 'dry' aggregate to the SSD condition, 29 kg/m^3 of water was needed on the basis of trial mixes. The water/cement ratios referred to in this thesis are the mass ratios of free-water to cement in the mix and are based on the aggregates being in a SSD condition. The reinforcement details are shown in Fig. 4.13.

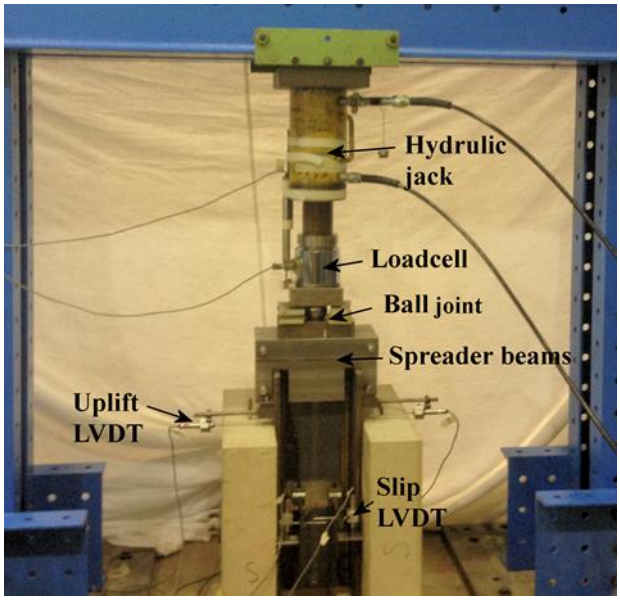

Fig. 4.11. Details of testing rig and specimen for LNSC pushout Tests 2

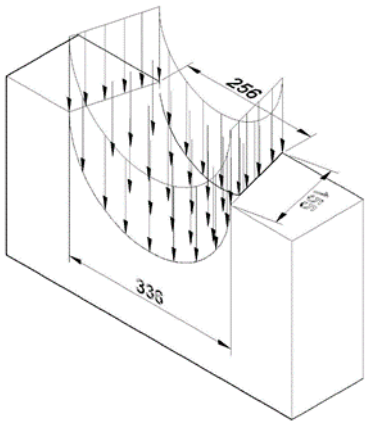

Fig. 4.12. Load distribution on slab pocket in LNSC pushout Tests 1 and 2

This reinforcement was chosen to eliminate tensile cracks in the concrete slab and to comply with the amount of reinforcement recommended by Eurocode 4 (BSI 2004a). All the reinforcements were of 10mm diameter. The concrete slabs were casted in timber moulds, covered by damped hessian and plastic sheets, and cured for minimum 7 days.

A reinforced concrete plug is shown in Fig. 4.14, and was designed to have a compressive strength of C50/60. The mix design quantities were: W/C = 0.35, water content = 158 kg/m^3, cement content = 451 kg/m^3, fine aggregate content = 733 kg/m^3, coarse aggregate content

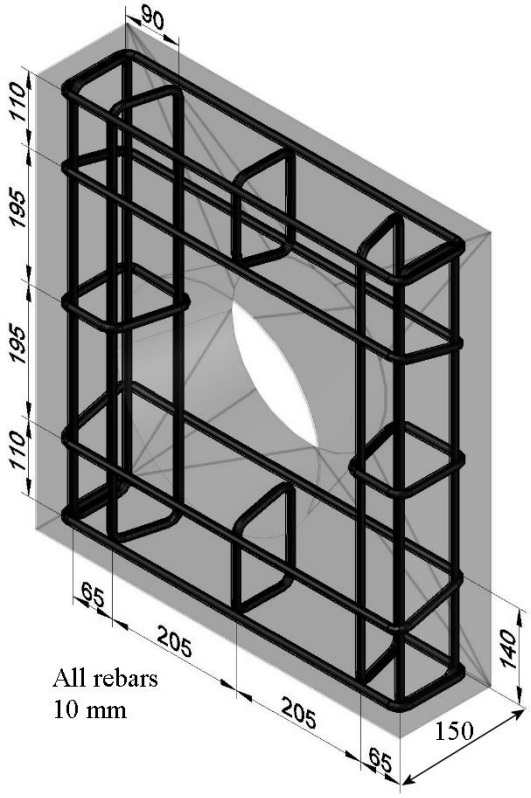

Fig. 4.13. Reinforcement details of LNSC pushout Test 1 and 2

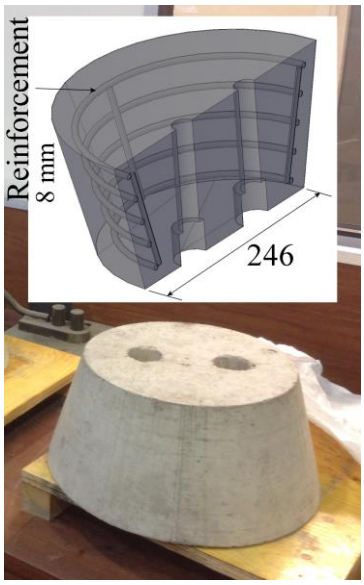

Fig. 4.14. Concrete plug with half inside view used in LNSC pushout Tests 1 and 2

= 1054 kg/m^3, and admixture super-plasticizer 'TamCem 60' = 0.8% of cement weight. The maximum size of coarse aggregate was 10mm, cement type was CEM II A-L 32.5 R, and 65% of fine aggregate passed the 600-micrometer sieve. Additional water of 25 kg/m^3 was used to bring the aggregate from dry to SSD condition.

The concrete plugs were casted in wood moulds with the exact dimensions shown in Fig. 4.15. Please notice that the thickness of the mould is optional, and the two posts are used to create the longitudinal holes for bolts' accommodation. All the reinforcements used in concrete plugs were 8 mm plain mild steel re-bars. The reinforcement was arranged as five circular rings evenly spaced along the height of the plug, and linked together by four bars distributed radially at 90 degrees, as shown in Fig. 4.14.

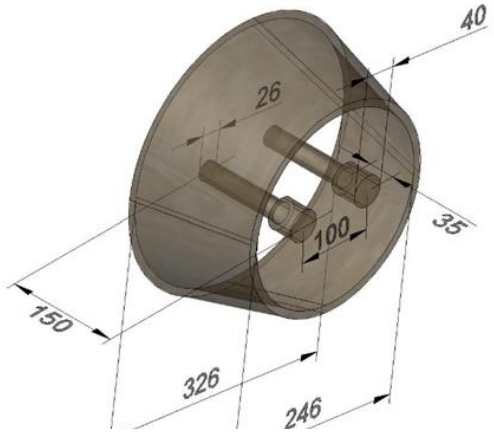

Fig. 4.15. Dimensions of concrete plug mould of LNSC pushout Tests 1 and 2

In order to connect the slab, concrete plug, and steel bolts together to resist the applied load, all the gaps (10 mm between concrete plug and slab pocket, and 10 mm between bolt and its longitudinal hole inside the concrete plug (see Fig. 4.9)) were filled with anchor grout (Lokfix S25 from FOSROC). This grout is usually used to anchor reinforcement bars in prestressed concrete to satisfy the requirement of BS EN 1504-6. The grout gains a compressive strength of 83 MPa in just 1 hour. Fig. 4.16 shows specimens from Tests 1 and 2 after grouting and preload tightening of bolts prior of pushout testing. Tightening of bolts to the proof load was ensured by DTI washers from BAPP Ltd. M16 DTI washers give the indication of the proof load when the bolt tensile load is in the range of 88 – 106 kN.

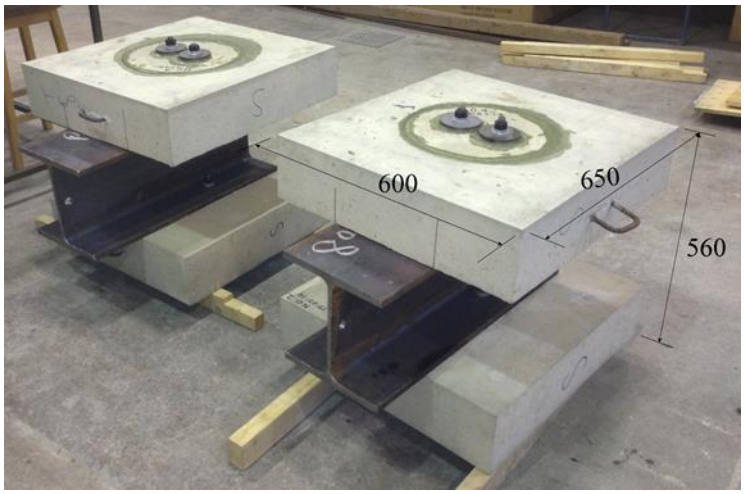

Fig. 4.16. Grouting and bolts tightening of the LNSC pushout tests 1 and 2

The bolts, nuts, and washers in Tests 1 and 2 were, according to BAPP Ltd delivery characteristic specification, and not as listed in Table 4.5. Preload bolts BS EN 14399-3 HR, M16, Length 250 mm, Grade 8.8, with proof load of 94.5 kN, ultimate load of 130 kN, and hardness Rockwell HRC 23-34. The nuts were M16, grade 10 per BS EN 14399-3, with proof load of 182 kN. The washers were M16 chamfered per BS EN 14399-5, with inside diameter 17-17.2 mm, outside diameter 29.48 - 30.0 mm, thickness 3.7 - 4.3mm, and hardness 300 - 370 HV (Vickers Hardness). DTI washer was M16 grade 10 according to BS EN 14399-9, internal diameter 16.75 - 16.85 mm, external diameter 35.00 - 36.80 mm, and thickness 3 – 6 mm.

The plate washers were fabricated for Test 1 and was reused in all other pushout tests. They were manufactured from EN24T steel according to BS EN 10204 in The University of Warwick Workshop to be: 90 mm outer diameter, 18 mm inner diameter, and 10 mm thickness. The 90 mm outer diameter was chosen to decrease the compressive stress in the concrete plug to lesser than 50% of ultimate compressive strength of concrete plug when the bolt is

preloaded to proof load. The 18 mm inner diameter was used to accommodate M16 bolts. The steel has a tensile strength of 1000-1150 MPa, yield strength of 850 MPa, and hardness condition V (through-hardening) of 293-352 Brinell. The 10 mm thickness and aforementioned hardness were necessary to increase the stiffness of the washer against bending under the proof load of the bolt. This is essential to minimise the stress concentration on the upper face of the concrete plug. The load inside each bolt is the proof load, which, for the Test 1 assembly, will be in the range of 88-106 kN according to M16 DTI washers' indications. It should be noted that plate washers and nuts were eliminated from the LNSC pushout Test 2 after a conclusion from LNSC pushout Test 1 that the anchorage grout had fixed the bolt to the concrete plug entirely without the need for plate washer and nut connection. Moreover, the four LVDT transducers that supposed to measure any uplift of the concrete plug (shown in Fig. 4.10) were removed for the same technical reason, as shown in Fig. 4.11. The concrete slabs were embedded into the strong floor using a grout, as seen in Figs. 4.10, and as recommended by Eurocode 4 (BSI 2004a), in order to prevent slabs sliding. A 'dental paste' was used for the grout as it was successfully used before by Oehlers (1980), and Yuan (1996) at the Structures Laboratory in School of Engineering, University of Warwick.

4.4.2 LNSC Pushout Preliminary Test 3

LNSC pushout Test 3 (Fig. 4.17) differs from pushout tests 1 and 2 in that the reinforced concrete plugs had an extra enlargement space for the M16 Grade 8.8 bolts to deflect (see Fig. 4.18).

Fig. 4.17. Overview of testing rig and specimen for LNSC pushout tests 3

This enlargement was made to check the Test 3 maximum slip capacity. The frictional resistance between the concrete plug and steel beam was minimized by machining the upper face of the flanges of the steel beam, and the grout between the bolts and plug holes was also eliminated. As a result, the only active element to resist the shear force is the bolt. The type of grout used to link the concrete plugs to the concrete slab was a mixture of 0.5 water/cement for simplicity and to reduce the cost. The grout was in a liquid state, and therefore, poured into the gap between the plug and the slab. However, it was prevented from flowing below the concrete plug by a commercial sealer. Detailed alignment procedures using adjustable bolts for accurately positioning the LNSC specimen at the centre of testing rig was used, as shown in Fig. 4.19.

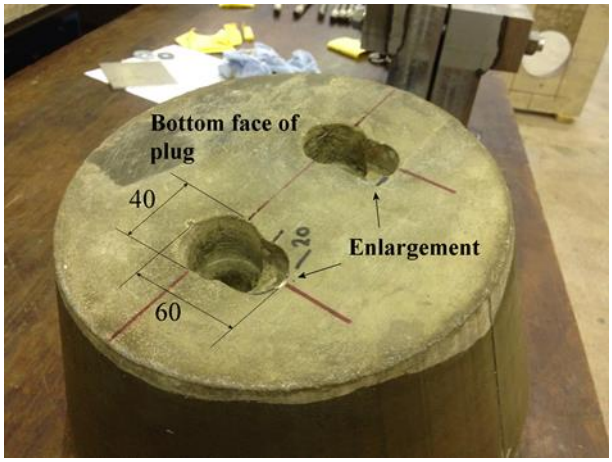

Fig. 4.18. Lower face of reinforced concrete plug showing extra enlargement for bolt hole

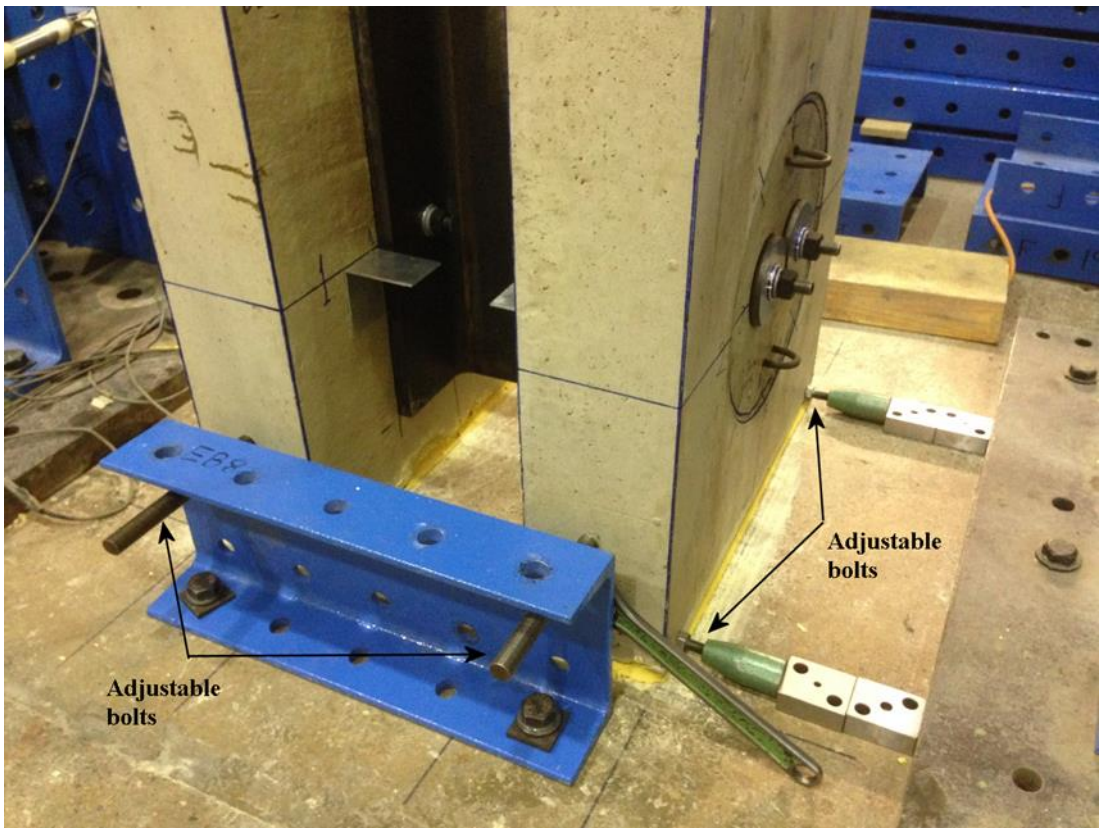

Fig. 4.19. Positioning the LNSC specimen

Fig. 4.20. Adding four transducers to measure bolt's slip inside its hole

Four new transducers were positioned in the inner side of the specimen (see Fig. 4.20) to measure the possible sudden displacement of bolt inside its hole when the frictional resistance between the double nut connection and the flange of the steel beam overcome. The transducers that were previously used (Fig. 4.10) to measure the differential displacement between the concrete plug and the concrete slab were removed after there was strong evidence, from pushout Tests 1 and 2, that complete fixity existed between the two parts. The transducers that were used to measure the slab uplift are still in position as can be seen in Fig. 4.17. Duration of the test was about 3 hours. The concrete compressive strength was evaluated using six 100 mm cubes for cones, and four 75 mm cubes for grouts, while the split tensile strength was estimated using one cylinder dia. 100 for plugs and 2 for grout.

4.4.3 LNSC Pushout Preliminary Test 4

In LNSC pushout Test 4, one important modification was corroborated. An initial locking nut mechanism was introduced to overcome the problem of sudden slip. In an ordinary doubled nut bolts (like Pavlović (2013), Kwon *et al.* (2011), and Dedic and Klaiber (1984)), it is difficult to bring all the bolts to work together at the same time and at the same level in resisting the applied shear. Each bolt has different clearance inside its hole which can be between 0 – 2 mm. Some bolts may act in bearing, friction, or both before other bolts act similarly. In the locking nut connection, both the middle nut and the chamfered countersunk seat opening of the bolt has the same inclination angle. By using locking nut connection, the aforementioned problem is eliminated. All bolts are perfectly connected to the chamfer

countersunk seat holes of the flange of the steel beam and hence initially acting in bearing. The upper opening of bolt hole was machined to have a chamfered of 120 degrees as seen in Fig. 4.21 to act as a countersunk seat for the nut. The full-length M16 nut already has the same inclination angle in one of its ends according to BS EN 14399-3 (BSI 2005c). A locking mechanism between the two could now be brought into operation in resisting the shear by tightening the double nut connection to the flange of the steel beam.

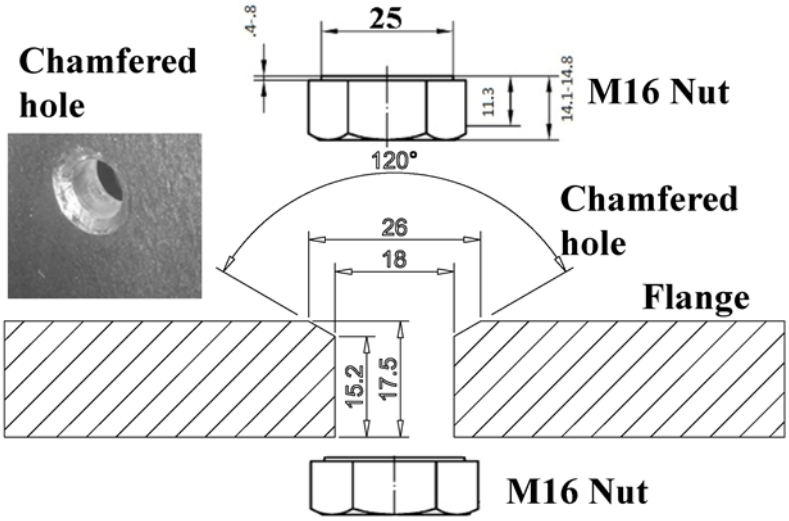

Fig. 4.21. Countersunk seat of 120 degrees chamfered bolt hole

Full proof preload exists between the lower and middle nut, while minimum preload between the middle and upper nuts (just ordinary hand wrench tightening according to Eurocode 3 (BSI 2005b)). A minimum friction resistance is therefore expected between the concrete and the steel, and the LNSC shear resistance is based on the bolt and its locking nut. The plug height was lower than the slabs thickness by 20 mm (see Fig. 4.22) to hide the upper nut and to allow for future covering by caps or grouting. This practice (using shorter plugs than the slab thickness) will be used in the rest of LNSC pushout tests.

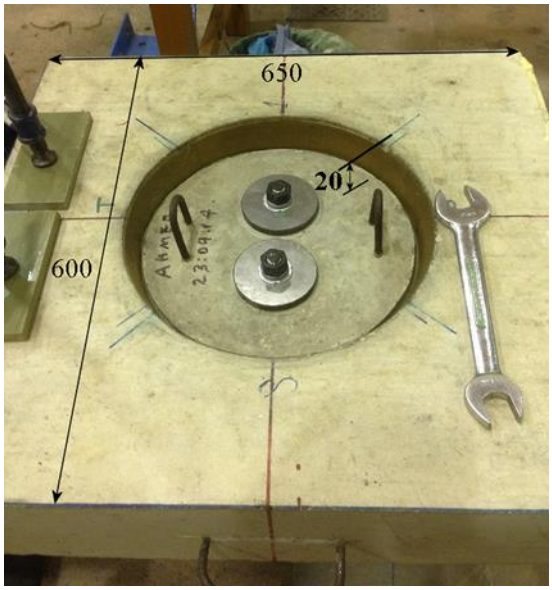

Fig. 4.22. Concrete plug lower than slab thickness

Slabs were designed with reduced amount of reinforcement as shown in Fig. 4.23, which represents a 50% reduction of the longitudinal reinforcement and 60% reduction of the transverse reinforcement compared to the corresponding amounts of reinforcement used in Eurocode 4 (BSI 2004a), while the concrete plugs were totally unreinforced as compared to Tests 1 - 3. The reason behind these is to examine new failure modes, specifically, in the concrete parts of the specimen.

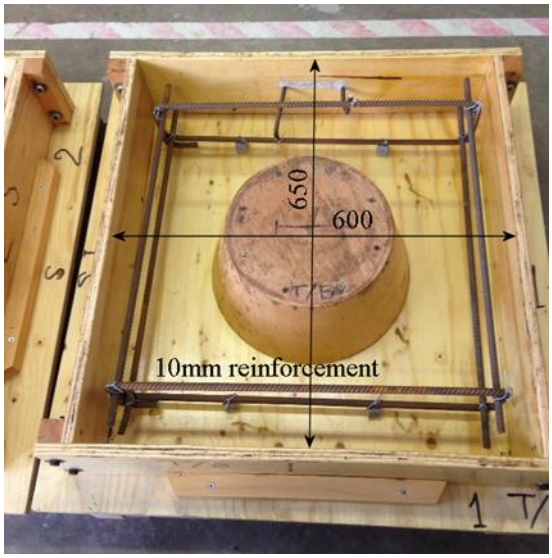

Fig. 4.23. Wood mould with reduced reinforcement ready for casting concrete

A release agent (Pieri® Cire LM-33 from Grace Construction Products) in two layers was applied to the matching faces of both the concrete plug and the concrete slab pocket (see Fig. 4.24). Such agent was chosen because only a very thin layer is required (120 m^2/kg) and can work on concrete surfaces. This release agent, therefore, will be used in the rest of the LNSC pushout tests.

Fig. 4.24. Applying the release agent to concrete plug and slab pocket

Fig. 4.25. Pouring grout into slab pocket

Once a grout of 0.5 water/cement mixture was poured into the slab hole (see Fig. 4.25), the concrete plug was slowly inserted forcing the grout to be distributed all around and filling all the gaps. Slight up-and-down movements of the plug for a few seconds will ensure no voiding are left. This was proved by examining the

grout after dismantling the specimen (after testing). A hand wrench was used to tighten the upper nut, and the fabricated connection is shown in Fig. 4.26.

Fig. 4.26. Concrete plug inserted into grouted slab pocket

Fig. 4.27 revealed that several safety beams were added to the testing rig. These beams used bolting connections that tightened by hand in order not to affect the structural performance of the testing rig. Four new LVDTs to measure the slab uplift at the level of bolts. Continuous constant loading rate was applied, as recommended by the Eurocode 4 (BSI 2004a), to overcome the possible problems associated with concrete creep or bolt relaxation. This technique will be used in all remaining pushout tests. Near the ultimate load and while the loading was almost constant, there was an unexpected increase in the load when it was discovered that the steel beam, because of the big displacement (15 mm), had reached the wood blocks. The test was immediately unloaded to zero, the blocks were removed, and the test continued again and retained to its previous position without losing any of its strength. The duration of this test was approximately 3 hours.

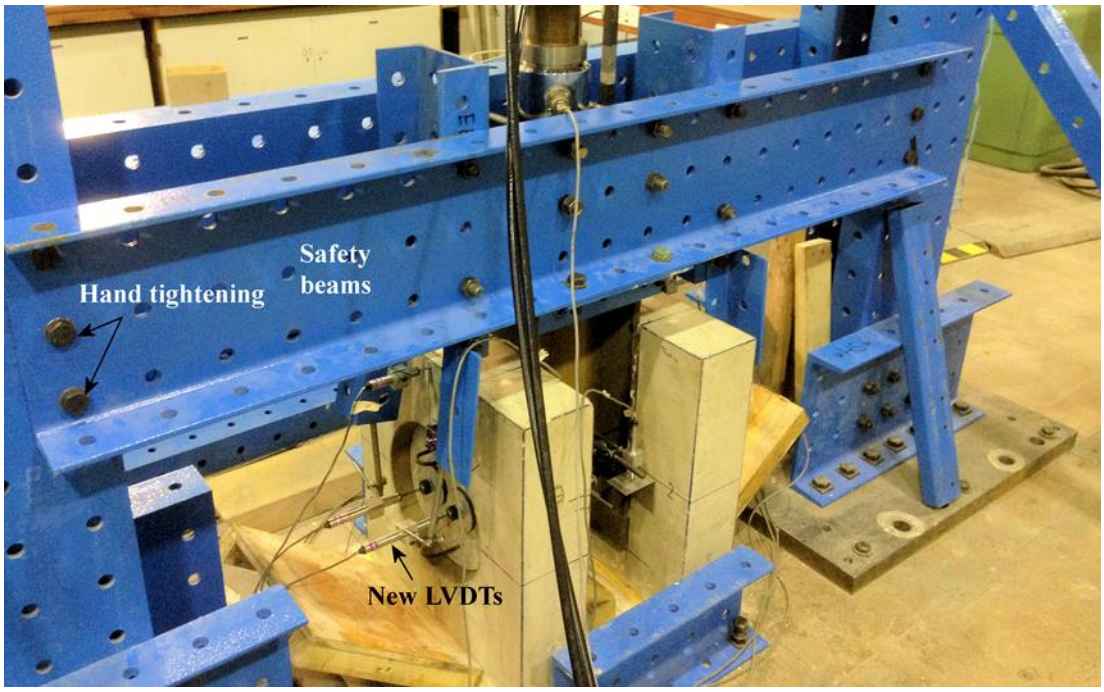

Fig. 4.27. LNSC pushout Test 4 overview

4.4.4 LNSC Pushout Preliminary Test 5

It was observed in Tests 1-4 that the handling of plugs was difficult due to their heavy weight (25 kg) and large size (diameter 326 mm). Furthermore, based on the results of Test 4 in relation to plug performance (Section 5.2.1.3), Test 5 abandoned the usage of the aforementioned plug. Fig. 4.28 shows that the slab pocket in Test 5 has a rectangular shape. Test 5 used small (diameter 90 mm) separate unreinforced precast concrete plugs for each bolt. Each pair of plugs were positioned inside a single pocket in each concrete slab. The overall dimensions of the concrete slab pocket are given in Fig. 4.29. The plug dimensions are those for the final design of the LNSC (Fig. 3.5(b)), and they will be implemented in the rest of LNSC tests.

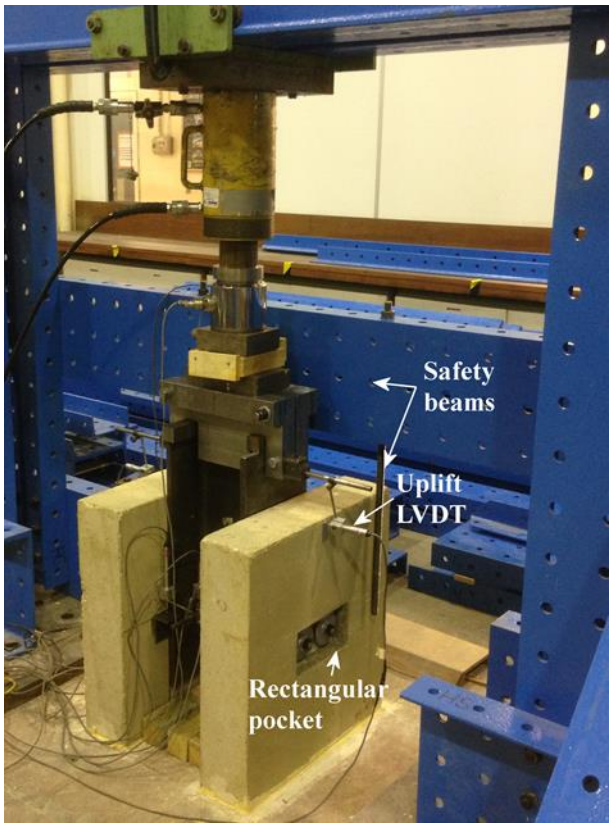

Fig. 4.28. LNSC pushout Test 5 overview

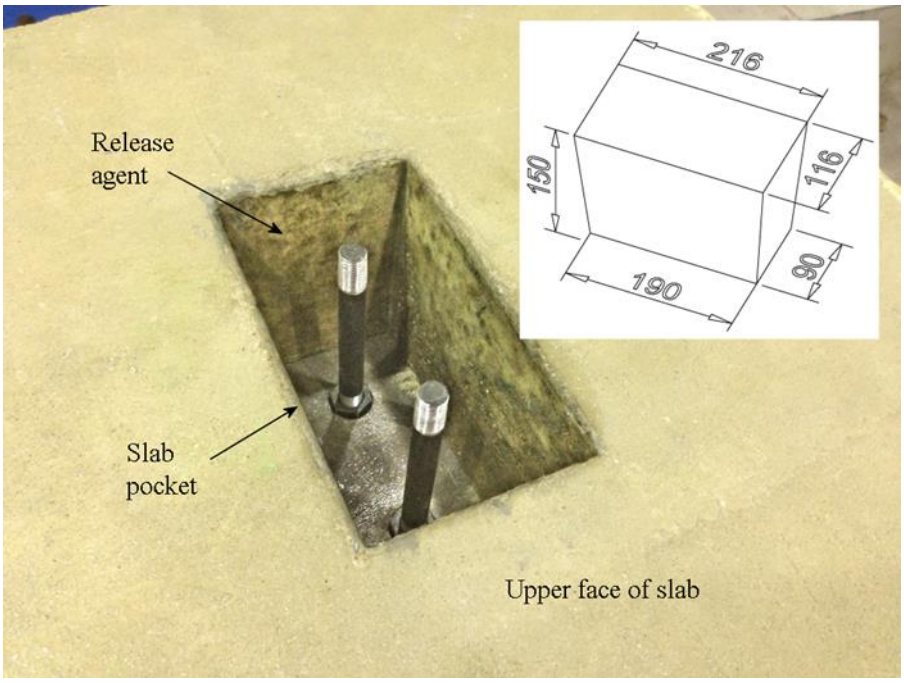

Fig. 4.29. Slab pocket overview and dimensions of LNSC pushout Test 5

The locking mechanism consists of a locking nut and a countersunk hole, and their dimensions are shown in Fig. 4.30. It is clear that by reducing the inclination angle of the locking mechanism from 120 degrees (Fig. 4.21) to 60 degrees (Fig. 4.30), the sliding force between the conical nut and the countersunk seat hole parallel to the inclined interface is reduced and the bearing force normal to the inclined interface is increased (refer to Section 3.2 for more enlightenment). This countersunk seat hole will be employed in the rest of LNSC tests.

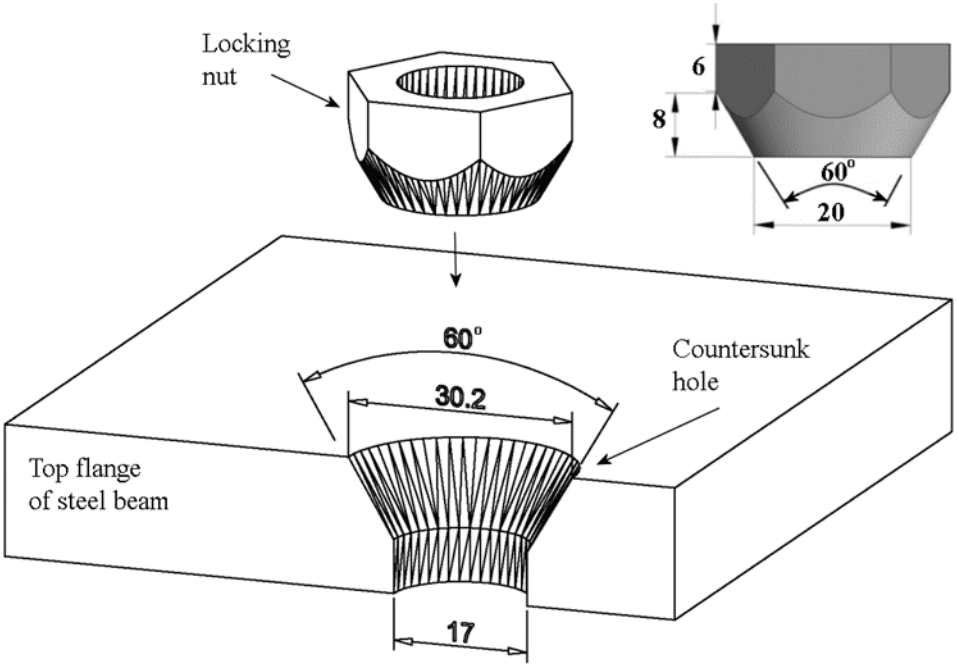

Fig. 4.30. Conical nut and half countersunk seat of LNSC pushout Test 5

Fig. 4.31 shows the positioning of the bolts with their locking nuts inside the countersunk seat holes in the flange of the steel beam, where a portion of the threaded length (weakest part) of the bolt will be vulnerable to shear forces during pushout test. The geometry of bolts was also changed from all-length threaded bolts (used in Tests 1 – 4) to bolts of smooth shank with 20 mm threads in one end and 70 mm threads in the other end, as shown in Fig. 4.31. It obvious that shearing the bolts through their smooth part will required higher shear force as compared to shearing them through their threaded parts. New grout was used to fill all the gaps between the bolt and the concrete plug and between the concrete plug and slab hole. This grout material consists of a mixture of 1:1 Portland cement (CEM II/A-L class 32.5N): fine sand (for internal plastering), 0.3 w/c, and 1.2% of cement weight superplasticizer (TamCem 60 from Normet). The same demoulding agent (Pieri® Cire LM-33 from Grace Construction Products) was applied on the surfaces of the slab pocket, as shown in Fig. 4.29 (but not to the outer surface of concrete plugs).

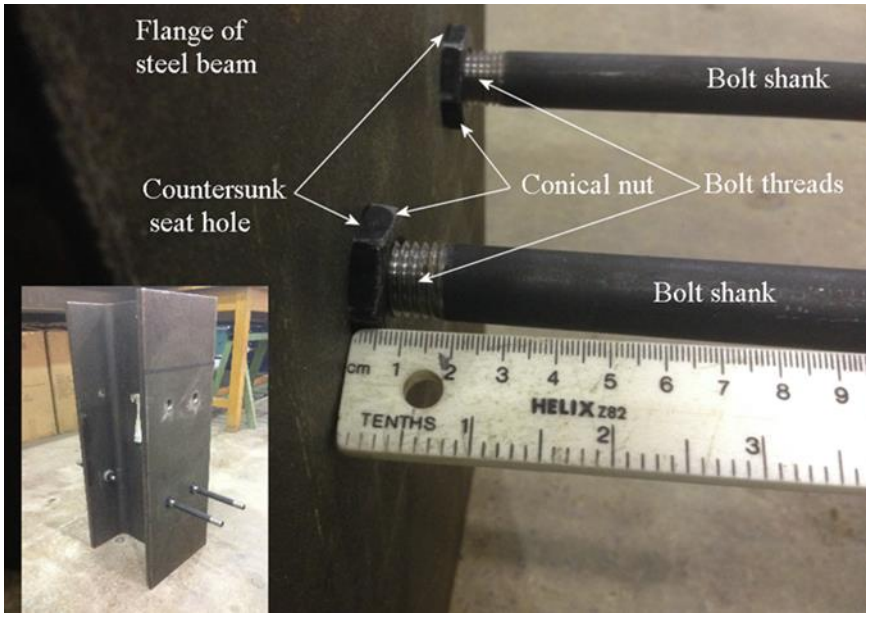

Fig. 4.31. Positioning bolts over steel beam of LNSC Test 5

4.4.5 LNSC Pushout Preliminary Test 6

Test 6 differs from Test 5 as follows. The slab pocket was changed from rectangular shape (Fig. 4.29) to oval shape (Fig. 4.32). It was found from Test 5 (Section 5.2.1.4) that the right-angle corners create difficulties in the demountability procedure. This slab pocket represents the final design (its exact dimensions can be found in Fig. 3.5a), and will be adopted in the rest of the LNSC tests.

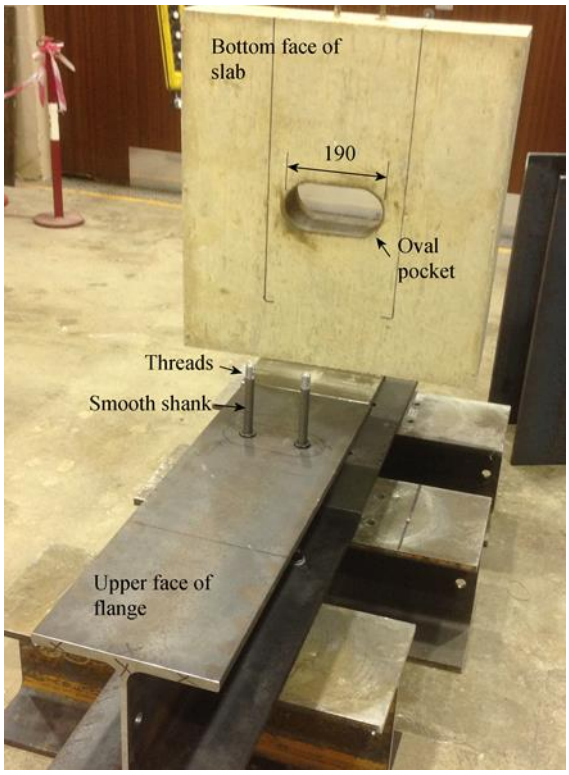

Fig. 4.32. Slab prior to position over a steel beam of LNSC Test 6

The bolts are of smooth shank with threaded ends; 20 mm at one end and 50 mm at the other. These bolts (but not the locking nuts) represent the final design and will be implemented in the rest of LNSC tests. Bolt threads seen in Fig. 4.31 were eliminated by removing 6.1 mm length of conical nut threads from its upper face (Fig. 4.33) and enforcing part of the bolt shank to be inserted inside the conical nut. In this way, the bolt thread is hidden inside the body of the

conical nut. Shearing-off the bolts should now take place in the shank of the bolt, which has gross cross-sectional area larger than the net cross-sectional area of the threads. It should be noted that the locking nut shown in Fig. 4.33 is slightly different from the final design shown in Fig. 3.4b (more details will be given in Section 5.2.1.6).

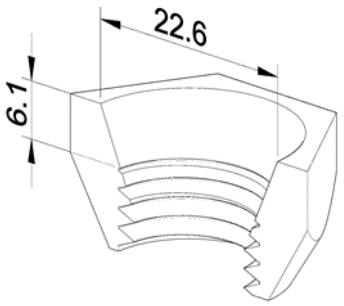

Fig. 4.33. Half locking nut used in LNSC Test 6

The grout consists of, based on trial mixes, 1:1 Portland cement (Quickcem from Hanson): fine sand (internal plastering sand), and 0.5 w/c. Quickcem cement is ideal for the slab pocket grouting because of its fast setting and hardening characteristics. Its workability duration is 7 minutes. The 0.5 w/c ensures a flowable grout without bleeding. Fine sand according to Table 4.4 is a vital requirement to avoid possible segregation of sand particles between the lower face of the plug and the upper face of the steel flange. This kind of grout is classified as part of the final design and will be used in the rest of the LNSC pushout tests.

The duration of Test 6 was 3 hours. The loading rate was under manual displacement control and was approximately 0.1-0.4 mm per minute. Material properties were listed in Table 4.2. The number of material specimens are as follow. Concrete compressive strength was evaluated using four 100 mm cubes for slabs, six 100 mm cubes for cones, and six 75 mm cubes for grouts, while the split tensile strength was estimated using two 100 mm cylinders for slab and plug.

Approximately the same amount of reinforcement recommended by Eurocode 4 (BSI 2004a) was used to reinforce the slabs. The latter detail for steel reinforcement is also constant for all the remaining LNSC pushout tests. A sample photo of the reinforcement is given in Fig. 4.4.

4.5 Preliminary pushout tests for FBSC

Six preliminary tests were performed to reach the final design of the FBSC in Section 3.3. These tests were carried out after pushout Tests 1 and 2 with LNSC. The author was therefore familiar with the test procedure, equipment, and safety requirements, as well as with the test rig and specimens, National Instrumentation, and LabVIEW programming. Bearing this in mind, specimens for tests 1 and 2 with FBSC were designed with dimensions, concrete

strengths, and slab reinforcement based on the findings the two LNSC tests. The following sections outline the six preliminary FBSC pushout tests.

4.5.1 FBSC Pushout Preliminary Tests 1 and 2

The main idea of the specimen of the FBSC is to get the full benefit of the friction that can be created at the interface between the lower face of the concrete plug and upper face of the flange of the steel beam. However, as a starting point for the tests, such friction resistance is not required. An overview of the test rig and the pushout specimen are shown in Fig. 4.34 which have the exact dimensions shown in Fig. 4.8.

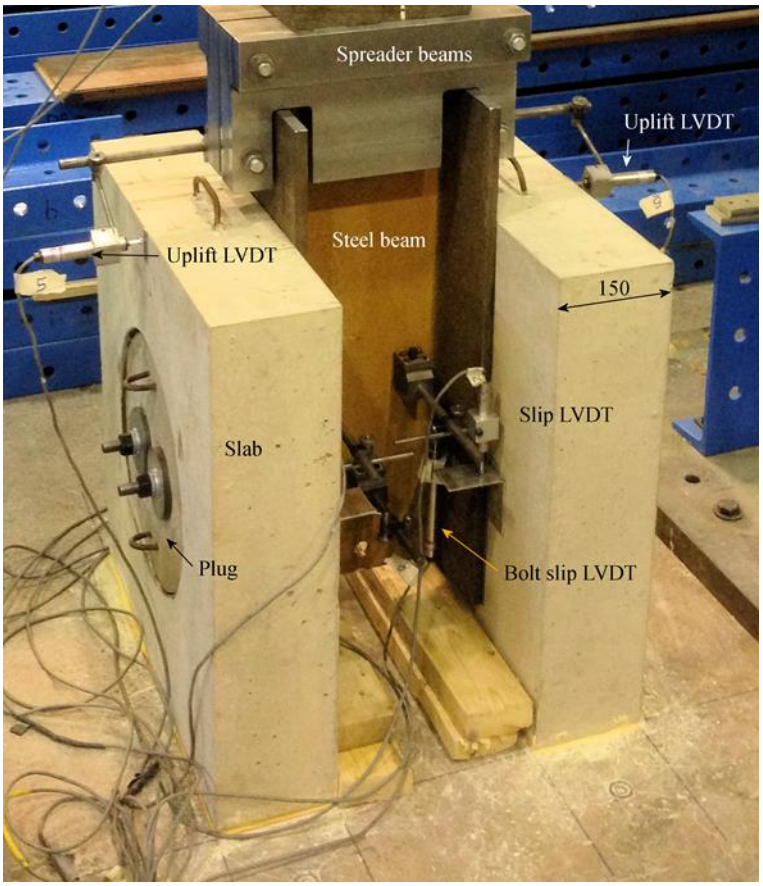

Fig. 4.34. Overview of FBSC Tests 1 and 2

Test 1 and 2 pushout specimens consists of one plug (exact dimensions in Fig. 4.15) in each pocket of the concrete slab. Each concrete plug contains two longitudinal holes to accommodate two preloaded all-length threaded M16 Grade 8.8 bolts. The configuration of the FBSC was the same as the LNSC in Fig. 4.9 with the exception that the middle nut has four M16 hardened washers per BS EN 14399-6 (BSI 2005d) (see Fig. 4.35) and they were left loose without any preloading. This was done to only hold the threaded bolts in position prior to final grouting of the slab's pocket, and at the same time to allow the threaded bolts to

deflect and create ductile failure before shearing-off. To achieve this goal, the grout was prevented from entering the gap between the bolt and plug hole and the interface between the lower face of the concrete plug and the upper face of the flange of the steel beam by using a commercial sealing agent. The sealant can be seen in Fig. 4.36.

No friction resistance was expected in this test because of the existence of the sealing agent; therefore, the failure load would represent the shear resistance of the threaded part of the bolt. It should be noted that proof load was applied to these bolts to check the effect of combined shear and tension. A demoulding agent (Pieri® Cire LM-33 from Grace Construction Products) was applied to the internal surfaces of the pocket of the concrete slab, as shown in Fig. 4.36. This demoulding agent will be used in the rest of FBSC tests.

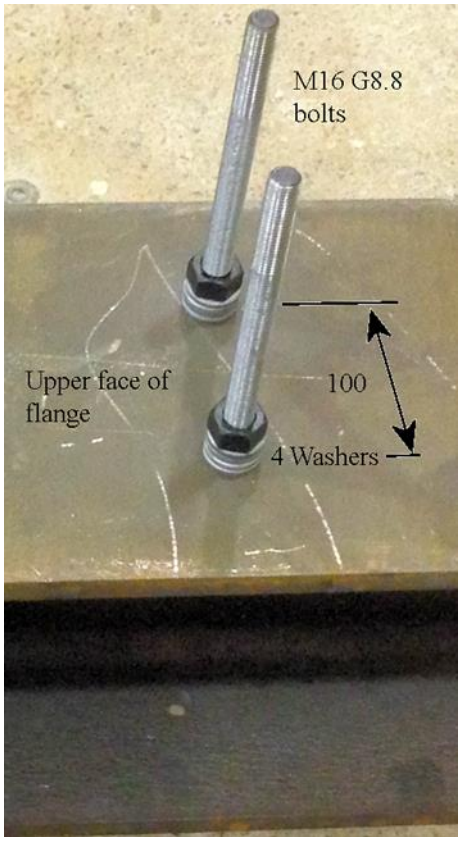

Fig. 4.35. Position of bolts with four washers and a nut in FBSC Test 1 and 2

A new grout (Epoxy Injection Grout from Parex) was used in Tests 1 and 2 to fill the 5-10 mm gap between the concrete plug and the pocket of the concrete slab. This grout is different from the final design and it was chosen because it can easily penetrate in thin gaps (i.e. 0.1 – 10 mm), it has a rapid strength gain (60 MPa in 1 day), and it has a workability time of 10 minutes at a temperature of 30°C.

Fig. 4.37 shows the reinforcement details used in the concrete slabs. The amount of reinforcement is about 50% of what is recommended from Annex B in Eurocode 4 (BSI 2004b). The reason behind this is to

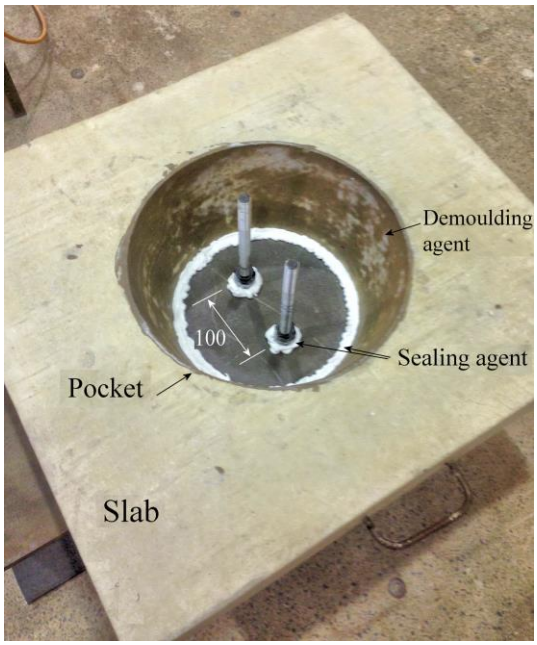

Fig. 4.36. Applying sealing and demoulding agents to slab pocket of Test 1 and 2

check the effect of reinforcement on the behaviour of the FBSC.

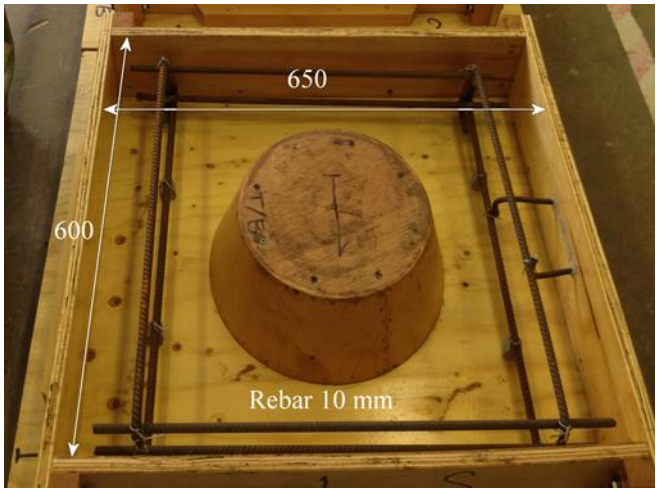

Fig. 4.37. Reinforcement used in FBSC Test 1 and 2

4.5.2 FBSC Pushout Preliminary Tests 3

In this test, bolts threaded along their whole length were used but without a middle nut or washers as compared to Tests 1 and 2. Based on findings of Tests 1 and 2 (Section 6.2.1.1), and to avoid sudden slip of bolts in their clearance holes in the flange, a chamfer countersunk seat was used. The countersunk seat, having an angle of 120 degrees, was machined in the inside opening of the hole in the flange of the steel beam (see Fig. 4.38). The reason behind this is to create an interlock with the full length hexagonal nut per BS EN 14399-3 that has the same inclination angle in one of its ends. The other side of the flange hole was not further machined. One of the technical problems of such type of connectors is how to hold the bolt in position prior to grout casting. As was discussed in Section 2.5, Dallam (1968) used spring chairs, while Lam and Saveri (2012) used a collar shaft (reduced diameter).

Fig. 4.38. Chamfer countersunk seat in FBSC Test 3

Test 3 used a handmade steel wire retaining ring (shown in Fig. 4.39) to hold the bolt in position without affecting its performance. A 0.5 water/cement ratio grout was used to fill all gaps between the bolts and plug hole and between the plug and the slab pocket.

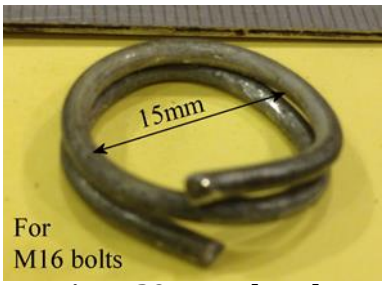

Fig. 4.39. Handmade retaining ring used in FBSC Test 3

4.5.3 FBSC Pushout Preliminary Tests 4

This test is similar to the LNSC Test 5 by having a rectangular conical pocket in each slab (Fig. 4.28) and small concrete plugs similar to those shown in Fig. 3.8. The chamfered countersunk seat has been changed from the inner face to the outer face of the flange and it still has the inclination angle of 120 degrees (Fig. 4.21). The handmade circular retaining ring (Fig. 4.38) was used again. The concrete slabs were reinforced with similar amount of reinforcement as recommended by Eurocode 4 (BSI 2004a), as shown in Fig. 4.40. This reinforcement details will be used in all the following pushout tests.

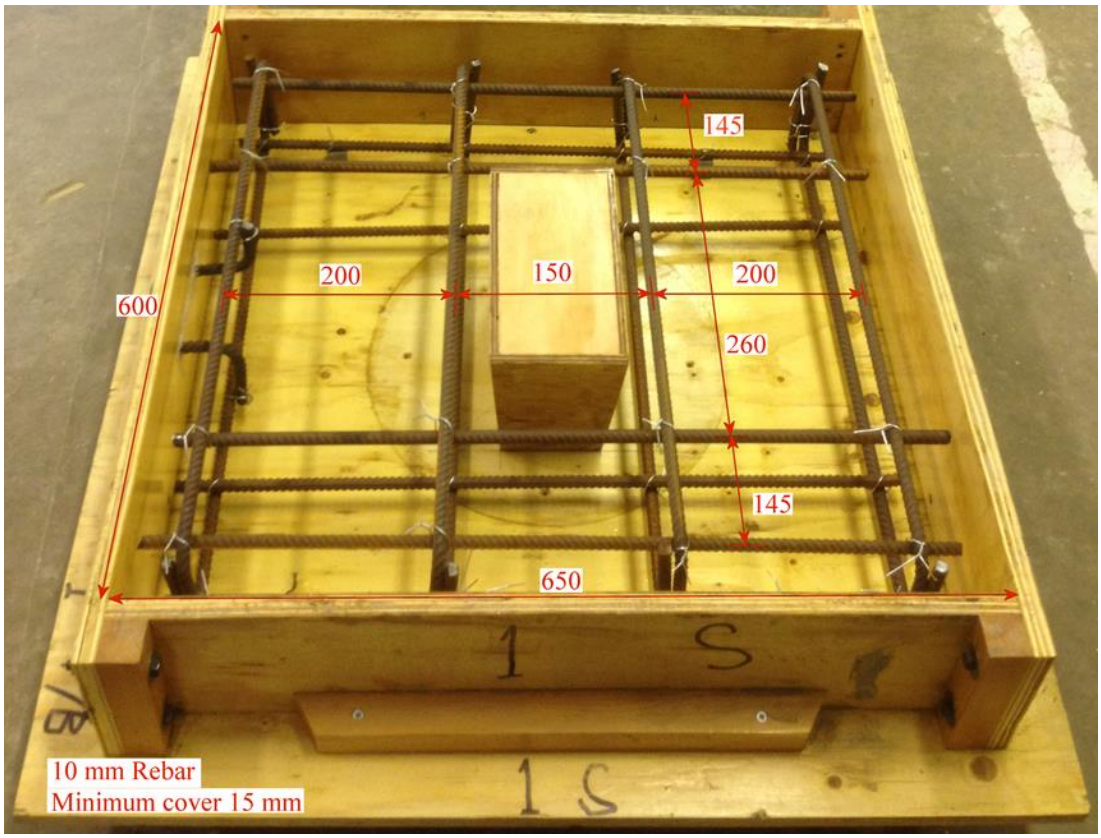

Fig. 4.40. Reinforcement used in FBSC pushout Test 4

It should be noted that although a countersunk seat hole does exist, no compatible nut was used. Instead, this seat was designed to be filled with grout to lock the bolt within its hole,

and therefore, to prevent the sudden slip of the bolting inside clearance holes when friction resistance between the concrete plug and the steel beam is overcome.

The bolts were not threaded along their whole length as before (i.e. Tests 1 – 3), but they have two 20 mm threaded ends (for nuts tightening) and a middle-unthreaded smooth part. In this way, the threads of the bolt are kept away from the shear failure plane which exists at the concrete slab-steel beam interface. The failure should always occur at the smooth part of the bolt which has a cross-sectional area larger than the net cross-sectional of the threads. Proof load was applied as a preload in each bolt to create considerable frictional resistance that can be used at the SLS. The grout of the final design listed in Table 4.1 was used to fill the gaps between the bolts and the plugs holes as well as the gaps between the concrete plugs and the concrete slab pockets. The grout mix design was explained in Section 4.4.5. The duration of the test was about 2.5 hours. The loading rate was approximately 0.1-0.2 mm per minute. The concrete compressive strength was evaluated using four 100 mm cubes for the slab, eight 100 mm cubes for the concrete plugs, and five 75 mm cubes for the grout. The split tensile strength was obtained using three cylinders (100 mm diameter and 200 mm length) for the concrete plugs and one cylinder test for the concrete slabs.

4.5.4 FBSC Pushout Preliminary Tests 5

An overview of the test is shown in Fig. 4.41. This test is similar to the previous test with one exception. The upper opening of the bolt hole was chamfered to create a countersunk seat with an inclination angle of 60° instead of 120°. In this way, a deeper seat is created which allows for more grout to settle and, hence, more resistance against sudden slip of bolt inside its clearance hole. Furthermore, the lower nut was used as a locking nut for each bolt to overcome the sudden slip. The handmade retaining ring was also used. The duration of the test was about 2.5 hours. The loading rate was approximately 0.1-0.2 mm per minute. The concrete compressive strength was measured using four 100 mm cubes for the slab, seven 100 mm cubes for the concrete plugs, and four 75 mm cubes for the grout. The split tensile strength was determined using one 100 mm cylinder for the concrete plugs.

Fig. 4.41. Overview of FBSC Test 5

4.5.5 FBSC Pushout Preliminary Tests 6

This test is like Test 5, except for the following. The pocket in the concrete slabs which has an oval conical shape, as shown in Fig. 4.42. The lower nut uses ordinary M16 nut instead of locking nut.

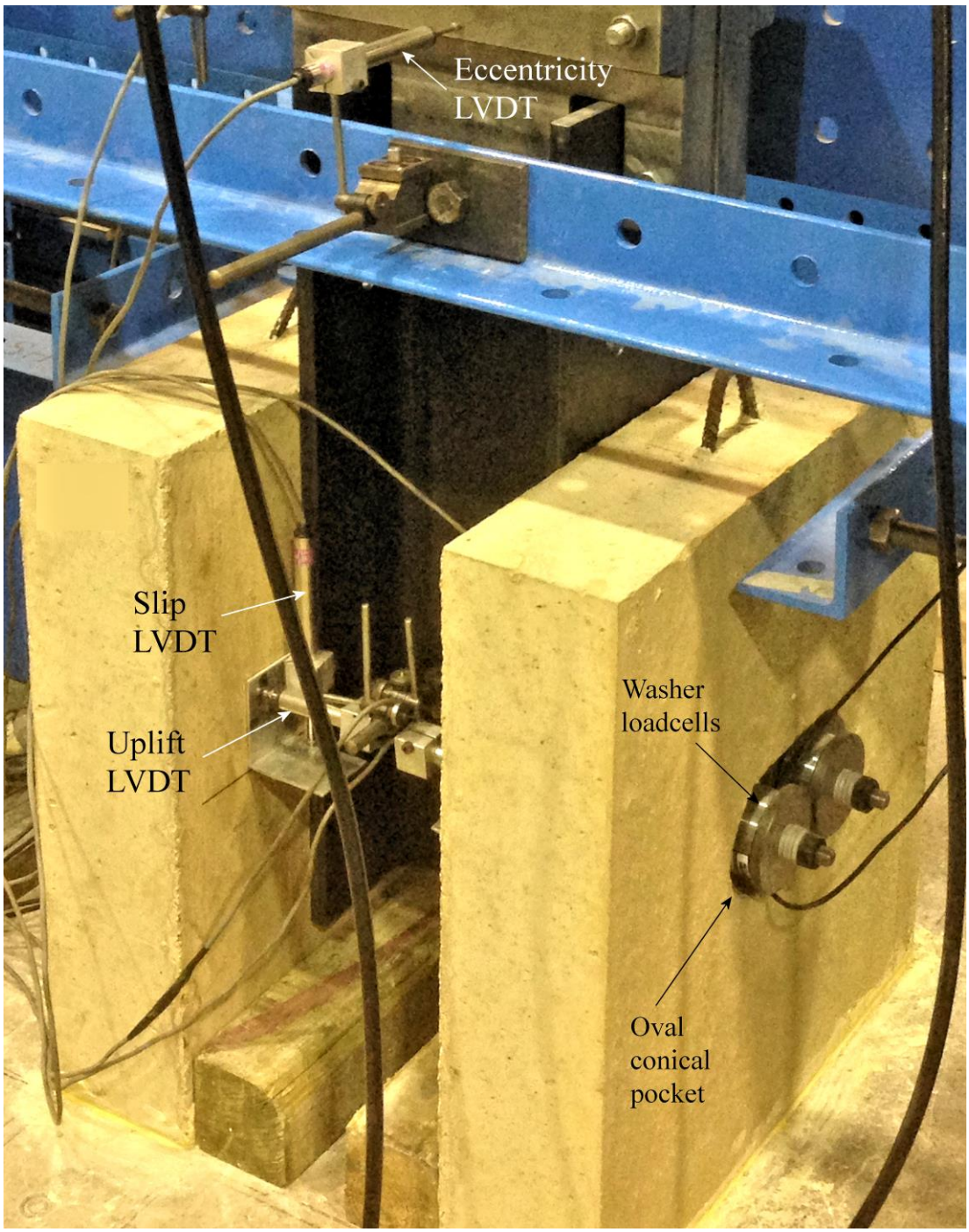

Fig. 4.42. Overview of FBSC Test 6

The testing rig was further stiffened by attaching additional channels to the column and beam elements. This was done to reduce the stored strain energy in the testing rig during

loading. A washer load cell (Fig. 4.42) was used for each bolt to precisely establish the preload, and to monitor the pretension during the pushout test. The preload was 63 kN, which is about 60% of the proof load. The bolts were held in position before grouting of the slab pocket by using standard retaining washers per BS EN 3386 (BSI 2012) (see Fig. 3.7) instead of the handmade rings (Fig. 4.38). The retaining washers (their details are given in Section 3.3) will be used in the rest of FBSC pushout tests. The concrete compressive strength was calculated using six 100 mm cubes for the slab, four 100 mm cubes for the concrete plugs, and six 75 mm cubes for the grout. The split tensile strength was obtained using two 100 mm cylinders for the concrete slabs and two 100 mm cylinders for the concrete plugs.

4.6 Steel-Concrete Composite Precast Beam Test

Experimental study of the behaviour of composite steel–concrete beam with FBSC is included in this thesis. The FBSC was chosen instead of the LNSC randomly. The structural behaviour of the composite beam is assessed under a monotonically increasing static load (four-points bending). With this arrangement, a pure bending zone with constant moment is created so that the flexural behaviour under pure bending could be studied. Such condition was absent in the pushout tests. The details of quasi-static test on one full-scale composite beam are reported. The following paragraphs outline the construction/preparation of the specimen, the testing procedure, the test set-up and the instrumentation used to measure the test responses. The results (Chapter 7) provide benchmark studies for numerical models or for the development of design procedures.

4.6.1 Test Setup

The simply supported composite beam is tested in a four-points bending, as shown in Fig. 4.43. The steel-concrete composite precast beam has length equal to 9.173 m and a UB457×191×89 steel section. The concrete slab specimen has 9.0×1.25×0.15 m dimensions. The simply supported beam has a span of 8.5 m between the supports. The beam used a roller bearing support in one end (left side of beam) and a pinned bearing support in the other (right side of beam) (Fig. 4.43). The supports were elevated 400 mm from the strong floor using concrete blocks (1.2×0.6×0.4 m) plastered to the strong floor to allow the composite beam to deflect freely. The overall heights of the left and right ends of the steel beam were carefully matched using several packing plates of high strength steel, to ensure horizontal alignment of the composite beam. Dental grout was used to embed the steel supports over the concrete blocks and in-between the packing plates. The pinned bearing support (right end) consists of two thick high strength steel plates (300×210×50 mm) with a

90^{o} wedge in between. The wedge was welded to the lower plate and has a rounded top (10 mm radius of curvature). The upper plate has a rounded groove (20 mm radius of curvature) in its base, and it can freely rotate over the rounded wedge.

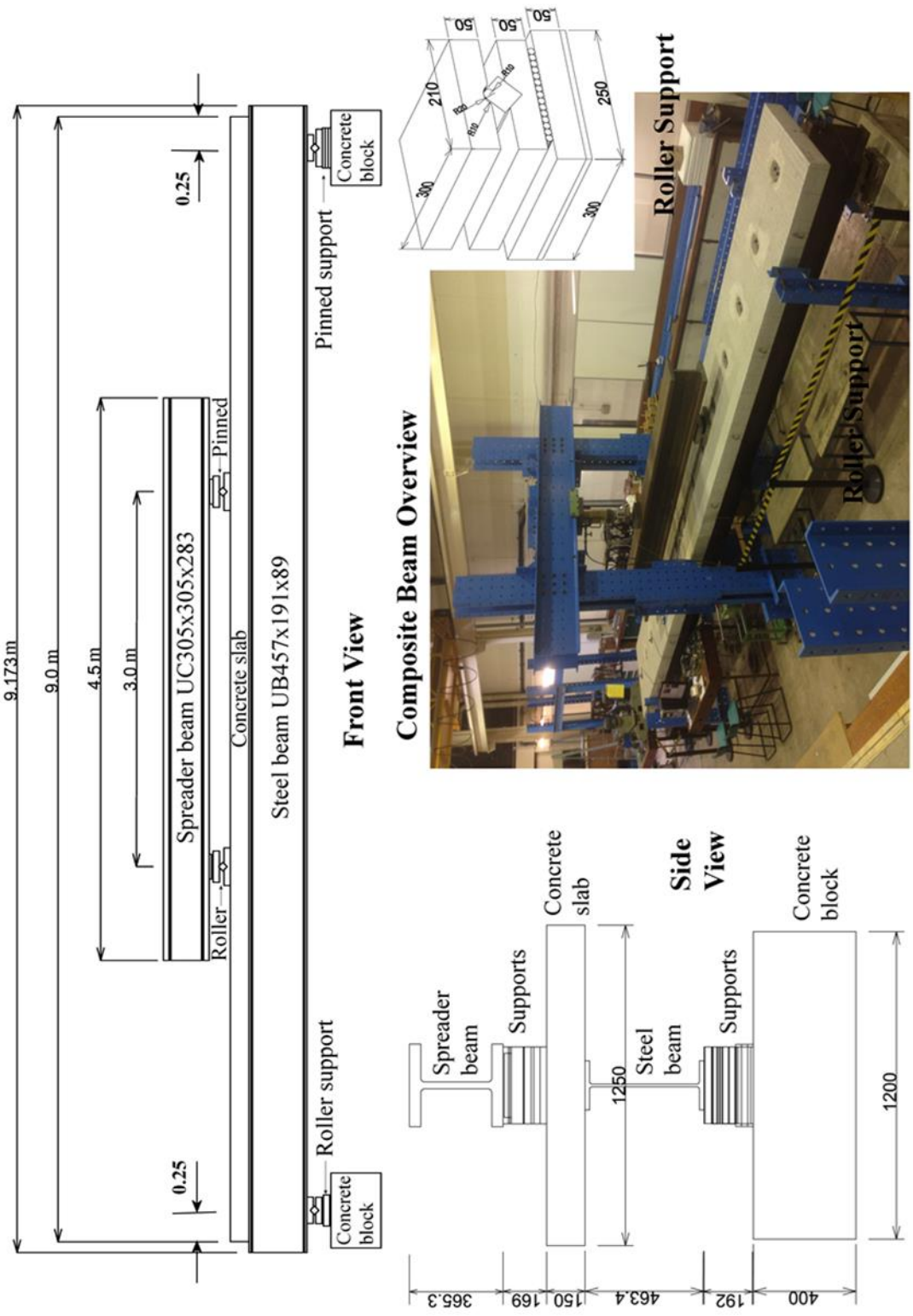

Fig. 4.43. Overview of the four-loads steel-concrete composite beam test

The geometry of the support is shown in Figs. 4.43 while its rotation performance before and after beam deflection is shown in 4.44. The roller bearing support (left end) is the same as the pinned bearing support with the exception that it rests on several cylindrical high strength steel rods (15ϕ12 mm). These rods can freely slide over another steel base plate (300×250×50 mm) to provide minimum resistance to horizontal displacement. In addition, the roller support a rotation ability provided by the steel wedge. This end support is shown in Figs. 4.43, and the roller performance before and after beam deflection is shown in 4.45.

It is essential at both supports to have upper bearing plates that have enough contact area (300×210 mm) with the steel beam to reduce the concentrated stresses in the lower flange of the end-sections of the steel beam to avoid any possible local buckling failure in the flanges. Otherwise, welding of additional steel stiffeners to the steel beam, above the supports, is needed. The welded stiffeners could modify the behaviour of the composite beam due to extra strength or residual stresses due to the heat of welding.

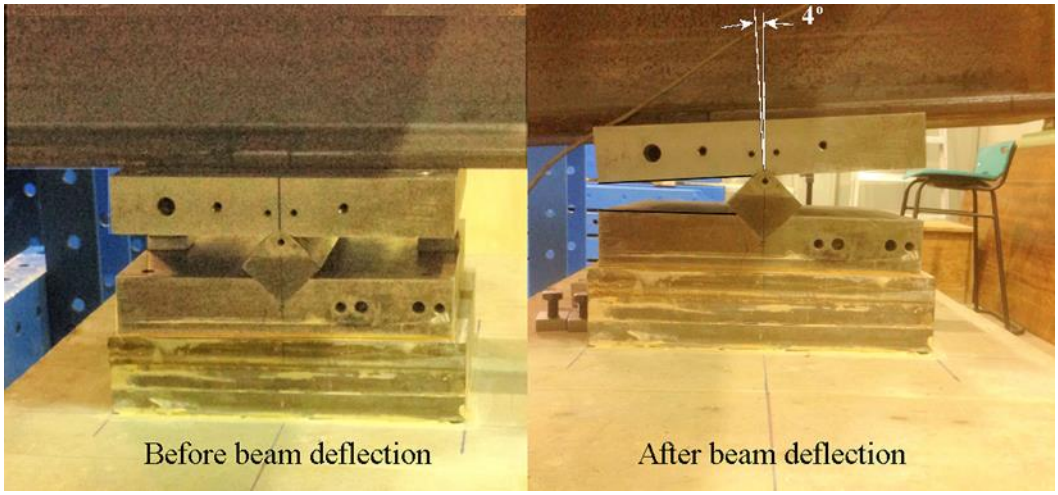

Fig. 4.44. Pinned bearing support (right end) between concrete block and steel beam

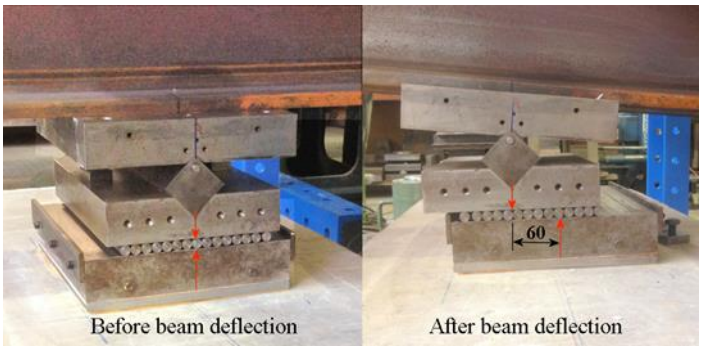

Fig. 4.45. Roller bearing support (left end) between concrete block and steel beam

The pinned and roller supports have an adequate contact area between their lower bearing plate and the concrete block to keep the compressive stress in the concrete blocks under 6 MPa when the applied load is maximum (i.e. 100t). As seen from Fig. 4.43, the testing rig was similar to the one used previously in the pushout tests, which basically consists of a steel frame with a 100t lifting hydraulic jack (including a compatible separate 100t load cell) in the middle. The hydraulic jack was successfully retested under pressure performance by a specialist company (Group HES Ltd) few days before the test. The load was transferred through ball joint to avoid any possible rotations due to eccentricity. The point load of the ball joint is converted to two points loads (3 m apart) using a stiff spreader beam of UC305×305×283 kg. It is calculated that the spreader beam will deflect vertically up to 2.0 mm under the maximum load of 100t. The stiff spreader beam is supported over the concrete slab (see Fig. 4.46) through pinned and roller supports with similar specifications as discussed previously. The two supports are shown in Fig. 4.47. All previous four supports were of high strength steel and designed to withstand an ultimate load of 200t, which is for a factor of safety of 4. It should be noted that all bolted connections in the rig were cleared from clearance gaps inside bolts' holes by relative shifting of connection plates one to each other until the bolts are in contact with holes' sides; therefore, all bolts will react in bearing immediately as the load starts.

Fig. 4.46. Position of stiff spreader beam over the concrete slab

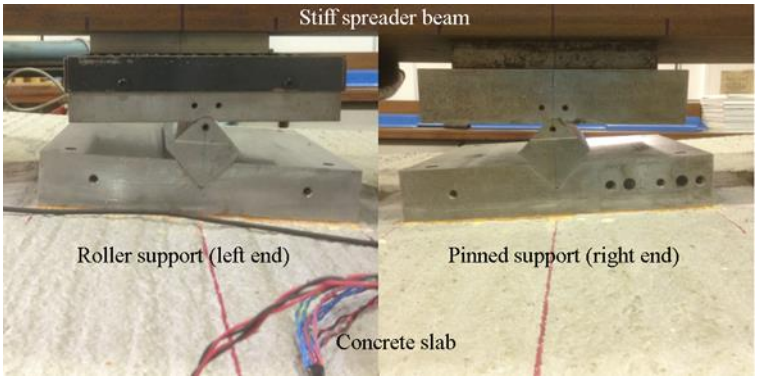

Fig. 4.47. Spreader beam's bearing supports after beam deflection

4.6.2 Specimen and Materials Properties

The steel-concrete composite precast beam has length equal to 9.173 m and a UB457×191×89 steel section. Three steel coupons were taken from the beam flange where severe yielding is expected to take place. It should be noted that the tensile strength of the flange is lower than that of the web. Tensile tests were conducted following BS EN ISO 6892-1 (BSI 2009b). Specimen strains were measured using an axial extensometer. The average values of the properties of the steel beam are as follows: tensile strength $f_{\mathrm{u}} = 457$ MPa, yield strength $f_{\mathrm{y}} = 355$ MPa, and modulus of elasticity $E_{\mathrm{s}} = 210.1$ GPa. A typical stress-strain relationship from one coupon test is shown in Fig. 4.48. Typical levels of strains were as follows: at the end of the elastic region is 0.001625; at the initiation of strain hardening is 0.015; at maximum stress is 0.12; and at fracture is 0.17.

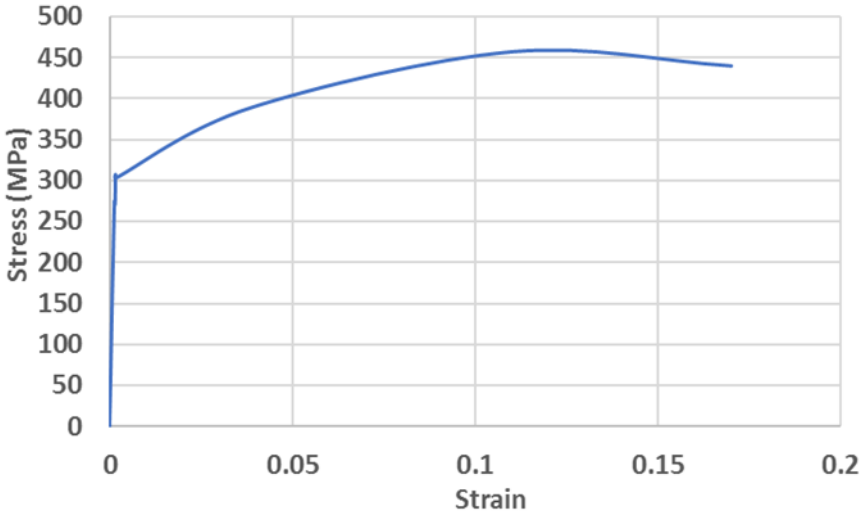

Fig. 4.48. Typical tensile stress-strain relationship of steel section

The steel beam is position over the pinned and roller bearing supports, as seen in Figs. 4.44 and 4.45, with span of 8.5 m (centre/centre) between them. The steel beam, on its own, was made horizontal by eliminating self-weight deflection by using two temporary steel supports

at the mid-length and 3 m apart, as shown in Fig. 4.46. Thirty M16 holes grouped as 15 rows and each row contain two holes were drilled on the upper flange of the beam. The longitudinal centre-to-centre spacing between the rows was 600 mm which leaves a length of 386.5 mm without holes at each end of the steel beam. The transverse centre-to-centre distance between the two holes of each row was 100 mm. Each M16 hole is machined to have an upper opening with chamfered countersunk seat illustrated in Fig. 3.4c.

The concrete slab for composite beam specimen had 9.0×1.25×0.15 m dimensions, with concrete average properties listed in Table 4.6. The mean concrete compressive and tensile strengths in these tables were obtained on the day of beam test according to BS EN 12390-3 (BSI 2009c), and BS EN 12390-6 (BSI 2009d) respectively. The compressive strengths of the slabs and plugs were evaluated by using 18 cubes of 100 mm sides; the compressive strength of the grout by using 12 cubes of 75 mm sides; and the tensile strengths of the slabs and plugs by using six cylinders of 100 mm diameter and 200 mm height. The modulus of elasticity was measured using three cylinders of 100 mm diameter and 170 mm height for the slab and plugs. In particular, three cylinders for the slab were used to evaluate the stress-strain curve (and the modulus of elasticity) through compression test. Three longitudinal strain gauges attached to each of the cylinders, as shown in Fig. 4.49. The stress-strain relationship of the three cylinders for the concrete slab can be found in Fig. 4.50. The average

Table. 4.6. Concrete average properties of composite beam test

Slab panels	**Compressive strength (MPa)**	**66**
	Tensile strength (MPa)	4.5
	Modulus of elasticity (GPa)	31
Slab mid-span	Compressive strength (MPa)	61
	Tensile strength (MPa)	3.7
Plug	Compressive strength (MPa)	89
	Tensile strength (MPa)	4.7
	Modulus of elasticity (GPa)	39
Grout	Compressive strength (MPa)	49

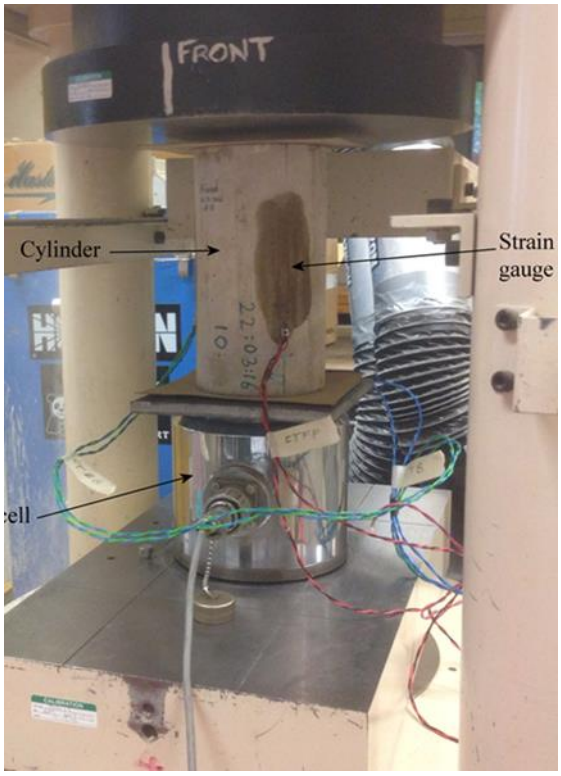

Fig. 4.49. Compression test on concrete cylinder with strain gauges

of the three strain gauges' readings represent the strain value for each of the three cylinders in Fig. 4.50.

The results of the three cylinders were also processed through polynomial regression to construct a second-degree nonlinear equation that reliably simulated the stress-strain relationship for this particular concrete as follows

$$\sigma = -5.50 \text{ x } 10^6 \, \varepsilon^2 - 3.39 \text{ x } 10^4 \, \varepsilon - 0.468 \qquad (4.1)$$

Where σ is compressive stress (in MPa), and ε is strain (in negative sign). It can be seen from Fig. 4.50 that the linear elastic part of the relationship ends at a strain of 0.0012, and that its maximum strength is reached when strain equals 0.0033. It can be observed that both steel section (in tension) and concrete slab (in compression) lose their elastic linear behaviour at a strain of approximately 0.001. Also, it can be concluded from the predicted curve of Equation (4.1) that concrete crushing may be assumed to occur at strain of 0.005. The strain at failure is typically around 0.005 for normal to high strength concrete (60-120 MPa) (Güler et al. 2012). It should be kept in mind that a great increase in strain capacity can be achieved when confinement from reinforcement is provided.

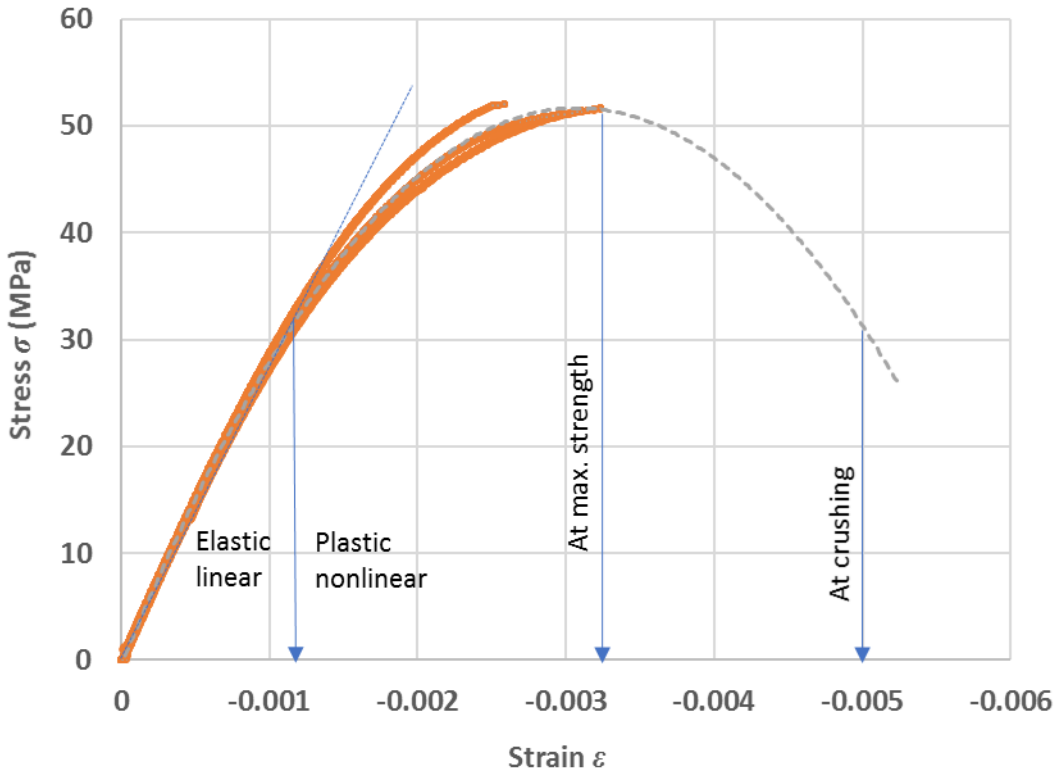

Fig. 4.50. Compression stress-strain relationship for slab concrete

The slab has fifteen pockets spread along the centre of the slab with a centre-to-centre spacing of 600 mm that leaves a length of 300 mm without pockets at each end of the slab, as shown in Fig. 4.46. The geometry of each pocket is the same as the one used in the final design of FBSC Test 6, as shown in Figs. 3.5a and 4.42. The demould release agent (Pieri® Cire LM-33 from Grace Construction Products) was applied to these pockets in two layers. The concrete slab was positioned over the steel beam so that each row of holes in the upper flange of the steel beam aligns with a pocket in the slab. Thirty M16 Grade 8.8 bolts per BS EN 14399-3 (Table 4.5) were positioned through the chamfered countersunk holes of the steel beam using retaining washers (Fig. 3.7) and M16 nuts per BS EN 14399-6. Each bolt was threaded from two ends (20 mm) while the middle part has a smooth shank. As used in the FBSC pushout Test 6 (Section 4.5.5), bolt thread was hidden below the level of the countersunk seat hole of the upper flange of the steel beam. A grout with the design in Table. 4.1 was poured inside the holes, then followed by gradually inserting one concrete plug for each bolt, followed by tightening the upper nut to the proof load to finish the construction process. The concrete plugs were the same with those used in the FBSC pushout Tests 4 – 6, as shown in Fig. 3.8. The upper nut used the same hardened plate washer in all pushout tests with specific characteristics listed before in Section 4.4.1. Careful attention was made to ensure a flat surface of the upper face of the concrete plug and the plate washer. Irregular interface may cause stress concentrations on the upper face of the plug, which result in plug crushing as the upper nut is tighten.

The concrete slab consists of two precast panels; each one has 4.05 m length, leaving a 0.9 m gap between them. The concrete used in the panels was a ready-mix design and truck delivered. The mix design was: 335 kg/m^3 cement CEM I (from CEMEX/ Rugby), 845 kg/m^3 sand (from CEMEX/ Berkswell), 1032 kg/m^3 aggregates (from Tarmac/ Hints), 1676 ml/m^3 superplasticizer type CSP340 (from CEMEX), max concrete size of aggregates 10 mm, water/cement 0.44, and slump of 50-60 mm. Similar proportions were used to cast the middle 0.9 m gap between the slab panels to produce a matching concrete through the whole slab (see Table 4.6). The longitudinal reinforcement from each panel extends into the gap with an overlap length of at least 800 mm. This was done because the lap is located in area of high moment, and a formation of plastic hinge might happen, and to comply with requirement of Clause (8.7) of Eurocode 2 (BSI 2004b). The gap was casted with concrete (see Fig. 4.51) to link the two panels together and to form the 9.0 m long slab. The reason for doing this is to simulate the actual construction method used in precast steel-concrete bridges, which usually result in tolerances in panels positions and levelling, as well as the

development of gaps between the concrete slab and the flange of the steel beam. It should be noted that because the slab test had the objective to check the behaviour of the FBSC shear connector, no longitudinal joints were used between the panels. This detail was present in order to make the results exclusively representative of the behaviour of the shear connector, without any additional factors that might affect the beam test results. It should be noted also that the concrete slab during the construction process was laterally supported by eight temporary steel supports, as shown in Fig. 4.52, to prevent any accidental tilting of the slab over the steel beam. After concrete hardening, the middle four lateral supports were removed while the four lateral end supports were kept (but did not touch the specimen, 1 mm gap) for structural safety reasons.

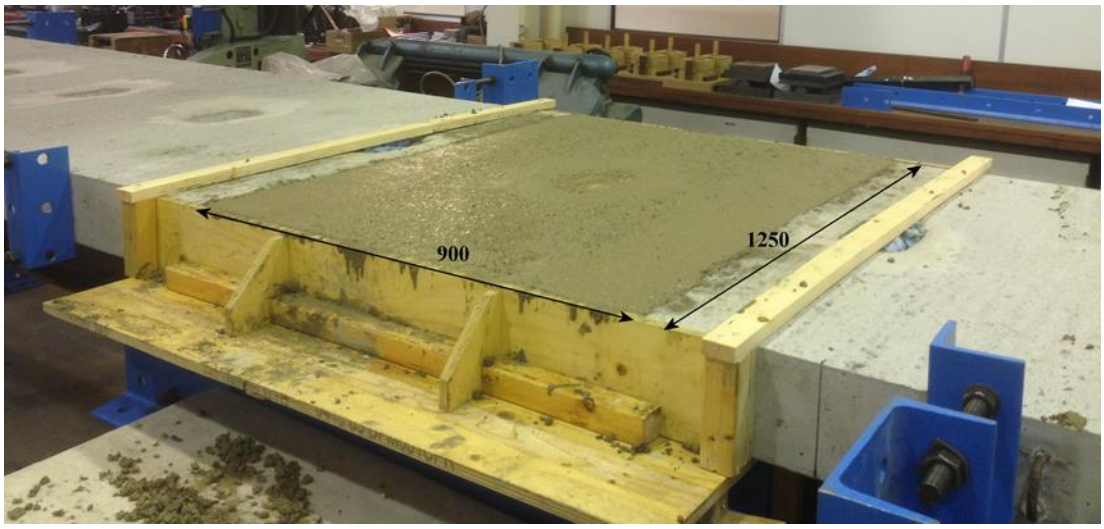

Fig. 4.51. Casting concrete in the gap between the concrete panels

Fig. 4.52. Lateral supports for concrete slab during construction

The concrete slab formwork and reinforcement is shown in Fig. 4.53. It consists of a lower mesh of reinforcement that consists of longitudinal rebars of ϕ12 mm at 250 mm spacings, except for the boundary bars where the spacing is reduced to 225 mm. The transverse reinforcement consists of ϕ10 mm at 200 mm spacings, except for the boundary bars where

the spacing is reduced to 175 mm. The upper mesh of reinforcement is the same as the lower one but the longitudinal bars are of ϕ10 mm and not ϕ12 mm. The reinforcement was ribbed bar, grade 500, according to EN 10080. Thus, the characteristic yield stress is assumed 500 N/mm^2 (not tested), and the modulus of elasticity is taken to be the same as that for steel beam. Concrete spacers of 20 mm were used under the bottom reinforcement mesh, which left about 12 mm cover for the top reinforcement mesh. It should be mentioned that less reinforcement was used as compared to standard pushout test (BSI 2004a), but still more than the minimum reinforcement required by Clause (9.2.1.1) for longitudinal reinforcement, and by Clause (9.2.2.5) for transverse reinforcement in Eurocode 2 (BSI 2004b). No special reinforcement detailing was made near slab pockets, despite the recommendations in Section 8 of Eurocode 4 (BSI 2005a). This was done, based on the results of Chapter 6.

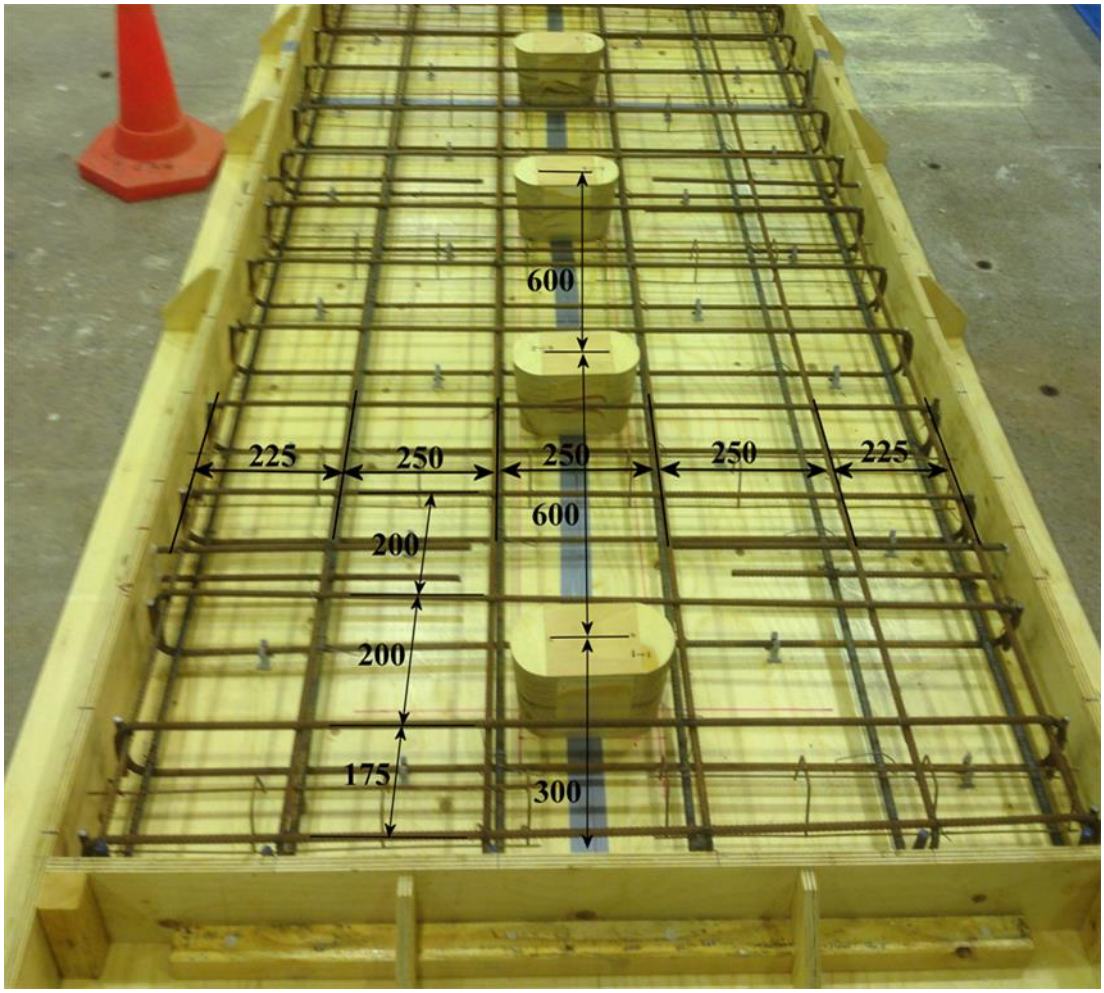

Fig. 4.53. Reinforcement for concrete slab

The concrete slab panels were casted in timber moulds, covered by damped hessian and polythene sheets, and cured for 7 days, then the moulds were opened and the opposite faces

of the middle gap were roughened-up with a special needle gun to be prepared for the in-situ concrete casting of the gap. The slab panels were lifted using embedded side hooks 1.0 m apart, as shown in Fig. 4.54, to represent the actual construction method for steel-concrete composite bridges, and positioned over the steel beam. During all these steps, the steel-concrete composite beam was temporary supported by two floor supports under the two points loads developed by the stiff spreader beam (i.e. at the centre and 3 m apart), which were in place until the pockets grout was completely hardened.

Fig. 4.54. Lifting of one concrete panel

4.6.3 Instrumentation

Figs. 4.55 and 4.56 show the positioning of LVDTs, load cells, and strain gauges used in the beam test. It should be noted that all load cells and LVDTs were recalibrated before testing. All strain gauges came from Techni-Measure. Concrete strain used type PL-60-11, while the steel strain used type YF-20 with 20% strain. The total number of LVDT transducers used in the test was 18. The slip between the concrete slab and the steel beam was measured near each FBSC (centre of slab pocket) and throughout the length of the beam using 13 LVDT transducers (S1 to S8 and S2R to S8R, but not for S2R and S3R where the slip is expected to be very small). Two LVDTs (S9 and S9R) were used to measure the slip between the concrete slab and the steel beam at each end of the concrete slab. One LVDT transducer (S10) at the mid-span of the beam and two dial gauges at 1.5 m from the beam centre (mid-length between S3 and S4, and mid-length between S3R and S4R) were installed to measure any possible uplift displacement of the concrete slab. Another LVDT transducer (S11), shown in Fig. 4.56, was positioned at the mid-span, normal to the web of the steel section and 300 mm below the upper flange, to give warning of any possible lateral deflection of the composite beam. The main mid-span mid-width vertical deflection was measured with a long

617 mm LVDT (S12), type ACT6000 from RDP Electronics Ltd, bolted to a column of the testing rig and attached to a smooth elastic plate glued to the upper face of the concrete slab (Fig. 5.56). The smooth elastic plate is essential as the mid-span section will slightly move longitudinally because of the roller-pinned supports mechanism. The main applied load was measured with a 100t load cell.

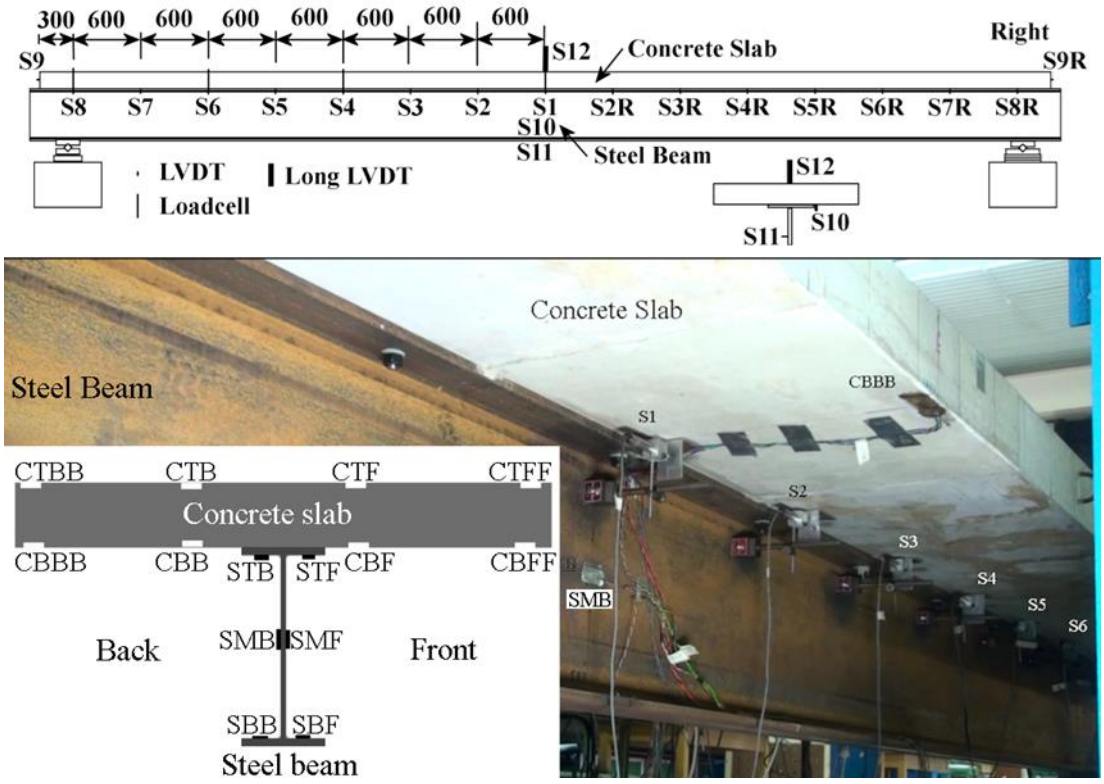

Fig. 4.55. Positions of load cells and LVDTs

The preload in the four bolts (S1, S4, S6 and S8 of Fig. 4.55) was measured with 200 kN washer load cells similar to those used in previous pushout tests (LNSC Tests 7-12 and FBSC Tests 6, 9, 10 and 11). The rest of the bolts were tightened using M16 DTI washers per BS EN 14399-9 (BSI 2009a) and a calibrated mechanical wrench. Strain levels at different locations at the mid-span section of the concrete slab and the steel beam were monitored during the beam test. Fig. 4.55 (bottom-left) shows the location and labels of strain gauges. Eight concrete strain gauges were used to measure the slab surface strain in the longitudinal direction. Four strain gauges at the top and four at the bottom of the concrete slab were used. In particular, two strain gauges were positioned on the edges (20 mm from the outside edge of slab) and two at the centre and just beside the slab pocket (140 mm from the centre line). The concrete surface was first grinded using a diamond tipped wheel to a smooth finish, and then, the manufacturer procedure was followed for the rest of the installation of the strain gauges. Six post-yield strain gauges were used to measure the strains at the mid-span steel section in

the longitudinal direction. They are arranged as two on the top flange, two at the mid-height of web, and two on the bottom flange.

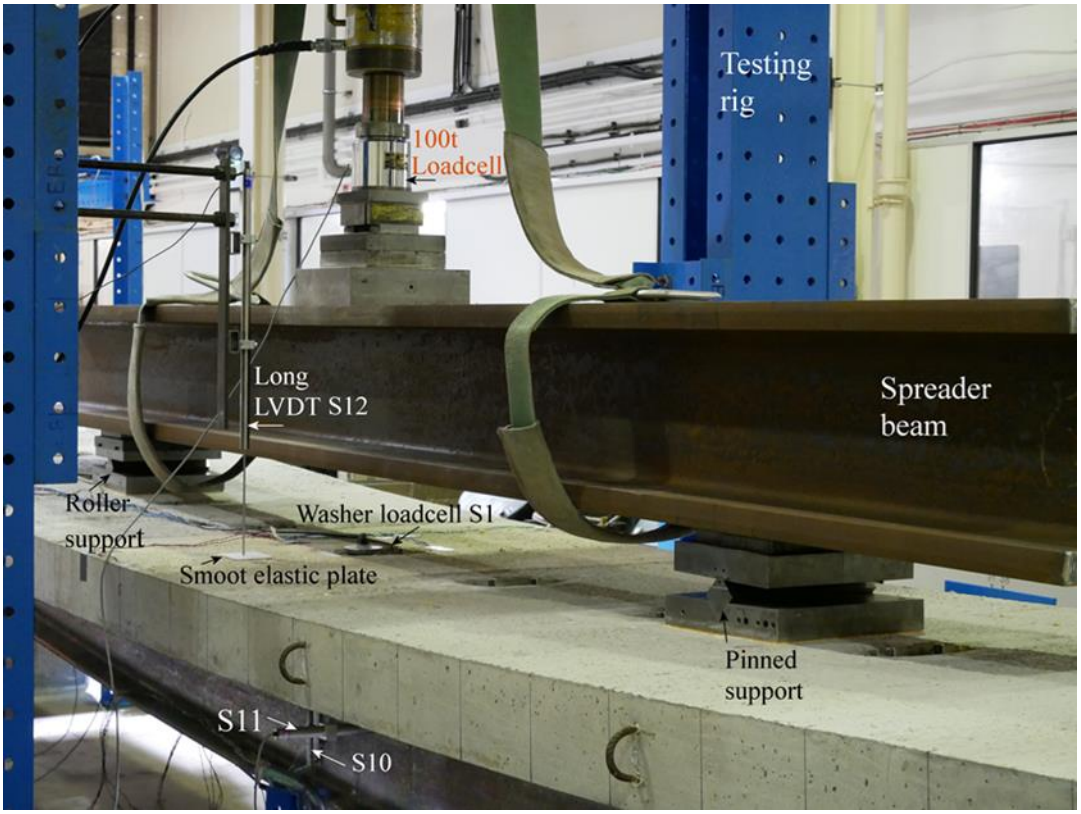

Fig. 4.56. Positions of S10, S11 and S12 LVDTs

The labelling used for the stain gauges (Fig. 4.55) is as follows: the beginning letter 'C' or 'S' stands for Concrete slab or Steel beam; the second letter represents the vertical location which would be 'T', 'M', or 'B', for Top, Middle, and Bottom; the third letter indicates the lateral location with respect to the central line of the composite section; therefore, it could be either 'F' for Front, or 'B' for Back; and the fourth letter is used only for the concrete slab to indicate the far Front using 'F', or the far Back using 'B'. Thus, the label CBBB shown in the photo of Fig. 4.55 represents a concrete strain gauge at the far back of the bottom face of the slab. In evaluating the strain profile or the neutral axis (N.A.) location, average values of strains are used for the top and bottom of the slab; top, middle, and bottom of steel beam. It should be noted that strain gauges on steel flanges were positioned at the inner faces (see Fig. 4.55), because of the concrete slab attachment to the upper flange, and because of technical difficulties and safety issues in the lower flange. All instrumentation was wired to a data logger from National Instruments and linked to a LabVIEW programme written specifically for this test to have continuous onscreen readings throughout testing.

4.7 Summary

The two novel shear connectors (LNSC and FBSC) will be tested with pushout tests and a composite beam test. Detailed description of the test setup and procedures, specimen dimensions, materials properties, and instrumentation were included. The development of the final design details of the LNSC and the FBSC through testing was described in detail. The connection developed from one plug in one pocket, to two plugs in one pocket. The geometry of plug was minimized. The slab pocket changed from circular conical shape into oval conical shape. The bolts modified from all threaded length to smooth shank with threaded ends. The reinforcement in plugs were omitted. The applied load was monitor by load cell, while washer load cells were used to measure the bolt preload and tensile force. The slip, separation, deflection, and eccentricity were measured by LVDT. Strain gauges were provided to quantity concrete and steel strains. All measurements were connected through National Instrumentation to a LabVIEW programme.

Chapter 5: Results and Discussions of LNSC Tests

5.1 Introduction

The results of the LNSC pushout tests are presented and discussed in this chapter. The LNSC experimental evaluation started with preliminary tests 1 to 6. The results of the preliminary pushout tests aided the author to identify optimum structural details of the LNSC that lead to superior demountability, shear resistance, slip capacity, ductility, and uplift resistance. The chapter provides full insight into the behaviour and failure mode of the LNSC along with meaningful comparisons with welded studs. Moreover, the results of the final parametric push-out tests are discussed in detail and highlight the effect of important parameters on the LNSC behaviour. From the final pushout tests, a design equation will be proposed for the shear resistance of the LNSC.

5.2 LNSC-Pushout tests

5.2.1 Preliminary Tests

The first six pushout tests were preliminary and served to investigate how different design details influence the structural behaviour of LNSC. The results of these preliminary tests led to the recommendation of the final robust structural details of LNSC.

5.2.1.1 *LNSC Pushout Preliminary Test 1 and 2*

A detailed description of LNSC preliminary pushout tests 1 and 2 was included in the previous chapter (Section 4.4.1). Both tests used very high strength grout, a double nut configuration similar to the work of Pavlović et al. (2013), and two bolts per plug. The preload inside each bolt can be assumed to be negligible (see previous chapter, Section 4.4.1), and therefore, the resulting shear strength of each pushout test is expected to represent the shear strength of the bolts without frictional resistance. The load-slip behaviour of the LNSC preliminary pushout tests 1 and 2 are shown in Fig. 5.1. It should be noted that, in Fig. 5.1 (as well as in all the shear load-slip displacement curves presented in this thesis), the shear load is the applied load divided by four (i.e. number of bolts), while the slip displacement is the average of the slip displacements measured close to the four bolts. The ultimate load is the maximum load in the shear load-slip displacement curve, while the slip capacity is calculated as the slip displacement corresponding to the ultimate load.

It should be further noted that Eurocode 4 (BSI 2004a) recommends calculating the slip capacity as the one that corresponds to the characteristic load value in the descending branch of the shear load-slip displacement curve.

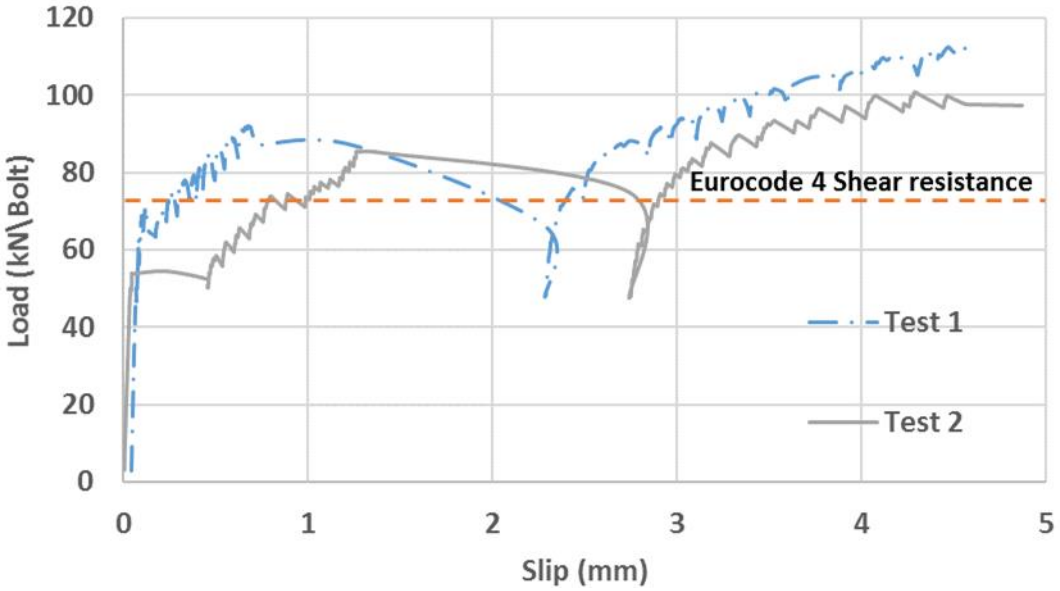

Fig. 5.1. Behaviour of LNSC in the preliminary pushout Tests 1 and 2

However, to reliably record the descending branch of a 'push-out test', a very stiff testing rig that does not store high strain energy at the instant of ultimate load (i.e. instant of sudden failure) is required (Johnson 1967). It can be seen in Fig. 5.1 that the test started at an initial slip displacement of 0.04 mm and not at zero slip displacement. The reason is the result of 25 cycles (recommended in Annex B of Eurocode 4) which showed a negligible effect that accumulates to only 0.04 mm slip. The 25 cycles are not shown in Fig. 5.1 for clarity. The preload in the double nut connection is the proof load, in the range of 88 -106 kN/bolt, and because this connection is basically a steel-steel friction interface, sudden slippage should occur at 0.2 × (88+106/2) = 19.4 kN/bolt (by assuming a static coefficient of friction between steel plates equal to 0.2). However, Fig. 5.1 shows that the sudden slip occurred when the shear resistance in the range 55-85 kN/bolt, which means that the effect of grout increased the chemical bonding and adhesion between the concrete plugs and the steel beam. The sudden slip was about 1.7 mm accompanied a loud acoustic emission as the bolts bear inside their holes. The load then dropped from 85 kN/bolt to about 50 kN/bolt, however this does not represent a drop in the shear resistance of the bolt as the load recovers with continued slip.

As can be seen from Fig. 5.1, the shear resistance of the LNSC in Tests 1 and 2 was higher than that of an equivalent welded stud according to Eurocode 4 (BSI 2004a). This was due to the material tensile strength difference and the effect of the developed friction. The shear resistance of M16 Grade 8.8 welded stud embedded into normal strength concrete is 73 kN/stud (as will be calculated in Section 5.2.3).

According to Clause 3.6.1(1) of BS EN 1993-1-8 (BSI 2005e), the shear resistance P_s of a Grade 8.8 bolt is given by (after omitting design partial safety factors)

$$P_s = 0.6\, f_u\, A_s \qquad (5.1)$$

where f_u is the tensile strength of the bolt, and A_s is the tensile stress area of the bolt where the shear plane passes through the threaded portion. In case the shear plane passes through the unthreaded portion of the bolt, A_s is the gross cross section area. From Table 4.5, $f_u = 889$ MPa, and from Bickford (1995), for M16 bolt, $A_s = 157\ \text{mm}^2$. Substituting f_u and A_s into Equation (5.1), $P_s = 84$ kN/bolt. The ultimate failure load in Test 1 was about 110 kN/bolt and that of pushout Test 2 was about 100 kN/bolt, which are higher than the shear strength P_s. The reason behind this is because of the interlocking friction between the high strength grout and the irregular face of the steel flanges. The previous statement can be explained by considering that a 4.5 mm slip has caused the bolts to stretch and as the bolt ends were restrained, tensile forces inside each bolt were developed. This effect compresses the concrete plugs against the upper face of the flange of the steel beam and creates friction resistance between the concrete plug and the steel beam.

It should be noted that the 4.5 mm slip capacity is less than the requirement of 6.0 mm in Eurocode 4 (BSI 2004a) for ductile shear connectors. The results of Tests 1 and 2 classify this LNSC as a non-ductile shear connector.

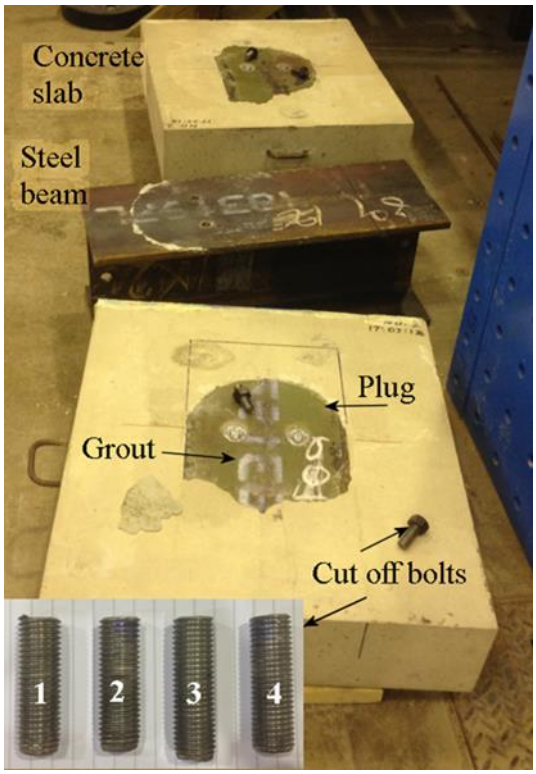

Fig. 5.2. Failure of LNSC Preliminary Test 1

Fig. 5.2 shows the failed specimen of pushout Test 1. The mode of failure in Tests 1 and 2 was early direct shear failure in the threaded part of the bolts with modest slip capacity. It can be seen in Fig. 5.2 that the grout is still glued to the bottom face of the concrete plug, while the imprint of scratches on both grout and steel beam indicate the existence of friction resistance. Moreover, the clean direct shear failure plane without noticeable bending in the fractured bolts indicates that no dowel action existed. For the locations of bolts 1 to 4, refer to Fig. 4.1.

Slab separation or uplift of the LNSC in Test 1 is shown in Fig. 5.3. The maximum separation was < 0.2 mm, which indicates that negligible displacements occurred on concrete slabs. Actually, the left slab was continuously moving towards the steel beam and not away from it, while the right slab separated from the steel beam at 80% of ultimate loading. Please notice that right and left slabs were indicated in Fig. 4.1.

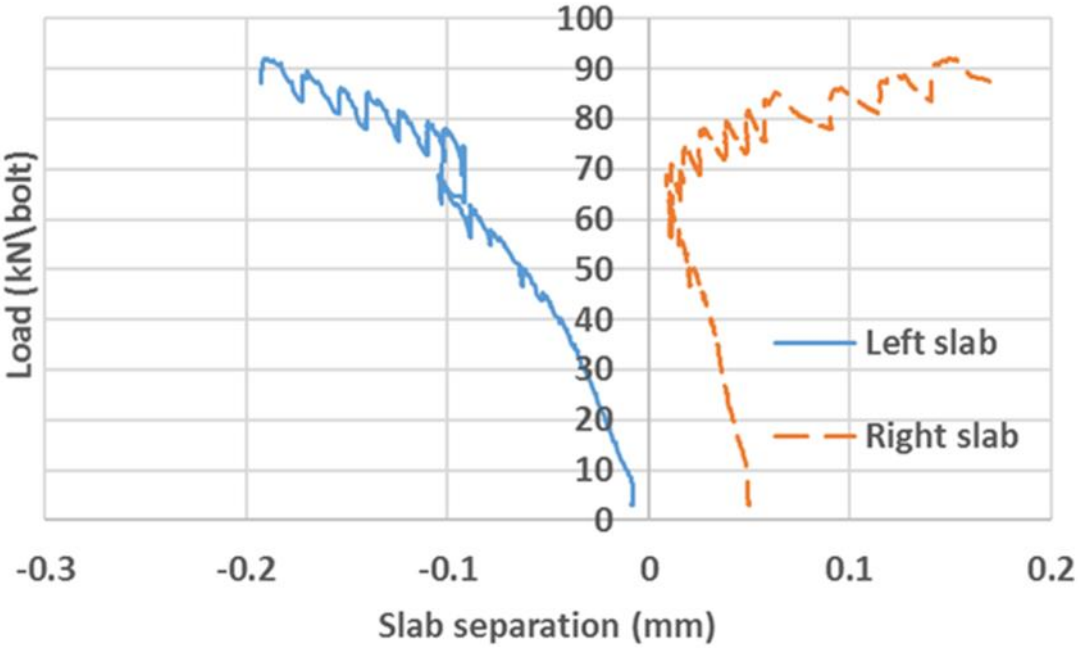

Fig. 5.3. Slab separation of LNSC preliminary pushout Test 1

Each plug was provided with two LVDTs (Fig. 4.10) to measure the plug movement relative to the slab. Fig. 5.4 shows the plug movement in the right slab during pushout Test 1, which indicates very small movements (i.e. < 0.06 mm). The plug, in the nonlinear part of loading, tried to tilt itself inside the slab pocket, i.e. the lower half of each plug tried to move up and slide over the slab pocket.

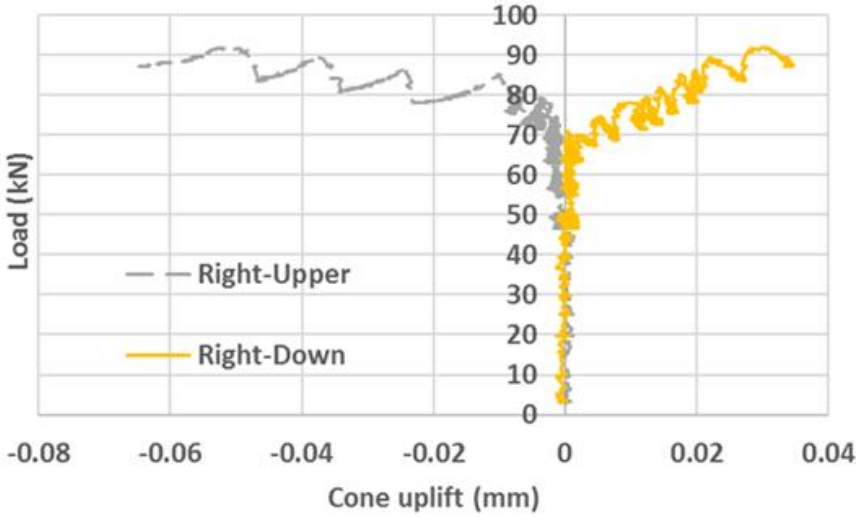

Fig. 5.4. Concrete plug movement during LNSC Test 1

5.2.1.2 *LNSC Pushout Preliminary Test 3*

Both LNSC pushout Tests 1 and 2 lack the required minimum slip capacity (i.e. 6 mm) of a ductile shear connector according to Eurocode 4, and it was difficult to distinguish between shear strength of bolt and other factors like grout adhesion. The specimen of Test 3 used two bolts per plug and a gap between the bolt and its hole (inspired by the work of Liu et al. (2014)) with an extra enlargement at the bolt base that equals 20 mm. The interface between the concrete plug and the steel beam was of a smooth machined finish; minimizing the effect of friction resistance. Further details can be found in Section 4.4.2. The load-slip behaviour of the LNSC preliminary pushout Test 3 is shown in Fig. 5.5.

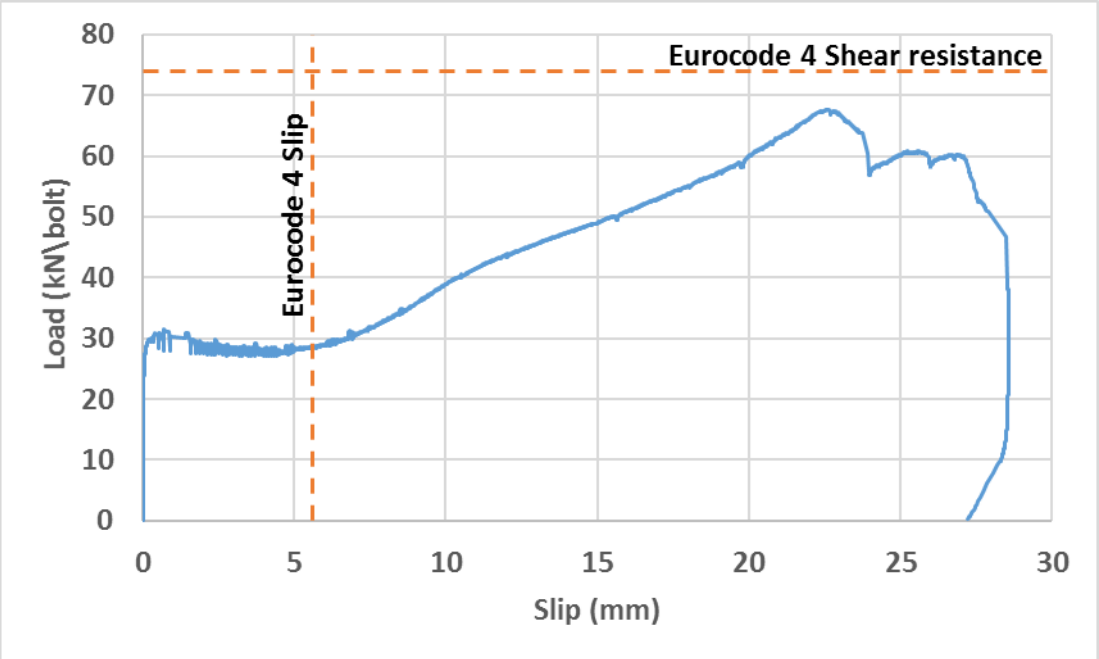

Fig. 5.5. Behaviour of LNSC preliminary pushout Test 3

It is evident that minimum friction resistance was available (30 kN/bolt compared to 85 kN/bolt of pushout tests 1 and 2). The effect of sudden slip (observed in Tests 1 and 2) was minimized. Due to the extra gap, the main behaviour of the bolt after the linear loading is bending of bolt, which resulted in a large slip capacity of about 23 mm at ultimate load, and finally led to the fracture of two of the four bolts (see Fig. 5.6). The ultimate load of the test was 68 kN/bolt, which is less than of an

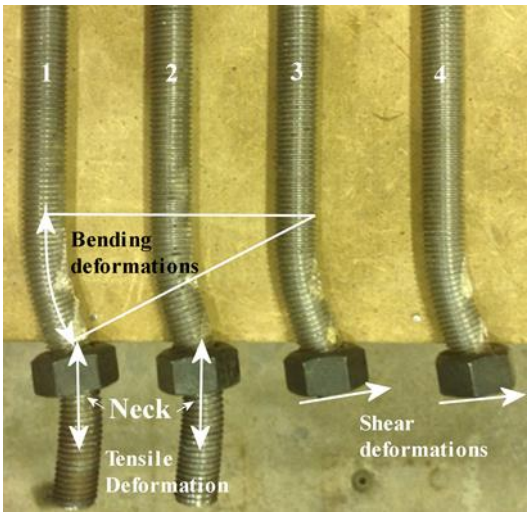

Fig. 5.6. Deflected shapes of bolts from LNSC Test 3

equivalent M16 welded stud at 73 kN/stud. It can be seen from Fig. 5.6 that a combination of shear, bending, and tensile deformations occurred in the bolts. A close look at the first two bolts on the left side of Fig. 5.6 show that formation of neck plastic zones has occurred, which indicates that the tensile force had exceeded the ultimate value. Figs. 5.5 and 5.6 showed that failure was due to excessive slip (≈28 mm), similar to the failure discussed by Oehlers and Bradford (1999). The maximum slab separation was relatively negligible and equal to 0.25 mm, while the maximum bolt slip inside its hole was 0.23 mm.

5.2.1.3 *LNSC Pushout Preliminary Test 4*

Test 4 was identical to that of Test 3, with the exceptions that the gap between the bolt and its hole was filled with a cement based grout, while there were no significant preloads inside the bolts (estimated to be about 10 kN using torque wrench). The proof load in the double nut connections was though maintained. A trial attempt for a locking double nut connection and the usage of a demould agent were also included. Section 4.4.3 provide more details. The load-slip behaviour of this preliminary test is shown in Fig. 5.7. The first thing to notice in this figure is that the sudden slip was minimized at 55 kN/bolt, but not completely eliminated. This indicates that the inclusion of a locking nut connection is a potential design. Secondly, there was an abnormal rising of load at 15 mm slip, which was explained in the previous chapter (Section 4.4.3). The shear resistance was larger than that of an equivalent welded stud according to Eurocode 4 (BSI 2004a). The shear resistance of M16 Grade 8.8 welded stud embedded into normal strength concrete is 73 kN/stud (as will be calculated in Section 5.2.3). In addition, the slip capacity and ductile failure behaviour were quite evident.

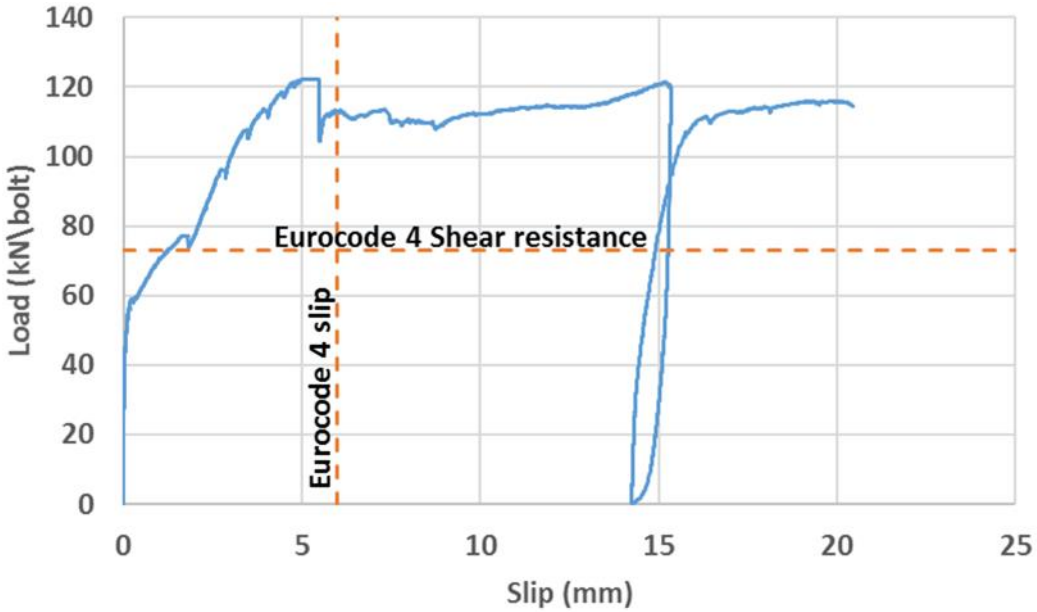

Fig. 5.7. Behaviour of LNSC preliminary pushout Test 4

Fig. 5.8 shows the deflected shape of the failed bolts after removing the lower nut for clarity. It can be seen from the photograph that some rotation occurred on the locking nuts relatively to their chamfered holes, which means that the locking nut was not perfectly stable inside its countersunk seat hole, although a proof load did exist in between the doubled nut connection (see Fig. 4.21). This conclusion indicates that the chamfered angle of the countersunk seat hole (i.e. 120°) need to be reduced, and its depth (i.e. ≈2 mm) need to be increased. Fig. 5.8 also shows necking plastic zones just below the locking nuts. The bolts undergo a very high tensile load that creates these plastic necks, and it seems that the rotation of the locking nut had contributed in increasing this tensile force. Due to the inclined position of the nuts, there was a sort of a prying action, where the nuts were used as lever arms that exerted additional tensile stresses on the bolt between the double nuts. Finally, Fig. 5.8 illustrates that the shear failure plane was in the threaded part of the bolt, which indicates an opportunity to increase the strength of the LNSC furthermore by forcing the shear failure plane within the smooth shank.

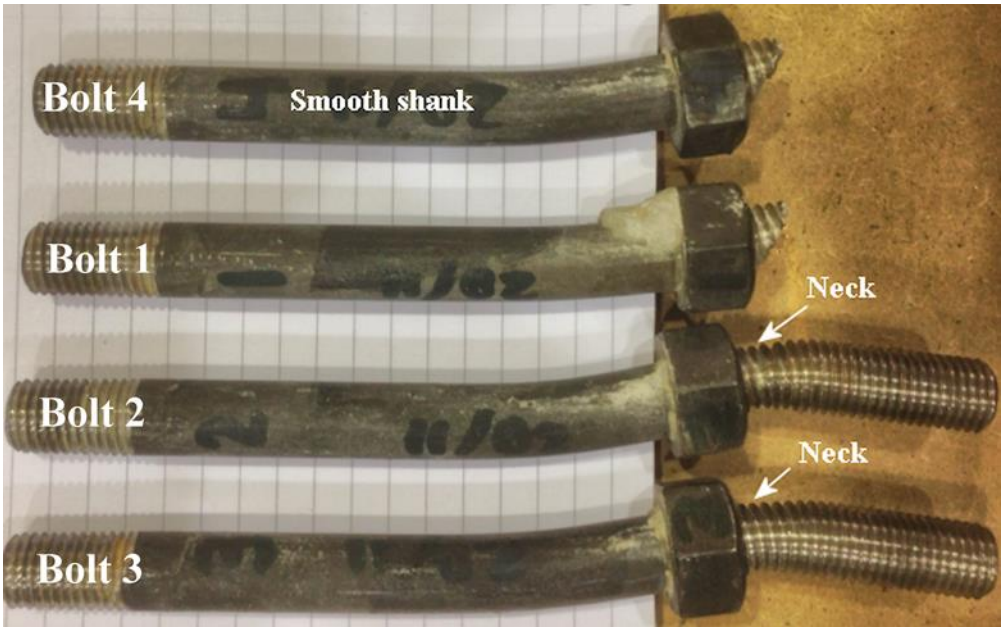

Fig. 5.8. Deflected shapes of bolts from LNSC preliminary pushout Test 4

Cracking in the concrete plugs was also observed as shown in Fig. 5.9. Several factors assisted in cracking the plugs, and they are: (1) the current inclination angle of the concrete plug sides; (2) non-preload inside the bolts, which reduces the triaxial stress state of the plug concrete and therefore reduces its compressive strength; (3) the addition of a demoulding release agent, which contributes to the instability of the plugs by minimising the friction resistance between the plug and the slab. Hairline cracks with maximum crack width of 0.3 mm were observed in the concrete slabs especially at the inner face of each slab which

indicates that there is a need to increase the amount of reinforcement. The maximum slab separation was 0.1 mm, which is negligible.

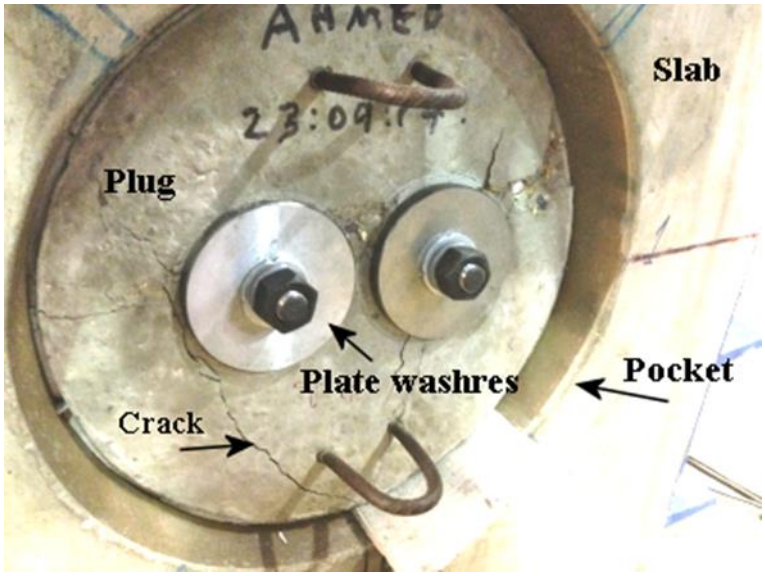

Fig. 5.9. Fracture of concrete plug of LNSC preliminary Test 4

5.2.1.4 *LNSC Pushout Preliminary Test 5*

During the aforementioned four tests, a sudden large slip occurred as a result of bolts sliding inside their bolt holes when the friction resistance at the steel beam-concrete slab interface was exceeded. To this end, Test 5 aimed to assess the behavior of a non-slip shear connector using a conical nut connection similar to that of the final LNSC (Fig. 4.3) with one exception; the connection does not completely hide the threads of the bolt inside the conical nut body, as shown in Fig. 5.10. In addition, and by building on previous tests results, a new design for the concrete plug and the slab pocket was adopted (see Section 4.4.4 for more details). The load-slip behaviour is shown in Fig. 5.11. It's clear from the curve that the presence of the conical nut and countersunk seat hole of 60° angle successfully eliminated any sudden slip. Additionally, the LNSC detailing increased the shear resistance compared to the previous pushout tests (e.g. double the shear resistance of Test 3). On the other hand, it has low slip capacity at 4 mm compared to the 6 mm requirement in Eurocode 4 for ductile shear connectors (BSI 2004a). It

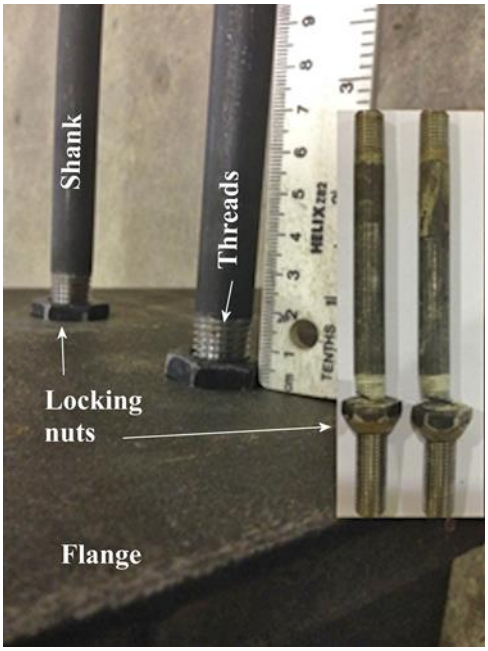

Fig. 5.10. Bolts of the LNSC before and after Test 5

should be mentioned that only two bolts fractured, which means that the resulting shear resistance may not represent the mean failure value for the four bolts.

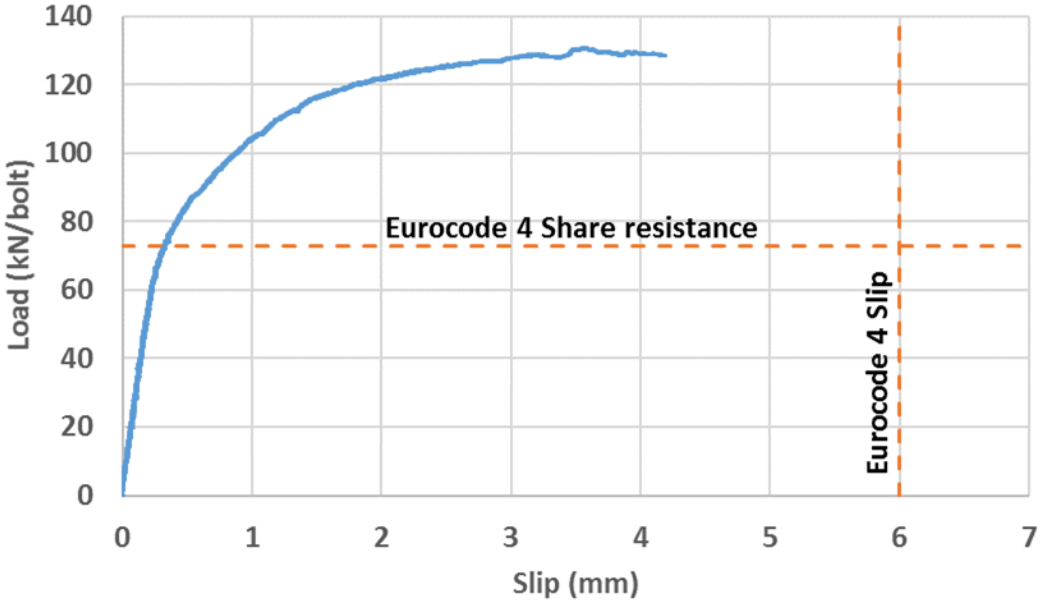

Fig. 5.11. Behaviour of LNSC preliminary pushout Test 5

It can be seen from Fig. 5.10 that the shear failure plane was almost direct shear without observable bending deformations, similar to the failure of Tests 1 and 2 (see Fig. 5.1). The main reason for this is the existence of threads near the shear plane, which concentrates the shear stresses in this zone. In addition, the surrounding grout around the bolts had a compressive strength of 58 MPa, which represents a stiff surrounding that bounded the bolt shank and prevented bending deflections. Local concrete crushing and powdering was noticed in front of each conical nut taking the shape of a wedge as shown in Fig. 5.12 due to concentration of high stresses.

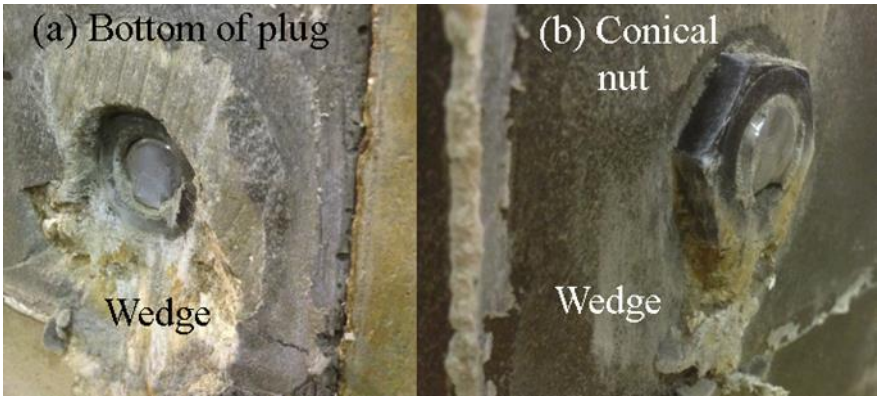

Fig. 5.12. Concrete wedge failure of LNSC Test 5, (a) slab face (b) beam face

The demountability was confirmed by pulling out the entire grout of the slab pocket, which contains two concrete plugs and two bolts with their conical nuts (see Fig. 5.13). It should be stated that the 90° four corners of the slab pockets produced difficulties in the aforementioned process due to geometry confinement. It can be seen from Fig. 5.13 that the release agent has successfully prevented chemical bonding between the grout and the concrete slab pocket.

Fig. 5.13. Pulled out slab pocket after LNSC Test 5

5.2.1.6 *LNSC Pushout Preliminary Test 6*

Finally, Test 6 was conducted on a specimen representing the actual robust structural details of the final LNSC, including the oval shape of the concrete slab and the normal strength grout. The tensile load inside the bolts was in the range 88-106 kN, while inside the double nut connection, it was about 67 kN (see Table 4.2). These values were estimated using a calibrated mechanical torque wrench and DTI washers. The tensile load inside the double nut connection should not be less than the proof load because it has been proved that this type of connections usually lose pretension easier than flat ones (Bickford 1995). 67 kN represents the tensile force after a loss of about 35% of its original proof load value. Furthermore, as 5 mm length of the internal threads of the conical nut were removed (see Fig. 3.4b), and a chamfered finish was created for this opening (Fig. 4.33). The reason behind these preloads and geometrical differences is to try to make the conical nut easier to rotate inside its hole to absorb more energy and to increase the ductility. Such ductility was absent in Test 5. Further details can be found in Section 4.4.5. The load-slip behaviour in Test 6 is plotted in Fig. 5.14. It is clear from the figure that pushout Test 6 achieved the highest results in shear strength, slip capacity, and ductile failure as compared to previous pushout tests.

The reasons behind this will be explained later in this section. The ultimate load per bolt was 198 kN, the corresponding slip capacity was 12.2 mm, and the slab uplift was < 1.0 mm.

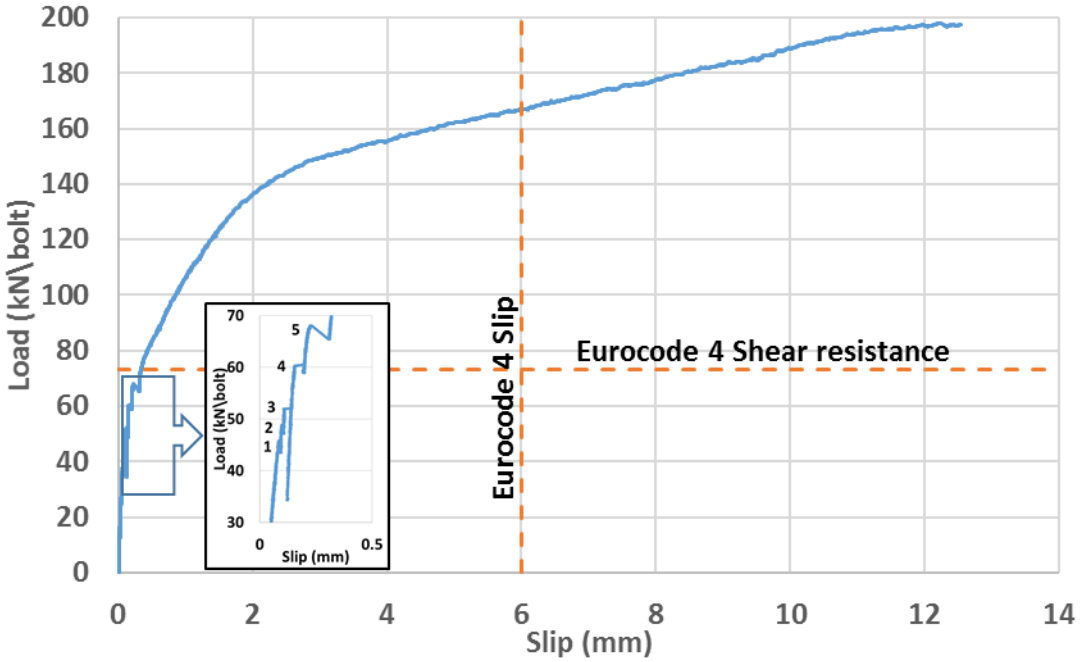

Fig. 5.14. Behaviour of LNSC Test 6

Fig. 5.14 shows that the LNSC Test 6 has three distinct load-slip phases. Initially, it behaves as a stiff shear connector, by achieving about 100 kN shear strength (50% of ultimate load) with only 0.86 mm slip (i.e. initial stiffness of 116 kN/m). Five tiny successive slips (hard to be seen in Fig. 5.14) were noticed at the beginning of the test. These slips are highlighted inside Fig. 5.14, and they are: (1) at 45 kN/bolt, adding 0.015 slip; (2) at 48.3 kN, adding 0.015 mm slip; (3) at 51.2 kN, adding 0.011 mm slip; (4) at 60.5 kN, adding 0.032mm slip; (5) at 68.0 kN, adding 0.043mm. The reason for these tiny slips are likely to be due to distinct small rotations (about 10 degrees in total) of the conical nuts inside their holes (as illustrated in Fig. 5.15); especially as the preload in this connection was about 64 kN (i.e. less than the proof load). It should be noted that the rotation was observed at the end of the test by inspecting the conical nuts. These rotations and slips can be avoided in the coming tests by increasing the preload from 64 kN to the proof load which is in the range of 88-106 kN. The first phase is the elastic

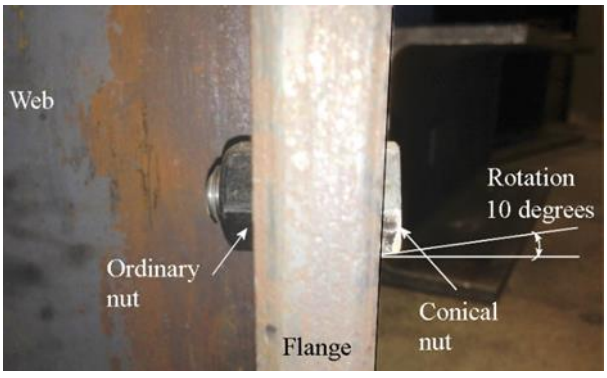

Fig. 5.15. Rotation of conical nut after LNSC Test 6

one where almost zero slip (i.e. < 0.86 mm) takes place and the only operated shear resistance is believed to be due to friction resistance between the plugs and the steel flanges. Once the frictional resistance is overcome, the second phase begins.

In the second phase, the LNSC behaves almost linearly with less stiffness until 131 kN (66% of ultimate load) at 1.78 mm slip (i.e. stiffness of 34 kN/mm). It is believed that two mechanisms are activated in this phase: formation of two plastic hinges (see Fig. 5.16), and bearing compression of the surrounding concrete. The combination of these two mechanisms is called *dowel action*. Although the preload force is constant, the internal tensile force changed during the pushout test. Once a slip occurs, bolt bending and elongation follows, which results in an increase in the bolt tensile force. This develops tensile stresses along its outer flank and less tensile stress along the inner flank. Because the bolt has two bending curvatures, the shear plane takes an inclined profile extending between these two high tensile zones, as illustrated in Fig. 5.16. Adding to that, the resultant tensile force in the bolt changed to be an inclined force with two components. One component creates compression on concrete and the other counters the external applied force. It can also be concluded from what is seen in Fig. 5.16 that the deflected profile of the bolt is within the lower part, roughly about 40 mm above the steel-concrete interface. This represents approximately two and a half bolt diameters or one third of bolt length between the upper plate and the interface.

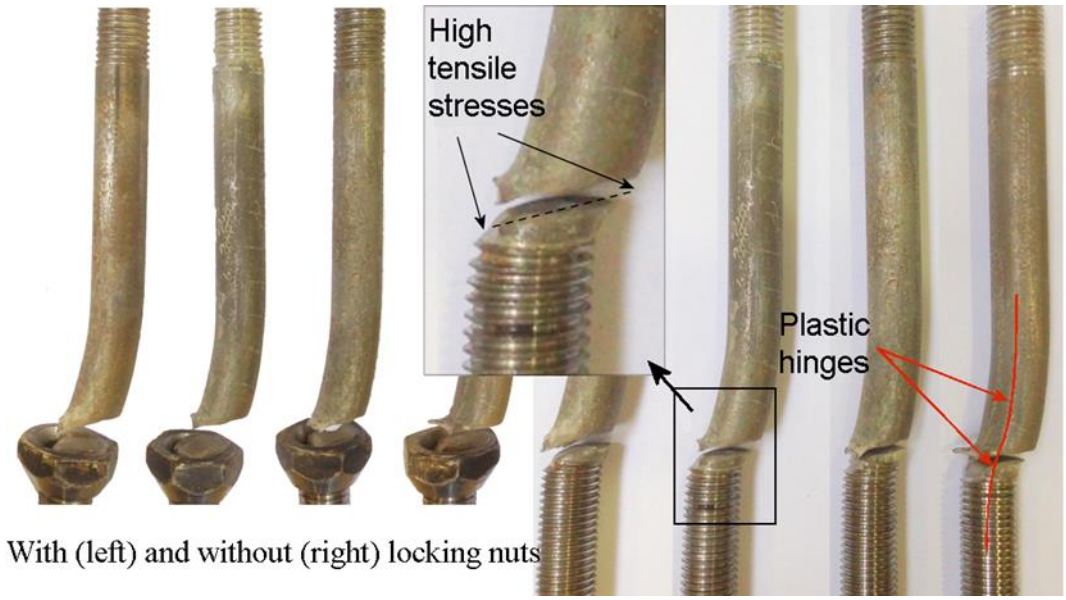

Fig. 5.16. Bolts deflected shape of LNSC pushout Test 6

The third phase started at 146 kN (73% of ultimate load) and 2.7 mm slip, and continued with an ascending linear response, but with lower stiffness of 6 kN/mm until ultimate failure at

198 kN and a slip of 12.2 mm. The failure was confirmed to be complete fracture failure of the four bolts, as can be seen in Fig. 5.16. The third phase is for a rapid increase in the flexural curvature of the lower plastic hinge due to shear deformations. This curvature leads to an increase in tensile stresses concentrated on the root of the first thread, indicating that the threads were not totally protected. At the end, crack initiated and rapidly propagated through the bolt cross-sectional area due to shear and tension forces at the same plane. It would be interesting to investigate what the change in shear resistance and slip capacity would be if the threads were completely hidden from the failure plane. This could be achieved by removing the chamfer finish from the upper open of the conical nut (see Fig. 4.33).

Replaceability was tested assuming no access to bottom side of (the bridge), and that all bolts have sheared-off. The steps are illustrated in Fig. 3.9. These steps were performed after push-out test. The idea was to make use of the 'deformed' shape of the bolts to create pull-out forces on the cones and on the whole pocket while keeping the slab still. The two plugs are grouped together by the grout as one unit, as Test 6 failure was local and did not significantly affect the grout.

Similar to previous pushout tests, the slabs were in near perfect condition after the test and the only failure observed was small local concrete wedge below each bolt as seen in Fig. 5.17.

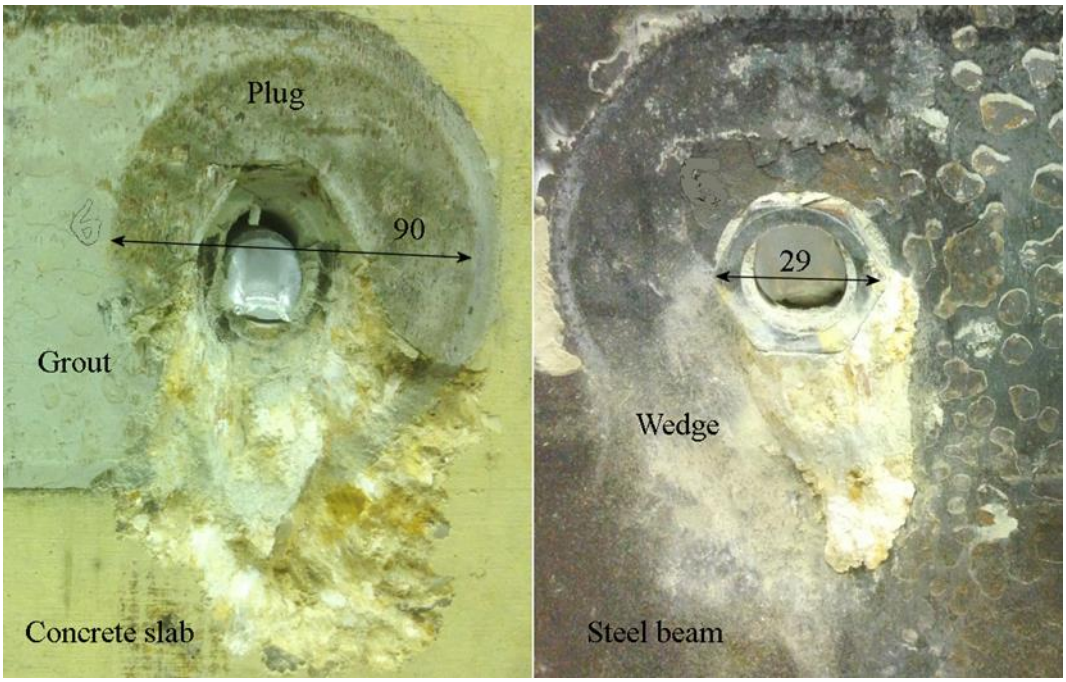

Fig. 5.17. LNSC Concrete wedge failure in pushout Test 6

The large surface area of the oval pocket participates to decrease the compressive and tensile stresses in the slab. The imprints on the steel flanges confirmed the concrete wedge failure, Fig. 5.17, without showing significant signs of frictional resistance scratches, as usually observed in friction-based push-out tests (see Chapter 6). It is worth mentioning that the steel flanges were not subjected to any special surface treatments in a trial to represent the expected situations in the field.

The pushout specimen was fixed at the lower end of each slab by grouting to the floor while the upper end was hinged by a steel ball. The function of ball is to prevent any possible specimen rotation from reaching the lifting cylinder or loading cell. Two transducers were used to check the movements of the upper end of the steel beam which represent the eccentricity of the applied point load. The cause of the eccentricity can be due to several factors related to tolerances in specimen dimensions and position or different performances between the four bolts. Fig. 5.18(a) specify common useful notations like 'flange direction', 'web direction', and bolts 1 to 4 locations. From the start of the test, an eccentric loading was recorded. At failure, the eccentricity reached a maximum of approximately 9.0 mm in the flange direction, which represents less than 1-degree rotation from the vertical axis. The 9 mm horizontal movement occurred with the existence of the ball joint, which is supposed to prevent any transversal movement. This means that the point load with its supports (testing rig) had moved slightly. The web direction experienced less movement being -1.7 mm at the ultimate load. As a result, it is expected that the two bolts (1 and 2) in the direction of the flange are having higher slips than the bolts on the opposite side (3 and 4). The point load is not perfectly distributed among the four bolts; being larger in the direction of movement and lesser in the opposite direction. A rough correction relationship using bilinear interpolation is suggested for such issue by having separate load components that corresponds to each bolt and to each slip.

Fig. 5.18b shows simulation of the five forces acting at the same elevation. These forces are the total applied load *P* (i.e. hydraulic jack) and the corresponding four load components for each bolt (i.e. P_{B1} to P_{B4}). *D*x and *D*y are the eccentricities of *P* from the centre. The variables *'a'* to *'d'* are the Cartesian distances of the eccentric load *P* to the bolts such that $a + b = 100$ mm, and $c + d = 260.3$ mm. The location of the eccentric *P* is therefore decided by $a = 50 + D\text{x}$, $b = 50 - D\text{x}$, $c = 130.15 + D\text{y}$, and $d = 130.15 - D\text{y}$. Using bilinear interpolation, the load components will be

$$P_{\text{B1}} = \left(\frac{a}{a+b}\right)\left(\frac{d}{d+c}\right)P \qquad (5.2)$$

$$P_{\text{B2}} = \left(\frac{a}{a+b}\right)\left(\frac{c}{d+c}\right)P \qquad (5.3)$$

$$P_{B3} = \left(\frac{b}{a+b}\right)\left(\frac{d}{c+d}\right)P \qquad (5.4) \qquad\qquad P_{B4} = \left(\frac{b}{a+b}\right)\left(\frac{c}{c+d}\right)P \qquad (5.5)$$

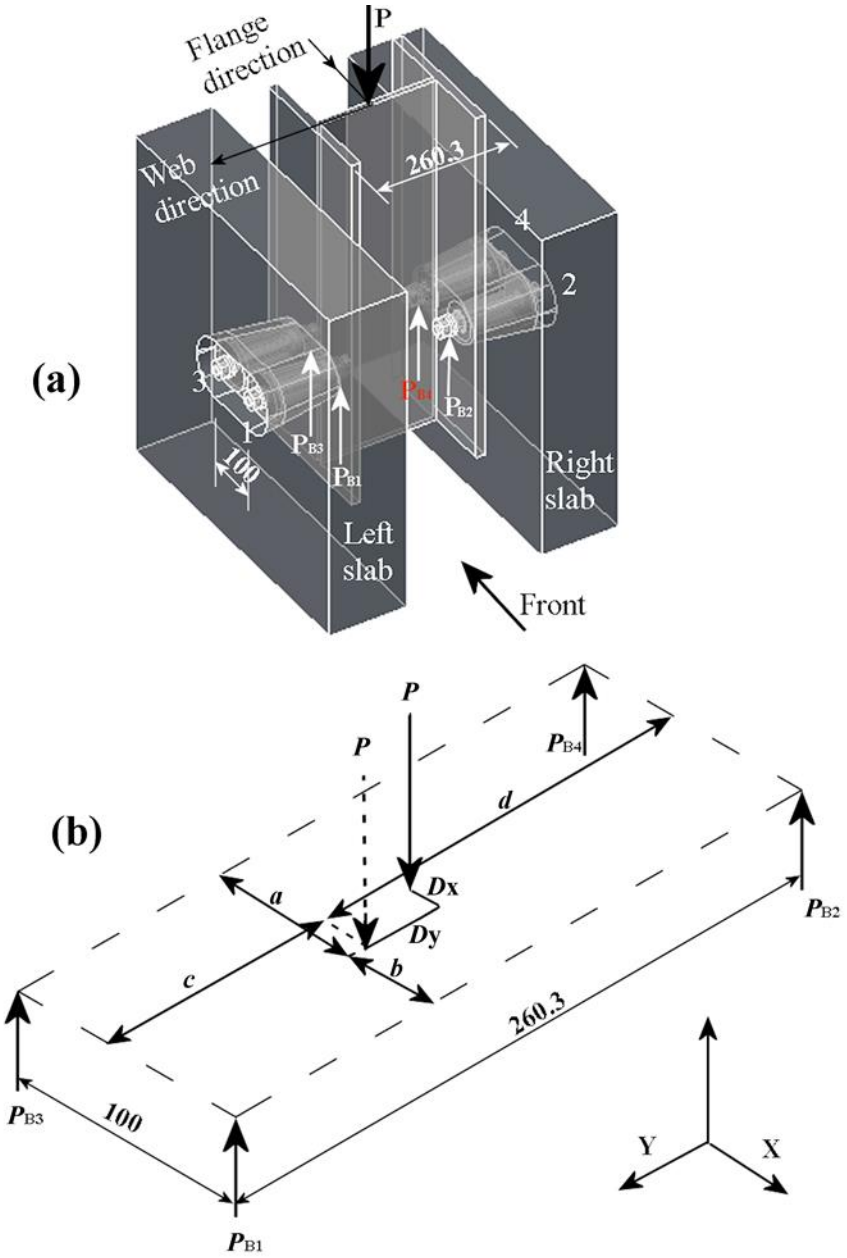

Fig. 5.18. Pushout specimen showing (a) common notations and (b) simulation of forces

Fig. 5.19 is a plot of the load-slip measurements at bolts 1 to 4 shown in Fig. 5.18. The figure shows five load-slip curves. The first four curves belong to the four bolts, while the fifth curve represents their mean. Each of the four curves has its own 'calculated' load and its own 'measured' slip, while the mean curve uses load *P* divided by four and average slip. It should be noted that in Fig. 5.19 there is no interpolation for slip values and the slips are the measured values near each bolt. It should be further noted that different dash type segments

(1 mm slip) were added to the end of each curve to help the reader to distinguish between the curves. Bolts 1 and 2 record the highest slip (at 15 mm). As can be seen from Fig. 5.19, the slip difference between the two sides in the direction of the flange (i.e. between bolts 1-2 and bolts 3-4) is continually increasing with loading until it reached a maximum of about 5.0 mm at failure. It is not clear if this is the result of the eccentric loading alone or in combination with other factors, like differences in bolts preloading. For this reason, the standard push-out test according to Eurocode 4 is based on using the studs in two levels, and four studs in each slab. As stated earlier, the failure of Test 6 was by shearing off all the bolts; therefore, the deviation of Fig. 5.19 is accepted.

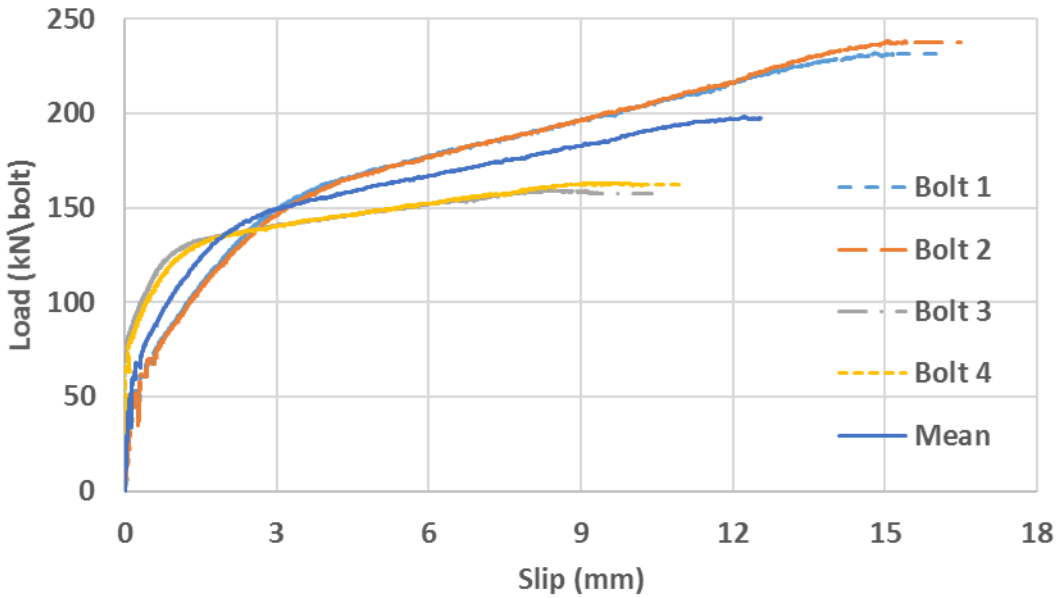

Fig. 5.19. Redistribution of load among 4 bolts of LNSC pushout Test 6

Plots for slabs separations (uplifts) are shown in Fig. 5.20. It is interesting to note that the right slab moved inwards toward the steel section and opposite to the left slab (refer to Fig. 5.18a for left and right slab positions), which indicates that the transducer readings were not only for slab separation measurements. Other effects of specimen tilting or shifting of load were also recorded. It should be noted that as the current pushout test has a single row of shear connectors, the connection between steel and concrete behave as hinges that cannot resist rotation. The behaviour above 125 kN/bolt shows different trends. This might be related to the third phase of the response and to the formation of concrete wedges (Fig. 5.17). The wedges are inserted in between the slab and the steel, and hence, increased separation. However, all the separations, until failure, were very small in comparison with the slips. Up to 25% of shear resistance, the separation of both slabs where almost zero. It is noteworthy that these measurements were taken at the upper end of the slabs; therefore,

slabs separations at bolts level would be, by linear interpolation, 50% of what shown in Fig. 5.20.

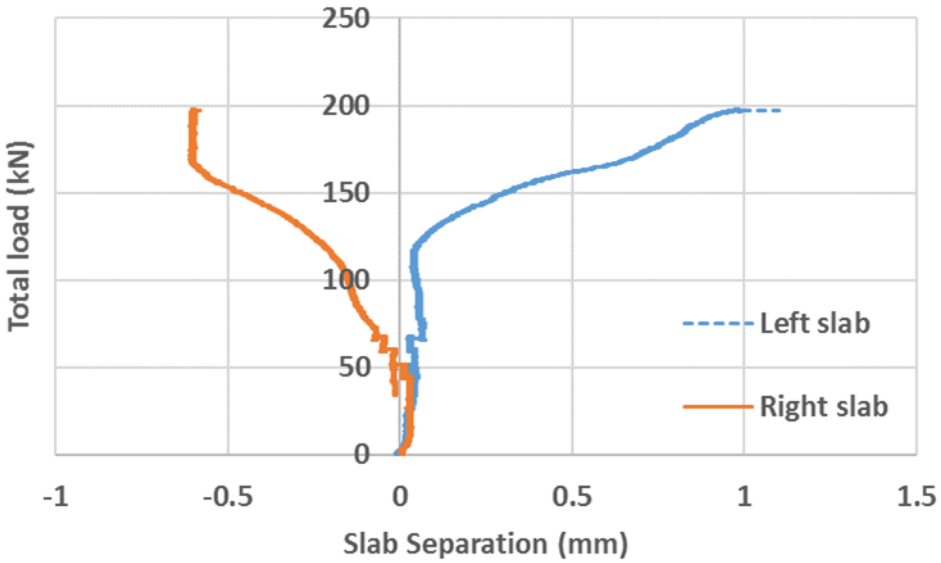

Fig. 5.20. Slab separation during LNSC pushout Test 6

Fig. 5.21 compares the shear load-slip displacement behavior from Tests 1 to 6 and highlights that the novel structural details of the LNSC in Test 6 result in superior structural performance including shear resistance, stiffness, ductility, slip capacity, and uplift capacity. All the tests show comparable initial stiffness. This is mainly due to friction resistance. It can be concluded from the figure that the sudden slip shown in Tests 1 to 5 is successfully eliminated in Test 6. Such sudden slip was also observed in all bolted shear connectors reviewed in Chapter 2. This has been done using the locking nut connection.

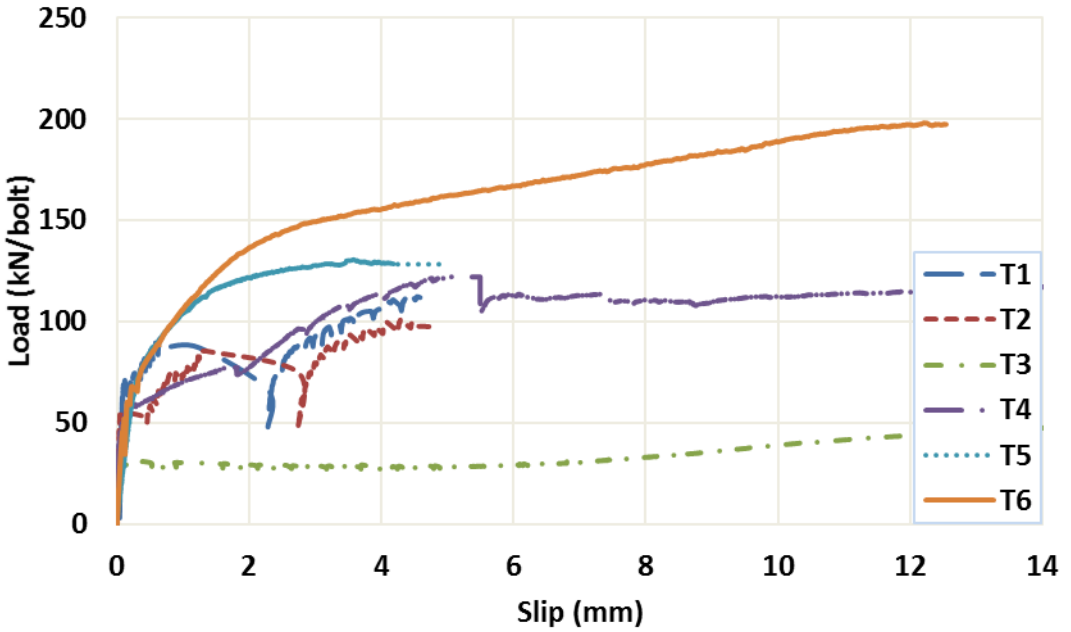

Fig. 5.21. Comparison of load-slip behaviour from LNSC pushout Tests 1 to 6

Test 6 has a higher shear resistance as compared to Tests 1 – 5 for the following reasons: (1) The failure mode consists of shearing off simultaneously the four bolts at the smooth inclined shank of the bolt (see Fig. 5.16). Shearing the four bolts means that the shear resistance is the average, which is the highest value that a pushout test can reach from the point view of test setup. (2) The smooth shank has a cross-sectional area larger than that of the threaded part. (3) Shearing the bolt at an inclined angle will result in a larger elliptical cross-section area as compared to a circular one, when the shearing is done at a right angle (i.e. Tests 1-5).

5.2.2 Characteristic Shear Resistance of LNSC

Design of composite structures is generally based on characteristic resistance of structural members. This is because of the variation of material properties, namely those of concrete slab, steel beam, and shear connectors. Normally, three pushout tests are conducted on nominally identical specimens to determine the characteristic shear resistance P_{Rk} per connector. If all three results are within 10% of mean shear resistance, then from Johnson (2012), and Eurocode 4 (BSI 2004a), $P_{\mathrm{Rk}} = 0.9\, P_{\mathrm{min}}$, where P_{min} is the lowest of the three measured shear resistances per connector.

The results from pushout Test 6 were followed by two additional push-out tests (i.e. Tests 11 and 12 in Table 4.2) with approximately the same test setup, test method and material specifications. Table 5.1 lists the shear resistances and slip capacities from the 'identical' Tests 6, 11, and 12. The very close agreement between the tests (CV are 2% and 6%) is evidence of consistent test procedures. The deviation (difference) of any individual test result from the average shear resistance is about 2%. This is significantly below the above-mentioned 10% limit of Eurocode 4. Thus, the characteristic shear resistance of the LNSC is $P_{\mathrm{Rk}} = 0.9 \times 189.5 \approx 171$ kN.

Table 5.1. Results of Tests 6, 11, and 12

Test No.	Shear resistance (kN/bolt)	Slip capacity (mm)
6	198.1	12.2
11	196.7	13.9
12	189.5	13.8
Average	194.8	13.3
Standard deviation	3.76	0.779
Coeff. of variation CV %	2	6

Fig. 5.22 compares the shear load-slip displacement behavior from Tests 6, 11, and 12. It should be noted that small dashed segments were added to the end of Tests 11 and 12 curves, to help the reader to distinguish between the curves. The load–slip curves were

consistent up to the maximum load. The subsequent curves agreed well until bolts fracture failure (where 6% differences in slip can be noticed). The results highlight that the robust structural details of the LNSC result in superior strength, superior initial stiffness, large slip capacity, and repeatability in the load-slip behavior as compared to previous connectors reviewed in Section 2.5.

In general, it is not possible for common conventional welded studs to establish such consistency in load-slip curves of push-out tests, and have a variation of shear resistance results of < 10% (see Fig. 2.3 and Xue *et al*. 2008). Moreover, Suwaed *et al*. (2016) provides a comparison among the LNSC and previously proposed demountable shear connectors (Section 2.5), and shows that the LNSC presents the highest shear resistance. It should be stated that the slight difference (6% in Table 5.1) in slip capacity between pushout Test 6 and the other two tests (11 and 12) is because of the countersunk seat finish of the upper opening of the locking conical nut. Some of the threads of the bolt in Test 6 were vulnerable to shear failure plane, while in the other tests, the threads were completely hidden and excluded from the failure shear plane.

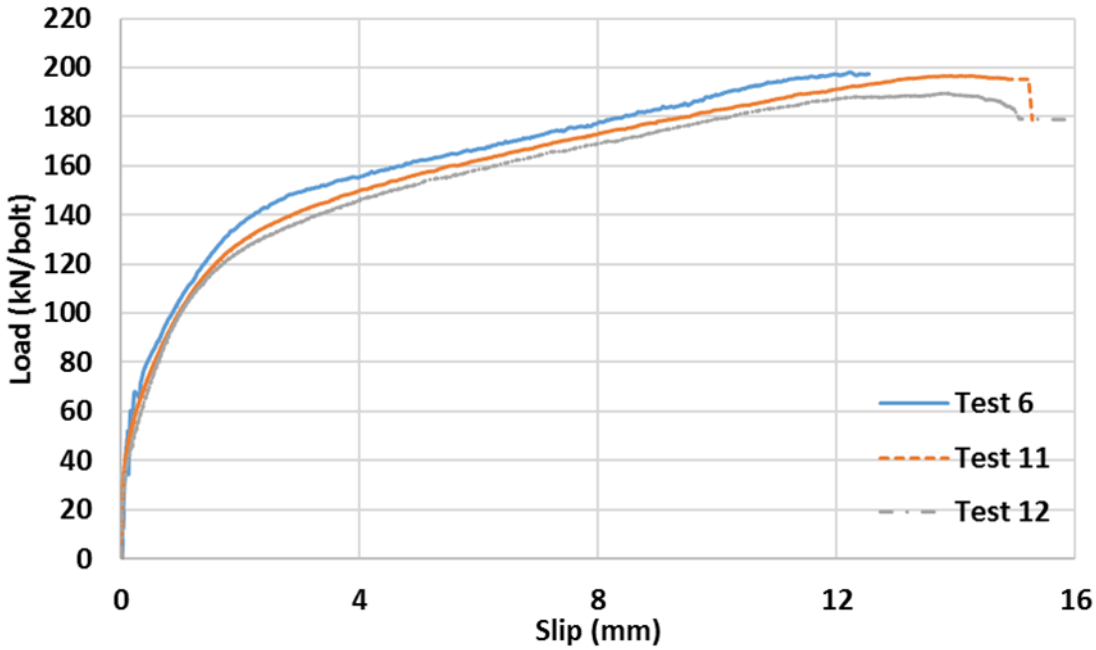

Fig. 5.22. Behaviour of LNSC from three identical push-out Tests (6, 11, and 12 in Table 4.2)

5.2.3 Comparison with Welded Studs

The shear resistance of the LNSC from Test 6 is equal to 198.1 kN for a concrete slab strength equal to 41 MPa, bolt diameter equal to 16 mm, and bolt tensile strength equal to 889 MPa.

According to Eurocode 4 (BSI 2004a), the shear resistance of welded shear studs is calculated as the minimum of (omitting the design partial factors)

$$P_{\mathrm{R}} = 0.8\, f_{\mathrm{u}}\, \pi \frac{d^2}{4} \tag{5.6}$$

and

$$P_{\mathrm{R}} = 0.29\, d^2 \sqrt{f_{\mathrm{ck}} E_{\mathrm{cm}}} \tag{5.7}$$

where d is the shank diameter of the welded stud, f_{u} is the ultimate tensile strength of the steel material of the stud, f_{ck} is the characteristic compressive cylinder strength of the concrete slab, and E_{cm} is the elastic modulus of the concrete. f_{ck} and E_{cm} can be calculated using the procedure used by Dai *et al.* (2015). By substituting, in Equations (5.6) and (5.7), the concrete slab strength (not plug strength), stud diameter, and tensile strength of the LNSC from Test 6, the shear resistance of the corresponding welded shear stud is calculated to be equal to 73 kN from Equation (5.7). Although this is nominal resistance, but similar values were obtained from tests conducted by Xue *et al.* (2008). Thus, the shear resistance of the LNSC is significantly higher (i.e. approximately 2.7 times higher) than that of comparable welded studs. The reasons for this are as follows, (1) using high strength steel (e.g. Grade 8.8 and above), (2) using high strength concrete (80-100 MPa) for the plugs, (3) the failure mode is due to steel bolts fracture and not to concrete splitting, (4) using smooth flowable grout around the bolts without variation in voids or aggregates sizes, (5) using friction resistance between the concrete plug and the steel flange, (6) shearing-off the bolts through their smooth shanks, (7) the shearing plane is of elliptical cross-section and not circular. It is noted that although a tensile strength of 889 MPa was used for the welded shear studs in the above calculations, Eurocode 4 does not allow the use of welded studs with tensile strength higher than 500 MPa (BSI 2004a); possibly because welding steel structural elements of dissimilar steel material grades (i.e. steel stud and steel beam) is not permitted (Clause 4.2.4 of BSI 2016). 'It should be noted that increasing amounts of carbon and manganese, which are necessary for higher strengths, make the steel harder and consequently more difficult to weld' (Ellobody 2014). Moreover, even if a stud with steel strength higher than 500 MPa could be used, the previous comparison shows that concrete strength would again govern the shear resistance.

The slip capacity of the LNSC from Test 6 is 12.2 mm, i.e. two times higher than the ductility limit of 6.0 mm for slip capacity of welded studs in Eurocode 4 (BSI 2004a) or the 1/3

diameter as recommended by Oehlers and Coughlan (1986). This large slip capacity could be exploited in the design of very long composite beams on the basis of the partial interaction theory (Johnson and May 1975). Partial interaction designs for very long beams cannot be achieved with welded shear studs due to their limited slip displacement capacity (Johnson 1981). Furthermore, it has been found that even the 6.0 mm slip capacity is not always feasible in common conventional welded studs, especially using lightweight concrete or profile sheeting (Johnson and Yuan 1998a).

It has been found (Johnson 2012) that the results of the pushout tests based on common conventional welded studs are widely scattered (e.g. see results in Xue *et al.* 2008). The LNSC does not show appreciable scatter in its behaviour (see Fig. 5.22) compared to the scatter seen in the behavior of welded shear studs, despite using the same test procedure of Eurocode 4. The alteration in welded studs shear resistance can be up to +/- 30% (Oehlers 1980). The main reason is that the smooth flowable grout used to fill all gaps between the elements in LNSC ensures uniform distribution of bearing stresses in the conical nut - grout, bolt shank - grout, and plug - grout interfaces. Such uniform distribution of bearing stresses cannot be ensured in the area around the collar of welded shear studs due to the existence of voids and/or the variation in local arrangement of the aggregate particles (Johnson 2004). Furthermore, as diameter of stud decreases, the scatter increases because of the corresponding collar size in relation to that of aggregate particles (Oehlers 1980).

5.2.4 Load – Slip Behaviour and Failure Mode

The shear force transfer mechanism of the LNSC initiates with friction forces in the steel flange - concrete plugs interface. The concrete plugs transfer these forces into the slab through the grout at their interfaces. When the shear forces exceed the friction resistance in the steel flange – concrete plugs interface, incremental slip occurs. Then apart from friction, shear forces are also transferred from the steel flange into the conical nut and the bolt shank through bearing. The conical nut and bolt shank transfer forces to their surrounding grout. Finally, these forces are transferred to the concrete plugs and then into the slab through the grout.

It should be noted that concrete is significantly stronger in triaxial compression, i.e. stresses can reach values equal to ten times the cylinder strength (Johnson 1967). Although there is no systematic research work on the relation between connector strength and the degree of containment of the connector (Yam 1981), Oehlers and Bradford (1995) estimate that the concrete adjacent to the collar of a welded stud can withstand 7.0 times its cylinder strength.

The part of the concrete plug in front of the conical nut is under nearly tri-axial stress confinement conditions. These conditions are compression of plug due to bolt preload, bearing of the bolt shank against plug and slab, and the restraint provided by the surrounding reinforcement in the slab. The plug, therefore, can develop stresses much higher than its 80-100 MPa cube compressive strength (listed in Table 4.2). Therefore, bolts will always shear off before a concrete plug fails. On the other hand, the existence of grout of ordinary strength (designed in Section 4.4.5) enables the bolts to deflect by crushing/powdering of the grout at the plug–bolt interface. Such bolt deflection enables the LNSC to develop its large slip capacity (i.e. >> 6 mm), absorb more energy, and ensure a ductile failure mode.

The shear load-slip displacement behavior of the LNSC (see Fig. 5.22) consists of three phases. The first phase covers slip displacements from 0.0 to 1.0 mm where the shear load reaches values up to 100 kN, i.e. approximately equal to 50% of the shear resistance, which means that the stiffness of the LNSC for M16 bolt is 100 kN/mm. Similar stiffness can be offered by 19 mm diameter welded studs according to Eurocode 4 (BSI 2004a), which suggests a superior stiffness with LNSC. Fig. 5.23 plots the results of pushout Test 12 for slip displacements up to 1.0 mm and shows that no slip occurs for shear loads lower than 12 kN.

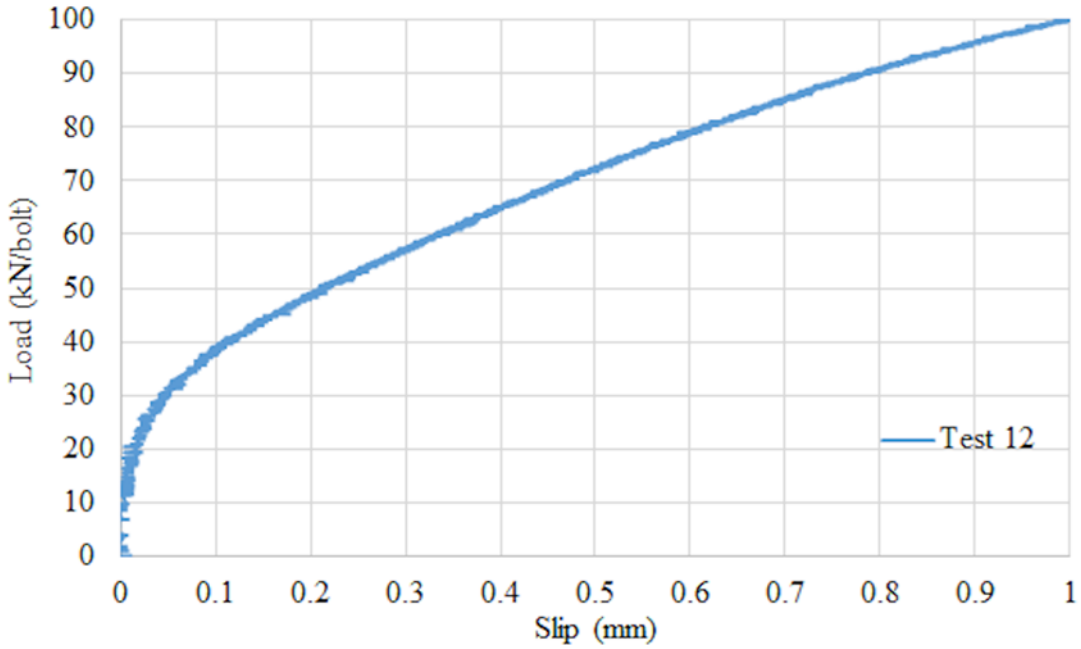

Fig. 5.23. Results of Test 12 for slip displacement up to 1.0 mm

This initial non-slip behavior is due to friction within the steel flange– concrete plugs interface. A friction resistance equal to 12 kN indicates a value of the friction coefficient equal to 0.5 (on the basis of the 26 kN bolt preload in Test 12 (see Table 4.2)), which is compatible with the recommendation of BS 5400 BSI (1979) and slightly below the 0.6 of BS EN 1993-2

(BSI 2006) for steel-concrete (uncoated and free from grease) interfaces. Please notice that bolt preloading is carried out before grout hardening, and therefore, 100% of the bolt preload is transferred as normal force into the steel flange-concrete plug interface. It should be mentioned that when the shear load exceeds the shear resistance, no sudden slip is seen in the behaviour of the LNSC due to locking nut configuration. Moreover, as the slip displacement increases, the length of the bolts increases and their internal forces slightly increase. The latter results in gradual increase of the friction resistance.

The second phase of the load-slip curve in Fig. 5.22 covers slip displacements from 1.0 to 2.5 mm where the shear load reaches values up to 130-150 kN, i.e. approximately equal to 75% of the shear resistance. In this phase, gradual yielding of bolts in combined shear and bending along with crushing/powdering of the grout in front of the conical nut and the bolt shank take place. At the end of this phase, the bolts form two short length regions of high plasticity (i.e. 'plastic hinges' due to combined shear, bending, and axial internal stresses) separated by a 30-40 mm undeformed length (as revealed from the defected shape of bolts after tests, Fig. 5.24).

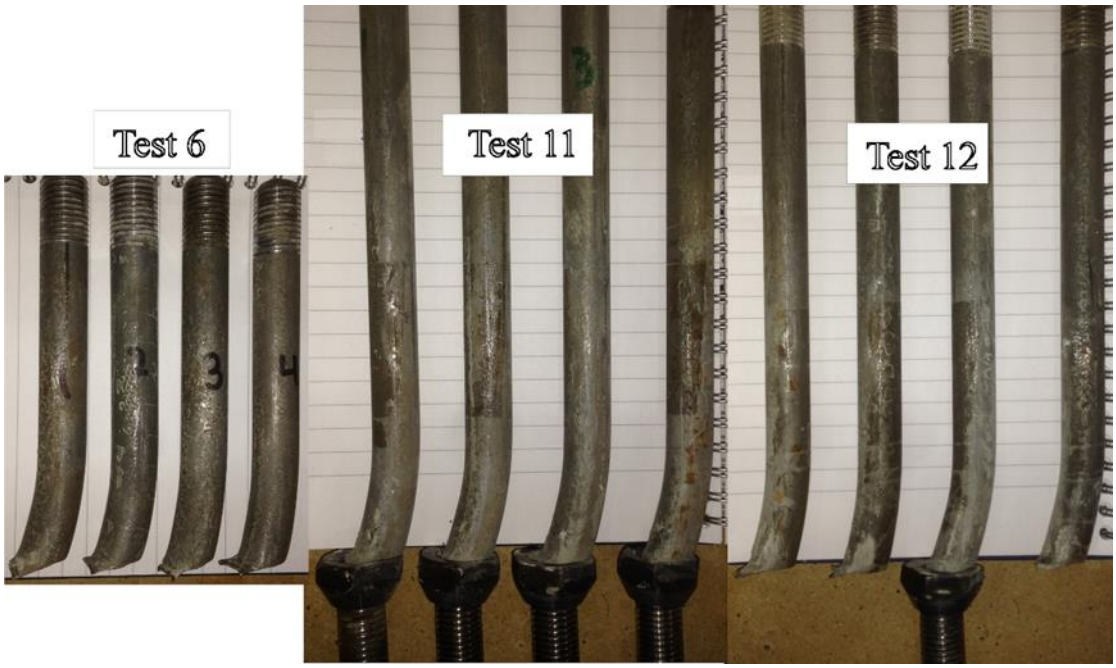

Fig. 5.24. Deflected shapes of the bolts from push-out Tests 6, 11 and 12

The last phase of Fig. 5.22 covers slip displacements from 2.5 mm to 14–15 mm, where the LNSC reaches its 180-200 kN ultimate shear resistance. The accumulated crushing\powdering of the in front grout and concrete plug form a concrete shear failure plane that passes through the grout-plug-grout-slab interfaces. The failure plane starts just

above the conical nut and ends just above the steel flange and forming a concrete wedge, see Fig. 5.17. The formation of concrete wedges shift the bearing stresses from the locking nut to the bolt shank, and finally leads to shear failure of the bolt shank through an elliptical cross-section just above the conical nut (see Fig. 5.24). It worth to notice that no necking zones were developed in the bolts of Fig. 5.24 as compare to Figs. 5.6 and 5.8 of Tests 3 and 4 respectively. This indicates that the tensile stresses in the bolts of the final design LNSC were below the yield strength.

It should be noted that deformations in the bolts of the LNSC are a combination of shear, flexural, and tensile deformations. Similar behaviour was observed in welded studs using advanced FEM models for the push-out test (Pavlović *et al.* 2013). The combination was 56% bending deformations, 37% shear deformations, and 7% tensile deformations. Unfortunately, this thesis does not contain FEM analysis, and no specific comparable combinations of deformations can be suggested. Even the two plastic-hinge failure mechanism was observed in welded studs (Molenstra 1990, and Ranković and Drenić 2002), as shown in Fig. 5.25 (for the complete definitions of Fig. 5.25 parameters, see Ranković and Drenić (2002)).

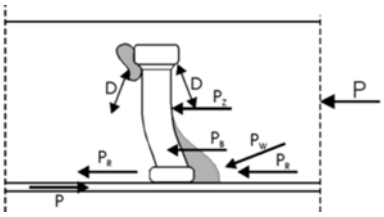

Fig. 5.25. Two plastic hinge mechanism of welded studs (Ranković and Drenić 2002)

It is interesting to note that concrete wedges in the slab were minor in the sense that they did not cause global cracking or splitting in the LNSC tests (see Fig. 5.26).

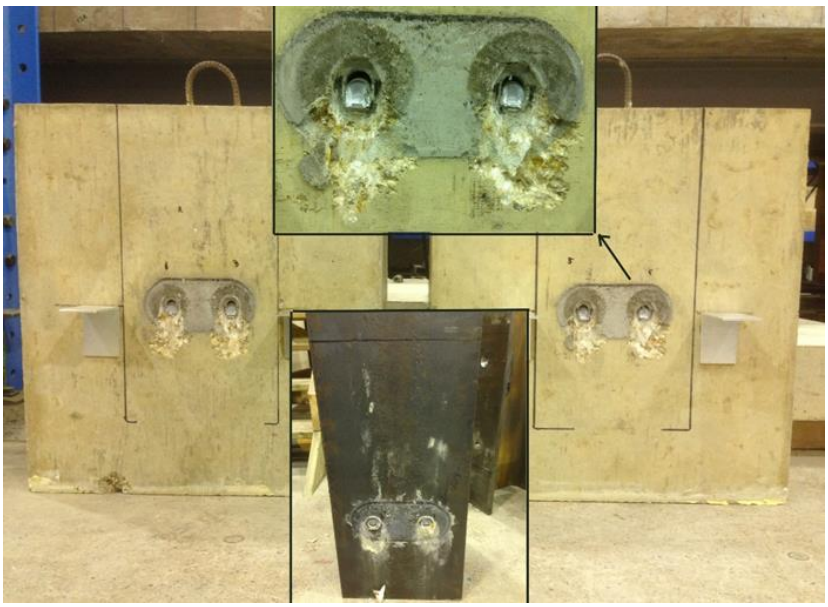

Fig. 5.26. Concrete wedges after push-out Test 6

The latter implies that contrary to welded studs, there is no need for additional reinforcement detailing in the transverse direction of the slab (Clause 6.6.5.3 of BSI 2005a).

5.2.5 Load – Slab Uplift Behaviour

Initially, during a standard pushout test, slabs compressed towards the steel beam (Oehlers and Bradford 1995, and Johnson 2012). Once a slip displacement occurred, an opposite behaviour is initiated. Slabs tend to separate, as they slide over the collar of welded studs (SCI 2016, Johnson 2012, and Hendy and Johnson 2006). Eurocode 4 (BSI 2004a) and other researchers (e.g. Yam 1981) recommend that the slab uplift (i.e. slab separation) should be no more than 50% of the corresponding slip displacement at a shear force equal to 80% of the shear resistance. Fig. 5.27 shows that the average slab separation, in Tests 6, 11, and 12, is less than 0.1 mm at 80% of loading, i.e. only 4% of the corresponding slip displacement.

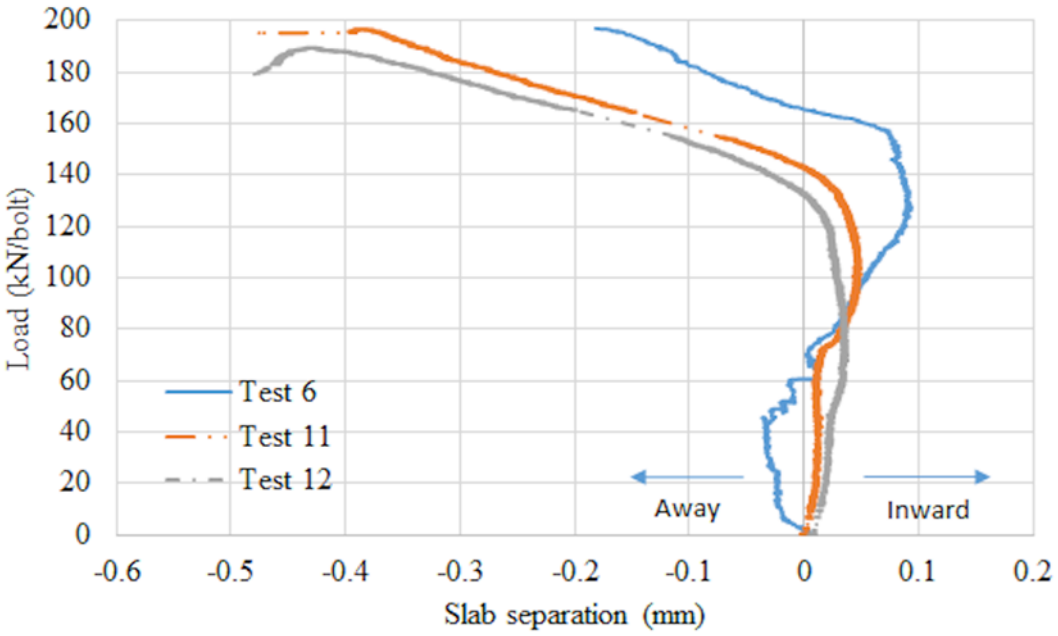

Fig. 5.27. Comparison of slab separation from Tests 6, 11, and 12

Pushout tests on welded studs of the same bolt diameter showed uplift displacements equal to 9-15% of the corresponding slip displacements (Spremić *et al.* 2013). A comparison of the three curves in Fig. 5.27 shows that Test 6 has the least separation (≈0.2 mm) as compared to Tests 11 and 12 (≈0.4 mm). This can be explained as follows. The only difference between pushout Test 6 and Tests 11 and 12 is in their slip capacities. Recalling that the main reason for slab separation is the tendency of slabs to ride up the conical nuts in the LNSC; Test 6 had relatively less slip as compared to Tests 11 and 12 (see Table 5.1), and hence less sliding of

the slabs over the conical nuts; and thereby less slab separation. It should be emphasized that such separations (0.2-0.4 mm) cannot considered to be serious as was the situation in blind bolts specimen shown in Fig. 5.28.

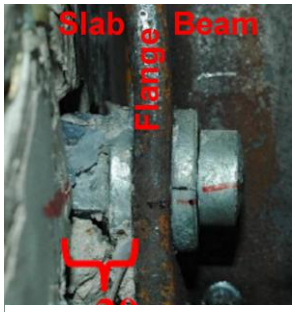

Fig. 5.28. Typical separation of blind bolts (Mirza et. al. 2010)

Fig. 5.29 shows the relationship between the average slip and the average tensile force of the bolts in Tests 11 and 12. Unfortunately, Test 6 did not used washer load cell to measure the tensile force. The figure indicates a linear correlation between the tensile force of LNSC and its corresponding slip displacement until fracture of bolts at about 15 mm slip. The tensile force at the onset of failure was 70-75 kN (i.e. 40% of the calculated bolt tensile resistance listed in Table 4.5). Furthermore, the angle of the line of action of this force from the vertical gradually increases as the slip displacement increases. Therefore, the internal bolt force has a vertical component that contributes to friction resistance and a horizontal component that directly contributes to shear resistance.

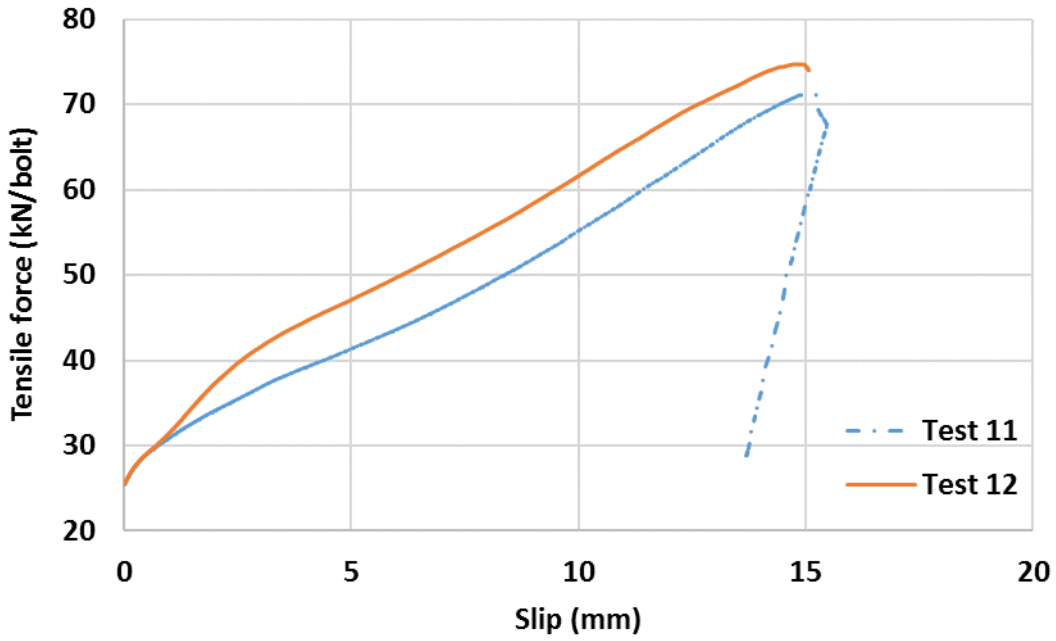

Fig. 5.29. Bolt tensile force-slip relationships from Tests 11 and 12

5.2.6 Design Equation

Eurocode 4 recommends that the shear resistance of a connector failing due to steel fracture to be calculated using Equation (5.6) (Hendy and Johnson 2006). As was mentioned repeatedly in this thesis (e.g. Section 5.2.1.6) that the failure mode of the LNSC is by bolt

fracture and not by concrete crushing/splitting. Thus, the shear resistance of the LNSC due to bolt shear resistance alone is (omitting partial design factors)

$$P_{\mathrm{R}} = 0.8\, f_u\, A_{\mathrm{s}}$$

In which, A_{s} is the cross-sectional area of the bolt's shank. For circular failure plane, $A_{\mathrm{s}} = \frac{\pi d^2}{4}$, and for elliptical failure plane, $A_{\mathrm{e}} = \pi \frac{d}{2}\frac{a}{2}$, where a is the maximum diameter of the ellipse and it is equal $a = \frac{d}{\cos\beta}$. Thus, $P_{\mathrm{R}} = 0.8 f_{\mathrm{u}} \frac{\pi d^2}{4\cos\beta}$

It should be emphasized that there is a tensile force T inside each bolt that is perpendicular to the steel flange. When the bolt slips, T will no longer be perpendicular, but it will be inclined from the vertical by an angle of β. T is transformed into two components. One component is vertical to the steel flange and equals $T_{\mathrm{V}} = T\cos\beta$, and the second component is horizontal and equals $T_{\mathrm{H}} = T\sin\beta$. T_{V} is responsible for the frictional resistance, as follows $P_{\mathrm{Friction}} = \mu\, T\cos\beta$, where μ is the coefficient of friction between concrete and steel. It should be mentioned that Eurocode 4 allows the addition of friction resistance to the calculated resistance of the shear connector, for example in composite columns using welded studs (BSI 2005a). The direction of T_{H} coincide with the direction of the bolt shear resistance, P_{R}. Thus,

$$P = P_{\mathrm{R}} + P_{\mathrm{Friction}} + T_{\mathrm{H}}$$

and by substituting and rearrangement,

$$P = 0.8 f_{\mathrm{u}} \left(\frac{\pi d^2}{4\cos\beta}\right) + T(\sin\beta + \mu\cos\beta)$$

In which, T is the tensile force in the bolts at the onset of failure. T was found (Section 5.2.5) to be equal to 40% of the calculated bolt tensile resistance listed in Table 4.5; therefore, $T = 0.4\, f_{\mathrm{u}} A_{\mathrm{s}}$, and $T = 0.4\frac{\pi d^2}{4} f_{\mathrm{u}}$. By substituting T into P

$$P = 0.8 f_{\mathrm{u}} \left(\frac{\pi d^2}{4\cos\beta}\right) + 0.4\frac{\pi d^2}{4} f_{\mathrm{u}}(\sin\beta + \mu\cos\beta)$$

and after rearrangement

$$P = \frac{\pi d^2 f_u}{4}\left(\frac{0.8}{\cos\beta} + 0.4(\sin\beta + \mu\cos\beta)\right) \tag{5.8}$$

Equation (5.8) indicates that shear resistance of LNSC is roughly proportional to the square of its diameter and depends on the ultimate tensile strength of the bolt material (but not the yield strength). A similar dependence can be found in conventional welded studs embedded in strong concrete (Yam 1981). For Tests 11 and 12, f_u is equal to 889 MPa from Table 4.5; d is equal to 16 mm from Table 4.2; μ is equal to 0.5; β is equal to 12.1° from Table 5.2. Substitution into Equation (5.8) gives a predicted shear resistance of 196.2 kN. This is < 1% higher than the average shear resistance from Tests 6, 11, and 12 listed in Table 5.1. It is interesting to note that by substituting μ = 0.5 and β = 12.1° into Equation (5.8), the shear resistance of the LNSC becomes equal to 1.1 times the bolt tensile resistance. The latter value is significantly higher than the pure shear resistance of a bolt of the same diameter, i.e. 0.6 times the tensile resistance (Equation 5.1). It can be concluded from this finding that, a connector deforming with multi-deformations for shearing, bending, and tension will have a higher shear resistance than a connector deformed in pure shear deformation. This is because the former connector can absorb more energy before failure. It should be noted that β measurements were performed after dismantling the pushout specimen.

Table 5.2. Angle 'β' of the deflected shape of the bolt from the vertical (in degrees) - M16 bolts of Tests 11 and 12

Test No.	Bolt 1	Bolt 2	Bolt 3	Bolt 4	Average
11	12.9	12.1	12.1	9.7	11.7
12	11.3	11.3	13.7	13.7	12.5
Average					12.1

5.2.7 Experimental Parametric studies

5.2.7.1 *Effect of Bolt Diameter*

Three bolt diameters, i.e. 12, 14, and 16 mm (while the rest of material properties and test setup are identical) were used in push-out Tests 7, 8, and 12 (see Table 4.2). The objective was to explore the validity of Equation (5.8), and to assess the slip capacity of the LNSC when the bolt diameter is less than the minimum allowed by Eurocode 4 (i.e. 16 mm). The shear load-slip displacement curves and the deflected shapes of the bolts from these tests are shown in Figs. 5.30 and 5.31, respectively. Results of these tests are listed in Tables 5.3 and 5.4 and show that all connectors have a slip capacity > the 6 mm limit in Eurocode 4 (BSI 2004a)) regardless of using diameters less than the minimum limit of 16 mm. Moreover, the values of the 7th column in Table 5.3 confirm that the LNSC shear resistance can be approximately obtained as 1.1 times the bolt tensile resistance.

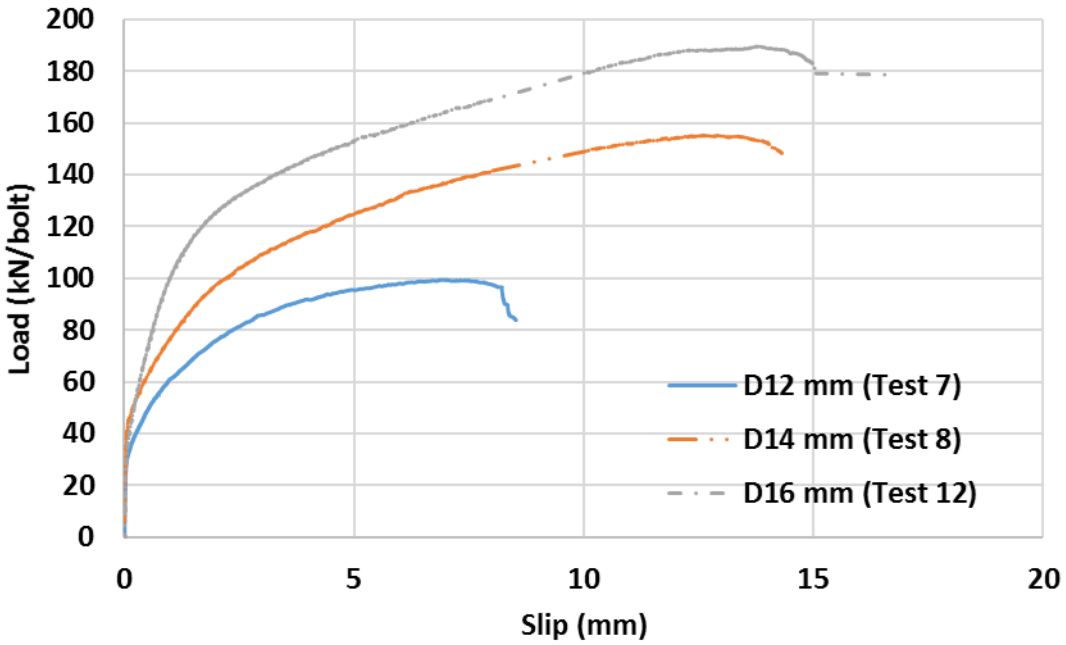

Fig. 5.30. Effect of bolt diameter on the load-slip behavior

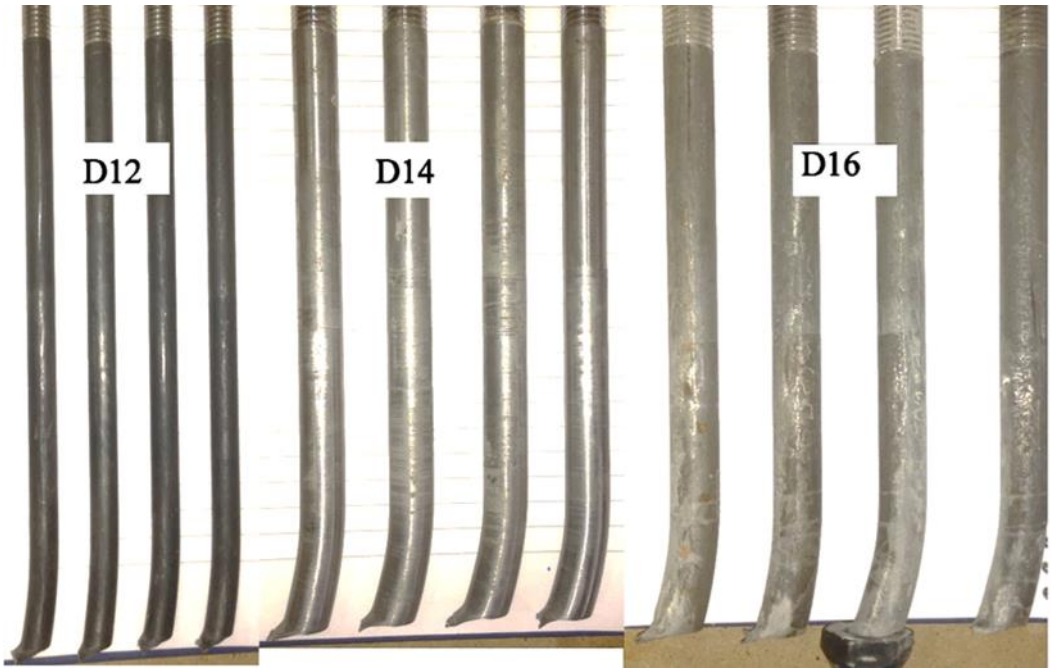

Fig. 5.31. Deflected shapes of D12, D14, and D16 mm bolts from Tests 7, 8 and 12

Substituting appropriate values for the M14 bolt into Equation (5.8) results in shear resistance equal to 149.2 kN, which is only 4% lower than the corresponding value in Table 5.3. Similarly, Equation (5.8) provides a shear resistance equal to 107.6 kN for the M12 bolt, which is only 8% higher than the corresponding value in Table 5.3. The above results show that Equation (5.8) is reliably predicting the resistance of LNSC for three different bolt

diameters in range 12 mm to 16 mm. It should be noted that Eurocode 4 defines having identical pushout tests as that with deviations in shear resistance of < 10% from the average.

Table 5.3. Results of Tests 7, 8, and 12

Test No.	Bolt dia. (mm)	Collar height (mm)	Conical nut width (mm)	Shear resistance (kN)	Slip capacity (mm)	Shear resist. / Bolt tensile resist. *	Bolt internal load / Bolt tensile resist. *
7	12	2.5	23	99.3	7.0	0.99	0.34
8	14	5.0	27	155.2	12.9	1.1	0.35
12	16	6.0	29	189.5	13.8	1.1	0.45
					Average	1.06	0.38
					Standard dev.	0.0596	0.0497
					CV %	6	13

***** Bolt tensile resistance is provided in Table 4.5

Fig. 5.32 shows the effect of bolt diameter on slab uplift displacement where the vertical axis represents the ratio of the applied load to the shear resistance, and the horizontal axis represents the ratio of the uplift displacement to the corresponding slip.

Table 5.4. Angle 'β' (in degrees) and length of deflected shape for M12, M14, and M16 bolts

Bolt Dia. (mm)	Bolt 1	Bolt 2	Bolt 3	Bolt 4	Avg.	Deflected length (mm)
12	7.7	9.9	8.5	9.9	9.0	28
14	10.5	11.3	11.3	12.1	11.3	35
16	11.3	11.3	13.7	13.7	12.5	40

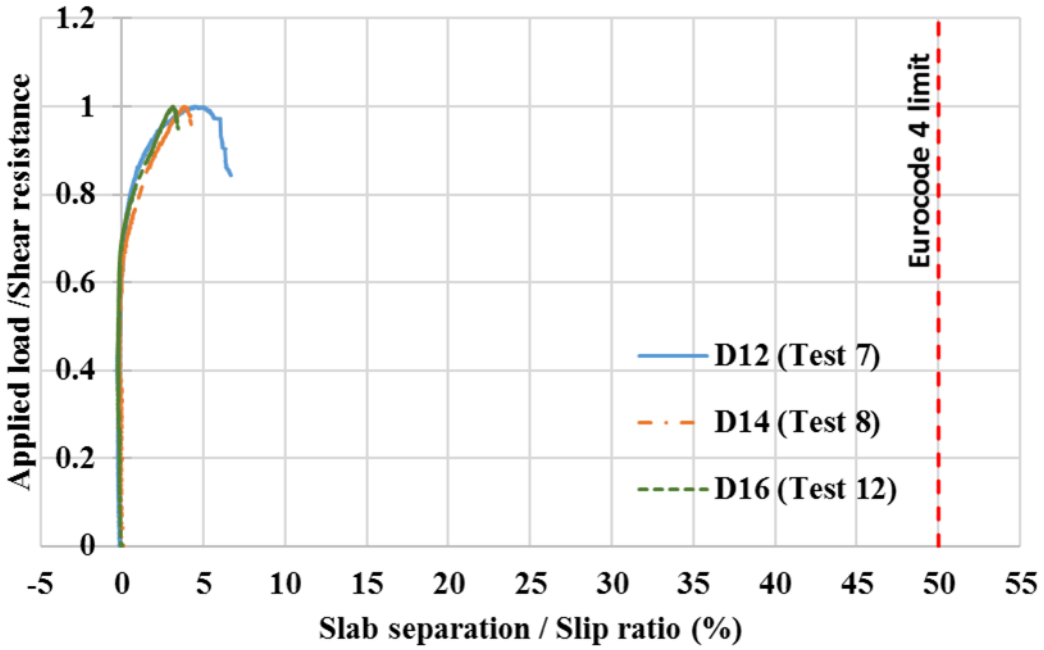

Fig. 5.32. Effect of bolt diameter of LNSC on slab uplift displacement

It is interesting to note that no uplift occurs for loads up to 60-70% of the shear resistance. Furthermore, at the onset of failure, the uplift displacements are equal to only 3%, 4%, and 5% of the corresponding slip for M16, M14, and M12 bolts, respectively, which are well below the limit of Eurocode 4.

5.2.7.2 *Effect of Plug Concrete Strength*

Push-out tests 10, 11, and 12 (see Table 4.2) investigated the effect of plug concrete strength (i.e. 50, 91, 96 MPa) on LNSC response. Test 9 used plugs having 80 MPa concrete strength, but because it failed due to accidental loss of bolt pretension, the measurements are not presented. The results of tests 10, 11, and 12 are presented in Tables 5.5 and 5.6, and in Figs. 5.33 to 5.37.

Table 5.5. Effect of plug concrete strength on M16 shear connector behavior

Test No.	Bolt diameter (mm)	Plug strength (MPa)	Shear resist. (kN)	Slip capacity (mm)	Shear resist. / Bolt tensile resistance*	β (degrees)
10	16	50	180.7	14.7	1.01	13.0
11	16	96	196.7	13.9	1.10	11.7
12	16	91	189.5	13.8	1.06	12.5

***** Bolt tensile resistance is provided in Table 4.5

Table 5.6. Comparison among the predictions of Equation (5.8) and the push-out tests results

Test No.	Bolt diameter (mm)	Plug strength (MPa)	β (degrees)	Shear resistance (kN)	Equation (5.4) (kN)	Difference %
7	12	91	9.0	99.3	107.6	8.0
8	14	95	11.3	155.2	149.2	-4.0
10	16	50	13.0	180.7	190.7	6.0
11	16	96	11.7	196.7	195.5	-1.0
12	16	91	12.5	189.5	196.8	4.0

Table 5.5 shows that changing the plug concrete compressive strength from C50 to C96 results in modest changes in the shear resistance (9% increase) and slip capacity (5% decrease) of the LNSC. These results further confirm that, unlike conventional studs which have 5 modes of failure (BSI 1994), or even 7 modes of failure (Johnson and Yuan 1998b), the LNSC has only one failure mode (for the parameters tested), i.e. bolt shear failure just above the locking nuts. It should be noted that concrete crushing failure is a non-ductile

failure mode and for that reason, it is not recommended, in current composite bridges practice, to use concrete of quality less than C35/45 (Vayas and Iliopoulos 2014).

Table 5.6 and Fig. 5.33 provide a comparison for the predictions of shear resistances from Equation (5.8) and the corresponding experimental values. It is shown that Equation (5.8) provides good estimations from five pushout tests with a maximum absolute deviation of less than 8%. It appears that Equation (5.8) can be used to predict the shear resistance of LNSC for: plug concrete cube strengths between 50-100 MPa; bolts with steel strength of 889 MPa; diameters from 12 to 16 mm; grout compressive strengths from 25 to 45 MPa; a full proof load of 88 – 106 kN between nuts 1 and 2 (see Fig. 3.3); an initial internal bolt force equal to 25 kN (which is usually achieved by ordinary wrench without preloading).

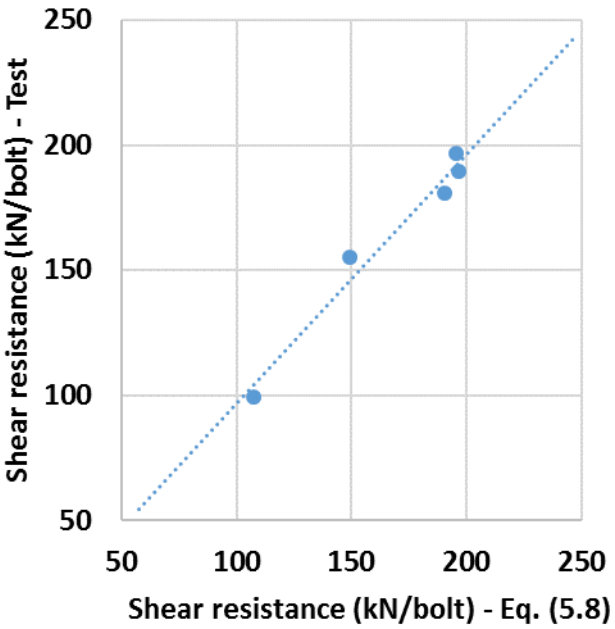

Fig. 5.33. Shear resistance comparison between the predictions from Equation (5.8) and the push-out tests

Fig. 5.34 shows the effect of plug concrete strength on the shear load–slip displacement behavior. The plug concrete strength has no effect for loads up to 32% of the shear resistance, which is similar to welded studs with concrete cube strength of the slab ranged from 20 to 70 N/mm (Oehlers and Coughlan 1986). An increase of the plug concrete strength from C50 to C96 increases the stiffness from 78 kN/mm to 106 kN/mm at a shear load equal to 50% of the shear resistance. Fig. 5.35 shows the bottom face of the slabs after failure of the specimens in Tests 10 and 11. No significant differences can be noticed between the C50 and C96 plug strength specimens. Moreover, Fig. 5.35 shows that concrete wedge has extended only within a 20-30 mm circular pattern inside the slabs.

Fig. 5.36 shows that as the plug concrete strength increases, less slab uplift displacement occurs. A 92% increase in plug concrete strength results in 33% reduction in uplift displacement at the onset of failure.

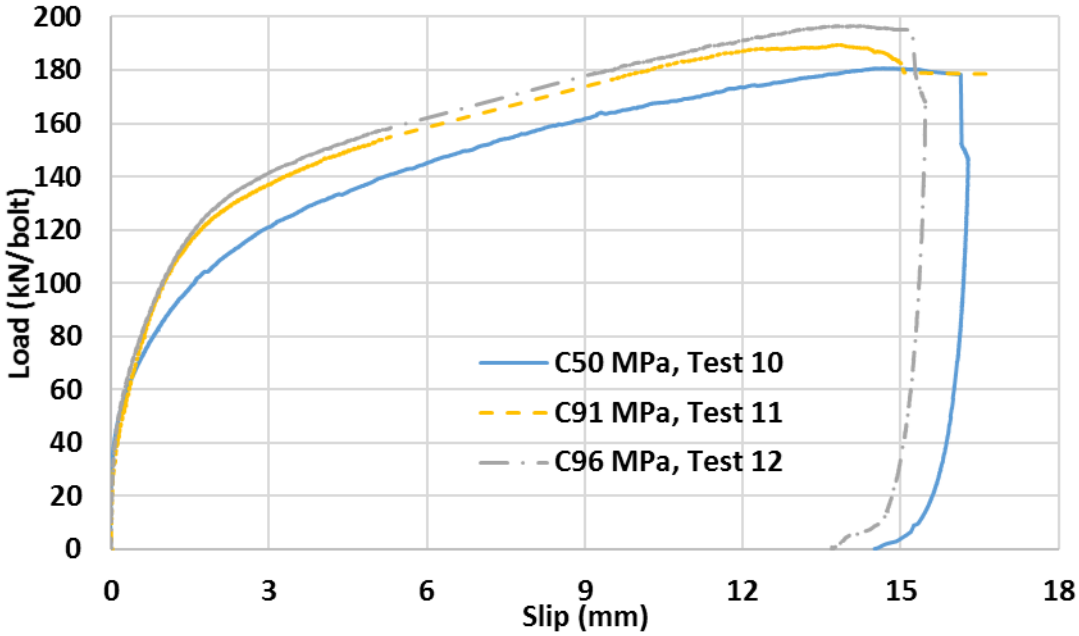

Fig. 5.34. Effect of plug concrete strength on load-slip behavior

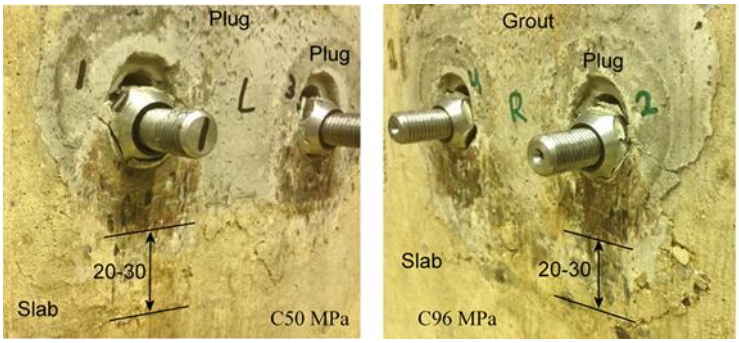

Fig. 5.35. Effect of plug concrete strength on concrete wedges

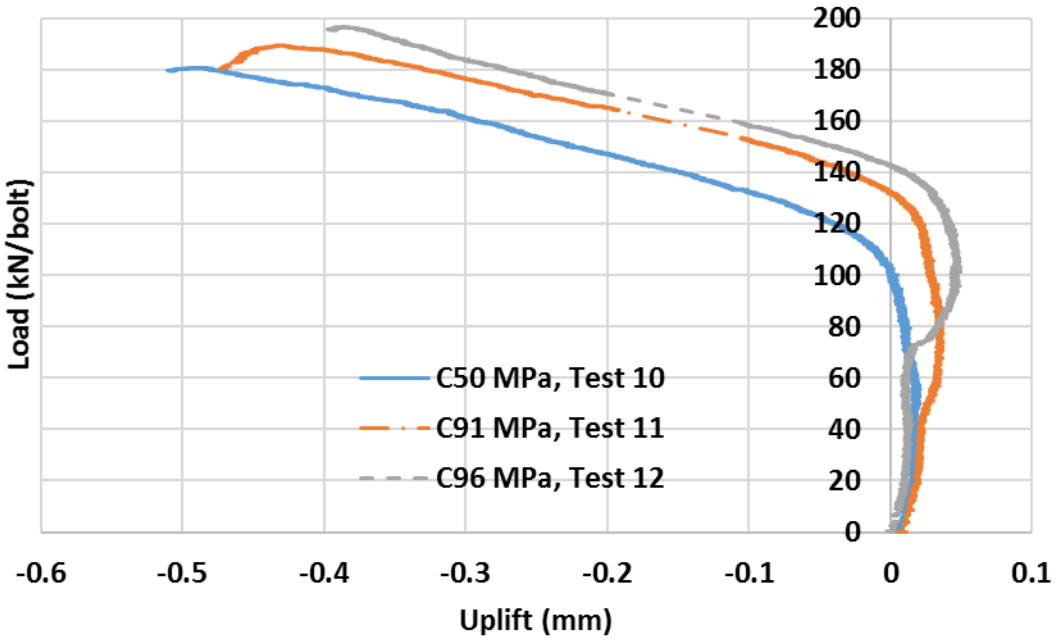

Fig. 5.36. Effect of plug concrete strength on slab uplift displacement

Fig. 5.36 also highlights that slab separation starts for loads higher than 50% of the shear resistance and has a maximum value that is < 0.5 mm at the onset of failure. These results further confirm that LNSC has superior stiffness and strength against slab uplift over comparable standard welded shear studs.

Fig. 5.37 shows the deflected shape of bolts after failure in Tests 10, 11, and 12. All bolts have similar deflected shapes; an observation that further indicates that plug concrete strength has little effect on LNSC response to shear loading.

Fig. 5.37. Deflected shapes of M16 bolts for different plug concrete strengths

5.3 Summary

The results of twelve LNSC pushout tests were presented and discussed in this chapter. The LNSC experimental evaluation started with six preliminary pushout tests. The results of the preliminary pushout tests promoted the author to identify optimum structural details of the LNSC (including locking nut, countersunk seat hole, hidden thread, separated conical plug, and oval conical slab pocket, flowable grout, plate washer) that led to superior demountability, strength (195 kN/bolt), slip capacity (13 mm), ductility, and uplift resistance (4% of slip). The chapter provided full insight into the behaviour and failure modes of the LNSC (including the three distinct phases of LNSC structural response, load-slip, load-uplift, and slip-bolt tensile force responses, and formation of two plastic hinges and dowel action). Meaningful comparisons with welded studs showed that the final LNSC shear resistance and slip capacity were 2.7 and 2 higher respectively. A simple design equation was suggested for the shear resistance of the LNSC with maximum deviation from the experimental average of less than 8%. Moreover, the results of the six parametric push-out tests were discussed in detail and highlighted the effect of bolt diameter and plug concrete strength on the LNSC behaviour.

Chapter 6: Results and Discussions of FBSC Pushout Tests

6.1 Introduction

The results of the FBSC pushout tests are presented and discussed in this chapter. The experimental program started with preliminary tests. These tests led to the development of the final robust details of the FBSC that provide demountability, superior shear resistance, slip capacity, ductility, and uplift resistance. The structural behaviour and mode of failure of the FBSC are discussed along with comparisons with welded studs. Finally, the results of the parametric experimental studies are presented with a useful design equation.

6.2 FBSC-Pushout tests

Eleven push-out tests were carried out with specifications listed in Table 4.3. These tests can be grouped into two categories: preliminary and final tests. The preliminary tests (Tests 1 to 6 in Table 4.3) are discussed in Section 6.2.1, while the final tests (Tests 7 to 11 in Table 4.3) are used to evaluate the characteristic shear resistance (Section 6.2.2)., and in two parametric studies (Section 6.2.7). Using the results of the final tests, a meaningful comparison with conventional welded studs is made (Section 6.2.3) and a design equation is proposed for the shear resistance (Section 6.2.6).

6.2.1 Preliminary Tests

The first six tests listed in Table 4.3 are preliminary and served to investigate how different design details influence the structural properties such as the shear resistance and ductility. Details of each of these tests were introduced and discussed in Chapter 4 (Section 4.5). The results of the preliminary tests led to the recommendation of the final robust structural details of the FBSC and they are discussed in detail in the following subsections.

6.2.1.1 FBSC Pushout Preliminary Tests 1 and 2

The description of the setups, specimens, material properties, test procedure, and test method can be found in Section 4.5.1. The load-slip curves of FBSC pushout tests 1 and 2 are shown in Figs. 6.1 and 6.2, respectively. The results in Fig. 6.1 show that the shear resistance of Test 1 is 57 kN/bolt and the slip capacity is 10 mm. The 25 load cycles (recommended by Eurocode 4 for identifying progressive slip premature failure) were included in Fig. 6.1 to show that even when the occurrence of load cycles is beyond the friction resistance limit, their effect on the overall performance of the test was negligible (i.e. < 0.5 mm slip). The results in Fig. 6.2 indicate that the shear resistance of Test 2 is 59 kN/bolt and the slip capacity is almost 12 mm. The resulting shear resistances of Tests 1 and 2 are 70% of the shear

resistance of high strength bolts (Grade 8.8) from Equation 5.1 and 80% of the shear resistance of comparable welded studs (Section 5.2.3). Fig. 6.3 shows the deflected shapes of the failed bolts after dismantling the pushout specimen. It can be seen from the figure that the bolts react mainly in shear without tensile or bending deformations.

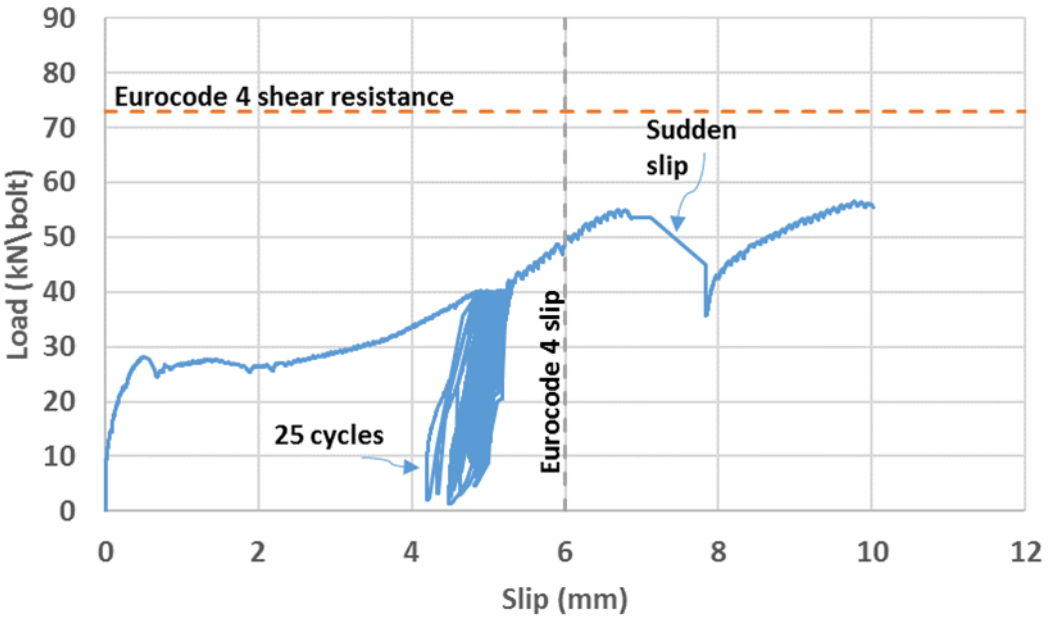

Fig. 6.1. Behaviour of FBSC Test 1

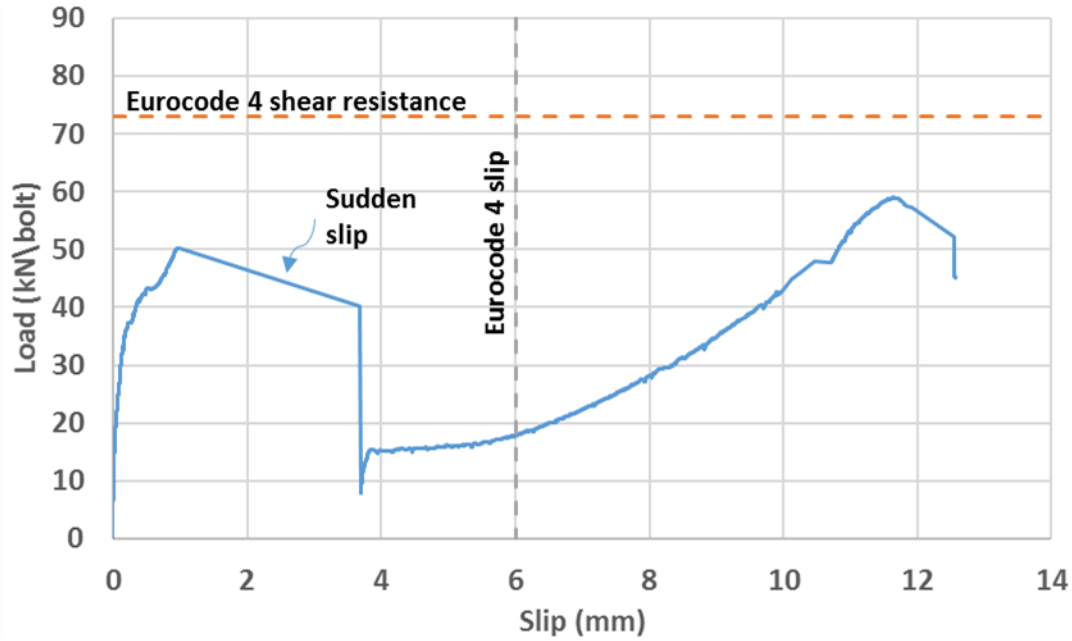

Fig. 6.2. Behaviour of FBSC Test 2

Tests 1 and 2 might experience eccentricities in loading, in specimen dimensions, in specimen position, and variations in preloads of bolts. In such cases, the resulted shear resistance is

more likely to be of the weakest bolt and not of the average. The photo in Fig. 6.3 supports this conclusion because it shows that not all bolts fractured.

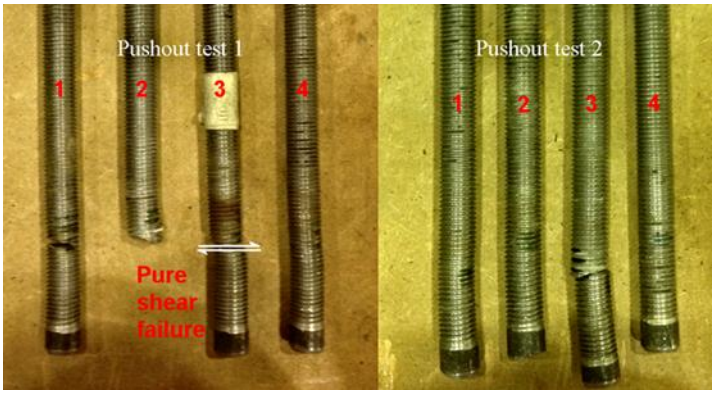

Fig. 6.3. Bolts deflected shape of Tests 1 and 2

Both tests achieved good slip capacity (i.e. 10-12 mm), and successfully exceeded the Eurocode 4 limit of 6 mm for ductile shear connectors. The maximum slab uplift displacement was 0.3 mm and 0.7 mm for Tests 1 and 2, respectively. The demountability was confirmed, as shown in Fig. 6.4, by using gentle taps with a plastic hummer that suggests that any mechanical pull-out method would work.

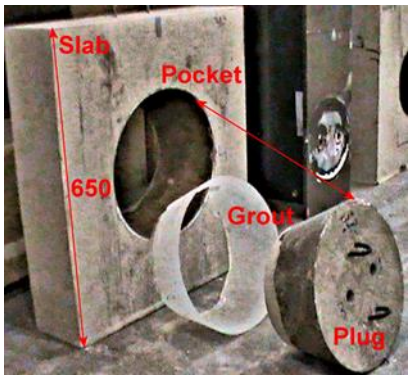

Fig. 6.4. Demountability of FBSC Test 2

Some cracks were observed after the tests in the centre of the concrete plugs, as shown in Fig. 6.5, which is believed to be the cause of plug tilting. The plug tried to tilt itself inside the slab pocket, i.e. the lower half of each plug tried to move up and slide over the slab pocket, similarly to LNSC Tests 1 and 2 (Section 5.2.1.1).

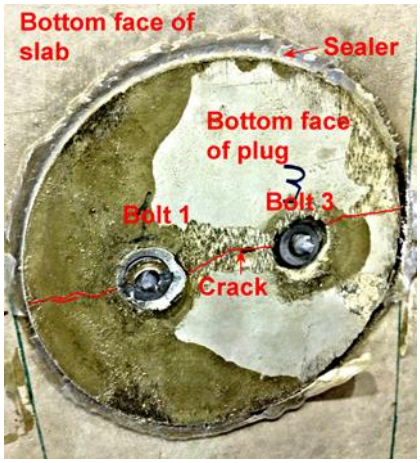

Fig. 6.5. Cracks in concrete plug of FBSC Test 2

6.2.1.2 FBSC Pushout Preliminary Test 3

The load-slip behaviour of Test 3 is shown in Fig. 6.6 and clearly represents an advance step in structural performance in comparison to the results from Test 1 and 2. The shear resistance of 89 kN and slip capacity of 7.3 mm are higher than the Eurocode 4 design limits (BSI 2004a). The slab uplift at the ultimate load was 0.18 mm. It seems that the usage of a locking countersunk seat and a nut in the inner side of the flange of the steel beam had contributed in reducing the sudden slip after friction resistance is overcome. However, it did not eliminate the sudden slip completely, which indicates that the slip should be controlled from the outer side of the flange of the steel beam.

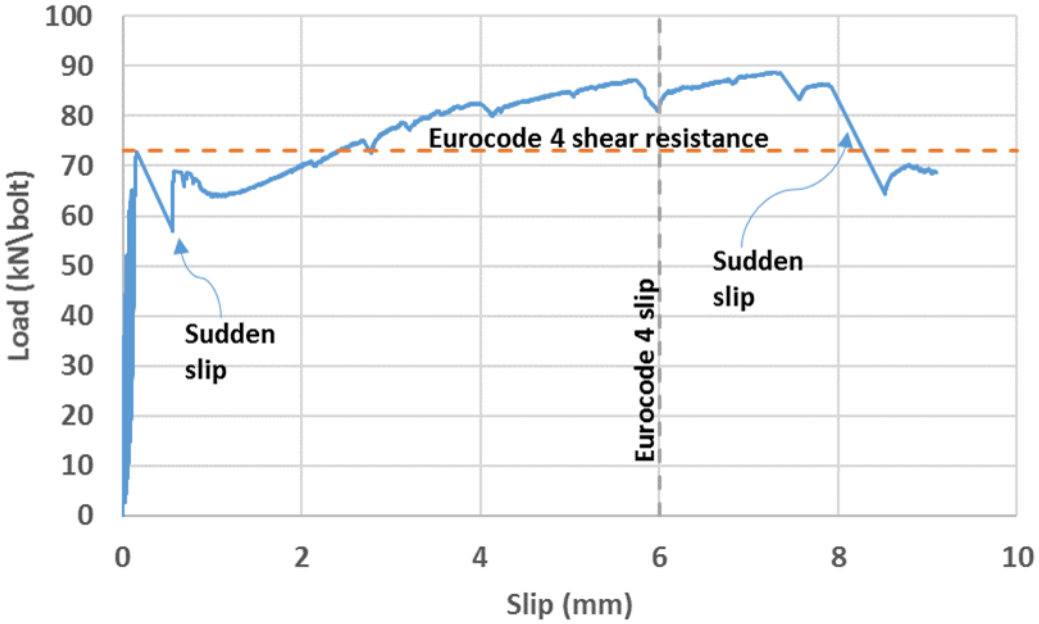

Fig. 6.6. Behaviour of FBSC Test 3

It should be noted from the results in Fig. 6.6 that the load's increase after the first sudden slip is slight (approx. 20%). This is most likely due to the low stiffness of the in-front grout because of the enlargement hole; therefore, excluding the enlargement hole from future tests is recommended. The 25 load cycles were included in Fig. 6.6 but they are hardly distinguished. Fig. 6.7 shows these cycles more clearly.

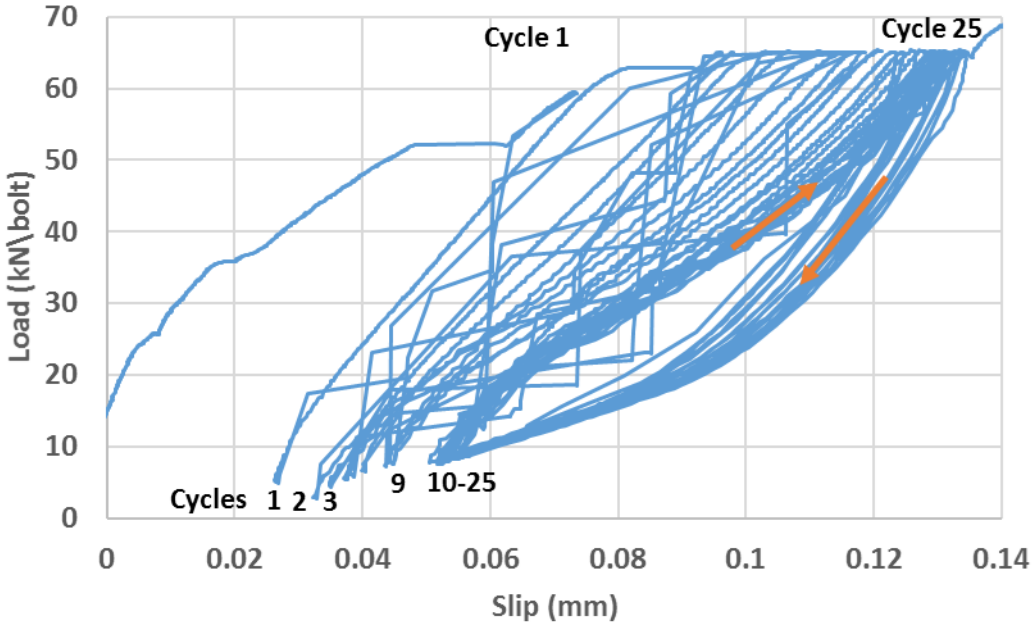

Fig. 6.7. 25 load cycles of the FBSC Test 3

Fig. 6.7 shows that the slip reduced after each load cycle (i.e. cycles 1-9) until reaching identical cycles at the end of the repeated loading procedure (i.e. cycles 10-25). It should be

noted that the main reason of these 25 repeated loadings is to ensure that if the connector tested is susceptible to progressive slip this will become evident (Johnson 2012). It can be seen from Fig. 6.7 that these load cycles did not form noticeable slips. In other words, the added accumulated slip after the 25 load cycles was about 0.05 mm and there was no evidence of progressive failure. Thus, the 25 cycles can be safely ignored in future FBSC tests as long as the frictional resistance exists. The deflected shapes of the failed bolts are shown in Fig. 6.8.

The photo in Fig. 6.8 shows considerable amount of bending deformations, which are related to grout crushing/powdering in front of each bolt, as shown in Fig. 6.9. Fig 6.8 shows that all bolts failed at inclined failure planes as compared to perpendicular failure planes observed in Tests 1 and 2. This indicates that when bending deformation exists, the failure plane is more likely to occur at an inclined angle.

Fig. 6.8. Deflected shape of bolts of FBSC Test 3

Fracture of the four bolts proves the precise specimen dimensions, positioning, and test procedure. Shearing the four bolts means that the shear resistance is the average, which is the highest value that a pushout test can reach from the point view of the test setup. In addition, it explains why the shear resistance from Test 3 is higher than that from Tests 1 and 2.

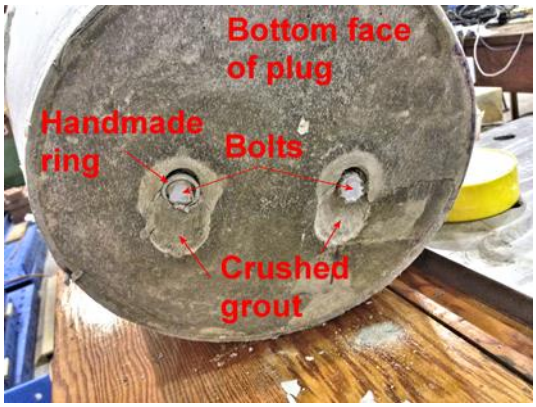

Fig. 6.9. Concrete crushing in FBSC Test 3

6.2.1.3 FBSC Pushout Preliminary Test 4

Test 4 differs from Tests 1-3 as follows: (1) Forming a countersunk seat hole of 120° (Fig. 4.21) at the outer face of the flange of the steel beam; (2) Using separated small plugs (diameter 90 mm); (3) The plugs have a conical shape with inclination angle of 5 degrees only; (4) Excluding the bolt's threads from the shear failure. The load-slip behaviour of Test 4 is shown in Fig. 6.10.

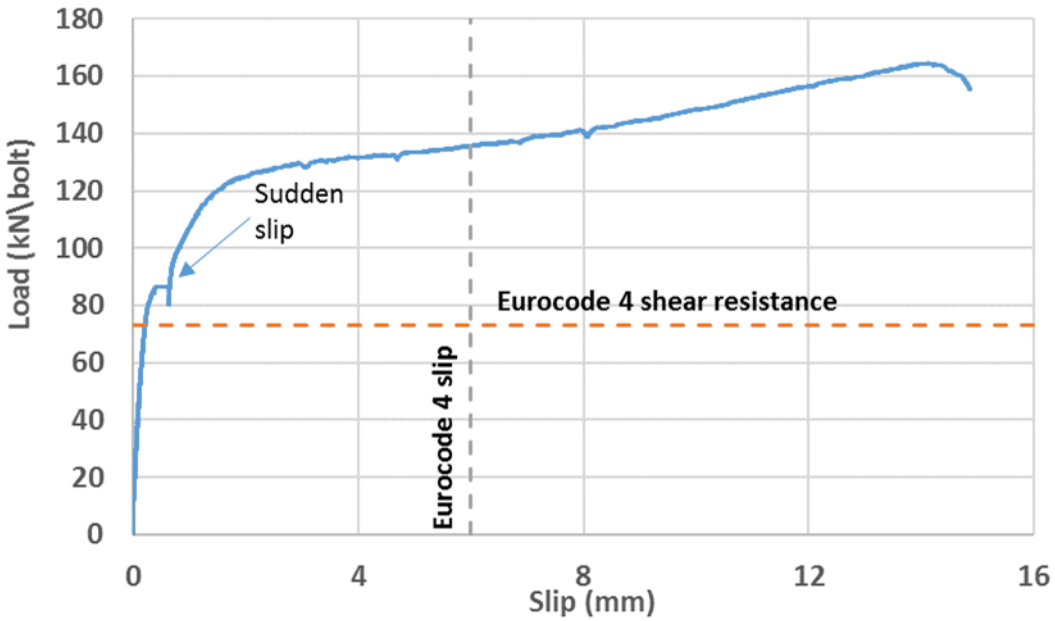

Fig. 6.10. Behaviour of FBSC Test 4

The shear resistance and slip capacity were 165 kN and 14.1 mm, respectively. These values represent further enhancements in both shear resistance and slip capacity compared to that of FBSC Tests 1-3 (e.g. they are higher than Test 3 shear resistance and slip capacity by 1.9). It is clear that the current design features in Test 4 had improved the FBSC structural performance. However, it seems from the load-slip results plotted in Fig. 6.10 that a small sudden slip (< 0.25 mm) still exists when the frictional resistance is overcome. This might be due to the shallow depth (2.3 mm) of the countersunk seat hole provided by the 120° inclination angle (Fig. 4.21). Decreasing this angle (to 60°) and thus increasing the depth of the countersunk hole (to 11.4 mm) allows more grout to settle inside the clearance hole. This is more likely to improve the FBSC performance against sudden slip. Slab uplift at the maximum load was only 0.3 mm. Failure of Test 4 occurred by cutting simultaneously the four bolts. Their deflected shapes (post-test) are shown in Fig. 6.11. The figure shows that the bolts undergo double curvature deflections due to the opposite relative movements between the steel flange and the concrete slab as well as due to the presence of the countersunk seat hole. The failure shear plane occurs at the flange-slab interface and passes through the inclined parts of the shanks. Hence, the resisting cross-sectional area is of

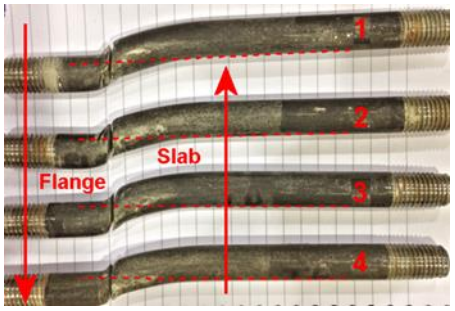

Fig. 6.11. Deflected shape of bolts of FBSC Test 4

elliptical shape, which explains partly the high shear resistance (165 kN/bolt) as compared to Tests 1-3.

Fig. 6.12 shows the two failed bolts embedded in the steel beam (left photo), inside the concrete slab (middle photo), and separately (right photo). The left photo in Fig 6.12 demonstrates that as the steel flange moves downward, the bolt moves upward inside its countersunk hole. This will crush the grout above the bolt inside the hole. The middle photo shows opposite movement of the bolt inside the plug. This will crush the grout below the bolt. It is clear from the right photo in Fig. 6.12 that the bolts undergo a combination of shear, double curvature bending, and tensile deformations, which is the result of plug crushing in front of the bolts and fracture of the bolts. It should be mentioned that concrete crushing was local (15-20 mm) and did not propagate to the rest of the concrete slab.

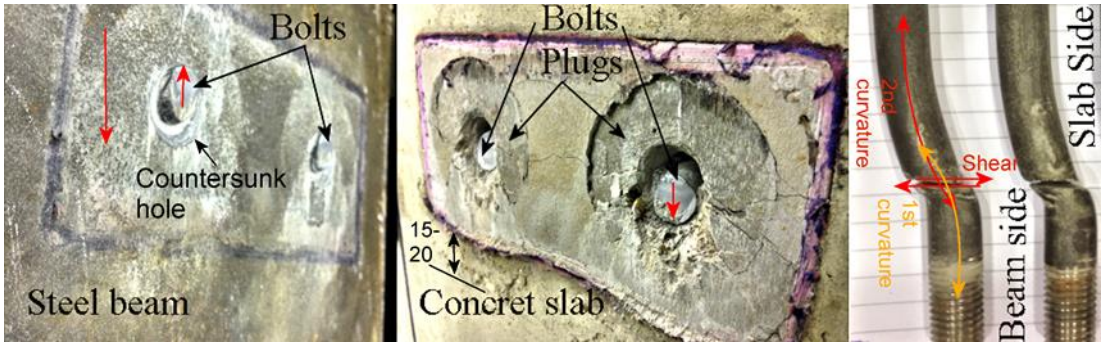

Fig. 6.12. Failed bolts in steel beam, concrete slab, and separately

6.2.1.4 FBSC Pushout Preliminary Test 5

Test 5 includes new modifications as compared to Tests 1-4 (as was explained in the Section 4.5.4). Briefly, the countersunk seat hole at the outer face of the steel flange had an angle of 60° (Fig. 3.4c) instead of 120° (Fig. 4.21), while the lower nut is used as a locking nut for each bolt. In this way, a deeper seat (i.e. 11.4 mm instead of 2.3 mm) is created which allows for more grout to settle and, hence, more resistance against sudden slip of bolt inside its clearance hole. The sudden slip was experienced in Tests 1-4. The load-slip behaviour of this test is shown in Fig. 6.13. It can be concluded from the load-slip curve in Fig. 6.13 that the shear resistance is 186 kN and the slip capacity is 17.4 mm. Both are higher than their equivalent from welded studs (i.e. 73 kN/stud and 6 mm) as well as from the previous FBSC tests (e.g. higher than the results of Test 4 by 13% in shear resistance and by 23% in slip capacity). It can also be confirmed from the same figure, that the sudden slip that normally occurs when friction resistance between the concrete and steel is overcome, is successfully eliminated. Results in Fig. 6.13 show that the response consists of three phases. Phase one starts with a linear relationship having high stiffness of 250 kN/mm until a load of 70 kN (i.e.

37% of failure load) and a slip of 0.28 mm are reached; followed by phase two with another linear relationship having less stiffness of 28 kN/mm until a load of 110 kN and a slip of 1.7 mm are reached. The third phase has stiffness of 5 kN/mm until the ultimate load of 186 kN and the slip capacity of 17.4 are reached. The last 0.5 mm slip of the load-slip curve is highlighted in Fig. 6.13. It shows that the FBSC load-slip curve has a plateau with no stiffness at the onset of failure, which indicates the fracture of the bolts. Between these three phases there are two nonlinear transition curves which represent a change in the response. Likely, the first transition represents the overcome of friction resistance while the second one represents the yielding of materials (steel and concrete) in shear and bending.

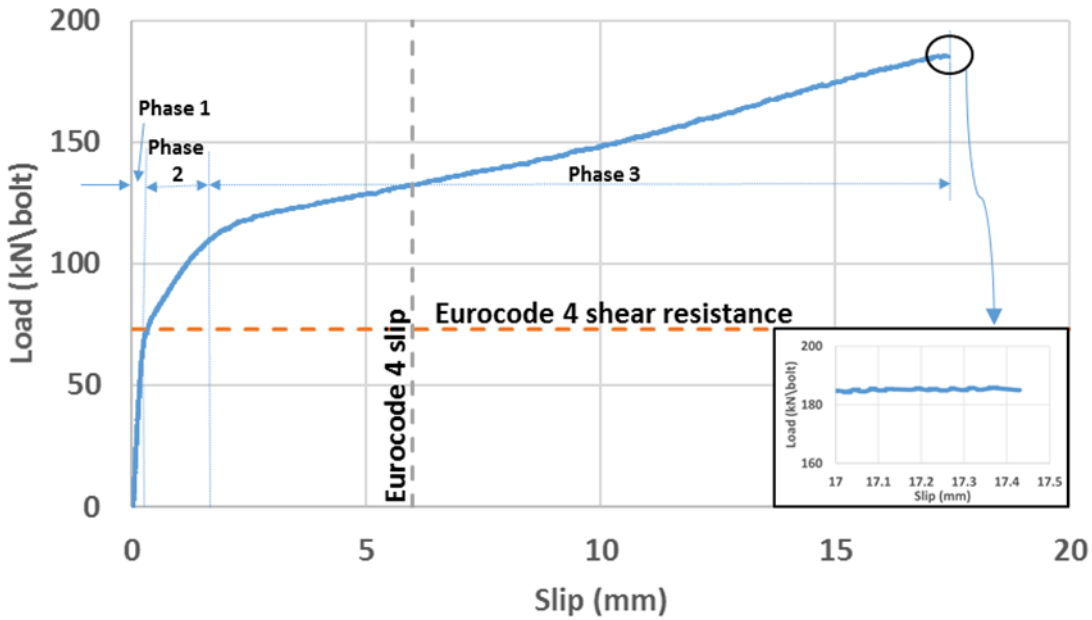

Fig. 6.13. Behaviour of FBSC Test 5

Slab separations (uplifts) are measured at the upper end of each slab, in similar way to what is shown in Fig. 4.34. The results are shown in Fig. 6.14. As was seen in all previous tests, minor negligible separations were recorded. Almost, the slabs are reflected similarly in magnitude and reversely in direction. In particular, the left-side slab separated from the steel beam (by maximum of 0.4 mm), while the right-side slab moved closer (compressed) to the steel beam (by < 0.8 mm). This is the evidence that slab separation readings of pushout test were affected by other factors, like specimen tilting. A closer look at the results in both Figs. 6.13 and 6.14 shows that each nonlinear transition interval in the load-slip curve caused noticeable changes in the corresponding load-separation curve.

Fig. 6.15 shows the failure mode as observed in three locations, namely, in the concrete slab, in the steel beam, and in bolts. It is clear from Fig. 6.15(a and b) that extremely high

compression stresses caused the grout and concrete in front of each bolt to crush to a powder state. Figs. 6.15b reveals that as the steel section moves downward during the pushout test, the bolts bend upward inside their countersunk holes. This will crush the grout above the bolts. The opposite is true for the bolts inside the concrete slab, as they bend downward inside their plugs. This will crush the grout below the bolts. The amount of crushed concrete in the slab is larger than that in the steel section. This explains why a gap is created above each bolt at the concrete slab, as shown in Fig. 6.15a, but not at the steel section, as shown in Fig. 5.15b.

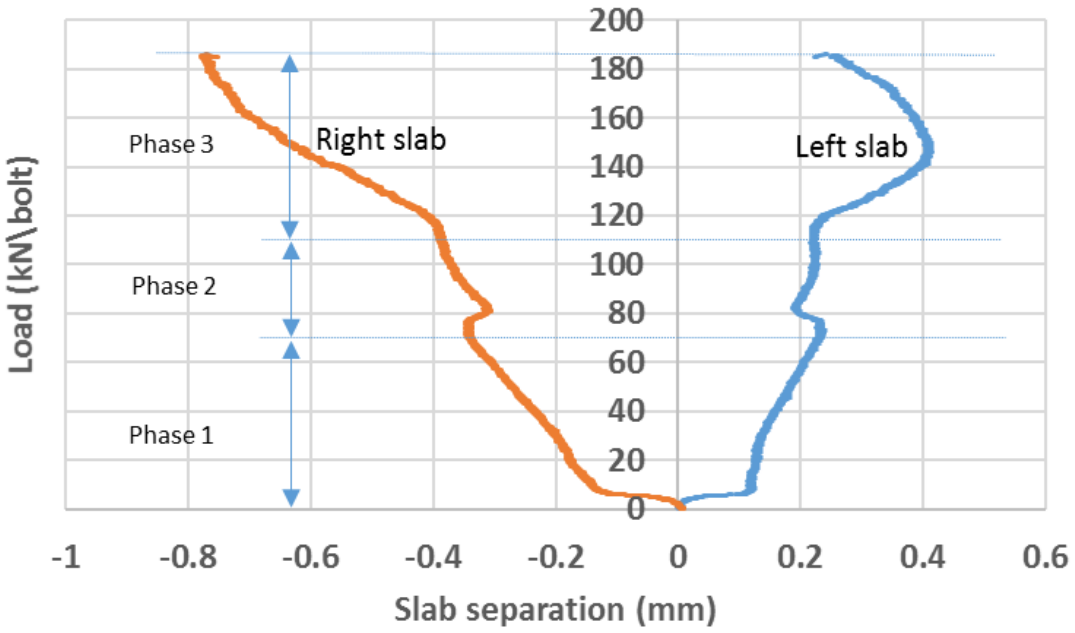

Fig. 6.14. Slab separations of FBSC pushout preliminary Test 5

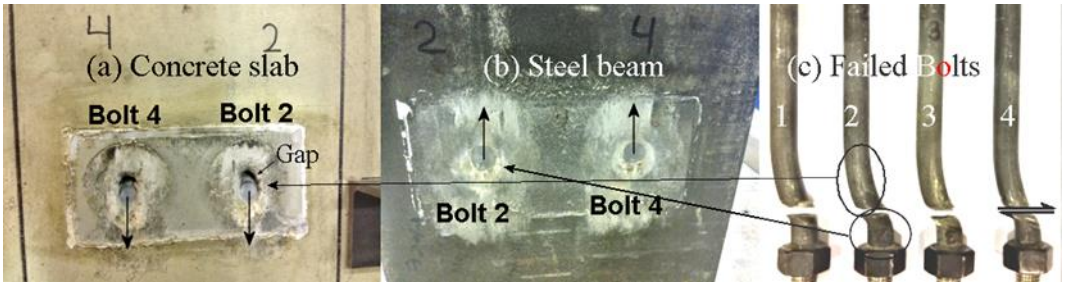

Fig. 6.15. Failure of FBSC Test 5 in (a) concrete slab (b) steel beam and (c) failed bolts

These opposite bends (curvatures) in each bolt are shown in Fig. 6.15(c), where a kind of 'S' shape results. This indicates the formation of two plastic hinges due to bending moments concentrations. It is obvious that the plastic hinges were developed before bolts shearing

off. More energy was absorbed (led to a higher shear resistance, 186 kN/bolt), and a delay in failure was achieved (led to a high slip capacity, 17.4 mm).

The movement of each bolt relative to its clearance hole is shown in Fig. 6.16. It is clear that the locking nuts could not prevent these movements. On the other hand, no sudden slip occurred during Test 5, due to the grouted countersunk holes. Bolts 1 and 3 (their positions can be seen in Fig. 5.18) showed some instability near the failure load, possibly due to the installation of locking nuts at the inside face of the flange. Excluding this performance feature from future tests, by using ordinary nuts, would be advisable.

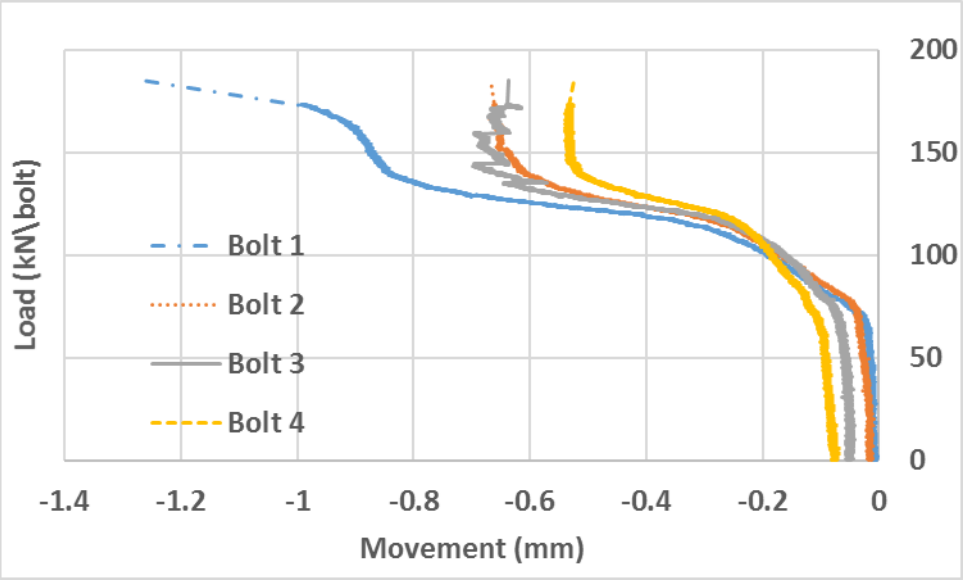

Fig. 6.16. Bolt's movement inside its hole of FBSC pushout Test 5

6.2.1.5 FBSC Pushout Preliminary Test 6

Test 6 specifications were described in Section 4.5.5. In brief, Test 6 represents the final design for FBSC as explained in Sections 3.3, 4.2, and 4.3. The load-slip behaviour in Test 6 is shown in Fig. 6.17. The results in the figure shows that the resistance force and slip capacity was 206 kN and 16 mm. This FBSC has a secant stiffness (at 50% of shear resistance) of 85 kN/mm, although it started with a stiffness 7–8 times higher than that, as can be seen in the first linear part (at 25% of shear resistance) of the load-slip curve. It is believed that the shear resistance was initially due to friction and chemical bond effects, and when these were overcome, a slight slip (0.17 mm) occurred. The reason for this slight slip might be due to tinny clearances between the bolts and their grout created by preload adjustment that took place before Test 6. The preloads were adjusted to ensure equal tensile forces among the four bolts. It should be noted that during this test, the author was eager to record as much as practically possible of the falling branch in the load-slip curve, especially after increasing

the stiffness of the testing rig (Section 4.5.5) to reduce the stored strain energy at the instant of ultimate load (i.e. instant of sudden failure), and that was reflected in few false load drops of the load-slip curve, as can be seen in Fig. 6.17. However, after each false drop, the load was easily recovered back to its original value. The best procedure to be adopted at the instant of failure is to decrease the displacement rate of the hydraulic jack to almost zero. This can be done by closing the valves of the hydraulic jack. During this period, the effects of concrete creep, steel relaxation, and the stored displacement energy in testing rig are more pronounced. Hence, the falling branch of the load-slip curve was recorded, as shown in Fig. 6.17.

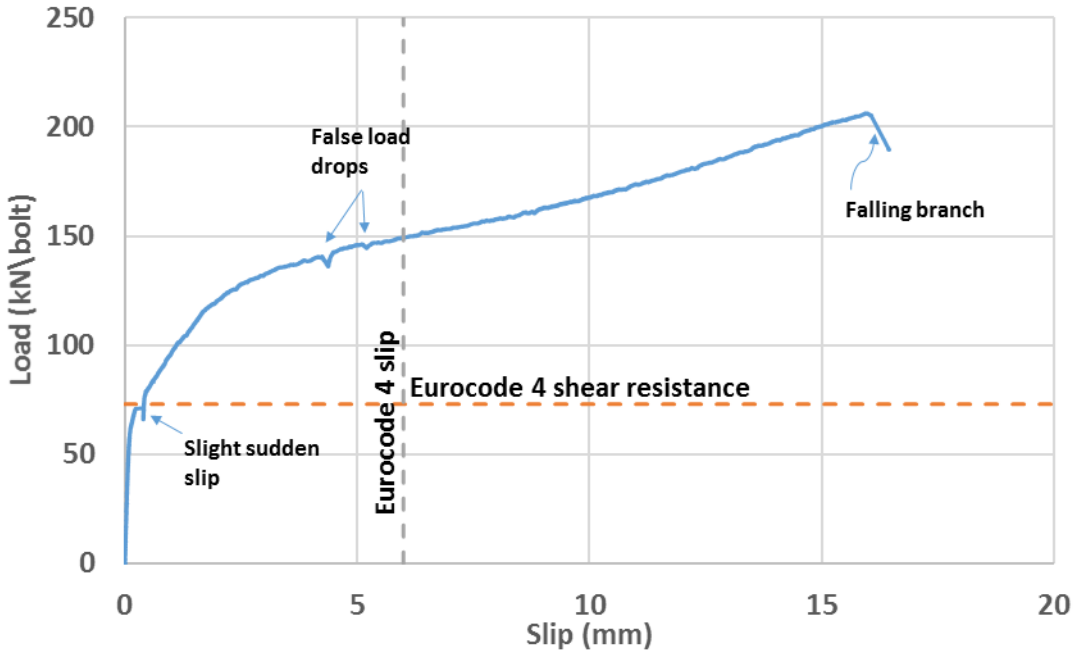

Fig. 6.17. Behaviour of FBSC Test 6

The importance of having a falling branch in the load-slip curve is to increase the measured slip capacity even more. Eurocode 4 defines slip capacity as the slip at the falling branch of load-slip curve and when the maximum load dropped by 10% (BSI 2004a). The falling branch of Test 6 represents a load drop of 8% from the maximum load, in which the slip was increased from 16 mm to 16.5 mm. It should be further noted that the end of the test was the author's decision and not owing to fracture of the bolts. The author was confident that the bolts had yielded and the maximum shear resistance has been reached or, at least, about to be reached. The reason behind this decision is that the shape of bolts and their surrounding grout/concrete at the instant of failure can be observed, assuming that the dismantle of the pushout specimen will not affect the failure mode.

The steel section in a pushout test can tilt around two axes (i.e. when its upper end moved laterally), as illustrated in Fig. 5.18 (more explanations can be found in Sections 5.2.1.6, 4.2 and 4.3). Fig. 6.18. shows the eccentricities of the applied load during Test 6. These eccentricities represent the measurements of the two LVDTs shown in Fig. 4.1. It should be mentioned that the test setup in Test 6 was so precise that the measured eccentricity of the hydraulic jack was less than 1.5 mm in direction of the web (compared to 9 mm in LNSC Test 6). The results from Fig. 6.18 suggest that specimen is tilting toward Bolt 3 and away from Bolt 2; therefore, the slip at Bolt 3 is expected to be the maximum one and that at Bolt 2 to be the minimum one.

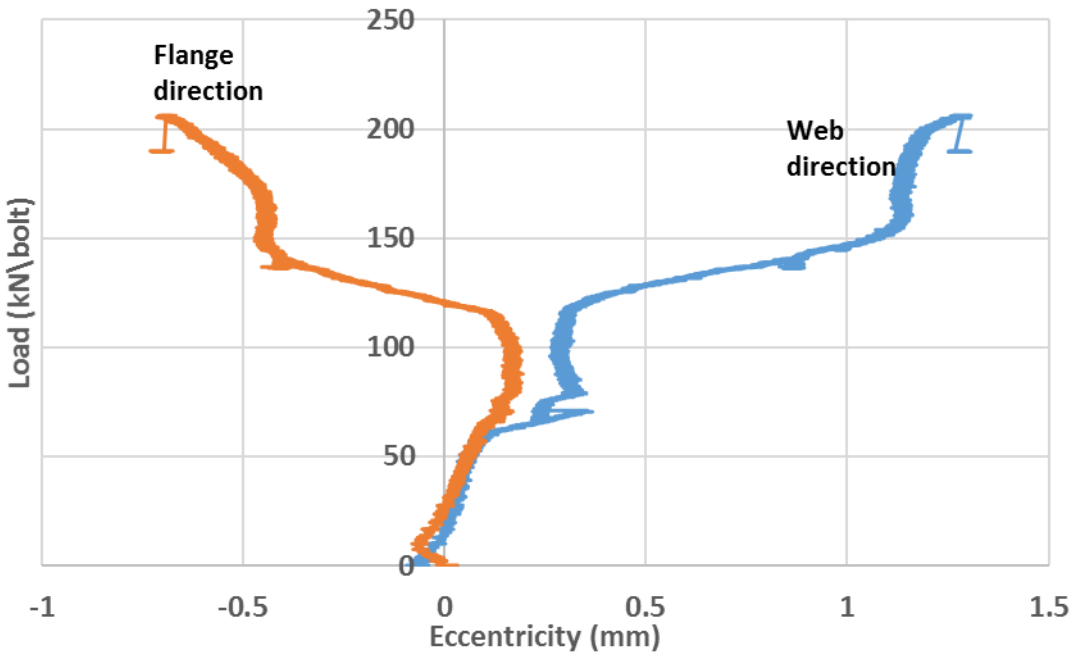

Fig. 6.18. Eccentricity of load during FBSC Test 6

In order to overcome the eccentricity issue, the applied load is redistributed among the four bolts (their locations are shown in Figs. 4.1 and 5.18) according to their positions from the eccentric load using bilinear interpolation and Equations 5.2 to 5.5 (explained in Section 5.2.1.6). Fig. 6.19 is a plot of the load-slip measurements at bolts 1 to 4 where their mean is shown in Fig. 6.17. The figure shows four load-slip curves that correspond to the four bolts. Each of the four curves has its own 'calculated' load and its own 'measured' slip. It should be noted that in Fig. 6.19, there is no interpolation for slip values because the slips are the measured values near each bolt. It should be further noted that different dash type segments (1 mm slip) were added to the end of each curve to help the reader to distinguish between the curves. Bolts 3 records the highest slip capacity (at 16.4 mm), while Bolt 2 records the lowest slip capacity (at 15.5 mm). This conforms to the results of Fig. 6.18. The differences

between the four load-slip curves are relatively small (< 10 kN/bolt in shear resistance, and < 1 mm in slip), which provides strong evidence of a consistent test procedure.

The separations in Test 6 were measured as close as possible to each bolt and are reported in Fig. 6.20. The maximum separation is 0.38 mm at Bolt 2 (bolts positions are shown in Fig. 5.18). It can easily be concluded by comparing the results from Fig. 6.20 to the slab separations recorded in Sections 5.2.1 and 6.2.1, that Test 6 has the maximum stiffness against slab separation.

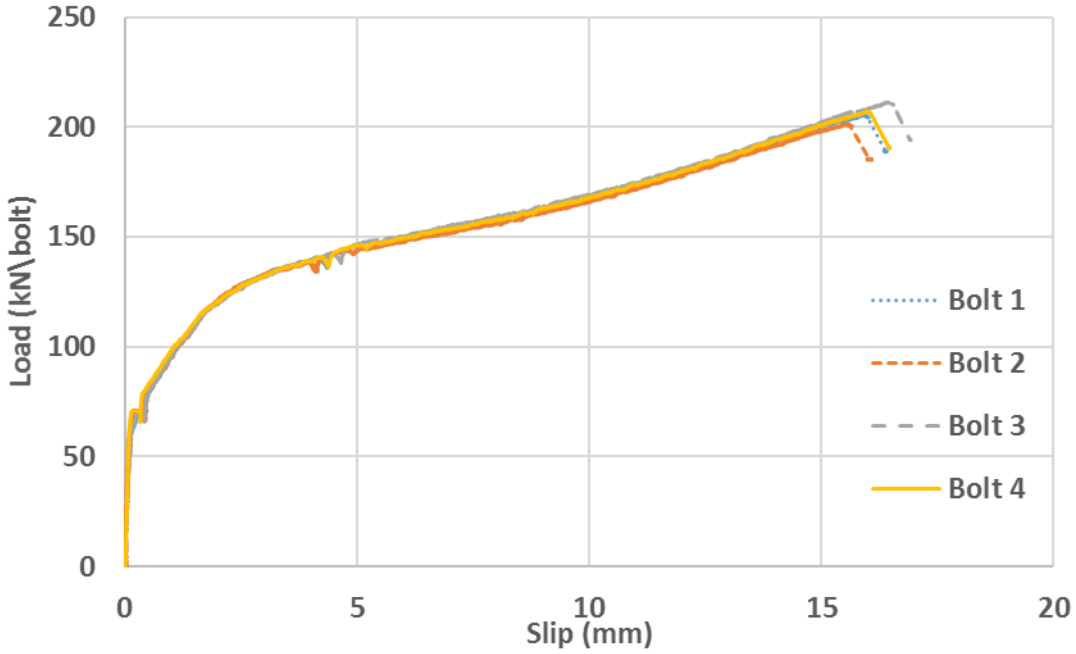

Fig. 6.19. Redistribution of load among 4 bolts of FBSC Test 6

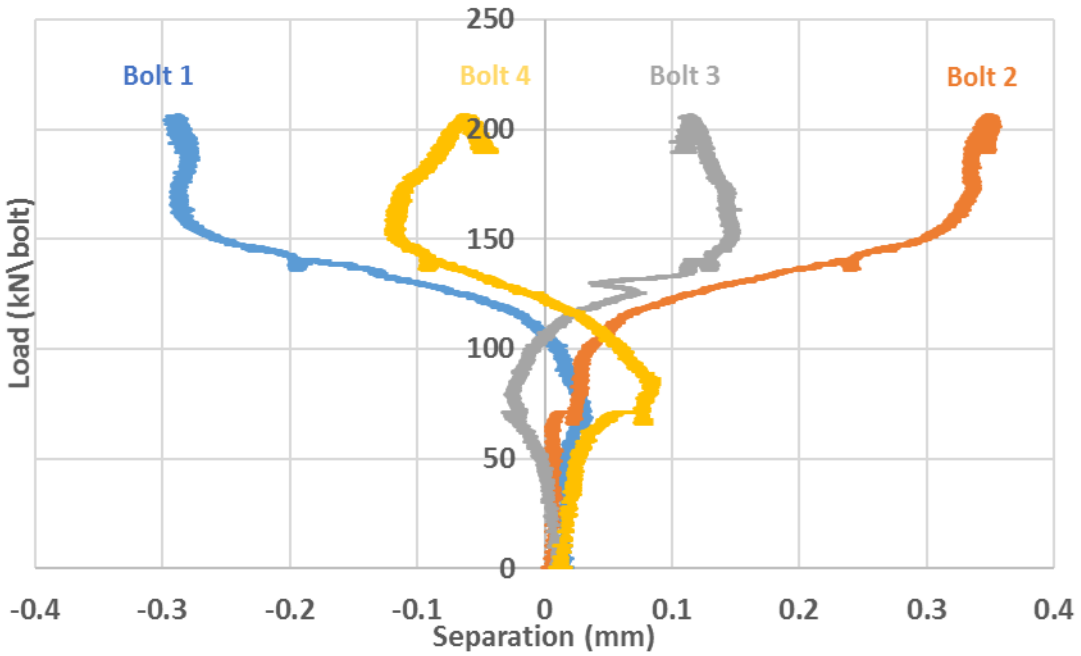

Fig. 6.20. Slab separation resistance of the FBSC Test 6

It can be seen from Fig. 6.20 that Bolts 1 and 2 have almost the same separation but in opposite direction (i.e. positive sign means separation, while negative sign means compression). The same is true for Bolts 3 and 4, but with lower separations. In other words, each slab has separation and compression at the same time. This shows that slab separation readings from pushout tests having four shear connectors at one level are affected by other factors like tilting of the pushout specimen.

Fig. 6.21 shows the relationship between the slab separation of each bolt and its slip displacement.

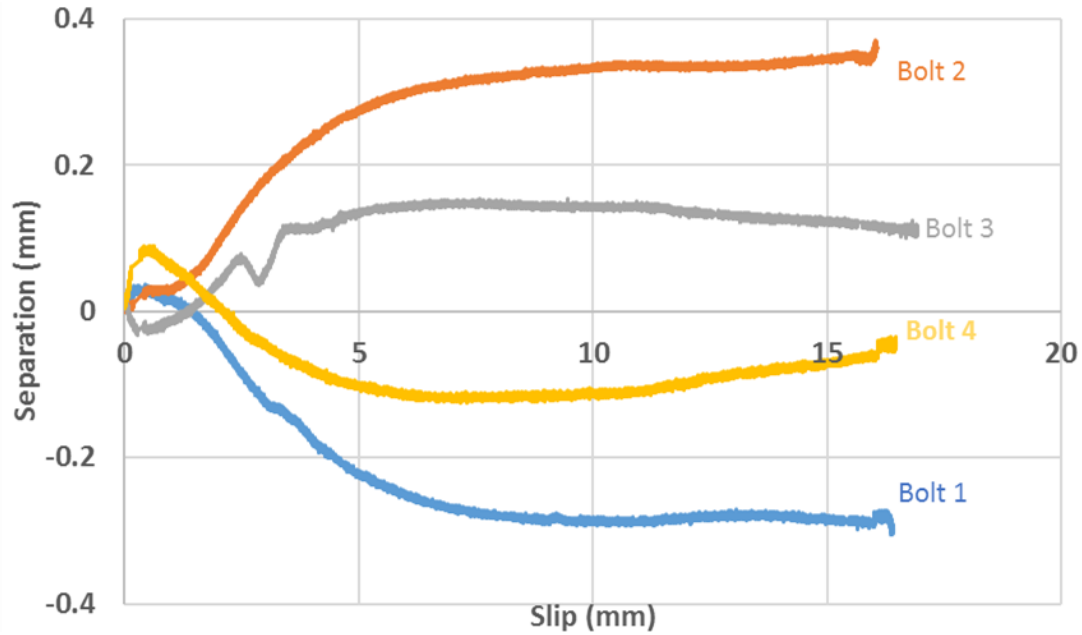

Fig. 6.21. Slab separation-slip relationship of the FBSC Test 6

It can be seen from separation-slip curves plotted in Fig. 6.21 that the separation/compression increases as the slip is increased until a slip of 5-7 mm, while afterwards, less variations are recorded. Again, Bolts 1 and 3 behave like mirror images of Bolts 2 and 4, respectively. If the assumption that double plastic hinges are developed during this slip duration (i.e. > 5-7 mm) is true, then they provide an inclined slide along the steel bolts for the slab to slide over. Thus, a similar behaviour should exist near the four bolts (i.e. near all bolts, the measurements should record separations). But, because the measurements near some of bolts show separation and near others show compression as slip increased, separation readings are not entirely related to the deflected shape of the bolts. Instead, they are more likely related to specimen tilting. It should be noted that the transducer reading is for slab separation and not for plug separation. Not every slab separation should be reflected by a similar separation at the plug, and the opposite is true.

This assumption can be seen to be valid because there is a release agent of wax-based material between the two members and because the separation/contraction readings are just a fraction of millimetre (see Figs. 6.20, 6.21).

The tensile force inside each bolt was recorded in relation to its corresponding slip and plotted in Fig. 6.22. The general behaviour shows a small increase (0.8-1.8 kN/mm) before 10 mm slip, while there is significant increase (3.6-4.3 kN/mm) after that. It is clear from Fig. 6.22 that, the status of tensile forces inside bolts are not affected by the eccentricity of the applied load (Fig. 6.18) or separation of slabs and tilting of the pushout specimen (Figs. 6.20 and 6.21), as these effects are mainly acting on the slabs. The tensile forces inside the bolts are related to separation of plugs. After a slip limit of 10 mm, the tensile force inside a bolt shows significant increase. This is believed to be due to the deflected shape of the bolts. After 10 mm slip, a more obvious deflected shape of the bolt is formed. The deflected shape of the bolt represents an inclined slide for the plug to slide over (ride-up). This will stretch the bolt and therefore the tensile force is increased at a rate of 4.3 kN for every 1 mm slip. The average tensile force in Test 6 at ultimate load was 100 kN, which represents 59% of the bolt tensile resistance, and 63% of the bolt yield resistance, which means that all the tensile deformations are elastic and most of the deformations developed at the onset of failure would be due to shear forces and bending moments.

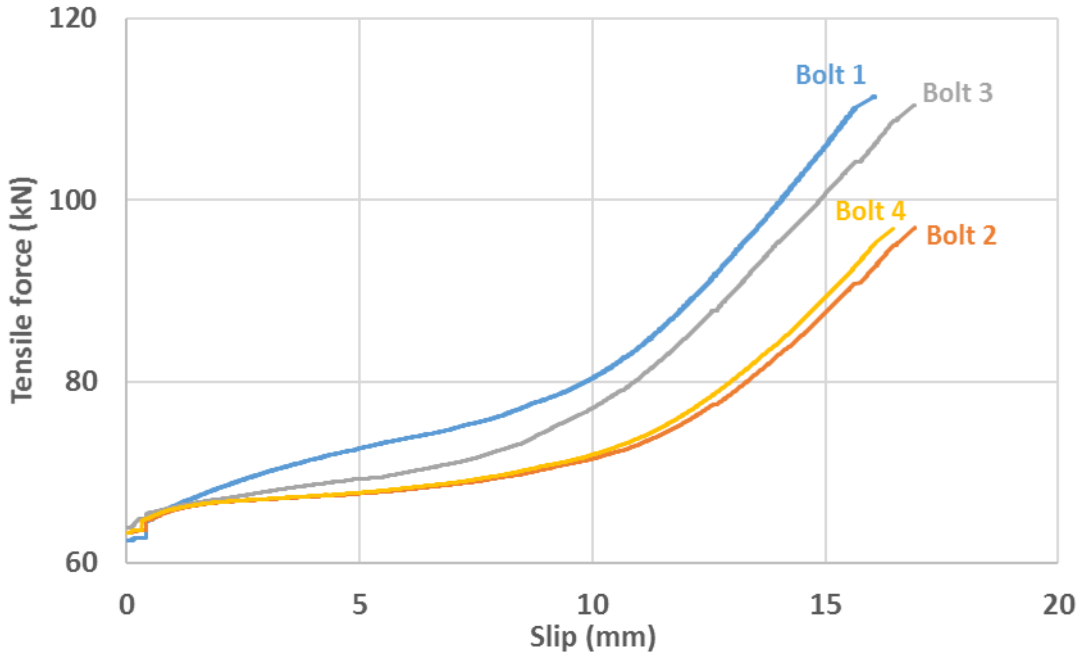

Fig. 6.22. Effect of slip on bolt tensile force of FBSC Test 6

The failure modes are illustrated in Figs. 6.23 and 6.24. It is clear from the photo in Fig. 6.23 that the measured slip from the deflected shapes of bolts are less than the recorded slips from pushout test as the later includes the effect of elastic slips, bolts slips inside their holes, and bolts rotations inside their holes. It can also be observed that the deflected shape has two plastic hinges that are 20-40 mm apart, then accompanied by a combination of shearing and tensile deformations concentrated in a length of 5-6 mm, which is the height of the countersunk seat hole, and with a deflection angle (β) with average value of 45°. Fig. 6.24 shows that the grout in the countersunk seat compressed to form a cushion for the deflected shape of the bolt.

Fig. 6.23. Deflected shapes of bolts for FBSC Test 6

Fig. 6.24. Concrete crushing for FBSC Test 6

6.2.2 Characteristic Shear Resistance of FBSC

As was explained in Section 5.2.2, the characteristic shear resistance P_{Rk} can be determined by conducting three pushout tests on nominally identical specimens. Eurocode 4 states that if the results are within 10% of mean shear resistance, then $P_{\mathrm{Rk}} = 0.9\,P_{\mathrm{min}}$, where P_{min} is the lowest of the three measured shear resistances (per connector) (BSI 2004a).

Table 6.1. Results of Tests 5, 6, and 11

Test No.	Shear resistance (kN/bolt)	Slip capacity (mm)
5	185	17
6	206	16
11	179	14
Average	190	15.7
Standard deviation	11.5	1.2
Coeff. of variation CV %	6	7.6

The results from Tests 5 and 6 were followed by one additional test (i.e. Test 11 in Table 4.3) with identical test setup, test method and approximately similar material specifications (Table 4.3).

Table 6.1 lists the shear resistances and slip capacities from these tests. The very close agreement between the tests (CVs are 6% and 7.6) provides evidence of consistent test procedures. The deviation (difference) of any individual test result from the average shear resistance is about 6%. This is significantly below the aforementioned 10% limit of Eurocode 4. Thus, the characteristic shear resistance of the FBSC is $P_{\mathrm{Rk}} = 0.9 \times 179 \approx 161$ kN.

Fig. 6.25 compares the shear load-slip displacement behavior from Tests 5, 6, and 11.

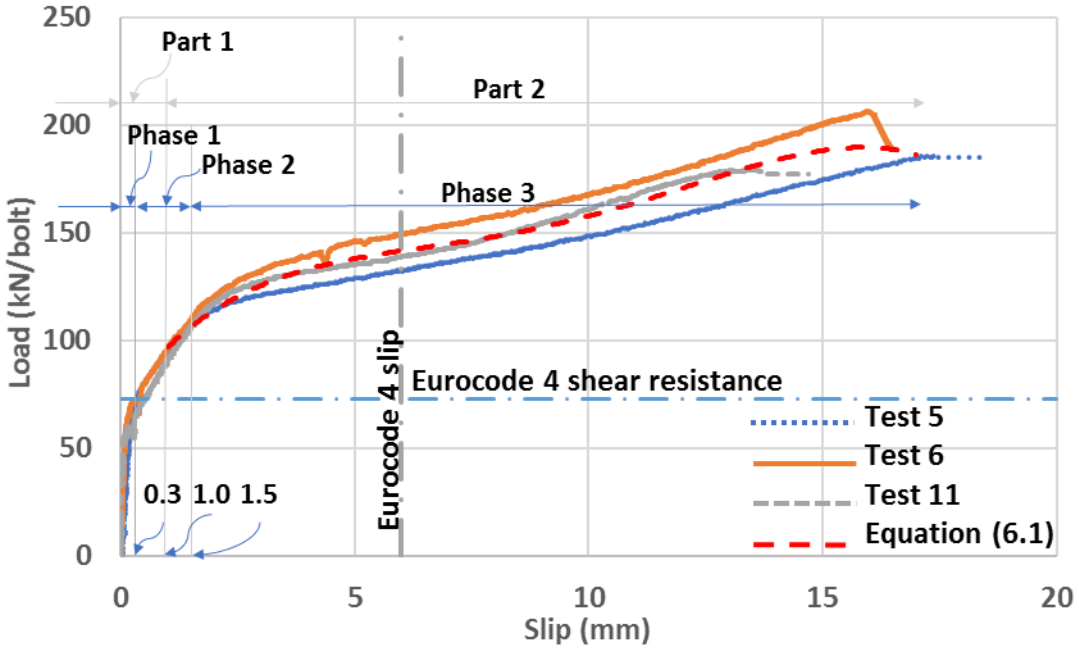

Fig. 6.25. Behaviour of three identical FBSC pushout tests

Please notice that the small dashed segments (1 mm slip) were added to the end of Tests 5 and 11 curves to help the reader to distinguish between the curves. The load–slip curves were consistent up to the maximum load. The subsequent curves agreed well up to fracture of bolts (where 6% and 7.6% differences in shear and slip can be noticed). The results from Fig. 6.25 highlight that the robust structural details of the FBSC result in superior shear resistance (avg. 190 kN/bolt), superior initial stiffness, large slip capacity (avg. 15.7 mm), and reliability in the load-slip behavior (CV are 6% in shear and 7.8% in slip) as compared to previous connectors reviewed in Section 2.5. Suwaed *et al*. (2016) provides a comparison among the FBSC and LNSC and the previously proposed demountable shear connectors (Section 2.5) and shows that the FBSC and LNSC provide the highest shear resistance (e.g. 1.3 times higher than the shear resistance of the load-slip curve in Fig. 2.15b).

In order to develop an expression that is representative of the load-slip curve of the FBSC, the curve can be considered to consist mainly of two parts. Part one is linear and it is from 0 to 1 mm slip, and part two is nonlinear and it is from 1 mm slip until failure. Part one can be represented simply by using the secant initial stiffness of the connector, as follows $P_i = 97 \times S$, in which, P_i is the shear force of the FBSC in kN/bolt, and S is the slip in mm. Part two can be represented by a best-fitting curve. The equation that govern the best-fitting curve can be constructed using a fourth-degree nonlinear polynomial regression. The nonlinear equation is as follows

$$P_i = -1.04 \times 10^{-2} S^4 + 3.88 \times 10^{-1} S^3 - 4.93 S^2 + 29.5 S + 72 \qquad (6.1)$$

If S = slip capacity, then $P_i = P$, where P is the shear resistance. Equation (6.1) will be proved to be useful when evaluating the shear resistances of the FBSCs from their slips in Section 7.2.5.

Equation (6.1) is drawn in Fig. 6.25, and it shows good agreement to the three tests. The maximum divergence in shear resistance of any of the three test from the value of Equation (6.1) at the slip capacity listed in Table 6.1 is < 8%. The divergence is minimized for slip displacement lower than the slip capacity. For example, at a slip of 10 mm, Equation (6.1) predicts the shear resistance equal to 158 kN/bolt, while from the load-slip curves plotted in Fig. 6.25, the shear resistance from Tests 5, 6, 11 are 149, 168, and 161 kN/bolt respectively. Thus, the absolute differences between the results from Equation (6.1) and Tests 5, 6, and 11 are 6%, 6%, and 2% respectively. Please recall that Eurocode 4 considers any three pushout tests as identical if the deviation in shear resistance of any test from the average is less than 10% (BSI 2004a). It should be noted, however, that Equation (6.1) was derived using

the boundary conditions of Tests 5, 6, and 11, including using M16 bolts with specific material properties listed in Table 4.5, and using slabs, plugs, and grout with material properties listed in Table 4.3. Thus, Equation (6.1) can only be used within these conditions. Further tests are required to extend its application to other practical situations. It can be seen from the load-slip curve of Test 11 shown in Fig. 6.25 that the shear resistance was slightly less than the average (i.e. the difference is 6%). The reason was the fracture of only one bolt. The shear resistance in this case represents the resistance of the weakest bolt and not the average.

Fig. 6.26 shows the deflected shapes of the failed bolts of Test 11. A closer look at Bolt 2 shows that because of some irregularity (bump) in the upper face of the flange of the steel beam near the edge of the countersunk hole, an irregular shear plane (cut) exists in the deflected part of the shank. From Fig. 6.26, it can be measured that the shank would be in direct contact with the bump when the bolt is deflected to a slip of about 11-12 mm. This contact will increase the shear stresses and reduce the bending moment in Bolt 2 as compared to the other three bolts. This response is an explanation for the results for Test 11 in Fig. 6.25, where its load-slip curve start to degrade for slip > 12mm.

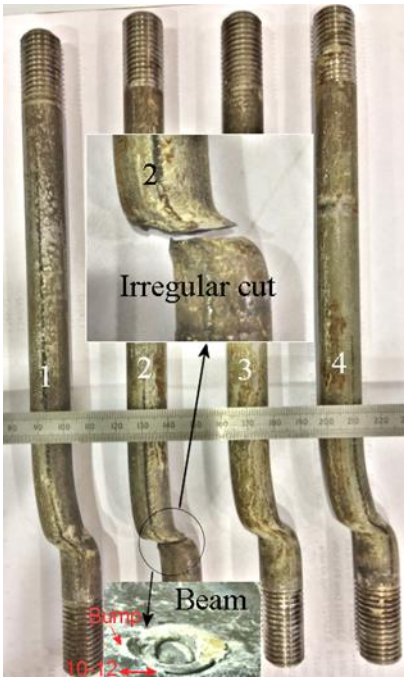

Fig. 6.26. Deflected shapes of bolts of FBSC Test 11

The tensile forces inside the four bolts are plotted in Fig. 6.27 with respect to the applied load per bolt. No noticeable changes can be observed up to 120 kN/bolt of loading (i.e. 67% of shear resistance), which represents the third phase in a typical load-slip behaviour of the FBSC (e.g. Fig. 6.13). It is interesting to note that the tensile force inside Bolt 2 reduced after the load limit of 120 kN/bolt, and that might be related to the aforementioned irregular shear plane (Fig. 6.26). One assumption can be suggested, i.e. that the bump was initially under the plug, and when slip reached 2 mm the plug started to slide-down gradually which caused reduction in Bolt 2 tensile force via bolt relaxation. It is clear from the curves plotted in Fig. 6.27 that the only bolt that fractured is Bolt 2 since it is the only bolt that had a decrease in tensile force at the end of the curve. One can conclude that if the fracture of Bolt 2 did not occur, it would be possible to record a higher shear resistance and slip capacity for Test 11. It should be noted that Bolts 1, 3, and 4 showed an increasing trend in tensile forces even at the onset

of failure although the applied load was slightly dropping (as shown in Fig. 6.27). This indicates that the tensile force was not directly related to the applied load, instead it was related to the slip progress because the slip was continuously increasing. This increase can be seen in Fig. 6.25. Thus, if an assumption is made that no failure occurred for Bolt 2, then a new relationship can be roughly estimated, as shown in Fig. 6.28. Each curve was extended to a slip of 16 mm (from Test 6) and each curve used data before the start of Bolt 2 failure. Based on that, the average tensile force would be 91 kN which is close to the result of 100 kN from Test 6. It is therefore concluded that the bolt tensile force inside the FBSC will have at the onset of failure a value equal to 55% of tensile resistance of the bolt.

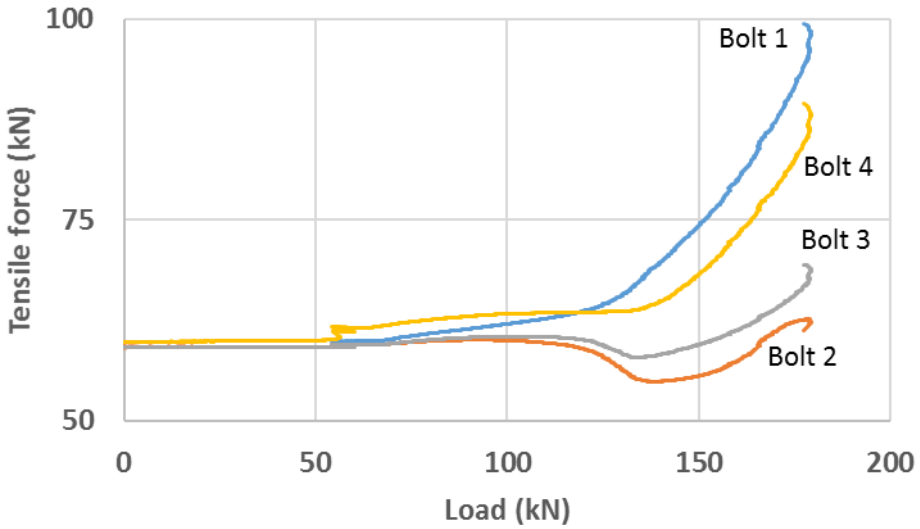

Fig. 6.27. Bolts tensile forces of FBSC Test 11

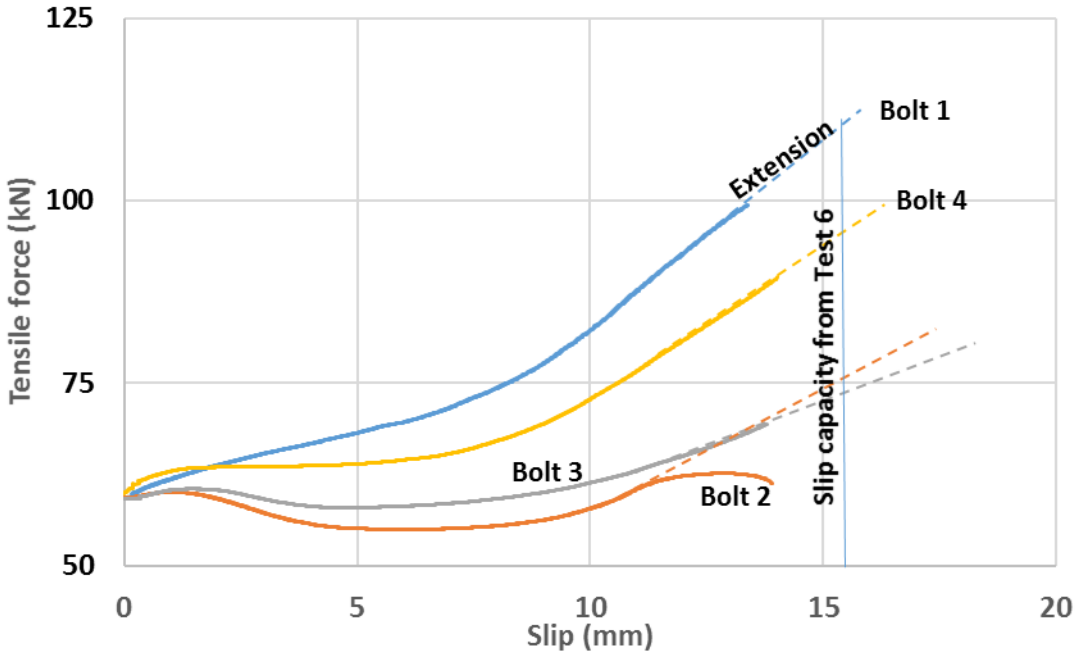

Fig. 6.28. Effect of slip on bolt tensile force of FBSC Test 11

Fig. 6.29 shows plotted results for the slab separation in Test 11, where the positive signs represent a compression displacement and the negative signs represent a separation displacement. The maximum slab separation was about 0.25 mm near bolts 2 and 3 (refer to Fig 5.18), despite that they have minimum tensile forces (Fig. 6.28), while a compression of less than 0.2 mm was recorded near bolts 1 and 4, despite that they have maximum tensile forces (Fig. 6.28). These results prove that there is no correlation between the slab separation and bolt tensile force, and they also support the previous observation that separation readings were effected by other factors like specimen tilting.

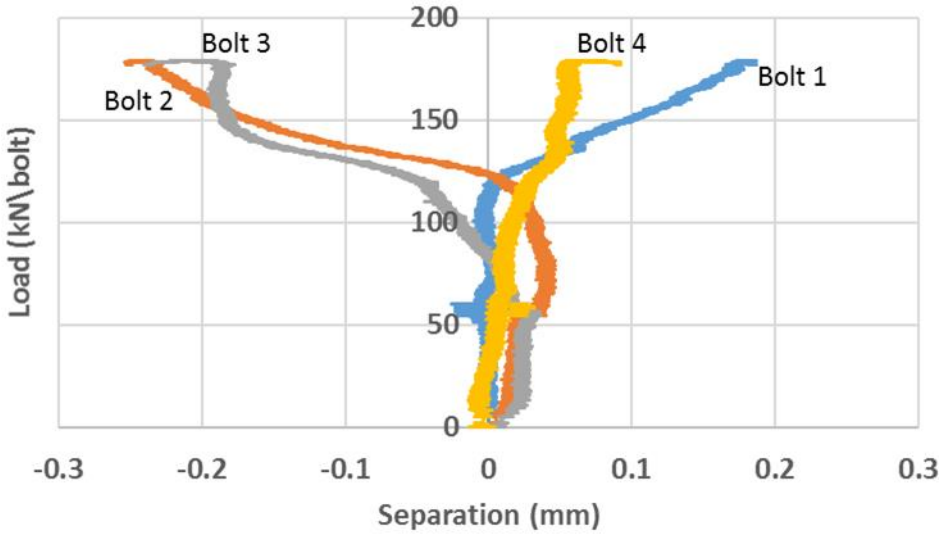

Fig. 6.29. Slab separation of FBSC pushout Test 11

The photo in Fig. 6.30 shows the crushed concrete in the bottom face of the slabs in Test 11.

Fig. 6.30. Concrete crushing of FBSC Test 11

It can be noticed that the bolts deform with two plastic hinges, and the concrete in front of the bolts crushed with a wedge shape and was converted to a powder state. The extent of the wedges was small (about 20 mm) and did not reached the slabs, as was the case in Test

6 (see Fig. 6.24). This supports the previous conclusion that it would be possible to increase the shear resistance of Test 11 if the irregular shear plane with Bolt 2 was absent.

Fig. 6.31 shows the specimen tilting during FBSC Test 11 (refer to Fig. 5.18 for movements directions). It is clear from the figure that slight movements (< 0.4mm) were recorded until the start of fracture of Bolt 2. Initially the specimen was tilting towards Bolt 1 and away from Bolt 4, and when Bolt 2 starts to fracture a new trend for both movements was established by tilting the specimen toward Bolt 2 and away from Bolt 3. The later movements were not enough to shift the load toward Bolt 2, and the majority of load was still on Bolt 1. This indicates that the failure of Bolt 2 was not because of resisting a high percentage of loading owing to eccentric loading but because of the irregular shear plane failure of the bolt.

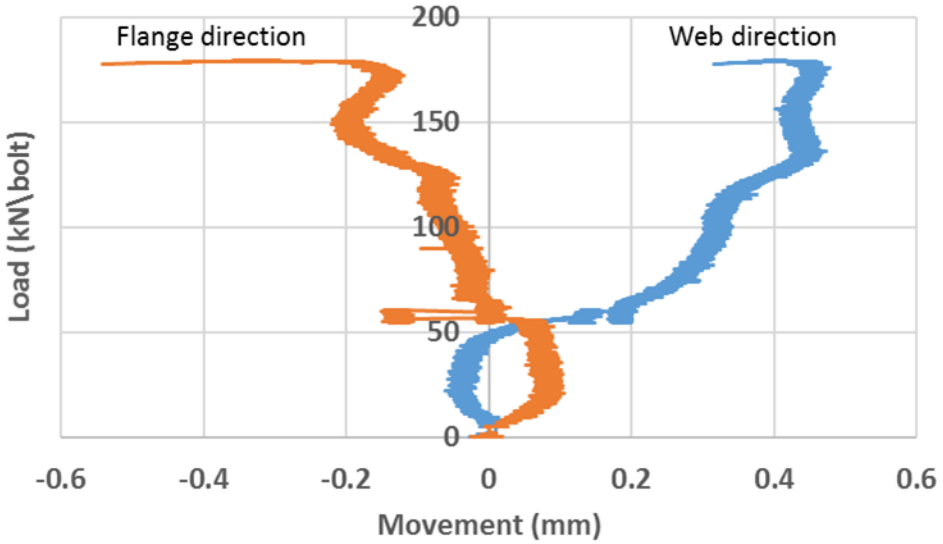

Fig. 6.31. Eccentricity of load of FBSC Test 11

6.2.3 Comparison with Welded Studs

The results of FBSC pushout test 6 will be compared with the results of an equivalent welded stud per Eurocode 4 (BSI 2004a). FBSC pushout Test 6 uses M16 Grade 8.8 bolts (tensile strength = 889 MPa from Table 4.5) and concrete slabs with cube compressive strength equal to 50 MPa from Table 4.3. The shear resistance of Test 6 is 206 kN/bolt. By following the procedure in Section 5.2.3, the shear resistance of welded studs is 73 kN/stud for Ø16 mm, Grade 8.8 (tensile strength = 889 MPa), and slab with cube compressive strength = 50 MPa. Thus, the FBSC shear resistance from Test 6 is 2.5 times higher than that of equivalent welded stud. Furthermore, the slip capacity of the FBSC from pushout Test 6 is 16.0 mm. The clip capacity adopted by Eurocode 4 for ductile welded stud is 6.0 mm. Thus, the FBSC slip capacity from Test 6 is larger by 2.7 times than its comparable welded studs. It should be

mentioned that although studs with Grade 8.8 were assumed in previous comparison, welding of high grade steel like 8.8 and above to normal grade mild steel is not permitted (BSI 2016).

6.2.4 Load – Slip Behaviour and Failure Mode

Fig. 6.25 plots the load-slip behaviour of the FBSC from three 'identical' tests. The load-slip curves consist of three main phases. The first phase, which starts from 0.0 mm slip to a range of 0.1 to 0.3 mm slip corresponding to loads from 55 to 70 kN (i.e. about 25% of shear resistance), is characterised by linear elastic deformations in concrete slabs and the steel beam. The applied forces are transmitted smoothly from steel beam to the concrete slabs through friction resistance at the interface. A closer look to this phase shows that it starts of a complete no-slip resistance until a load of 2 – 10 kN, followed by few one-tenths of millimetre slips, which is hard to be seen in Fig. 6.25. The calculated initial stiffness of the M16 FBSC during the 2-10 kN loading period is extremely high and equal to 230–900 kN/mm (as compared to 100 kN/mm for Ø19 studs). The static friction coefficient can be calculated by dividing the load of phase one (e.g. 55 kN/bolt from Test 11 of Fig. 6.25) by the preload of the bolt (e.g. 59 kN from Test 11 of Table 4.3). Thus, for Test 11, the friction coefficient is 0.9, which is larger than the expected between concrete and steel members (i.e. ≈ 0.5-0.6). Based on that, other factors had contributed (in addition to the frictional resistance) in increasing the shear resistance during phase one. These factors are the chemical bond (adhesion) between the grout and the steel flange and the interlock connection between the irregularity at the top face of the steel flange (see Fig. 6.32) and the grout. No noticeable slip can occur until the chemical bond and the interlock connection are crushed.

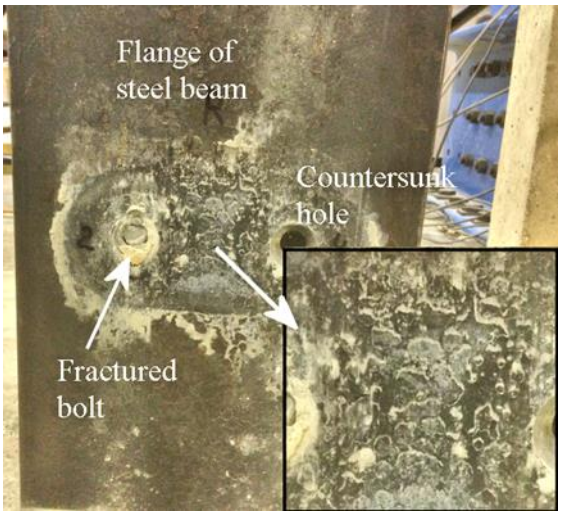

Fig. 6.32. Irregularity at the flange of FBSC Test 11

As the applied force increases, the friction resistance of FBSC is overcome, and the bolted connection starts resisting shear force through bearing. Some slight sudden slippage (e.g. Fig. 6.17) may occur if there are gaps between the bolts and their surrounding grouts and concrete. The reason for this is preload

adjustment mentioned in Section 6.2.1.5). Otherwise, the elastic linear performance will continue until a slip of 0.3 mm, which indicates the beginning of phase two.

Phase two consists of linear load-slip relationship and covers slip displacements from 0.3 to 1.5 mm, where the shear load reaches values up to 110 kN, i.e. approximately equal to 58% of the shear resistance. The deformations are related to bolts bending and bearing against the surrounding grout and concrete. The aforementioned interlock and chemical bond connections are lost; therefore, the stiffness of phase two is less than the stiffness of phase one. It should be noted that Eurocode 4 considers the stiffness of a connector at 50% of shear resistance. The 50% of average shear resistance (from Table 6.1) is 95 kN, and by substituting this into Equation (6.1), the corresponding slip is equal to 0.91 mm. Thus, M16 FBSC stiffness is $95/0.91 = 104$ kN/mm. The corresponding stiffness that can be offered by a welded stud is 100 kN/mm for $\emptyset 19$ mm according to Eurocode 4 (BSI 2004a), which shows the superior stiffness of the FBSC.

Phase three covers slips from 1.5 mm to 14 – 17 mm, where the load reaches the ultimate value in the range of 179 – 206 kN. It should be mentioned that plastic deformations of a bolt in FBSC consists of a combination of shear, bending, and tensile deformations. It is interesting to note that this phase is nonlinear for a short interval, linear for most of its part, and ends with nonlinear in a downward curve. The beginning can be assumed as a transition from elastic to plastic deformations, the linear part is pure plastic deformation, which is similar to the plateau part in the standard tensile tests, and the last part indicates shear failure of the bolts. This is an important feature of FBSC, as the slip at fracture is about 11 times the slip at which plasticity commences (i.e. phase three in Fig. 6.25). The response of the FBSC is approximately like the well-known stress-strain relationship of steel. Therefore, there should be no major concern in composite beam design to ensure that the connectors do not fracture prematurely before developing the beam plastic capacity. It should be mentioned that the comparable ratio in welded studs is 3 (Oehlers and Bradford 1999). In case of welded studs, the slip capacity is 'relatively small about 30% of the diameter of the connector. There is, therefore, a distinct possibility that the connectors may fracture before the composite beam achieves the strength predicted by partial-shear-connection analyses.' (Oehlers and Sved 1995).

6.2.5 Load – Slab Uplift Behaviour

As was recorded in all previous pushout tests in this chapter, where one level of shear connectors is used to connect the concrete slabs to the steel beam, there are other factors

interfering with the slab separation readings. There are different behaviours (separation and contraction) within the same slab and near each bolt. It is interesting to note that, it has been proved (Oehlers and Bradford 1995, and Johnson 2012) from equilibrium of forces of a typical pushout test, that there are internal horizontal forces that push the opposite slabs toward the middle steel beam. The magnitude of one of these horizontal forces is

$$H = F\frac{h_2}{2h_1} \tag{6.2}$$

where H is the horizontal force on each slab, F is the applied load on each slab, h_1 is the distance from the centre of the shear connector to the floor, and h_2 is the half thickness of the slab.

By substituting the appropriate values from the standard pushout test used in this research (Fig. 4.1) into Equation (6.2), the horizontal force H would be equal to 3% of the total applied load on each FBSC (assuming four bolts only). Thus, in each pushout test there is a horizontal force that compresses each slab towards the steel beam. The magnitude of this force is, for example in Test 6, equal to 12 kN. In conclusion, no separation is possible unless an uplift force larger than 12 kN is applied on each slab. The uplift force in pushout tests was said to be the result of the following (Johnson 2012): When slip exists, slabs tends to ride up a stud's collar, or in this case, a bolt's deflected shape. Fig. 6.33 shows the bottom face of a slab after detached from the steel beam at the end of Test 11. Please notice that when slab slides over stud/bolt shank, it actually stretches it without sliding, because of the constraint of stud's head/bolt's plate washer at the other end. In order for the separation to happen, a concrete wedge separated from the grout-plug-slab in front of the bolt will develop. The deflected shape of the bolt will create an inclined slide for the slab to slide-over. Equilibrium of forces at this stage indicates that, the delivered applied load to the slab will have, now, two components; one of them tries to shear off the bolts and the other tries to separate the slab from the steel beam. The later will be resisted by the tensile force of the bolt. No separation is possible unless the tensile forces of each slab are exceeded. To explore this idea, let us take Test 11 as example. Fig. 6.33 shows that the deflected shape of the

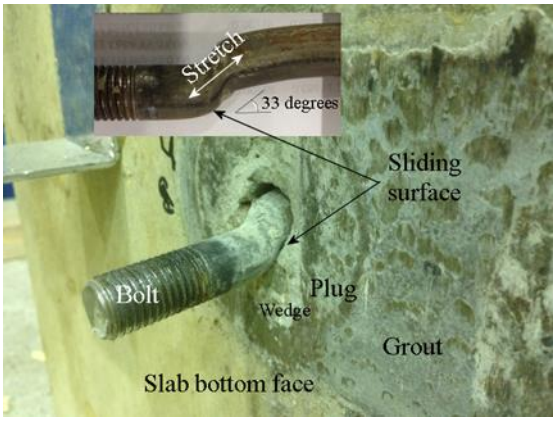

Fig. 6.33. Bolt resistance to slab separation from FBSC Test 11

shank has a 33° angle from the vertical. From the shear resistance of Test 11 listed in Table 6.1, the sliding force at the onset of failure is 179 × cos (60) = 89.5 kN. Assuming the friction angle between the bolt and the grout is 0.5, then the frictional resistance would be 179× 0.5 × cos (30) = 77.5 kN; the resulted sliding force would be 89.5 – 77.5 = 12 kN, which is less than the tensile force (88 kN) of Bolt 4 from Fig. 6.27. Even if the aforementioned frictional resistance is exceeded, the sliding force (89.5 kN) would be less than the summation of the bolt tensile force (88 kN) and the aforementioned horizontal compression force H (i.e. $^{12}/_{2} = 6$ kN). In conclusion, no separation is expected to occur due to the post yield shape of bolts in Test 11.

The other possible causes of slab separation are the eccentricity of loading and tilting of the pushout specimen. These influences may exist due to several reasons, like imperfect positioning of the specimen under the hydraulic jack; nonhomogeneous material properties like concrete in slabs, plugs, or grouts; unlevelled embedment of slabs on the floor; and unsymmetrical dimensions of specimen. In fact, this type of separation is related to the boundary conditions of this particular pushout test. The pushout test used in this research consists of a steel beam sandwiched between two concrete slabs using one row of bolts in each slab, which makes the connection between the three parts similar to pinned joints that cannot resist rotations. Thus, if the upper end of the specimen moves laterally, it will cause the specimen to tilt, and therefore it affects the structural performance of the shear connectors. Because the base of the slabs is grouted to the floor, any tilting of steel beam in the web direction will change the separation/compression of slab relatively to the steel beam. It should be mentioned that in all FBSC pushout tests, there was always some random gaps (<2 mm) between the concrete slabs and steel beam and the only interface with full surface contact is between the concrete plug and the steel flange. Fortunately, the recorded separations in all pushout tests were small (< 0.5 mm) and are known to have a negligible effect on the behaviour of the FBSC.

6.2.6 Design Equation

The FBSC bolt in service will experience torsion (due to tightening procedure), tension, shear, and bending stresses. Other actions that affect the behaviour of FBSC are the relationship between the tensile force inside the bolt and the friction resistance between the plug and steel beam or the interaction between the bending moment at the smooth shank of the bolt and the stiffness of the surrounding concrete (i.e. grout and plug). Thus, the derivation of an exact mathematical design equation (without approximations) for computing the shear

resistance seems to be a very complicated if not impossible task. Instead, most of Code of Practice manuals and related research use empirical equations (Oehlers and Bradford 1995). These equations are derived empirically from pushout and beam tests (e.g. see the work of Oehlers and Johnson (1987)).

Because FBSC does not have a collar or a locking nut, Equation (5.6) cannot be used. Instead, Equation (5.1), which represents the shear resistance of high strength bolts, can be adopted, after some modifications. The equation should incorporate: (1) the effect of friction resistance of the steel beam–concrete interface; (2) the effect of the inclination of the deflected shape of the bolts; and (3) the effect of shear failure through an elliptical cross-section of the bolt. Similar calculations were included in Section 5.2.6, and they will not be repeated here. To this end, the shear resistance of the FBSC is

$$P = 0.6 f_{\mathrm{u}} \left(\frac{\pi d^2}{4 \cos \beta} \right) + T(\sin \beta + \mu \cos \beta) \tag{6.3}$$

and after rearrangement:

$$P = \frac{\pi d^2 f_u}{4} \left(\frac{0.6}{cos\, \beta} + \frac{T}{F_{\mathrm{u}}} (sin\, \beta + \mu\ cos\, \beta) \right) \tag{6.4}$$

in which, T is the preload of bolts, and F_{u} is the tensile resistance, while the rest of variables are as defined before. Please remember that the tensile resistance is from Table 4.5 and it is based on the nominal cross-section area and not on tensile stress area (see Section 4.3 for more details).

The validity of Equation (6.4) is first evaluated by using the results from Test 6. The test used preload T of 60 kN with β = 45° (from Fig. 6.23); therefore, the shear resistance is equal to P = 214 kN, which is only 4% different than the test result of 206 kN (Table 6.1). Please recall that as long as the difference is < 10% (i.e. Eurocode 4 definition for identical tests), the results are accepted.

6.2.7 Experimental Parametric studies

The aims of the parametric tests were to explore the effect of certain parameters, namely bolt diameter and preload, on the behaviour of the FBSC and by doing so, to increase the reliability of the tests and to check the appropriateness of Equation (6.4). The effect of plug's concrete strength was ignored based on the conclusion that it had negligible effect on the connection shear resistance.

6.2.7.1 Effect of Bolt Diameter

Three different diameters for bolts, namely 12, 14, and 16 mm were used in FBSC pushout Tests 8, 10, and 6 respectively. The reasons behind this choice was to check the slip capacity of FBSC below the Ø16 mm limit in Eurocode 4 and because the capacity of the testing rig and strong floor cannot tests using bolts larger than 16 mm. Material properties of these tests are listed in Table. 4.3, while pushout test results are listed in Table 6.2 and plotted in Fig. 6.34. It can be seen from Table 6.2 that although three different diameters were used, and three different shear resistances were recorded, the shear resistance relative to the tensile resistance was almost the same; having an average ratio of 1.12. Please note that Equation (5.1) gives the typical ratio of shear/tensile resistances for Grade 8.8 bolts, which is 0.6. This explains that the superior shear resistance of the FBSC is not because of the high strength material alone but also due to other factors like frictional resistance.

Table 6.2. Results of FBSC Tests 6, 8, and 10

Test No.	Bolt dia. (mm)	Shear resistance (kN/bolt)	Slip capacity (mm)	Deflection angle β (degrees)	Shear resistance/ tensile resistance*	Bolt internal load/ tensile resistance*
6	16	206	16	45	1.15	0.59
8	12	108	12.6	33	1.08	-
10	14	156	13.2	39	1.14	0.51
				Average	1.12	0.55
				Standard deviation	0.031	0.04
				CV %	3	7

***** Bolt tensile resistance is provided in Table 4.5

Table 6.2 also reports that the internal tensile forces in the bolts are moderately stretched to about 55% of their tensile resistance at the onset of failure. Furthermore, information in Table 6.2 proves that as the bolt diameter increases, the slip capacity of FBSC also increases and that it has a value that is almost equal to the bolt diameter. It interesting to know that Eurocode 4 (BSI 2004a) suggests a single value of 6 mm for slip capacity of ductile shear connectors, regardless of stud's diameter, and at the same time limits stud's diameter to be not less than 16 mm. Information in Table 6.2 proves that when using FBSC with bolt diameter less than 16 mm, the connector will achieve more than double the slip requirement of Eurocode 4 (BSI 2004a). It can be concluded from the results in Table 6.2 that Tests 8 and 6 further confirm the behaviour of Test 6, and thereby increase the reliability of FBSC. Fig. 6.34 shows consistent load-slip curves for the three different diameters which support the previous conclusion. The aforementioned three distinct phases in the load-slip curve for M16

bolts (Fig. 6.25) can also be recognized for M14 and M12 bolts. It can be claimed that the structural performance of FBSC is confirmed from five nominally identical pushout tests, further increasing confident and reliability.

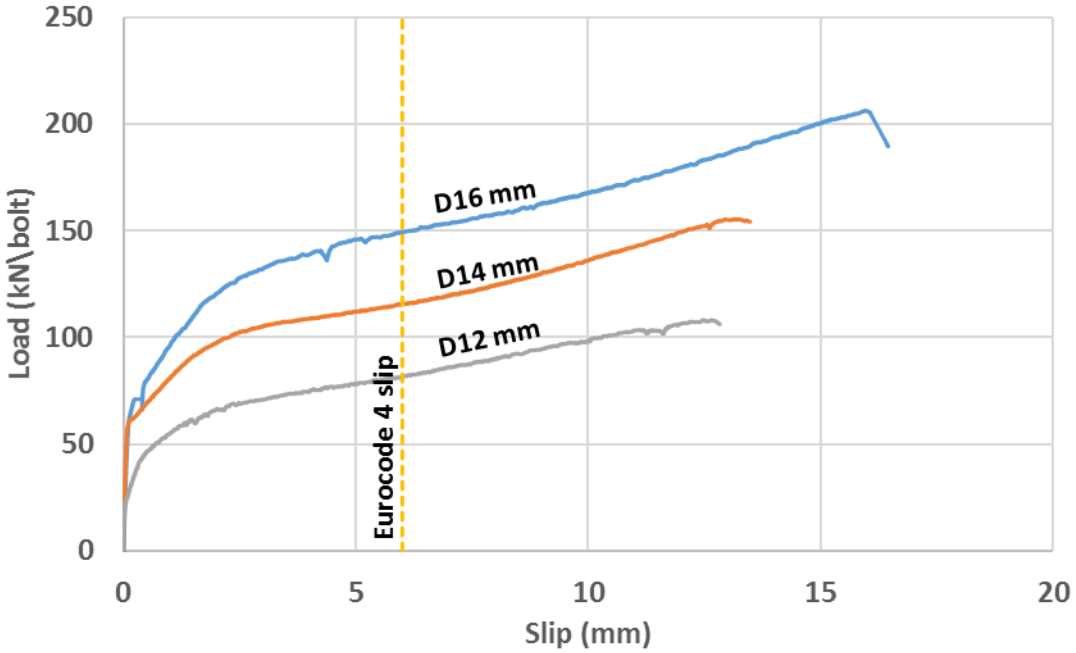

Fig. 6.34. Effect of bolt diameter on the load-slip behaviour of FBSC

BS 5400-5 (BSI 2005f) provides nominal static shear resistances of welded studs for different characteristic concrete strengths and diameters. For a slab of a characteristic compressive cube strength equal to 40 MPa (i.e. higher than the average concrete strength of FBSC Tests 6, 8, and 10 in Table 4.3), stud height in the range of 75 to 100 mm, and stud diameters from 13 to 25 mm, Table 6.3 lists the corresponding nominal shear resistance.

Table 6.3 Shear resistances of welded studs for different diameters

Diameter (mm)	13	16	19	22	25
Shear resistance (kN/stud)	52	82	109	139	168

Fig. 6.35 shows the effect of changing the bolt and stud diameter on the FBSC and stud shear resistances from Tables 6.2 and 6.3. It interesting to notice that the FBSC relation in the figure is linear, which provides evidence of consistent test procedures and material properties used in Tests 6, 8, and 10. In other words, the straight line confirms that the only variable in these tests is the diameter of the bolt. From Fig. 6.35, the FBSC shear resistance *P* can be evaluated using simple linear regression, as follows

$$P = 24.5d - 186 \qquad (6.5)$$

The influence of diameter change on the behaviour of welded studs shear resistance is also included in Fig. 6.35. The stud shear resistance P_{stud} can be calculated using simple linear regression, as follows

$$P_{\text{stud}} = 9.6d - 73 \tag{6.6}$$

From Equations (6.5) and (6.6) and for every 1 mm increase in diameter, the shear resistance increases by 24.5 kN in the FBSC and by 9.6 kN in the welded studs (i.e. the increase in shear resistance of FBSC is 2.6 higher than that of welded studs). It can be concluded from the welded studs line of Fig. 6.35 that the linear influence of the diameter on the shear resistance persists even when d > 16 mm. This may support the linear regression extension line (FBSC) of Fig. 6.35 for d > 16 mm, which claims that the FBSC shear resistance can reach 430 kN/bolt when the diameter is 25 mm. Theoretically, this is true, if certain conditions exist: (1) The pushout failure is by fracture of bolts without any premature failure modes; (2) No plugs crushing due to bolts preloading; (3) No local failure in the steel flange due to bolts bearing on the holes. However, according to the test results reported herein, Equation (6.5) is only valid for $12\ \text{mm} < d < 16\ \text{mm}$, and for the specific data provided in Tables 4.3, and 4.5; especially the tensile strength of Grade 8.8 bolts. More pushout tests are required to confirm the linear regression (FBSC) line of Fig. 6.35 when $16\ \text{mm} < d \leq 25\ \text{mm}$.

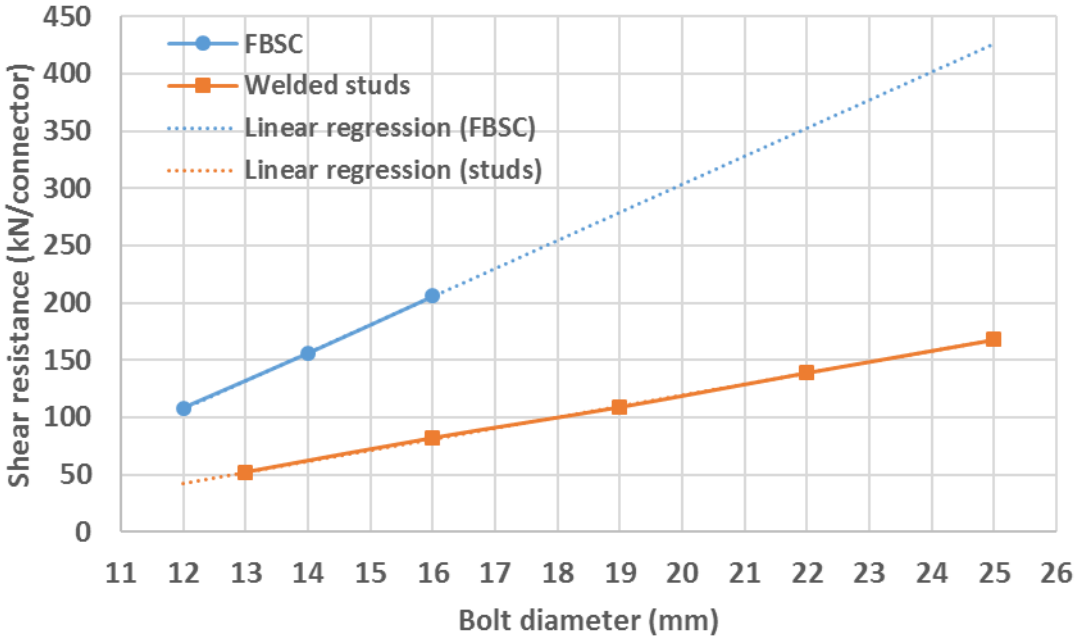

Fig. 6.35. Effect of bolt's diameter on shear resistance from Tests 6, 8, and 10

The validity of Equation (6.4) can be checked using information from FBSC pushout Tests 8 and 10, which correspond to M12 and M14 bolts respectively. Tests 8 and 10 have preloads

of 18.8 kN, and 55.5 kN, respectively. Fig. 6.36 shows the deflected shapes of the fractured bolts from Test 8 with 12 mm bolts. In this figure, the average deflection angle β is 33°. Fig. 6.37 shows the fractured bolts from Test 10 with 14 mm bolts. The figure gives an average deflection angle β of 39°. By substituting appropriate values into Equation (6.4), the shear resistances would be 107 kN and 163 kN, respectively. These values have differences of 1% and 5% with respect to the corresponding pushout tests results.

Fig. 6.36. Bolts deflected shapes of FBSC Test 8

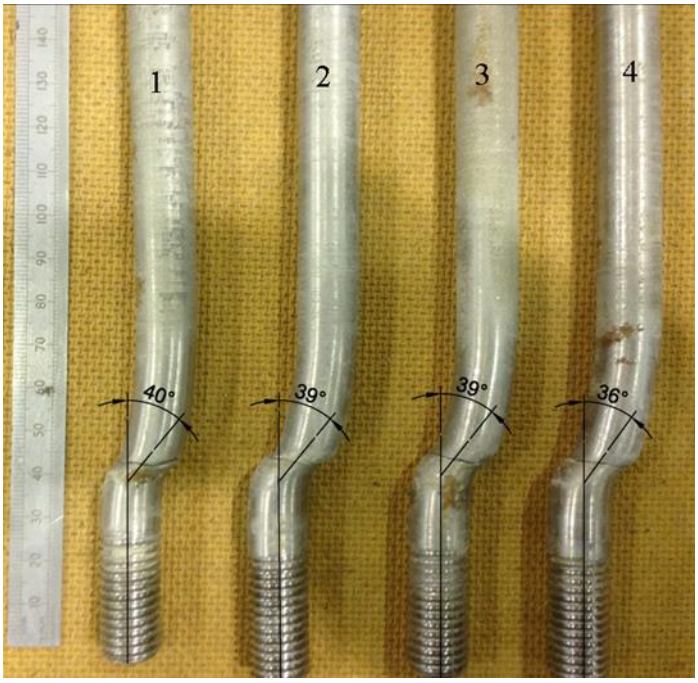

Fig. 6.37. Bolts deflected shapes of FBSC Test 10

FBSC pushout Tests 8 and 10 also recorded the load eccentricities, slab separations, and bolts tensile forces. Thus, it is useful to list this information here. Fig. 6.38 shows the eccentricity of load in the web and flange directions (for web and flange directions see Fig. 5.18) in Test

8, which proves a continuous movement in the direction of flange which led to an increase in slips in Bolts 1 and 2 and reduction in Bolts 3 and 4, as shown in Fig. 6.39.

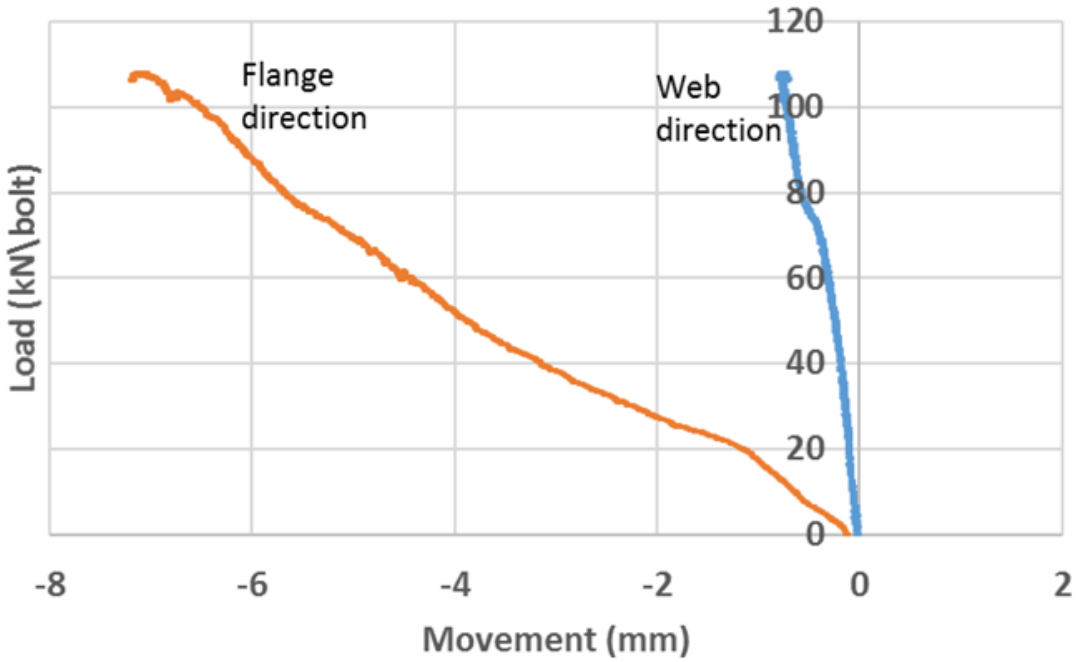

Fig. 6.38. Eccentricity of load during FBSC pushout Test 8

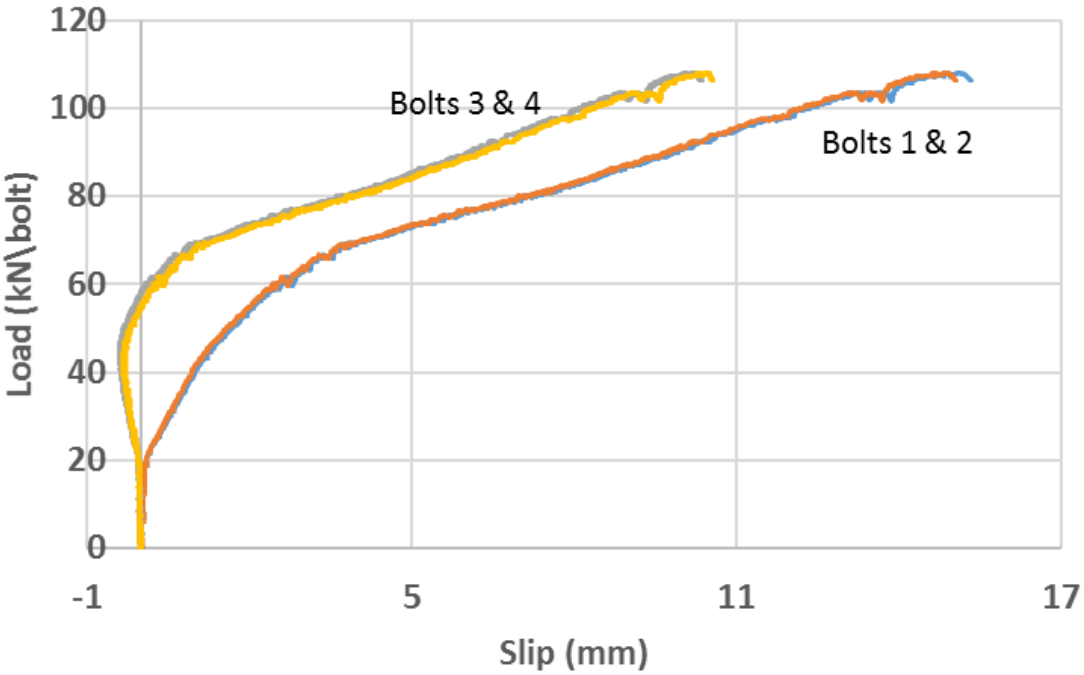

Fig. 6.39. Load-slip behaviour of 4 bolts of FBSC pushout Test 8

The load-slip curves plotted in Fig. 6.39 support the suggestion from Test 6 (Section 6.2.1.5) that the eccentricity of load (Fig. 6.38) creates tilting of the pushout specimen, which in turn affects slips. For example, the slips of Bolts 3 and 4 (Fig. 6.39) were of negative values in the beginning of the test. In order to overcome the eccentricity issue, the applied load is

redistributed among the four bolts (their locations are shown in Figs. 4.1 and 5.18) according to their positions from the eccentric load using bilinear interpolation and Equations 5.2 to 5.5 (explained in Section 5.2.1.6).

Fig. 6.40 plots the load-slip measurements at Bolts 1 to 4 shown in Fig. 6.39. The figure shows four load-slip curves of the four bolts. Each of the four curves has its own 'calculated' load and its own 'measured' slip. The results plotted in Fig. 6.40 indicate that Bolts 1 and 2 have higher shear resistance than Bolts 3 and 4, which indicates that a slight improvement in shear resistance might be achieved if the load eccentricities were eliminated. It should be noted that the failure of FBSC pushout Test 8 was by fracturing of the four bolts. Based on this, the shear resistance of Test 8 is the average of the four bolts and the results are accepted.

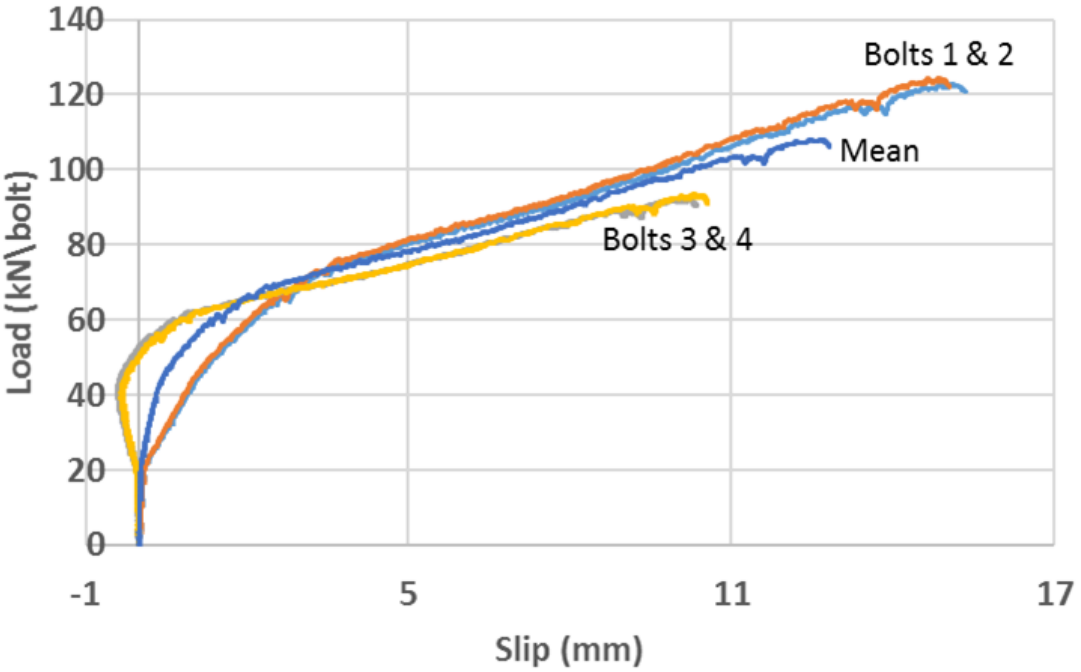

Fig. 6.40. Redistribution of load among 4 bolts of LNSC pushout Test 8

Fig. 6.41 shows slab separation of FBSC pushout Test 8. The maximum separation is 0.4 mm. This figure shows that there are opposite displacements (i.e. separation and compression) in each slab near the bolts. This indicates that the uplift LVDTs measurements (shown in Fig 4.42) were interfered by other factors, like tilting of pushout specimen (Fig. 6.38). It should be noted that positive signs represent compression of a slab towards the steel beam, which proves that there was initial gap between the two.

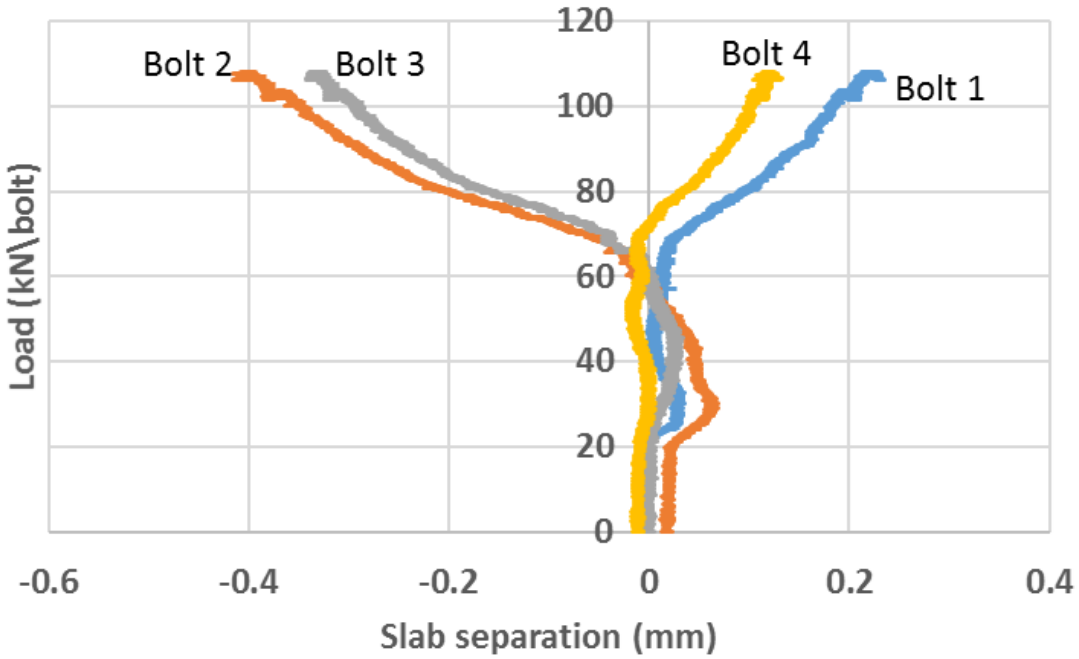

Fig. 6.41. Slab separation of FBSC pushout Test 8

6.2.7.2 Effect of Bolt Pretension

It should be noted that, not all FBSC pushout tests used washer load cells to measure the preload of bolts. In fact, only FBSC pushout Tests 6, 9, 10, and 11, used washer load cells. The preload of the other pushout tests was evaluated through standard DTI washers but one can anticipate low accuracy from the specifications of these DTI washers as they give a wide range of the expected preload, for example, M16 DTI is for a range of 88–106 kN, which means an average of 97 kN with a variation of -/+9%. In addition, the DTI washers only give a measured preload at the instant of bolts tightening and not when the friction resistance is overcome. Please note that some of the preload is lost with time (Section 3.3.1). In order to clarify this point, the preload of four bolts with diameter of 14 mm of FBSC pushout Test 10 were monitored for 7 days after tightening and before the performance of pushout test. The bolts were initially preloaded to about 60 kN tensile force (about 44% of tensile resistance). Fig. 6.42 shows preload loss during the first 7 hours after tightening, which is a variation between 3.4% to 11.6% of its original value. These results were also reported in Table 6.4, which contains, in addition, the preload loss after 2 and 7 days. The positions of Bolts 1 – 4 are shown in Fig. 5.18. It can be seen from Table 6.4 that bolt preload lost about 11% of its original value after only 7 days. It can be seen from Fig. 6.42 that the preload rapidly decreases following the initial tightening, then decreases at a slower rate following a logarithmic curve. The preload-time curve for Bolt 4 after tightening, for example, can be

represented by best-fitting nonlinear regression logarithmic equation with < 1% deviation, as follows:

$$T = -1.02\ln(t) + 54 \qquad (6.7)$$

in which, T is the preload after the loss in kN, and t is the time after tightening in hours.

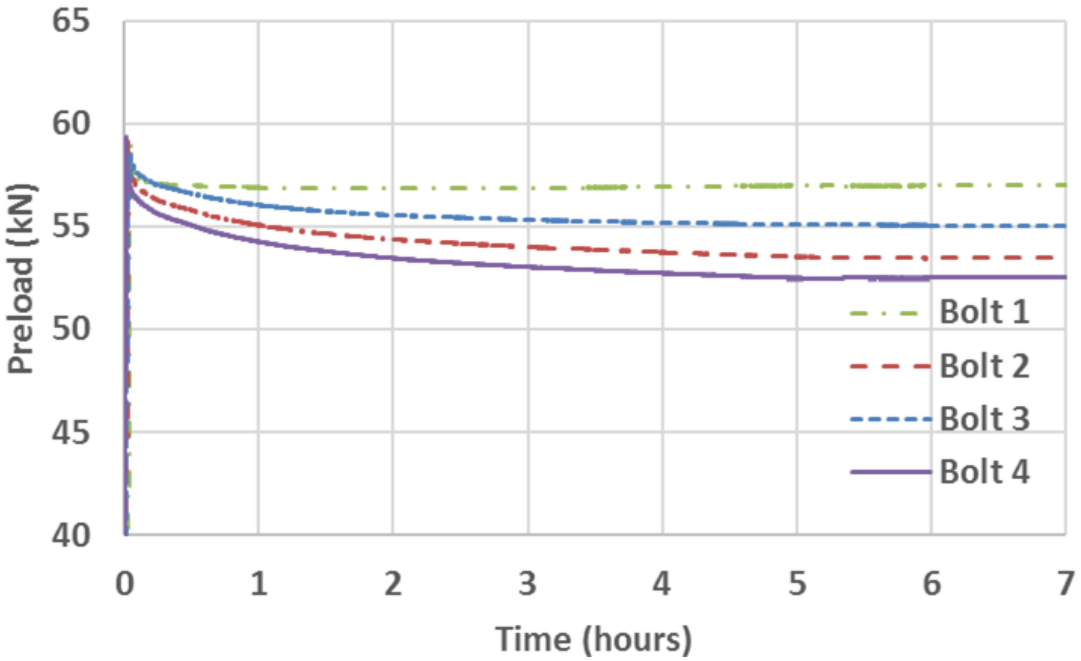

Fig. 6.42. Preload loss of four bolts of FBSC pushout Test 10

Table 6.4. Preload loss of FBSC pushout Test 10

Bolt No.	Preload loss (%)		
	7 Hours	2 Days	7 Days
1	3.41	3.55	7.16
2	9.91	10.02	11.56
3	6.46	6.58	9.37
4	11.55	12.52	15.36
Avg.	7.67	8.17	10.86

The preload-time curves plotted in Fig. 6.42 shows that the amount of preload loss varies greatly between the four bolts. This depends on several factors like: (1) shrinkage of grout and plug; (2) creep of grout, plug, nuts, washers (i.e. hardened, DTI, and plate washers), and flange of steel beam; (3) relaxation of bolt material (Johnson and Buckby 1986); (4) self-loosening of nuts combined with torsional relaxation of bolts after tightening procedures; (5) friction between the nuts and bolts threads; (6) friction between the nuts and their underneath washers; (7) accuracy of fit of parts together as related to tolerance variations

(Bickford 1995). Similar loss rates were found in the references, for example, a loss of 2-11% of preload immediately after tightening, followed by another 3.6% in the next 21 days was recorded for similar high strength bolts by Bickford (1995).

Thus, the preload of pushout tests that used only DTI washers to establish it needs to be rechecked. One way to do this is by relating the measured preload to the frictional resistance at first slip (i.e. to the load at which the friction resistance is overcome). It is possible to derive a relation between the two from pushout tests that used washer load cells, then apply that relationship to pushout test that did not use washer load cells. In this way, the corresponding preload for each pushout test can be estimated. It should be noted that it is not possible to relate the preload to frictional resistance through the usual concrete-steel coefficient as the interface involves an interlock connection between the irregular face of the steel and the in-situ grout, which is compressed by the concrete plug base. Table 6.5 reports the relationship between the preload and the load at first slip from four FBSC tests that used washer load cells to set the preload.

Table 6.5. Relation between preload and load at 1st slip

Pushout test No. (1)	Preload (kN) (2)	Load at 1st slip P_{1st} (kN/bolt) (3)	Friction coefficient (4)	Deviation (%) (5)
6	63.3	71.02	1.12	5.05
9	77.2	79.3	1.03	3.70
10	55.5	61.3	1.10	3.55
11	59.75	60.19	1.01	6.39
Average			1.07	

The second column in this Table represents the average of internal tensile forces of four bolts for each pushout test, the third column represents the load at which the frictional resistance is overcome, the fourth column gives the friction coefficient, which is simply the ratio between the load at first slip and the preload (i.e. column (3) / column (2)), while the last column reports the deviation (i.e. % difference) of each pushout test friction coefficient from the average value obtained from all tests. The required relation was found to be

$$T = 0.94P_{1\mathrm{st}} \tag{6.8}$$

in which, $P_{1\mathrm{st}}$ is the shear force (in kN/bolt) at which first slippage occurs, that indicates overcoming the frictional resistance at the concrete-steel interface. Table 6.5 shows that the maximum deviation was less than 6%, which represents reasonable improvement to the

previous deviation of 9% involved in DTI washers' preload estimation. Thus, using Equation (6.7), the preload values written in Table 4.3 for those FBSC pushout tests that did not use washer load cell and have similar interface condition between concrete and steel can be re-estimated as listed in Table 6.6. It interesting to note that only for Test 8 the prediction of Equation (6.8) shows large preload loss (64%), which may explain the low ratio of shear resistance to tensile resistance (i.e. 1.08 instead of 1.14-1.15) in Table 6.2.

Table 6.6. Re-estimation of preload in five FBSC tests

Pushout test No.	Bolt's diameter (mm)	Preload (kN)		
		DTI (avg.)	Equation (6.8)	Loss (%)
3	16	97	68.4	29
4	16	97	81.1	16
5	16	97	66.7	31
7	14	75	62.0	17
8	12	52	18.8	64

After evaluating all the preloads of the FBSC pushout tests using Table 6.6, the effect of the preload on the shear resistance of the FBSC can be assessed. Tests 7, 9, 10 use three different preloads (i.e. 62, 77, and 55 kN respectively). The results of the tests are listed in Table 6.7, while Table 6.8 and Fig. 6.43 illustrate the effect of preload variations on the behaviour of the FBSC.

Table 6.7. Results of FBSC Tests 7, 9, and 10

Test No.	Bolt dia. (mm)	Shear resistance (kN/bolt)	Slip capacity (mm)	Deflection angle β (degrees)	Preload/ tensile resistance*
7	14	134	14.4	21	0.45
9	14	141	12.4	19	0.56
10	14	156	13.2	39	0.41

* Bolt tensile resistance is provided in Table 4.5

Table 6.8. Effect of preload on behaviour of FBSC of three pushout tests

Pushout test No.	Preload (kN)	Load at 1st slip P_{1st} (kN/bolt)	Shear resistance P (kN/bolt)	Deviation of P from average (%)
9	77.2	79.3	140.5	2
7	62.0	65.9	134.1	7
10	55.5	61.3	156.0	8
Average of P			143.5	

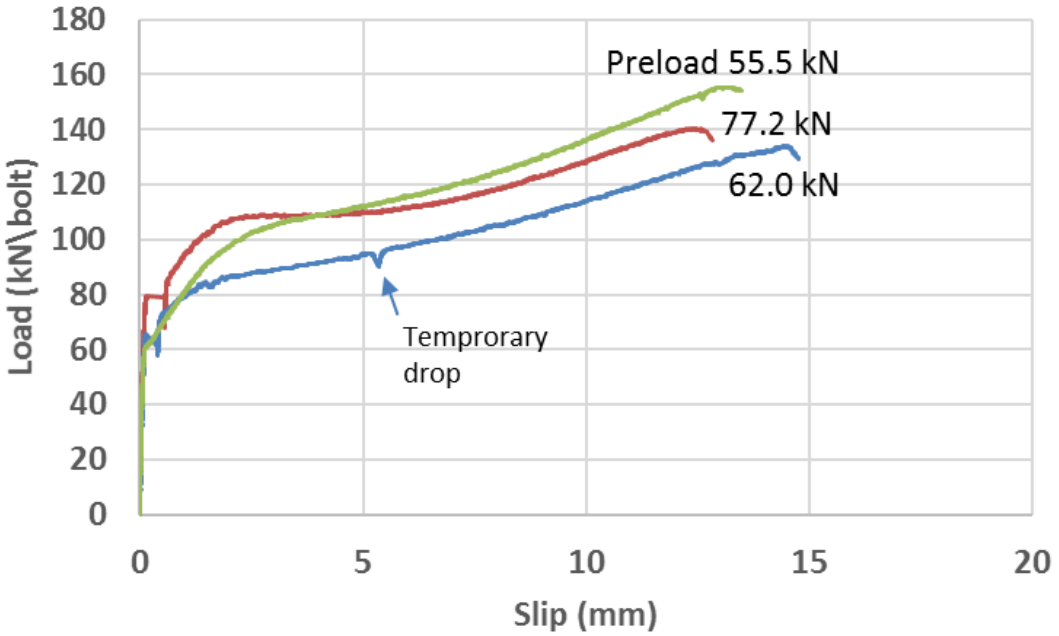

Fig. 6.43. Effect of preload on load-slip behaviour of three pushout tests

Table 6.8 and Fig. 6.43 show that when preload dropped from 77.2kN (i.e. 56% of tensile resistance) to 55.5 kN (i.e. 40% of tensile resistance), two consequences were observed: first, as preload increases, the load at 1st slip increases (i.e. frictional resistance). This finding can be seen easily by comparing the three curves up to 0.2 mm, as shown in Fig. 6.44. The latter figure shows that an increase of 40% in preload results in an increase of frictional resistance by 29%. The second finding is that as preload increases furthermore, the shear resistances from the three tests did not show consistent trend. Actually, the deviation of any shear resistance from the average of the three tests was less than 8%; recalling that Eurocode 4 consider any three tests to be identical if the shear resistance of any individual test deviates in less than 10% (BSI 2004a). Tests 7, 9, and 10 can be considered as identical, and the changes in their preload values did not show a clear reflection on the shear resistance. Further tests are recommended especially using wider range of preload variations.

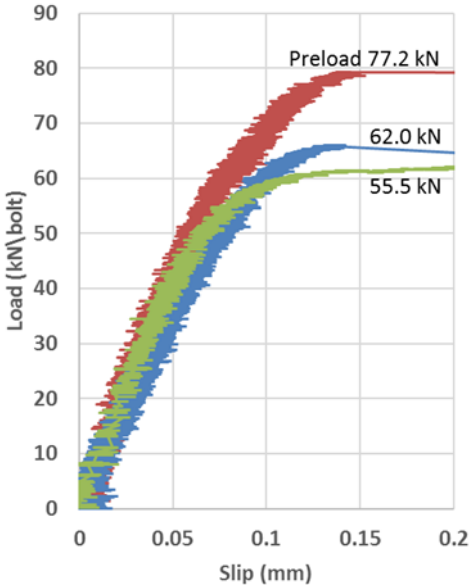

Fig. 6.44. Effect of preload on beginning of load-slip behaviour of three tests

All in all, preloads in the range 55 to 77 kN did affect the load at first slip; that might be of interest to SLS design, but did not significantly change shear resistance for ULS design.

It should be noted in Fig. 6.44 that, changing the preload in FBSC did not affect the initial stiffness of the connectors despite having different frictional resistances. Thus, any recorded slip before overcoming the frictional resistance of a connector is not literally a slip between the bottom face of the concrete plug and the top face of the upper flange of the steel beam. It is more likely to be related to elastic stiffness of the part of slab under compression in front of the conical plugs. It is interesting to observe from Fig. 6.44 that since the curves show an enlargement of the slip axis, the sensitivity of the LVDT is approximately +/- 0.01 mm and the curves do not start from perfect zero but have a negligible deviation of +/- 0.01 mm. This is true in all pushout tests and the beam test performed in this research.

It should be noted in Fig. 6.43 that there was a 'temporary drop' in load-slip curve of Test 7 close to a slip of 5 mm. An unexpected fire alarm caused the stoppage of testing for about 1 hour. During this period, all the pressure valves of the hydraulic jack were closed. However, the effects of creep and relaxation in concrete plugs and steel bolts were obvious. Fortunately, the testing was continued and the load-slip curve retained to its original path as seen in Fig. 6.43.

The validity of the design equation, i.e. Equation (6.4), can be further evaluated using the results from Tests 7, 9, and 10 listed in Table 6.6. Equation (6.4) gives shear resistances of 139 kN, 148 kN, 156 kN for Tests 7, 9, and 10, with differences of 4%, 5%, and 5% respectively. In summary, the justification of Equation (6.4) was made via the application of the equation to five different tests. The results are listed in Table 6.9 and are shown in Fig. 6.45, which indicates a maximum difference of 5%. It appears that Equation (6.4) can be used to predict the shear resistance of FBSC for: plug concrete cube strengths between 65-100 MPa; bolts with steel strength of 889 MPa; diameters from 12 to 16 mm; grout compressive strengths from 35 to 50 MPa; an initial internal bolt force (preload) in the range of 40% to 70% of tensile resistance.

Table 6.9. Comparison among the predictions of Equation (6.4) and pushout tests results

Test No.	Shear resistance (kN/bolt)	Equation (6.4) (kN/bolt)	Difference %
6	206	214	4
7	134	139	4
8	108	107	1
9	141	148	5
10	156	163	5

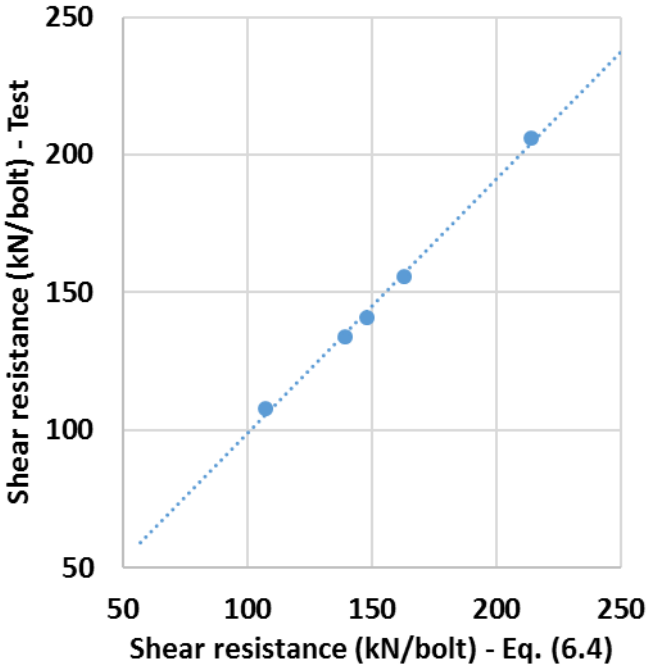

Fig. 6.45. Shear resistance comparison between the predictions from Equation (6.4) and the push-out tests

6.3 Summary

The results of eleven FBSC pushout tests were presented and discussed in this chapter. The experimental program includes six preliminary pushout tests. These tests led to the development of the final robust details, which include frictional resistance, countersunk holes filled with grout, separated conical plugs, oval conical slab pockets, hiding of bolt threads, and formation of two plastic hinges in the bolt of the FBSC. These design features provide FBSC with demountability, superior strength, slip capacity, ductility, and uplift resistance. The structural behaviour, failure mode, load-slip relationship, load-uplift relationship, and bolt tensile force-slip relationship of the FBSC were discussed. The results show that the structural response of the FBSC consists of three phases and that the slip at failure was about 11 times the slip at which plasticity commenced. Comparisons with welded studs show that the shear resistance and slip capacity of FBSC is higher by 2.5 and 2.7 times, respectively. Bolts preload loss was recorded using washer load cells and a practical equation for preload estimation was suggested. Results from the parametric experimental studies, including bolt diameter and preload, were presented. Finally, a simple design equation for FBSC shear resistance was introduced giving against the test results a maximum deviation of 5%.

Chapter 7: Design and Analysis of Composite Beam Test

7.1 Overview

The results of the test on the composite beam using FBSC are presented in this chapter. The construction/preparation of the specimen, testing procedure, test setup, material properties and the instrumentation used to measure displacements, strains, and forces were outlined in Section 4.6. The specifications of the FBSC were documented in Section 3.3, and its behaviour from pushout tests was described in Section 6.2.4. The main purpose of the beam test is to evaluate the performance of the FBSC under flexural action and under the effect of the differences in stress and deformation conditions between a beam test and a pushout test. For example, in a beam test, the applied load is not the direct cause of slippage, as was the case in pushout testing. Bending of the composite beam produces variation in strains between the concrete slab and the steel beam and hence slippage is developed. Additionally, the concrete slab is resting on the steel beam by its own self-weight; therefore, the self-weight and the applied load compress the slab against the steel beam. These parameters and many more do not exist in a pushout test. The behaviour of the composite beam using the FBSC is assessed by recording the applied load, beam deflection, FBSC slip, FBSC tensile force, concrete slab separation, concrete slab strains, and steel beam strains. The results are shown in Figs. 7.1 to 7.31. In general, the composite beam behaved as expected. At low loads, the behaviour of the composite beam with FBSC was linearly elastic, while at higher loads plastic deformations were clearly visible.

7.2 Design of Composite Beam

A composite beam can be designed by assuming that either the steel beam, concrete slab, or shear connectors govern the design. Full composite connection is assumed when either the concrete or steel parts of the composite section yield and that there are enough shear connectors to maintain an equilibrium of forces between them through shear forces at the interface. Usually, the neutral axis of the composite section at the maximum bending is designed to be in the concrete slab, while the steel section is under tension. However, because this composite beam is used to check the performance of the new shear connector, a large slip is required (FBSC slip capacity is 16 mm), and for that reason, partial shear connection design is chosen. In partial design, there are two neutral axes; one in the steel beam section and one in the concrete slab section. Such situation will produce a longitudinal expansion at the bottom side of the concrete slab and a longitudinal contraction at the topside of the steel beam. The FBSC slip is the relative displacement at the interface of the

slab and steel beam. The composite beam is provided with a degree of shear connection of 70% (the design is in Section 7.2.2). The spacing between shear connector rows is 600 mm and each row contains two FBSCs (100 mm c/c apart) (Fig. 4.46). The FBSC is based on the final design used in FBSC pushout Tests 6 to 11. In particular, the shear connection uses: (1) M16 high strength 8.8 bolts of unthreaded shank and 20 mm threads at the ends (material properties of the bolts are listed in Table 4.5); (2) Plugs with detailed geometry shown in Fig. 3.8, and material properties listed in Table 4.6; (3) Grout with mix design and properties listed in Tables 4.1 and 4.6 respectively; (4) Retaining washers with specific dimensions shown in Fig. 4.7 and designed in Section 3.3; (5) Slab pocket of exact shape shown in Fig. 3.5a; (6) Countersunk holes of specific dimensions shown in Fig. 3.4c. The specimen dimensions and material properties were outlined in Section 4.6.2. In brief, the steel beam has 9.173 m length, UB457×191×89 section, and average material properties of $f_y = 355$ N/mm^2, $f_u = 457$ N/mm^2, and E_s= 210.1 GPa. The concrete slab has geometry of 9×1.25×0.15 m with average concrete material properties of $f_{cu} = 61\ \mathrm{N/mm^2}$ and $E_c = 31\ \mathrm{GPa}$, (all the other material properties are listed in Table 4.6).

7.2.1 Full Shear Connection at Ultimate State

Referring to Fig. 7.1 where $b = 1250$ mm is the concrete slab nominal width, and $h_1 = 150$ mm is the concrete slab nominal thickness, the axial strength of concrete is equal to

$$F_c = 0.45\, f_{cu} b h_1 = 0.45 \text{ x } 0.061 \text{ x } 1250 \text{ x } 150 = 5147 \text{ kN}$$

and the axial strength of steel is equal to

$$F_s = f_y A_s = 355 \text{ x } 11.400 = 4047 \text{ kN}$$

where $A_s = 11400$ mm^2 is the nominal area of the steel section.

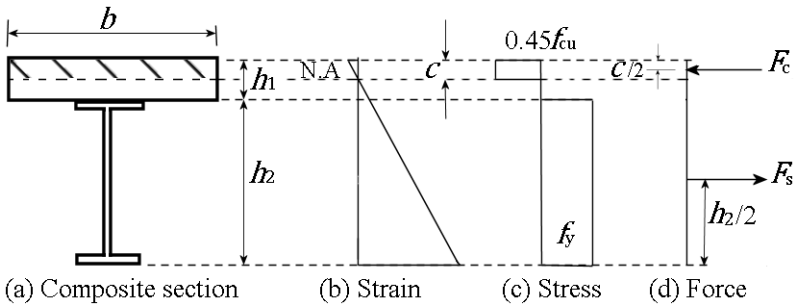

Fig. 7.1. Full shear connection analysis

It should be noted that, according to design codes, the effective width may be chosen larger than 1250 mm (see clause 5.4.1.2 in Eurocode 4 (BSI 2004a)), but this test is a single

composite beam where the stresses along its concrete slab width are expected to be almost constant. This assumption will be checked later in Section 7.3.3. As $F_s < F_c$, the neutral axis (N.A.) is in the concrete, and the axial strength of steel is governing the ULS design. The tensile force in the steel element acts at the mid-depth of the steel element. The compressive force in the concrete element, which is in this case equals the tensile force of the steel, acts over an area of concrete of depth c, as shown in Fig. 7.1. This means that in order to sustain equilibrium, the whole steel element had to yield in tension, the concrete above (N.A.) had to fully yield in compression, and the remainder of the concrete below the (N.A.) has to be cracked under tensile stress. By equating the concrete force F_c with concrete stress over an equivalent area of depth c, and solving for c gives the depth of the (N.A.) from the top fibre of concrete equal to 118 mm. Knowing the magnitude and positions of both the tensile and compressive forces in the composite section, the full shear connection moment capacity, M_{fp}, can be found by taking moments of forces which gives, $M_{fp} = 1306\ \text{kN.m}$. In order to achieve this moment capacity, the strength of the FBSCs in each shear span (i.e. half-length) of the beam must be greater than or equal to the governing force in the composite section, which is in this case the concrete force (i.e. 4047 kN). The total strength of the FBSCs in the whole beam must be at least 8094 kN. The shear resistance of one FBSC from pushout tests is approximately 190 kN (see Table 6.1); therefore, the required total number of the FBSCs to achieve full shear connection is 43.

7.2.2 Partial Shear Connection at Ultimate State

It should be emphasized that the minimum degree of shear connection according to Eurocode 4 (BSI 2004a) for composite beams with 8.5 m span and $f_y = 355$ N/mm^2, can be calculated to be 57%. Davison and Owens (2012) explained that the minimum limit is introduced in order to ensure adequate deformation capacity of the shear connectors as defined by the characteristic slip of 6 mm. As the FBSC had slip capacity of 2.7 times the 6-mm limit, it is practical to use partial shear connection with more confident. Thus, by assuming 70% degree of shear connection, the required number of FBSCs in the two shear spans of the composite beam will be 30. The shear connectors are distributed along the shear spans as pairs at a spacing of 600 mm < 800 mm (i.e. Eurocode 4 limit). Thus, the shear strength of FBSCs in one shear span $F_{FBSC} = (30/2)\times 190 = 2850\ \text{kN}$. As the shear strength of the FBSCs is less than the axial strength of concrete (i.e. 4047 kN), the resultant force in both steel and concrete elements of composite beam must equal to the strength of FBSCs, and hence the shear strength of FBSCs governs the design of the composite beam. In partial shear connection, neither the steel nor the concrete elements are fully yielded in one

direction, and hence each one of them has its own (N.A.) (Oehlers and Bradford 1995). By referring to Fig. 7.2, the axial force in concrete slab is the axial force in the compression concrete part (i.e. 2850 kN) minus the tensile force of the yielded reinforcement (i.e. 340 kN), i.e. 2850 – 340 = 2510 kN. The concrete neutral axis (N.A.1 in Fig. 7.2) can be found by equating the axial force in the concrete slab with concrete stress of an equivalent area above the (N.A.1), as follows

$$c_1 = \frac{2510000}{0.45 \times 61 \times 1250} = 73 \text{ mm}$$

which coincides approximately with the mid-depth of the concrete slab. The strain at the reinforcement is equal to 0.0032 > 0.001625 (i.e. elastic limit Section 4.6.2), which proves that the assumption of yielded reinforcement was accurate.

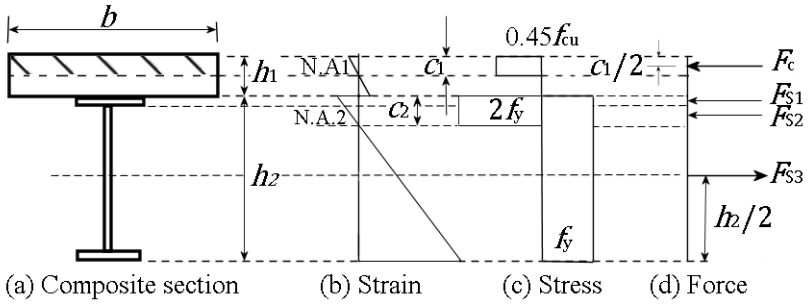

Fig. 7.2. Partial shear connection analysis

It should be noted that the calculation of concrete resistance used the coefficient 0.45 instead of the usual 0.85, because the compressive strength of concrete used in current calculations is taken from average experimental cube tests and not from characteristic cylinder compressive strength.

The steel neutral axis (N.A.2 in Fig. 7.2) can be calculated (by assuming that it is within the top flange and that $F_{S2} = 0$) by equating the tensile force below the (N.A.2) with the sum of compression forces in the concrete (i.e. 2850) and in part of the steel section that is under compression above the (N.A.2), as follows

$$c_2 = \frac{(4047 - 2850) \times 1000}{191.9 \times 2 \times 355} = 9 \text{ mm}$$

where the nominal width of the top flange is 191.9 mm. Hence (N.A.2) is found to be inside the top flange of steel section at a distance from the interface equal to 9 mm, which can create a compression force of 4047 – 2850 = 1197 kN. Based on this finding, part of the steel

section would be under compression. Its capacity could be reduced due to possible local buckling of the flange or web. The steel section UB457×191×89 kg is classified as *Class 1* section, where a full plastic moment of the cross section can be developed, and it has a sufficient rotation capacity to form a plastic hinge without reduction by local buckling (see clause 5.5 of Eurocode 3 (BSI 2005b)). This design feature will be confirmed later in Section 7.3.1.

By taking moments of forces around (N.A.2), for example, the moment capacity of the composite beam with 70% degree of shear connection is

$$M_{\mathrm{p70\%}} = 4.047\left(\frac{463.4}{2} - \frac{9}{2}\right) + 2.51\left(150 - \frac{73}{2} + \frac{9}{2}\right) - 0.34(25+9) + 1.197(\frac{9}{2})$$
$$= 1210\ \mathrm{kN.m}$$

The latter is 93% of the full shear connection moment capacity (i.e. 1306 kN.m), due to 30% reduction of the degree of shear connection. Thus, the partial shear connection method can be considered more economical in designing steel-concrete beams as compared to full shear connection method. It should be emphasized that the previous finding does not depend on the type of shear connector, but in case of FBSC the reliability of design is increase due to the large slip capacity of the M16 FBSC (i.e. 16 mm compared to 6 mm of Ø19 mm welded studs).

It should be noted that, the previous calculations assumed that shear connectors are needed along the entire length of the beam, even though, there is no longitudinal shear force in the middle part between the two point-loads. Five pairs of FBSC were distributed using the same spacing of 600 mm. These additional connectors, sometimes (see Dallam and Harpster 1968), are not included in the calculations as they do not significantly contribute to the shear strength of the shear connectors as will be seen later (Section 7.3.2). However, to follow the standard practice in composite beams (Yam 1981), i.e., distributing shear connectors at equal spacings along the whole length of the beam, and to resist any uplift forces if they exist in the middle part, these additional shear connectors are included. Thus, the total number of shear connectors would be 30, which provide a degree of shear connection of 70%.

It should be kept in mind that the previous calculations are based on rigid plastic analysis which usually gives conservative results compared to tests because of several assumptions, i.e. by considering that the maximum strength of steel is the yield strength and ignoring strain hardening, by ignoring the effect of reinforcement in the compression zone of the concrete

slab, and by ignoring the tensile strength of concrete. Also, the shear strength of the FBSC was taken from pushout tests results, assuming roughly that the behaviours of FBSC in pushout and beam tests are identical, which will be further discussed in Sections 7.3.1 and 7.3.2.

7.3 Analysis of Composite Beam

7.3.1 Load-Deflection Behaviour

Fig. 7.3 and Table 7.1 present the deflection results of the composite beam with FBSC, while Fig. 7.4 shows the deflected shape of the beam at the end of test.

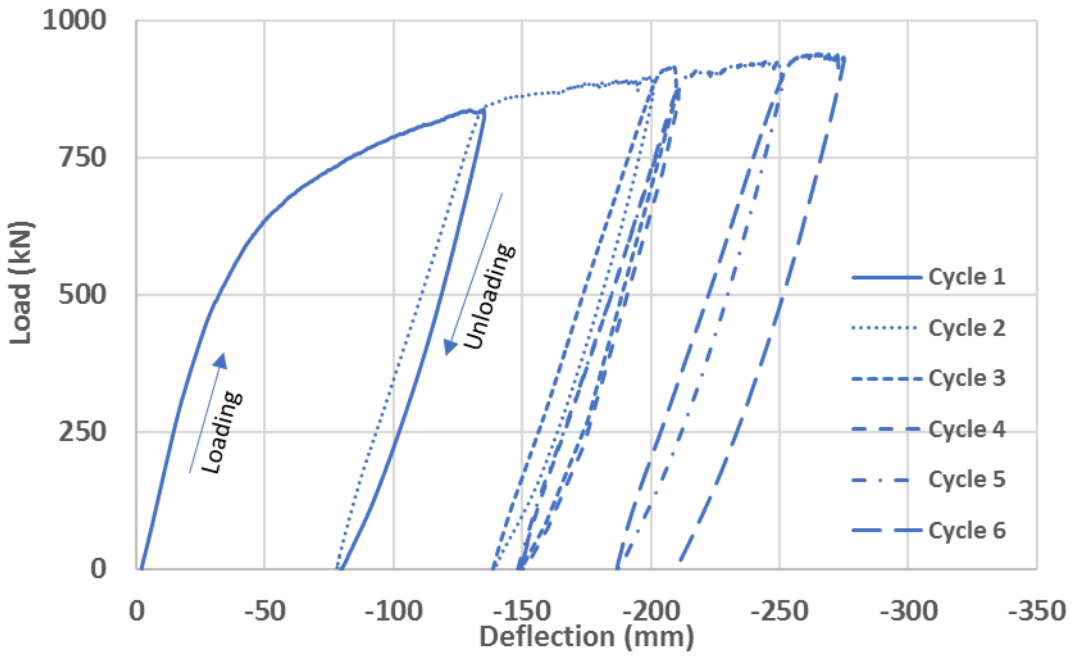

Fig. 7.3. Behaviour of composite beam with FBSC during beam test

Table 7.1. Load-deflection results of beam test with FBSC

Load cycle No.	Maximum Load (kN)	Maximum Deflection (mm)	Residual Deflection (mm)
1	838	135	80
2	897	201	139
3	914	210	149
4	878	211	150
5	926	251	187
6	939	275	209

Fig. 7.3 shows the load versus deflection relationship where 'Load' represent the reading of the 100t load cell shown in Fig. 4.56, while the 'deflection' represents the measurement of long LVDT S12 shown in the aforementioned figure. A common technical problem in full-

scale beam tests with spans (e.g. 8.5 m) is that due to large vertical displacement (e.g. > 200 mm), the hydraulic jack is run out of stroke during the test (e.g. Dallam and Harpster 1968). This also occurred in this beam test as the capacity of the 100t hydraulic jack is 175 mm and of the 200t is 150 mm, while the maximum vertical deflection is 275 mm (Table 7.1). Fortunately, after the first cycle of loading, there was enough residual deflection for additional bearing plates to be placed between the jack and the composite beam, as shown in Fig. 7.5. This procedure was repeated five times, which explains the six load cycles presented in Fig. 7.3 and Table 7.1. The term 'maximum' in Fig. 7.3 and Table 7.1 is the highest value reached for each cycle of loading, while the 'residual deflection' represents the remaining deflection at mid-span after removing the load after each cycle. The maximum deflection recorded at the end of test is 275 mm, as shown in Fig. 7.4, which represents a ratio of *L*/31 as compared to the maximum allowed SLS deflection for simply supported beams (but not for bridges) of *L*/200 (Davison and Owens 2012) or *L*/360 (Yam 1981). No similar limits were specified for bridges in BS EN 1994-2 (BSI 2005a) and BS EN 1993-2 (BSI 2006). Vayas and Iliopoulos (2014) state that 'there exist no code-prescribed deflection limit for road and pedestrian bridges'. Johnson and Buckby (1986) explained this as follows: 'Highway bridges (but not railway bridges for high-speed trains) turn out to be so stiff for other reasons that limitation of deflection need rarely be considered in design.' Vayas and Iliopoulos (2014) suggest an SLS vertical deflection limit of *L*/600 for railway bridges when the speed is < 80 km/h.

Fig. 7.4. The deflected shape of the composite beam

The elastic deflection at the mid-span of a four point-loaded composite beam, with full interaction between concrete and steel, from beam theory, is given by

$$\Delta_{\text{th}} = \frac{W\ a}{24\ EI}(3L^2 - 4a^2) \qquad (7.1)$$

where Δ_{th} is the elastic deflection, W is one point load, a is the distance from the point-load to the start of the beam, L is the beam span, E the modulus of elasticity, and I the moment of inertia. It should be noted that EI, for deflection evaluation, are based on the transformed section method (Davison and Owens 2012).

It should be noted that the test was stopped after cycle 6 without a collapse failure. The reason for this is due to several factors, as follows: (1) The experimental results exceeded the expected calculations; (2) The maximum applied load approached 100t, which is close to the testing rig capacity; (3) Safety concerns related to the stability of several bearing packing plates under the load, as can be seen from Fig. 7.5(b). The maximum load was 939 kN associated with a mid-span deflection of 263 mm. Please note that, the load was stopped at a deflection of 263 mm, but the beam continues to deflect until 275 mm due to creep, and after this stage, the beam was unloaded, and the deflection reduced to 208 mm of residual deflection. The maximum load is exerting a maximum bending moments of 1292 kN.m, which is constant moment along the middle part between the two point-loads of the spreader beam. Additionally, the maximum shear force of 463 kN, can be located from the aforementioned two point-loads to the ends of the composite beam, while the middle part between the two point-loads has negligible shear force but not zero (due to the minor effect of self-weight loads).

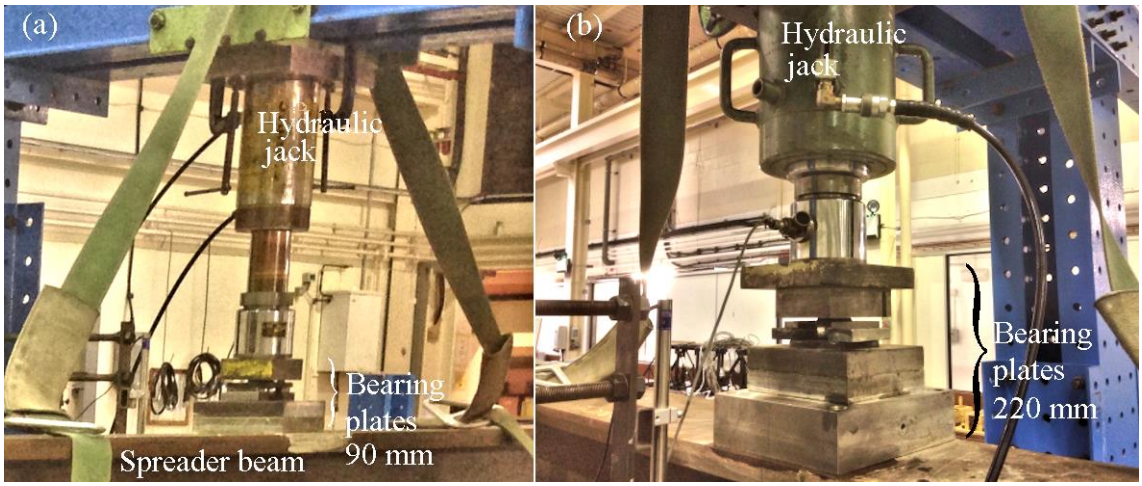

Fig. 7.5. Packing bearing plates in (a) 1st, and (b) 6th cycles of loading

It can be concluded from simple bending moment and shear force diagrams (not shown) that under the spreader beam's point loads, there exist maximum shear V_{max} and maximum moment M_{max} at the same point of the span. In such cases and according to Eurocode 3 (BSI 2005b), if the applied shear (i.e. $V_{\text{max}} = 939.3/2 = 470$ kN) is higher than 50% of shear

resistance of the steel section, a reduction in bending resistance of the beam is required. The shear resistance (*V*) can be calculated using:

$$V = \frac{f_y}{\sqrt{3}} h_2 t_w \tag{7.2}$$

in which, h_2 is the height of the steel section and t_w is the thickness of the web of the steel section. After substitution into Equation (7.2), the shear resistance would be equal to 997 kN, which is larger than double V_{max}. The influence of the applied shear when combining the bending moment can be ignored during this test.

The full-connection plastic moment capacity of the composite beam is $M_{fp} = 1306$ kN.m (Section 7.2.1). By comparing this value with the maximum bending moment recorded from the test, which is 1292 kN.m, a conclusion can be drawn that the composite beam with FBSC had reached a strength equivalent to its full plastic bending capacity during the last cycle of loading. Thus, both steel and concrete might had reached their yield strengths. The next subsections will check this assumption. It should be noted that the calculations of M_{fp} is based on rigid-plastic analysis, which assumes that the materials are fully yielded with an infinite deformation capacity that can be assumed from the plastic plateau. The rigid-plastic analysis method can be considered as an upper limit to the strength of composite beams. This can only occur if none of several premature failure modes occur first. Such failure modes include (Oehlers and Bradford 1995) (1) lateral-distortional buckling of steel beam, (2) local buckling of the steel plates, (3) fracture of shear connector; (4) splitting of concrete slab. The beam was designed to avoid failure modes 1 and 2, while the superior performance of FBSC ensures that modes 3 and 4 do not take place.

The load-deflection response of first load cycle reaches about 90% of the plastic moment capacity, as shown in Fig. 7.3 (because of the reason explained earlier). All the other load cycles start with a linear part, followed by a small nonlinear load-deflection response. Thus, for purpose of clarity, the combination of loading behaviour in the first cycle, and the build-up of nonlinearity in loading cycles 2-6, is shown in Fig. 7.6. The Y-axis represents the maximum bending moment at the mid-span, while the X-axis represents the corresponding mid-span vertical deflection.

It should be noted that, during the construction of the composite beam, the beam was propped by two supports (as was explained in Section 4.6.2) and that this situation represents the zero-deflection, and zero-moment state. When the supports were removed,

a deflection of about 2 mm was recorded at mid-span, without any changes in all other measurements like strains, slips, separations, and tensile forces.

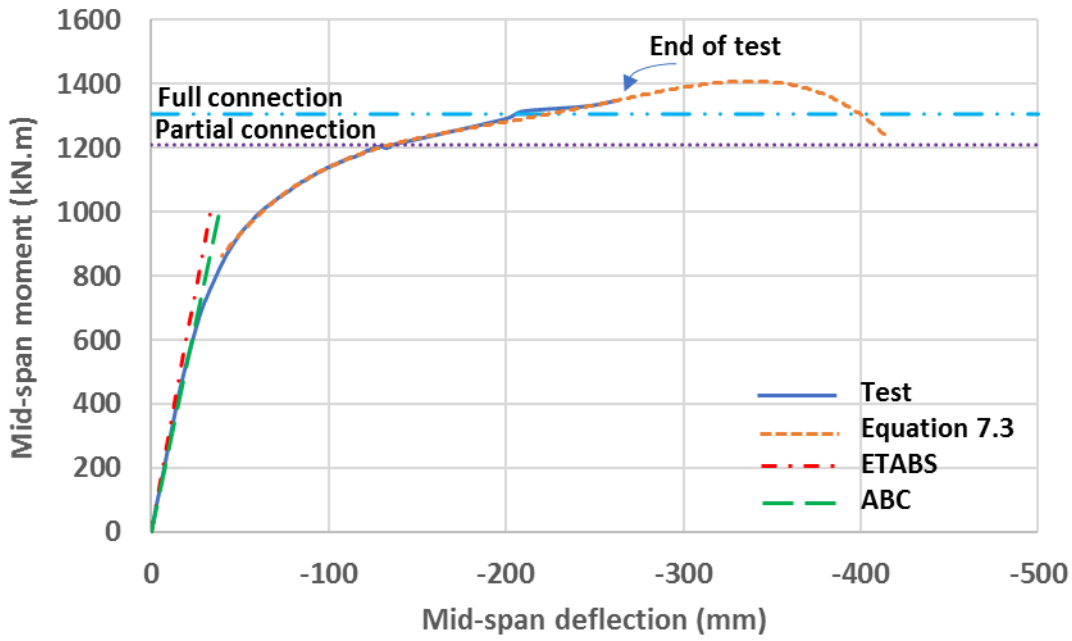

Fig. 7.6. Behaviour of composite beam with FBSC during beam test

That deflection was due to self-weight of the composite beam (i.e. uniformly distributed load of 5.3 kN/m plus two concentrated hogging moments of 0.17 kN.m at the ends of span), and due to self-weight of the spreader beam (i.e. two point-loads of 6 kN, three metres apart). One of the beneficial features of a spreader beam is that it has a self-weight approximately equal to the weight of an ordinary car and a distance between its point loads approximately equal to the distance between car axles; therefore, it roughly simulates the vehicle loading in actual bridges. These two types of loads caused an initial resultant bending moment at mid-span equal to 57 kN.m, which have been included in Fig. 7.6 and those to follow, but not in Fig. 7.3 or Table 7.1. Thus, having a car-weight over the composite beam only causes a bending moment of 4% of its plastic bending capacity with maximum deflection of 2 mm. It should be noted that, by adding the initial bending moment, the maximum applied bending moment is 1348 kN.m, and it is now more obvious that the composite beam with FBSC reached and exceeded the partial connection plastic moment capacity (i.e. 1210 kN.m) and even exceeded the full plastic capacity (i.e. 1306 kN.m). These calculated resistances are shown by horizontal lines in Fig. 7.6.

As was explained earlier in this section, the composite beam yielded when the vertical deflection was 275 mm without a collapse failure. The test was stopped due to technical safety cautions. Thus, the ultimate moment and deflection were unknown. However, a rough

estimation can be made as follows. Fig. 7.6 shows that a best-fitting curve, Equation (7.3) curve, can be made for the nonlinear part of the moment-deflection response. The best-fitting curve was formulated from a 4th degree polynomial nonlinear regression, as follows

$$M = -2.69\times10^{-7}\Delta^4 - 2.43\times10^{-4}\Delta^3 - 0.08\Delta^2 - 12.46\Delta + 478.47 \qquad (7.3)$$

where M is the bending moment (in kN.m), and Δ is the vertical deflection at the mid-span (in mm). The deflection is assumed to be for the negative sign convention. The expression will be valid to vertical deflections ≥ 40 mm. It should be stated that Equation (7.3) is only representative of this particular beam test with FBSC and cannot be generalized for other practical situations. If the curve of Equation (7.3) is extended beyond the maximum measured deflection of 275 mm (i.e. 'end of test' as shown in Fig. 7.6), a prediction of the failure moment can be obtained. Three pieces of evidences are given in Section 7.3.2 to support this proposal. The predicted maximum moment and the corresponding deflection are found to be 1415 kN.m and 340 mm respectively. These predicted results are close to the test results. This finding means that, if the prediction is true, the beam was at about 95% of failure moment when the test stopped. Failure of the composite beam designed with FBSC can be due to (1) crushing of concrete slab at top surface of mid-span; (2) fracture of the FBSCs at the ends of the beam; (3) fracture of the steel beam at bottom surface of mid-span. The latter is unlikely to happen first due to the high ductility of the steel beam.

It can be concluded from the test information in Figs. 7.3 and 7.6 that there is a linear variation in moment-deflection response up to 50-55% of maximum bending moment. After that, a nonlinear response is followed with a reduction in stiffness. The latter consists of a gradual increase in moment with substantial increase in slip until the test was stopped. Fig. 7.3 shows that the unloading path does not coincide with loading path. The latter is due to residual deflection. However, the load path of the second cycle is very close to the unload path of the first cycle, and so on in the subsequent cycles. Surprisingly, all the loading cycles have almost the same initial stiffness (at 50% of maximum moment). This can be explained by recalling that the initial stiffness of any loading cycle is dependent on the friction resistance of FBSCs. No significant changes in initial stiffness can be noticed from loading cycles. Nevertheless, this explanation will be further discussed when outlining the results of FBSC bolt tensile force. This observation could be useful in estimating the performance of composite beams with FBSC, which have been in service for a long time, or even have been under severe loading conditions, by measuring their current stiffness.

Two software programmes for steel-concrete composite beam design were used to predict the moment-deflection relationship of the composite beam up to SLS of 50% of moment capacity. ETABS2016 is from Computers and Structures, Inc., and ABS is from ArcelorMittal Commercial Sections. Both programmes use the finite element method to idealize the steel-concrete composite beam and have the ability to handle partial shear connection design. For beams with partial composite connection, the programmes calculate the deflections assuming an elastic distribution of stresses, where the strain in both the concrete and the steel is proportional to the distance from the elastic neutral axis of the transformed section (CSI 2015). In other words, the programmes cannot calculate the slip between the concrete slab and steel beam and therefore do not include its effect on the calculation of deflection of the composite beam. Hence, they are helpful at early stages of loading were full interaction can safely be assumed to exist. Fig. 7.6 shows the results of both programmes, and as can be seen the composite beam test and the two numerical predictions are very close together up to about 700 kN.m. In conclusion, vertical deflection of the composite beam with FBSC can be calculated reliably for SLS purpose using elastic theory like Equation (7.1).

7.3.2 FBSC Slip

When there are no shear connectors between the concrete slab and the steel beam, and thus no resistance to slip at the interface, the analysis is referred to as *no-interaction*. When there is a kind of glue between the concrete slab and the steel beam, and thus the analysis assumes no slip, then this is referred to as *full-interaction*. Lastly, when the analysis assumes a controlled slip at the interface, this is referred to as *partial interaction*. It was believed (Oehlers and Bradford 1995) that 'all composite beams with mechanical shear connectors exhibit partial interaction, since the mechanical shear connectors have to slip before they resist shear.' Thus, in welded studs, for example, they must slip in order to function as shear connectors and transmit the shear forces between concrete and steel. This is essential to maintain static equilibrium of forces in the composite section as explained earlier in this chapter. However, 'tests have shown that even when full interaction is achieved, slips between the slab and the flange do exist at very small loads' (Molenstra 1990). The only possible way to simulate full interaction using welded studs is to increase their number to the extent that they enhance the natural chemical bond between the concrete and steel at low loads, which leads to the inconsistency that 'shear connectors are unnecessary as long as they are there' (Yam 1981).

Fig. 7.7 shows the relationship between the bending moment at mid-span and the slip at the right-end of the concrete slab (S9R in Fig. 4.55). This slip was chosen because it is 0.8% higher than that at left end (S9). No slip (i.e. full-interaction) can be observed until the bending moment had reached approximately 500 kN.m. At this level of moment, the mid-span deflection is 20 mm (i.e. *L*/425) (see Fig. 7.6) and exceeded the SLS limit of *L*/600 (Vayas and Iliopoulos 2014) (i.e. 14 mm). In other words, the structural performance of FBSC used in a 70% partial connection composite beam ensures full-interaction between the concrete slab and the steel beam for deflections exceeding the SLS deflection limit by 30%. Increasing the bending moment further, reduces the stiffness of the FBSC until reaching a moment of about 900 kN.m (74% of partial capacity) and a slip of less than 2 mm, where a non-linear relationship initiates. Gradual increase in bending moment with considerable increase in slip is followed until the end of the test (where the measurement records 13 mm slip).

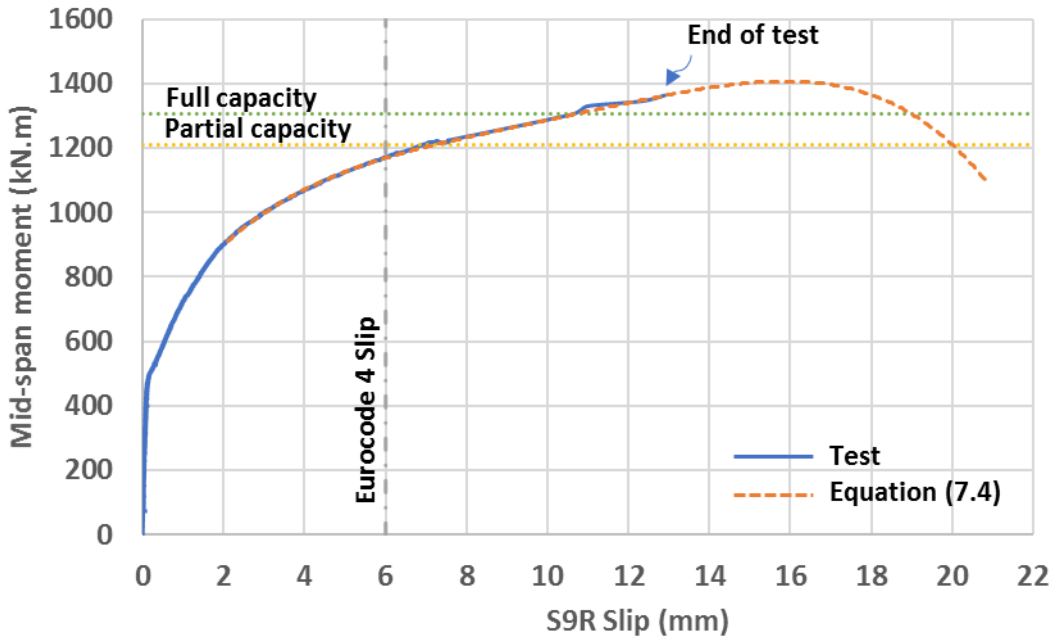

Fig. 7.7. Moment-slip behaviour during composite beam test

Fig. 7.7 shows that it is feasible to assume full-interaction analysis, using 70% partial shear connection, until about 40% of partial connection moment capacity and to about 50% with less than 1 mm slip.

By comparing the load-slip curves in Figs. 6.25 and 7.7, it can be seen that compatible behaviour of the FBSCs exist between the composite beam and pushout tests. The same three phases of the load-slip curve that were repeatedly experienced in FBSC pushout tests can be recognized in Fig. 7.7. The first phase represents frictional resistance and chemical

bond, which are due to bolts preloads (i.e. 88-106 kN). As was explained in Section 4.6.3, all bolts were tightened to proof load via DTI washers, however, four of them were equipped with washer load cells for continuous measure of the bolts tensile forces. For example, let us consider FBSC S8, which is the last connector in the left end of the beam, as shown in Fig. 4.55. A slip of 1 mm was recorded at a moment of 800 kN.m. The corresponding tensile force recorded for FBSC S8 at a slip of 1 mm was 100 kN. The shear resistance of the FBSC at the same slip of 1 mm can be found from Equation (6.8), as follows: $P_{1\mathrm{st}} = \frac{100}{0.94} = 106$ kN/bolt, where $P_{1\mathrm{st}}$ is the shear resistance at first slip. This is true if the behaviours of the FBSC in the pushout and beam tests at 1 mm slip are identical. This proposal is supported by the fact that, both pushout and beam tests share the same boundary conditions in the interface between the concrete plug and the steel beam and the same bolt preloads. Using Equation (6.1) for a slip of 1 mm, $P = 97$ kN/bolt, which is 91% of $P_{1\mathrm{st}}$. Thus, by using Equation (6.1), it is possible to predict the shear resistance of all shear connectors in the beam test from their slips (presuming slip $\geq$ 1 mm). On the other hand, the corresponding stiffness of the FBSC, from Equation (6.1), is equal to 97 kN/mm and it can be used to calculate the shear resistance of any connector that have a slip ≤ 1 mm. The sum of shear forces in all the connectors in half length of the beam is equal to the concrete compressive force at mid-span section (from static equilibrium).

Furthermore, Fig. 7.7 shows that the maximum slip in the composite beam was approximately 13 mm, which is about 80% of the FBSC slip capacity from pushout tests (i.e. 15.7 mm from Table 6.1). No shear connector was about to fracture when the beam test had stopped. This is based on the assumption that the behaviour of FBSC is the same in the pushout and beam tests. As was explained earlier (Section 7.3.1), the beam test was stopped due to health and safety. The beam test could not record the ultimate moment when the slip reaches the slip capacity of the FBSC. A rough estimation can be made to solve this issue as follows. Fig. 7.7 shows a best-fitting curve, i.e. Equation (7.4), is used for the nonlinear part of the moment-slip behaviour of the composite beam test. The best-fitting curve was constructed using a 4$^{\mathrm{th}}$ degree polynomial nonlinear regression, as follows

$$M = -0.038705S^4 + 1.58487S^3 - 24.25S^2 + 191S + 603 \qquad (7.4)$$

in which, S (in mm) is the slip at the ends of the beam. Equation (7.4) is valid for slips > 2 mm and it has a CV of 0.01%. If the curve of Equation (7.4) is extended beyond the maximum measured slip of 13 mm (i.e. 'end of test' as shown in Fig. 7.7), a prediction of the failure moment can be obtained. The predicted moment at the onset of failure is 1406 kN.m (at the

mid-span), and so from Equation (7.4) the corresponding slip is 15.9 mm (at the end of the beam). Please notice that the predicted slip is 99% of the average measured slip capacity of the FBSC (from pushout tests, Table 6.1). Thus, this is the first evidence to support the prediction of the failure mode since the slips from two different tests are identical.

Equations (7.3) and (7.4) were independently developed. In particular, Equation (7.3) was developed based on mid-span deflection measurements, whilst Equation (7.4) was developed based on slip measurements. When both equations are extended beyond their measured data, they predict the same failure moment (the difference is 0.6%). This is the second evidence to support the prediction of failure mode.

Fig. 7.8 shows the effect of mid-span vertical deflection on slip of shear connectors on the left side of the composite beam. Referring to Figs. 4.55 and 7.9, S8 represents the shear connector near to the left end of the concrete slab, while S2 represents the shear connector near to mid-span. The rest of the connectors were distributed between S2 and S8 at 600 mm spacings. It can be seen from Fig. 7.8 that a linear relationship, between deflection and slip exists straight away after overcoming the initial frictional resistance of all shear connectors; despite the fact that both of them (deflection and slip) have a nonlinear behaviour with respect to the applied moment. Shear connectors S6-S8 behave identically, while S5 and S4 slightly different with maximum lag between them of about 2 mm. Thus, if fracture could happen with this pattern, then, shear connectors S5-S8 could fracture at the same time. This can be presumed based on pushout tests experience. By extending the curve for S8 in Fig. 7.8 until it reaches the slip capacity of 15.9 mm the corresponding vertical deflection would be 340 mm, which is the same as the predicted one from Equation (7.3), as shown in Fig. 7.6. This is the third evidence to support the predicted failure mode.

It should be noted that the maximum measured slip of 13 mm is occurred, if the 8.5 m beam deflects by 275 mm (i.e. $L/31$). Theoretically, this means that the composite beam can be lengthened, for example, to 30 m span and have the same slip of 13 mm, if it deflects to the same $L/31$ (i.e. 968 mm). In other words, the 30 m beam can deflect to about one metre without fracturing the FBSCs (assuming other failure modes are prevented). On the other hand, the vertical deflection at a slip of 6 mm (i.e. for welded studs) is 110 mm (i.e. $L/77$) from Fig. 7.8. By comparing the deflections from FBSC and welded studs, a conclusion can be drawn that the beams with FBSC have a factor of safety of 19 compared to 8 in welded studs from the SLS limit of $L/600$. This indicates that the composite beams equipped with FBSC can

be suggested for long spans composite beams due to the large slip capacity of the FBSC. More tests are required to prove this suggestion.

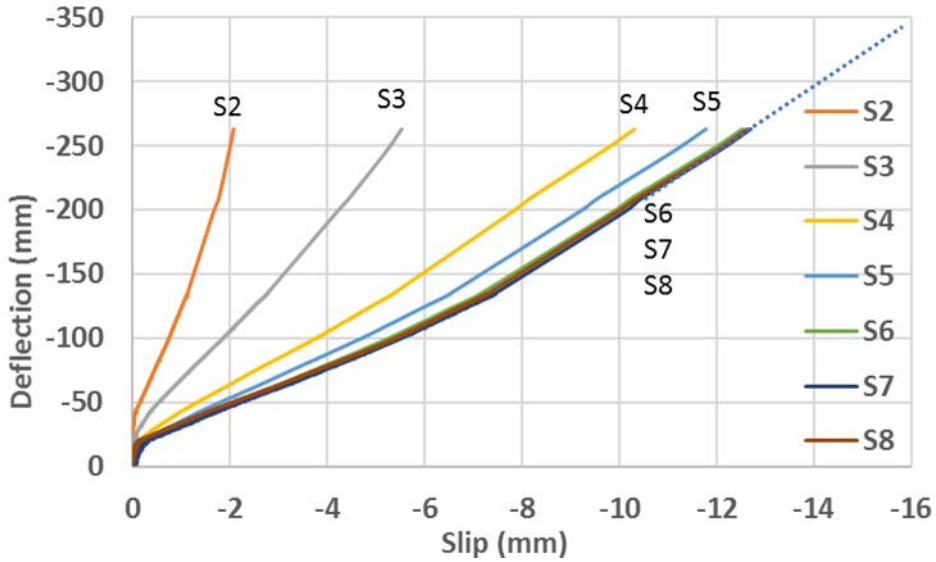

Fig. 7.8. Deflection-slip behaviour of composite beam

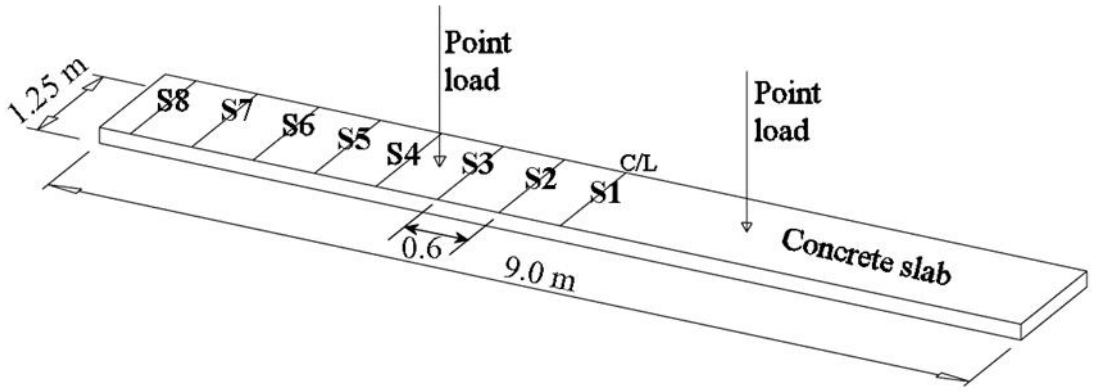

Fig. 7.9. Locations of load cells S4, S6, and S8 on the concrete slab

Fig. 7.7 shows the requirement of slip capacity recommended by Eurocode 4 (BSI 2004a) (i.e. 6 mm) for a ductile shear connector. It shows that, the moment capacity of the composite beam at a slip of 6 mm was 1171 kN.m, i.e., 97% of partial capacity and 90% of full capacity. In other words, limiting the slip to 6 mm does guarantee the development of plastic capacity as partial shear connection moment capacity. Partial and full shear connection capacities were reached exactly at slips of 7 mm and 11 mm respectively. Thus, FBSC, with its superior slip capacity of 16 mm, enabled the composite beam to achieve full development of partial and full shear connection capacities at only 45% and 70% of their slip capacity respectively and even it exceeded them without premature failure. It should be noted that as both the FBSC and welded studs do enable the composite beam of developing its plastic capacity at a slip of 6 mm, and as these two connectors are extremely different in their shear resistances,

then a conclusion can be drawn that the plastic resistance capacity is not affected by the shear resistance of shear connector, as long as the slip capacity is not less than 6 mm.

Eurocode 4 recommendation of 6 mm slip for welded studs in concrete solid slabs is based on assumption that several limitations were fulfilled (BSI 2004a). In reality, many of pushout tests on welded studs were stopped before reaching 3 mm (Johnson 2012). Furthermore, according to Eurocode 4, slip capacity is that on falling branch of the load-slip curve and after the maximum load dropped by 10% (BSI 2004a). Thus, welded studs that have 6 mm slip capacity, provide less than that at their maximum shear resistance.

Fig. 7.10 shows the distribution of slips along the length of the composite beam at different levels of applied moment, where the X-axis represents the distance (in metres) from the mid-span, while the Y-axis represents the corresponding slip (in mm) measured near each shear connector. It can be seen that almost constant maximum slip levels (e.g. 13 mm at 1364 kN.m moment) distributed along the shear spans (i.e. from point-load to beam end), then sharply decreases to zero at the mid-span. It can be concluded from Fig. 7.10 that in zones of no shear and constant moment, the shear connectors contribute little to the shear resistance, which explains why some designers ignore them (see Dallam and Harpster 1968).

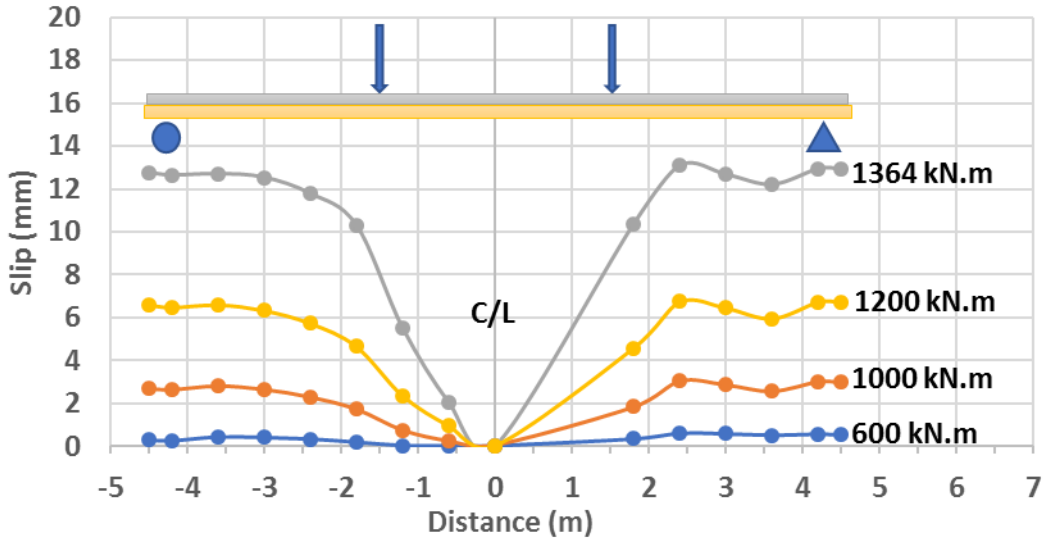

Fig. 7.10. Distribution of slips along composite beam length

7.3.3 Concrete and Steel Strains

Strain levels at different locations at the mid-span section of the concrete slab and the steel beam were monitored during the beam test. Fig. 4.55 shows the location and notations of strain gauges. The strains profile and the location of neutral axis (N.A.) before the start of the beam's test is shown in Fig. 7.11. The composite beam is under the self-weight of the

concrete slab, steel beam, and spreader beam. The location of N.A. was within the steel beam at 393 mm from the bottom of the section. It can be seen from Fig. 7.11 that the composite section is only sustaining low level of strains due to self-weight loadings; the maximum compression strain was 4.5×10^{-5} and occurred at the upper face of the concrete slab (CTB of Fig. 4.55), while the maximum tensile strain was 13×10^{-5} and occurred at the lower flange of the steel beam (SBF of Fig. 4.55). The strain profile takes almost linear shape, which indicates elastic behaviour and full interaction between the concrete slab and steel beam in the composite section.

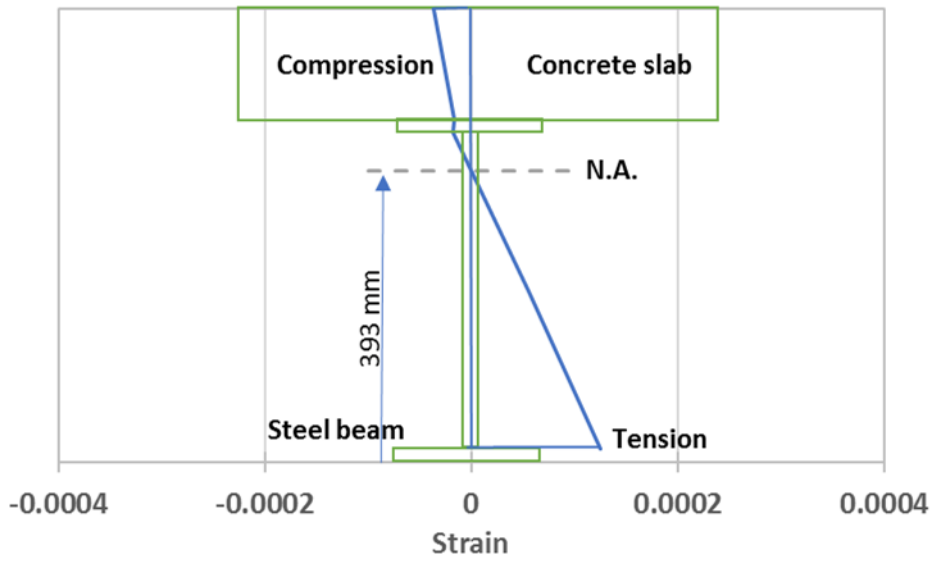

Fig. 7.11 Strains profile under self-weight loadings at mid-span section

Figs. 7.12 and 7.13 show the moment-strain relationships at several depths of the mid-span cross-section of the composite beam during the beam test. Fig. 7.12 shows strains on top and bottom faces of the concrete slab. The Y-axis represents the mid-span moment, while the X-axis represents the average direct strains from four readings (see Fig. 4.55). The whole section is under compression to a bending moment of 888 kN.m (73% of partial capacity) where the bottom face of the concrete slab gradually experiences tensile strains. Once the bottom face subjected to tensile strains, hairline cracks begin to propagate from the bottom face toward the top face, but hardly extends further than mid-thickness of the slab, as can be seen in Fig. 7.14 at the end of test. It should be noted that no readings of concrete tensile strains were included after a strain of 0.0003, because of cracking at the bottom face of the concrete slab that interfere with strain-gauges readings as can be seen in Fig. 7.15(4). It is clear from the photos in Fig. 7.15 that cracks concentrate near FBSC, because the bottom face of the concrete slab try to stretch while the FBSC encounters that action in opposite

direction. Furthermore, the strains, in Fig. 7.12, are linear to a bending moment of 750 kN.m (62% of partial capacity). After this point, the behaviour becomes nonlinear.

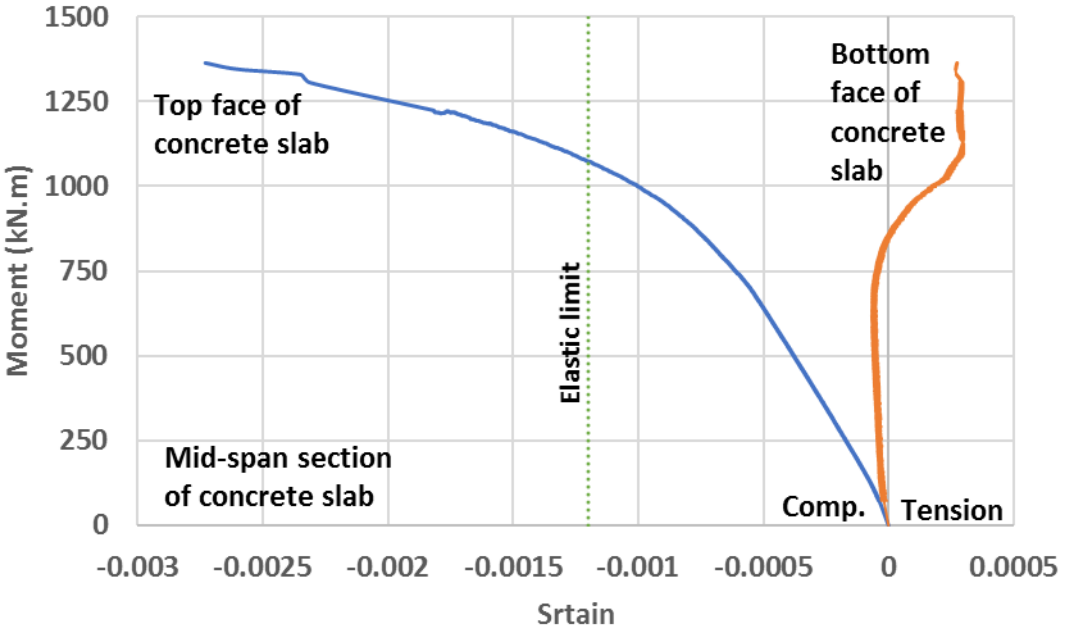

Fig. 7.12. Concrete slab strain behaviour during composite beam test

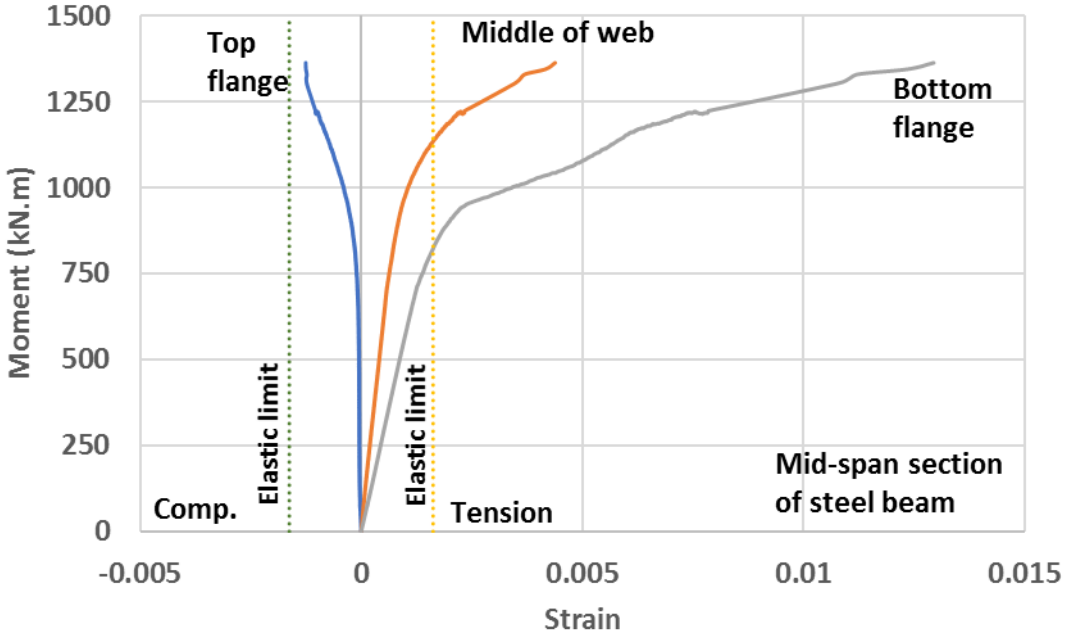

Fig. 7.13. Steel section strain behaviour during composite beam test

The compressive strain at the top face of the concrete slab during the beam test exceeded the concrete elastic limit at a moment of 1075 kN.m (i.e. 89% of partial capacity). It is interesting to note from Fig. 7.12 that, although the compressive strain almost reached 0.003, no concrete crushing occurred. This is because of the confinement provided by the

reinforcement. However, hairline longitudinal cracks were recorded only in the middle part between the point loads and at the top face of the concrete slab as will be explained later. The amount and distribution of reinforcement in the concrete slab can be found in Section 4.6.2. It should be noted that, in Fig. 7.11 and in all other figures to follow, the bending moments are similar to that of Fig. 7.6.

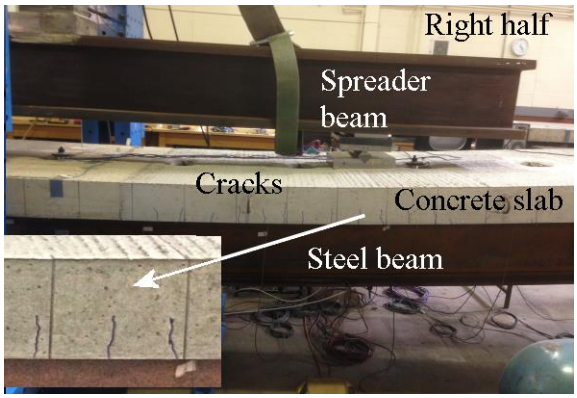

Fig. 7.14. Cracks in concrete slab during composite beam test

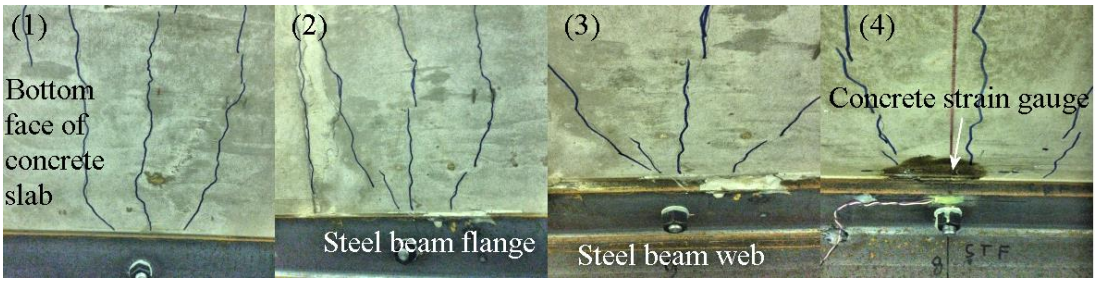

Fig. 7.15. Crack pattern in several bottom faces of slab during beam test

Fig. 7.13 shows the moment-strain relation at three vertical levels of the mid-span cross-section of the steel beam. Again, strain levels in the whole steel section were moderate and linear up to 750 kN.m (i.e. 62% of partial capacity). After this level, all strain gauges recorded a nonlinear response at different rates. The magnitudes of strains are related to their distance from the neutral axis; therefore, the bottom flange would experience more tensile strains than the others. Bottom flange strains exceed the elastic limit at a moment of 860 kN.m (i.e. 71% of partial capacity), mid-span deflection of 40 mm (i.e. $L/212$) and maximum slip of 1.7 mm (i.e. 11% of slip capacity). The strains at the middle of the web exceed the elastic limit at a moment of 1180 kN.m (i.e. 98% of partial capacity), mid-span deflection of 110 mm (i.e. $L/77$) and maximum slip of 6.2 mm (i.e. 39% of slip capacity). The strains at the top flange remain under elastic compression as shown in Fig. 7.13. By comparing the strain readings on the bottom face of the concrete slab in Fig. 7.12 with those at the top flange of the steel beam in Fig. 7.13, it is concluded that they have almost the same values up to a

bending moment of about 750 kN.m (i.e. 62% of partial capacity). This means that there is a negligible (relative displacement) slip at the interface and the behaviour is close to that of full interaction.

Figs. 7.16 to 7.20 illustrate strain profiles and neutral axis locations at the mid-span cross-section at different levels of bending moment. Fig. 7.16 shows the strain profile at 28% of plastic bending strength (i.e. 340 kN.m and 11.7 mm mid-span deflection), where there is no significant difference in the overall shape compared to the situation of self-weight shown in Fig. 7.11. The highest compressive strain was 25×10^{-5} (i.e. 15% of elastic limit) and occurred at the top face of the concrete slab, while the highest tensile strain was 60×10^{-5} (i.e. 37% of elastic limit) and occurred at the bottom flange of the steel beam. The neutral axis located inside the web of the steel beam. It should be noted that concrete strains are the average of four readings along the width of the slab (Fig. 4.55), and they do not represent the strains at the same line of steel strains (the difference is the flange thickness). This explains the slight recess in concrete strains from steel strains in Fig. 7.16.

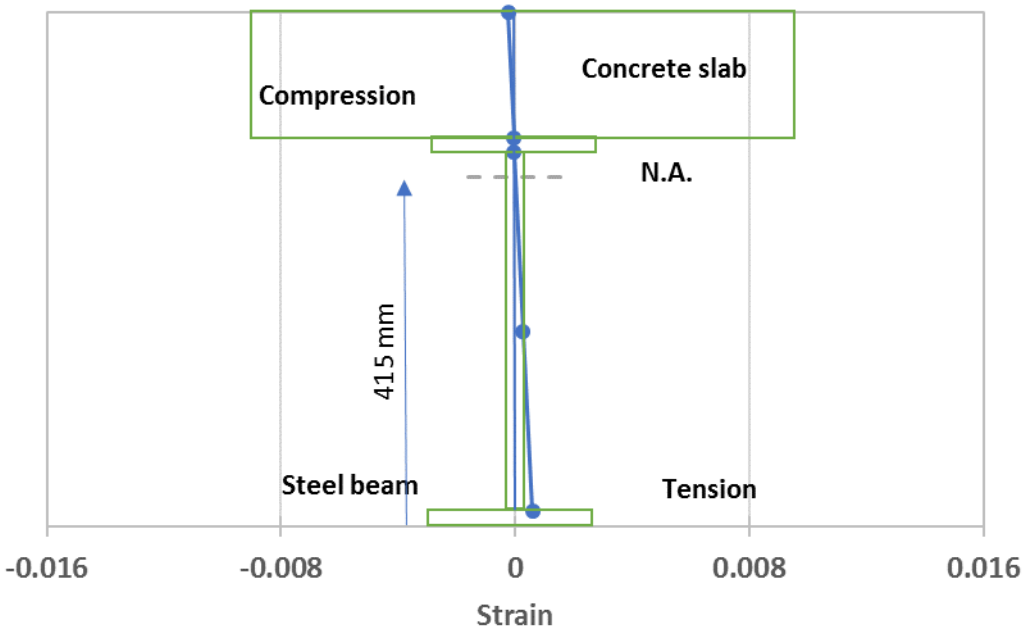

Fig. 7.16. Strains profile at 28% of bending strength of mid-span section

Fig. 7.17 proves that even if the bending moment is raised to 56% of partial plastic bending resistance, no considerable change is observed. The whole area of the mid-span cross-section of the concrete slab is still under compression, while the strain distribution over the depth of the composite section consists of a continuous straight line. By comparing the profiles in Figs. 7.16-7.17, it is concluded that as the moment increases, the neutral axis position shifts upward.

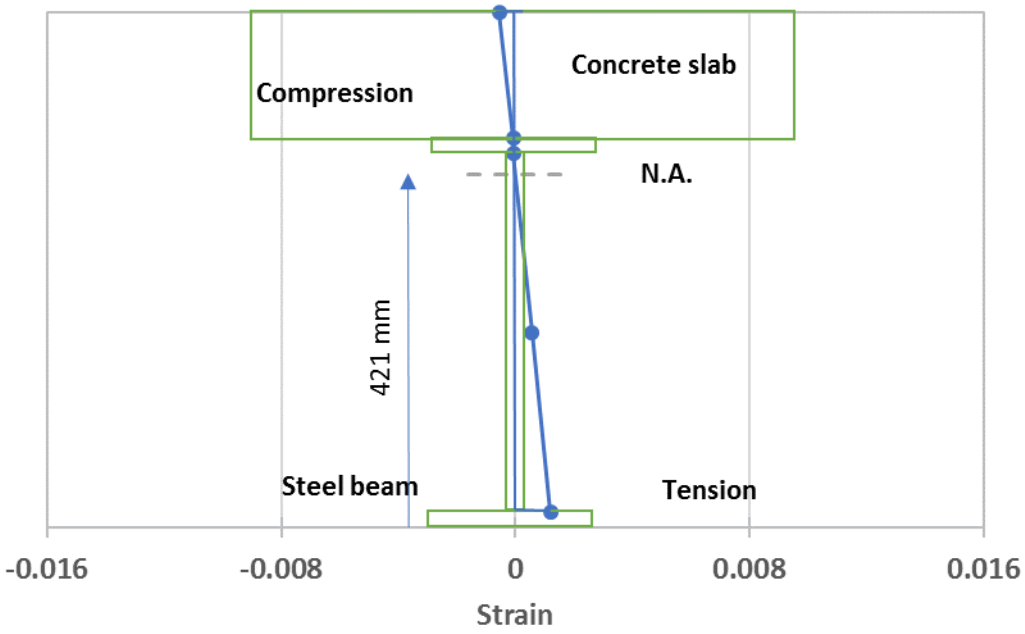

Fig. 7.17. Strains profile at 56% of bending strength of mid-span section

Fig. 7.18 shows the strain profile when the applied moment is equal to 1023 kN.m (i.e. 85% of partial capacity), the mid-span deflection is 67 mm (i.e. *L*/127) and the maximum slip is 3.3 mm (i.e. 21% of slip capacity).

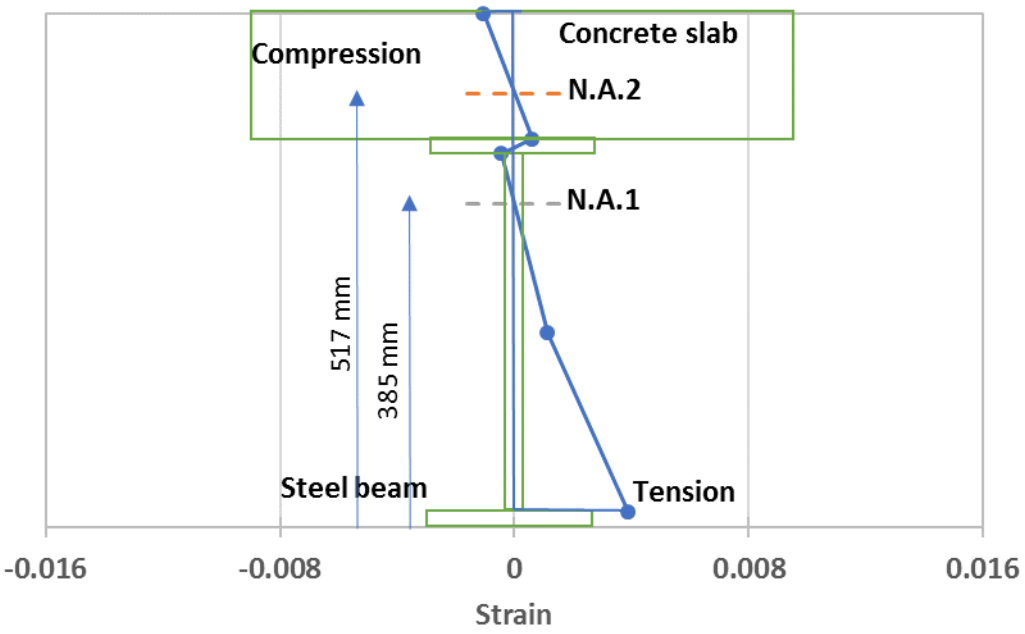

Fig. 7.18. Strains profile at 85% of bending strength of mid-span section

It is obvious that the composite section behaves in both partial-interaction and partial-connection. There is no longer one neutral axis, but instead, the concrete element and the steel element have their own neutral axes. Thus, each of them has compression and tension

zones at the same time. In such situations, the composite section should be under equilibrium of forces as follows: Tensile force in lower part steel section = Compression force in top part of steel section + upper part of the concrete section. To simplify the calculations, the tensile force of concrete and the compression forces in reinforcement are ignored. The lower flange of the steel section has a tensile strain equal to 0.00389, which is larger than the elastic limit (i.e. 0.001625), which means that the bottom flange has yielded. Its tensile force equals to 355/1000×191.9×17.7 = 1206 kN. On the contrary, the mid-height of the web has a tensile strain of 0.00113, which is below the elastic limit of steel. However, from Fig. 7.18 it can be calculated that a length of 214 mm of the web has also yielded; therefore, its tensile force equal to 355/1000×214×10.5 = 798 kN. Thus, the length of the elastic part of the tensile force is equal to N.A.1 – 214 – 17.7 = 153.3 mm. The strain in this length reduced linearly from the yield strain (i.e. 0.001625) to zero; and its tensile force is equal to 0.5× 0.355×153.3×10.5 = 286 kN. The total tensile force of the steel section is equal to 1206 + 798 + 286 = 2290 kN. The top flange of the steel section has a compression strain of 0.00044, which is below the elastic limit; therefore, the equivalent stress is equal to 210100 (i.e. E_s) ×0.00044 = 92 MPa. The compression force in the top flange is equal to 92/1000×191.9×17.7 = 313 kN and in the upper part of the web is equal to 0.5×92/1000×10.5× (463.4-385-17.7) = 29 kN. The total compression force in the top part of the steel section is equal to 313 + 29 = 342 kN. From equilibrium of forces, the compression force in the top part of the concrete slab is equal to 2290 – 342 = 1948 kN. The top face of the concrete slab has a compression strain of 0.00106, which is less than the elastic limit of concrete (i.e. 0.0012). Thus, the concrete slab is still in the elastic range and its stress can be calculated as follows 31000×0.00106 = 33 MPa (31000 MPa is modulus of elasticity of concrete, Table 4.6). The depth of the compression zone in the concrete slab can be calculated as 1948 / (1/2×1250×33/1000) = 95 mm and the position of N.A.2 from the bottom face of the steel beam is 518 mm. The bottom face of concrete has a tensile strain of 0.000614 (i.e. from similarity of triangles), which is higher than the tensile capacity of concrete that is usually assumed to be 10% of compression capacity. Thus, the lower part below the N.A.2 of the slab is cracked. The tensile reinforcement has a tensile strain of 0.000335, which is lower than the steel elastic limit (i.e. 0.001625) and can create a tensile force of only 48 kN (i.e. equal to 2% of concrete compression force). Ignoring its effect in the design of composite beams is an appropriate decision. However, for the purpose of analysis, the tensile reinforcement is included, and by trial and error method, its tensile force is equal to 46 kN, the depth of compression zone of concrete slab is 96 mm, the position of N.A.2 from the bottom face of

the steel beam is 517 mm and the compression force in the concrete slab is 1994 kN. Please notice that this distribution of force between the concrete slab and its reinforcement will not change the fact that the shear connectors should deliver the resultant force at the interface of concrete slab and steel beam, i.e., 1948 kN. Taking summation of moments of all previous forces around any axis inside the composite section gives 1093 kN.m, which is only 7% higher than the applied moment (i.e. 1023 kN.m). The difference may be due to simplifications and assumptions used in the calculation or due to variations in material properties.

From calculations, the compression force in the concrete slab at mid-span section is 1948 kN. This force shall be equal to the summation of shear resistances of all shear connectors in one shear span plus frictional resistance between the concrete slab and steel beam induced by the applied point load (i.e. in this case equals 346 kN). One way to calculate the shear force in each connector is to relate the shear force with the slip displacement using Fig. 6.25 and Equation (6.1). Alternatively, and for the sake of simplicity, Fig. 7.19 can be used.

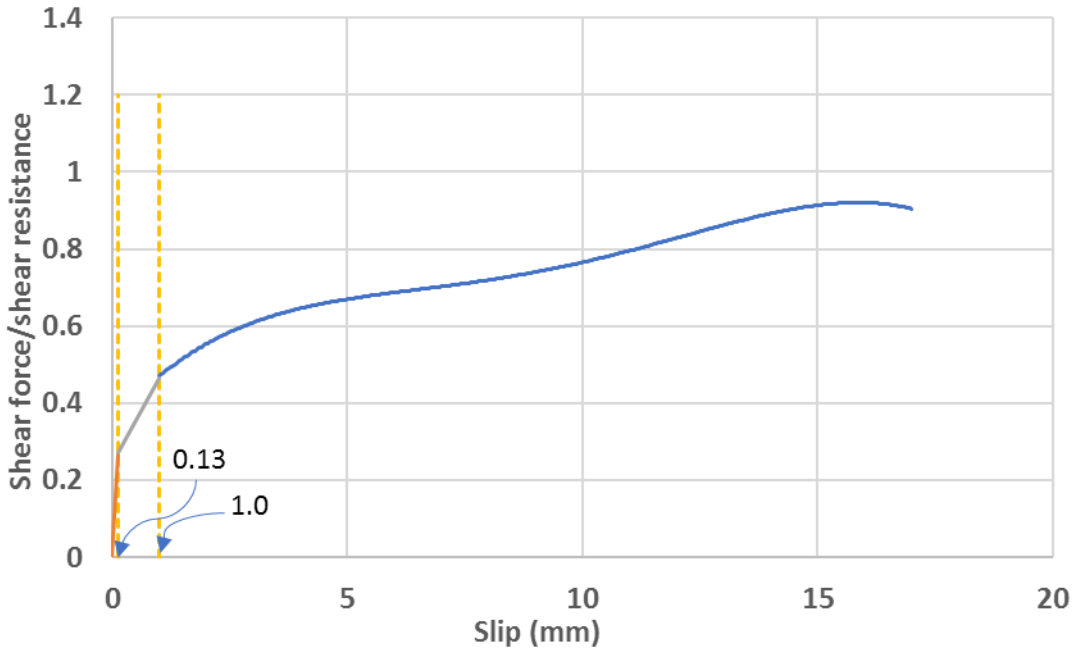

Fig. 7.19. Idealized load-slip curve for M16 FBSC pushout test

Fig. 7.19 plots a modified copy of the load-slip best-fit Equation (6.1) curve in Fig. 6.25. The Y-axis is the ratio of the shear force P_i to shear resistance P of a connector from FBSC Test 6 (and not the average). The reason for chosen Test 6 is because it produced the highest shear resistance of 206 kN/bolt. Three expressions are given for this ratio depending on slip magnitude S, as follows:

- For $0 < S \ll 0.13$ mm

$$P_{\mathrm{i}}/_{P} = 2.1\times S$$

- For $0.13 < S \ll 1$ mm

$$P_{\mathrm{i}}/_{P} = 0.22\times S + 0.24$$

- For $1\ \mathrm{mm} < S$

$$P_{\mathrm{i}}/_{P} = -5.05\times10^{-5}\times S^{4} + 1.884\times10^{-3}\times S^{3} - 0.02393\times S^{2} + 0.143\times S + 0.35$$

Then, from the summation of 15 shear forces (in a half-length) and the frictional resistance, the total compression force in the concrete slab is

$$F_{\mathrm{c}} = \sum_{\mathrm{i}=1}^{15} P_{\mathrm{i}} + \mu * F_{1} \qquad (7.5)$$

In which, F_1 is one point load (in kN).

Substituting the 15 slips from beam test into Equation (7.5) and solving for P

1948 = (-0.07+2(0.312+0.437+0.598+0.637+0.658+0.666+0.658)) ×P+ 0.5×346

1948 = 7.9 P+ 173

P= 225 kN/bolt

Thus, the FBSC shear resistance from beam test is 225 kN/bolt. That is 8% higher of the result from FBSC Test 6 (i.e. 206 kN). The latter finding indicates that the shear resistance of FBSC from beam tests is higher (or equal) than from pushout tests in this research. The reason behind this can be explained as follows. The FBSCs are placed at 15 rows along the composite beam. This enables redistribution of shear forces, so that the test gives the mean resistance of the shear span connectors which is the highest value that can be reached from the point of view of a test setup. It is interesting to notice that by using Fig. 7.19 and Equation (7.5), the contribution of shear connectors in the zero-shear zone (i.e. between the point-loads) is found to be 20% of shear resistance in the shear span. Thus, it could be understood why some designers (e.g. Dallam and Harpster 1968) ignore such zones when distributing the shear connectors.

Figs. 7.20 and 7.21 show strain profiles at 93% (i.e. 1160 kN.m) and 110% (1364 kN.m) of moment capacity and at deflections of 102 mm (i.e. *L*/83) and 267 mm (i.e. *L*/32) respectively. The tensile strain in the bottom flange of the steel beam changed from 0.00608 to 0.012939, which represents an increase from 5% to 11% of strain at ultimate tensile strength (i.e. 0.12

form Section 4.6.2). The compression strains in the top flange of the steel beam also changed from 0.00081 to 0.00125, which represents 77% of the elastic limit (i.e. 0.001625 from Section 4.6.2). Moreover, because the strain gauge is attached to the inside face of the flange, yielding at the outer face is assumed.

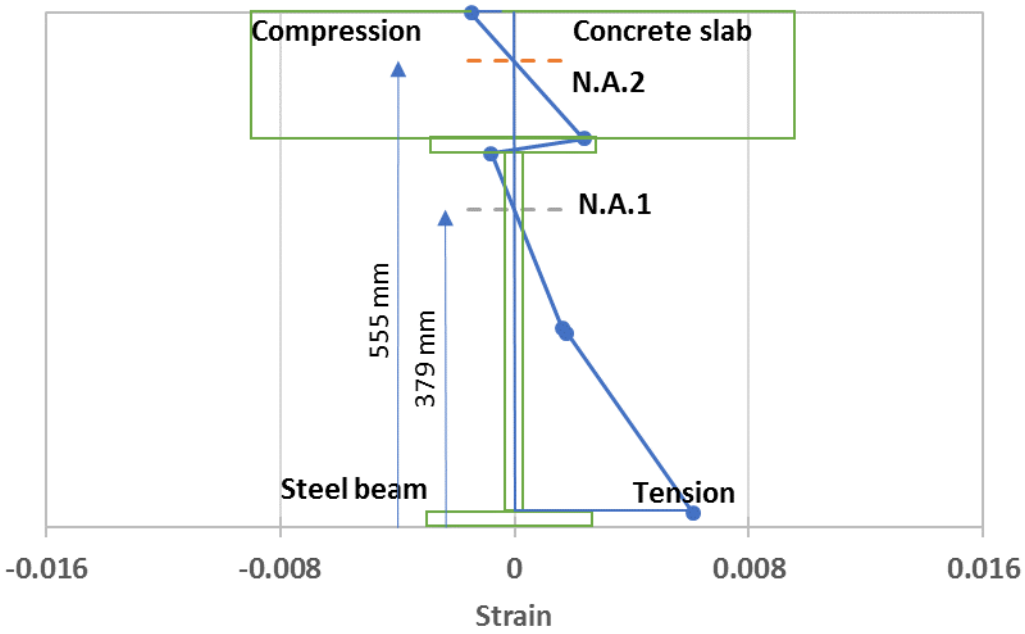

Fig. 7.20. Strains profile at 93% of bending strength of mid-span section

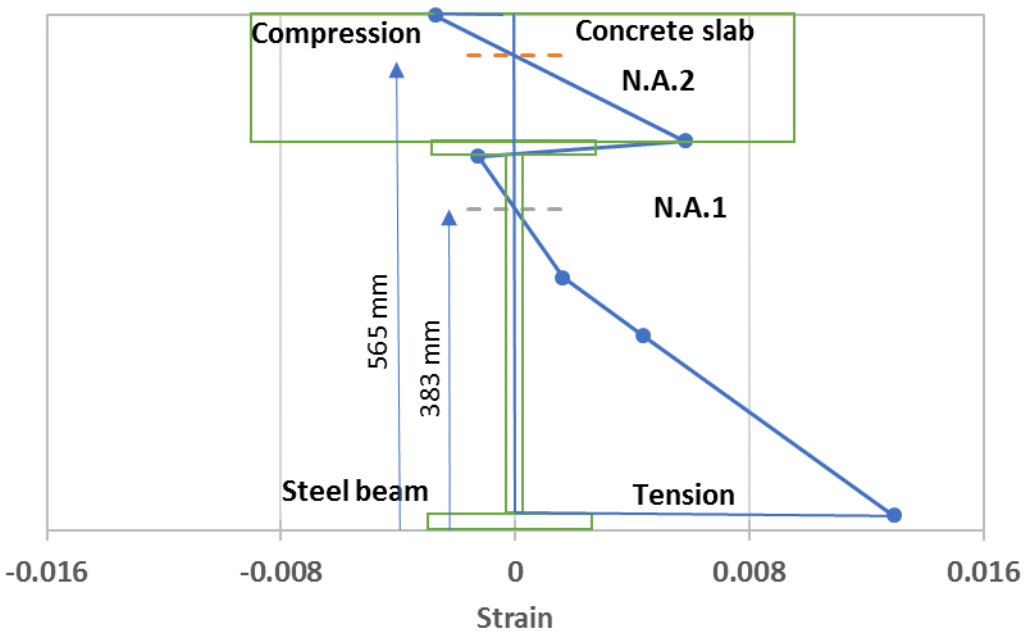

Fig. 7.21. Strains profile at 110% of bending strength of mid-span section

The expected failure might be crushing of concrete. Obviously, such failure should occur at the top surface (compression). Fig. 7.22 shows the mid-span distribution of compression strains across the width of the concrete slab. Four strain gauge readings were used to

develop this figure. Although it looks like that as moment increases, the difference between the strains increased, the numbers indicate a different situation. In particular, the strains at the edges of the width were about 0.6-0.7 of those at the centre for all cases. This explains the role of shear connectors (as dowels embedded into the concrete) in transferring the equilibrium forces between the concrete and the steel, which create a concentration of stresses in the middle zone of the slab. The latter is decreased towards the outside edges causing stress distortion. The decrease of stresses from the centre of width towards the edges is known as shear lag (Liang 2015). Fig. 7.22 shows asymmetry at > 50% of moment capacity. The strain at CTF was 14% higher than that at CTB at 110% of moment capacity. The reason of this is the lateral deflection at mid-span of the beam (S11 in Fig. 4.56) of about 10 mm.

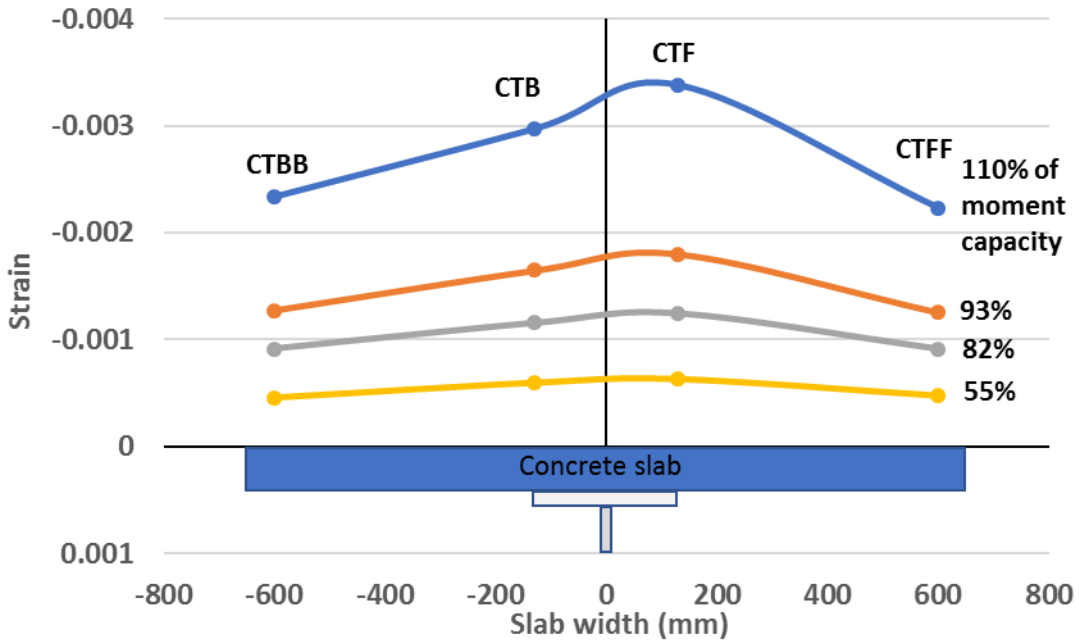

Fig. 7.22. Strain distribution along the width of concrete slab

Examination of top face of the whole slab shows that longitudinal hairline cracks are only visible in the part between the point loads (see Fig. 7.23) which is due to the shear lag of Fig. 7.22. It should be mentioned that less reinforcement was used as compared to standard pushout test (BSI 2004a) but still more than the minimum reinforcement required by Clause (9.2.1.1) for longitudinal reinforcement and by Clause (9.2.2.5) for transverse reinforcement in Eurocode 2 (BSI 2004b). No special reinforcement detailing was made near slab pockets, despite the recommendations in Section 8 of Eurocode 4 (BSI 2005a). This was decided on the basis of the results of Chapter 6, to prove that FBSC, contrary to welded studs (see Fig.

2.2), can efficiently distribute the bearing stresses and avoid any premature local failure in either the precast or the in-situ grout.

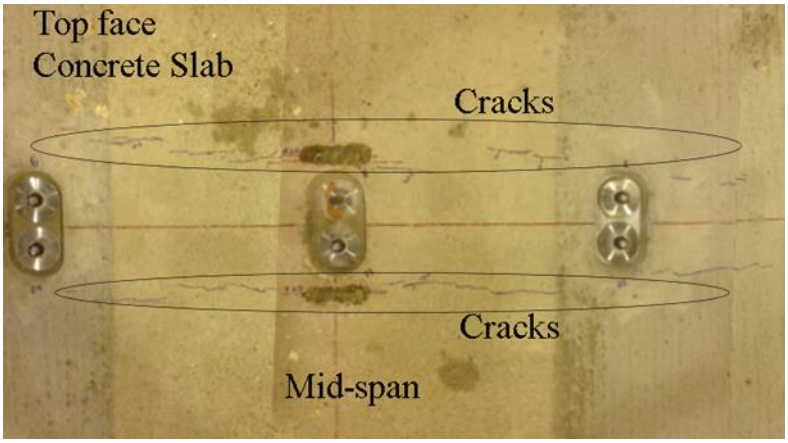

Fig. 7.23. Longitudinal cracks in concrete slab

7.3.4 Concrete Slab Separation

Slab uplift is unlikely to occur in the beam test because the applied load compressed the slab against the steel beam. However, one LVDT (S10 in Fig. 4.56) was used to capture any uplift that might occur due to flexural stiffness variation between the concrete slab and the steel beam during bending. Fig. 7.24 shows the mid-span moment-separation relationship. The maximum uplift was less than 0.2 mm. On the other hand, two dial gauges at 1.5 m from the beam centre (mid-length between S3 and S4 and mid-length between S3R and S4R in Fig. 4.55) recorded compressions of 0.26 mm and 0.55 mm under the left and right point-loads, respectively. Thus, the uplift in the beam test had a negligible effect on the behaviour of the composite beams. It should be noted that the existence of gaps between the concrete slab and top flange of the steel beam was checked before test and found that they are distributed along the length. None were found in the

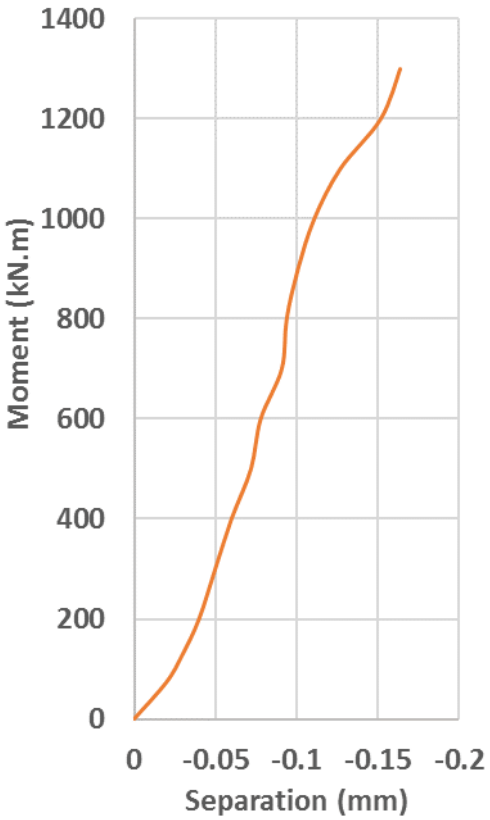

Fig. 7.24. Mid-span slab separation during composite beam test

middle part (i.e. the cast-insitu concrete) and they were normally less than 1 mm. This explains the 0.26-0.5 mm compressions.

7.3.5 FBSC Tensile Force

The tensile force inside the shear connectors was measured using washer load cells on four bolts on the left side of the composite beam, namely, S1, S4, S6, and S8, as shown in Fig. 4.55. S1 did not show any changes during the test due to symmetry and therefore its measurement is not included. The response of bolt tensile force was studied using the six load cycles and the test results are plotted in Figs. 7.25-7.30. Cycle 1 (Fig. 7.25) shows that as slip increases to about 2 mm, there is no change to the tensile force. At a slip in the range 5-8 mm, the tensile decreases slightly (about 15%) and is followed by another drop (about 50%) when the specimen is unloaded. This behaviour was observed during FBSC pushout tests (see Fig. 6.28), but not in LNSC pushout tests (see Fig. 5.28). The main difference between the two connectors, in relation to this observation, is that, the LNSC has a locking nut that ensure an initial perpendicular alignment to the steel beam, while the FBSC does not have a locking nut; therefore, can initially be slightly inclined in any arbitrary direction (not measured). Any slip induces direct stretching of the bolt, and therefore, increase in the tensile force, if the bolt is perpendicular to the shear force. On the other hand, the slip of FBSC, might be stretching or contracting the bolt, depending on the direction of the initial inclination. The main conclusion is that the tensile force can increases or decreases. Obviously, this hypothesis might be true if it occurs in the first cycle only and did not persist in following cycles. In the first 2 mm of slip usually no change occurs in the tensile force. This might be because of the chemical bonding between the bolt shank and the surrounding grout. The beam test setup, which is based on downward point-loads that force the slab to compress into the steel beam, might cause some additional relief in the bolt preload. Bending of bolts due to slip will stretch the shank of the bolts, and because bolt ends are restraints, the tensile force increases. This was repeatedly observed and explained in pushout tests. Lastly, variation in flexural stiffness between the concrete slab and the steel beam might cause some separation between them, and as a consequence, an increase in the tensile force. All in all, Fig. 7.25 and other load cycles, plots the combination of all these factors together, but it is impossible to identify the effect of each one. When the load is removed, the permanent (plastic) extension of bolts causes a reduction in the tensile force. It should be noted that, although the applied load was removed, the slips only slightly decreased and did not attain their initial values.

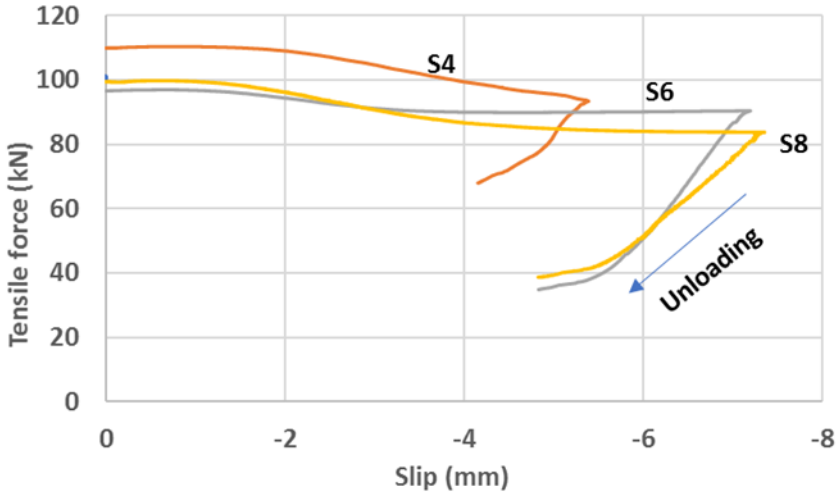

Fig. 7.25. Tensile forces inside bolts during 1st cycle of loading of beam test

In the following load cycles presented in Figs. 7.26 – 7.30, the tensile force behaviour shows a repetitive trend. As slip increases by 1-2 mm, the tensile force increases about 25%, then changes sharply to an almost constant value. This behaviour is quite difficult to explain, as it is neither related to load (i.e. moment), nor to deflection behaviour. For example, S4 in Fig. 7.26 is constant at 5.5-8 mm slips. At that slip, the moment was 1100-1200 kN.m in nonlinear part of the curve shown in Fig. 7.3. and this nonlinear behaviour had not been reflected on the tensile force behaviour. It is a safe proposal to say that the connector's tensile force is constant to a maximum slip of 2 mm and a vertical deflection of 50 mm (i.e. *L*/170). Moreover, the connector will have 80% of the preload at a slip of 4 mm and a deflection of 100 mm (i.e. *L*/85).

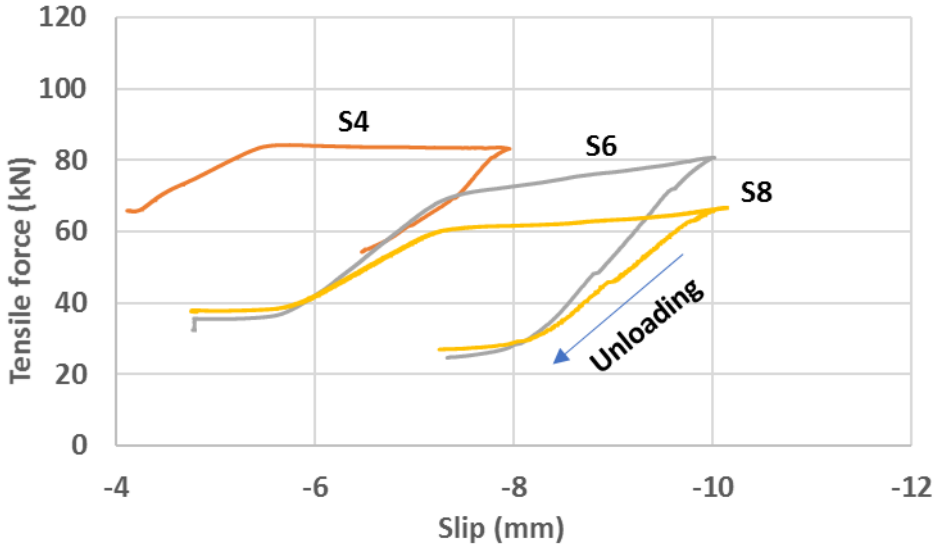

Fig. 7.26. Tensile forces inside bolts during 2nd cycle of loading of beam test

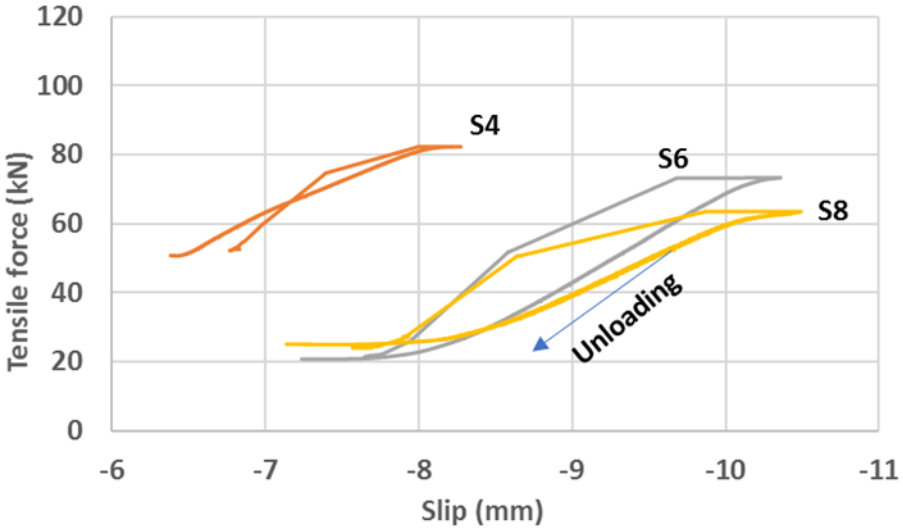

Fig. 7.27. Tensile forces inside bolts during 3rd cycle of loading of beam test

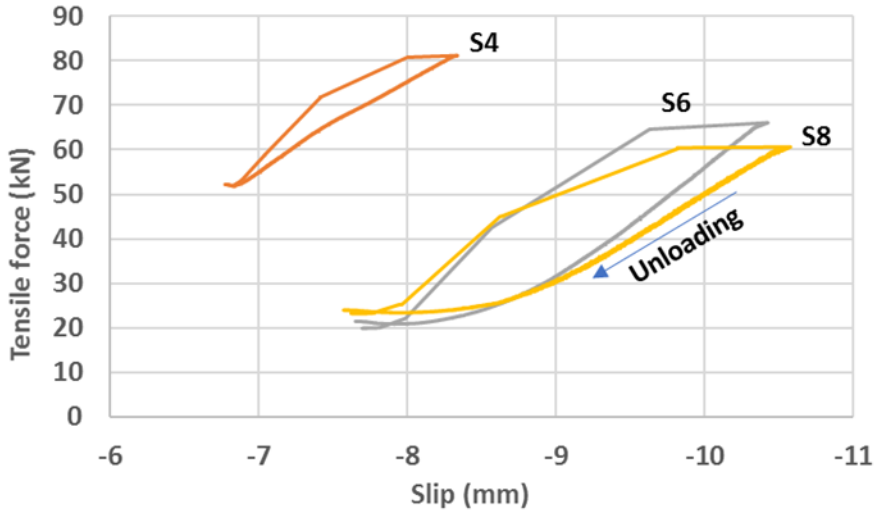

Fig. 7.28. Tensile forces inside bolts during 4th cycle of loading of beam test

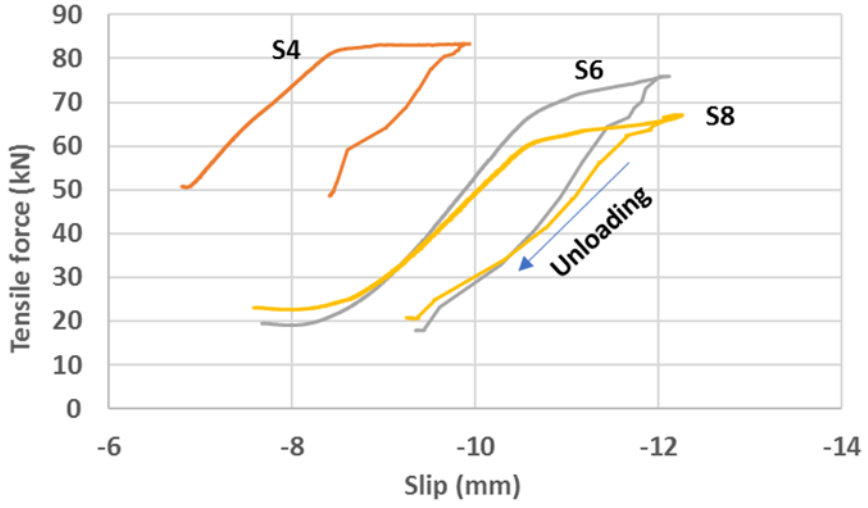

Fig. 7.29. Tensile forces inside bolts during 5th cycle of loading of beam test

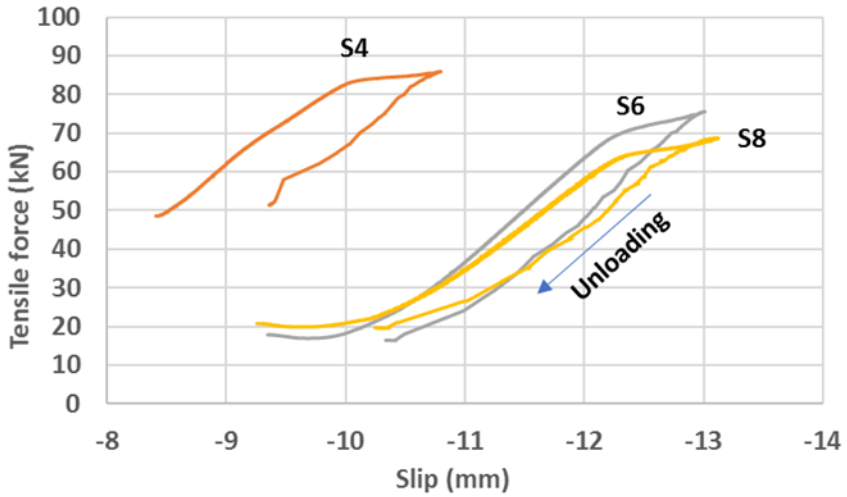

Fig. 7.30. Tensile forces inside bolts during 6th cycle of loading of beam test

7.4 Disassembly of composite beam

In the Civil Lab, performing disassembly before linking the two panels is straightforward and does not need to be evaluated by tests. Basically, the lower nuts can be removed and the panels can be lifted-up using the same procedure shown in Fig. 4.45. Doing the disassembly after a service (working) load is the most useful as it simulates the conditions in practice. However, it was found that this is beyond the capability of the Civil Lab as it required lifting the whole 9.0 m concrete slab. Doing the disassembly after the testing can be done by removing the lower nuts, splitting the concrete slab into two panels, and then lift them up. It was found that this is impractical, because it can be seen from Fig. 7.4 and Table 7.1 that the composite beam has deflected to 275 mm, and all the bolts are inclined from the vertical. The panels should be separated from the steel beam at an angle from the vertical, or the shear connectors are pulled-up which requires working above the slab. In both options, the safety regulations of the Civil Lab cannot be fulfilled.

7.4 Summary

A test on a full-scale precast steel-concrete composite beam of 9.0 m length using FBSC was performed. FBSCs were distributed along the length of the beam in pairs at 0.6 m spacings. The test was conducted in a four point-loads setup. To study the behaviour of the composite beam, the test gave readings for load (moment), deflection, slips, slab separations, concrete strains, steel strains, and tensile forces. The results showed that the resulted moment exceeded the partial and full connection moment capacity. Thus, the FBSC can be used in composite beams at partial shear connection of 70%. The structural merits of strength, stiffness, ductility, and slip capacity participated in the development of moment capacity without premature failure even when the composite beam had reached a vertical deflection

of about 275 mm (*L*/32) and both the steel beam and the concrete slab had reached their plastic limits. Using FBSC, it is feasible to assume full-interaction (i.e. no slip), partial connection (i.e. 70%) until 50% of plastic moment capacity. The deflection of composite beams designed with FBSC can be calculated reliably using elastic theory for SLS.

Chapter 8: Summary and Conclusions

8.1 Summary

Two novel demountable shear connectors, namely the Locking Nut Shear Connector (LNSC) and the Friction Based Shear Connector (FBSC), for precast steel-concrete composite bridges have been presented. Both connectors use high-strength steel bolts, which are fastened to the top flange of the steel beam using a locking nut or a grouted countersunk hole configurations that prevent slip of bolts inside their holes. The LNSC resembles in geometry the collar of welded shear studs and prevents local failure within the threaded part of the bolts to achieve higher shear resistance and ductility, while FBSC uses friction resistance to achieve higher shear resistance at SLS. The bolts are surrounded by conical precast high-strength concrete plugs, which have dimensions so that they can easily fit within the precast slab pockets. Grout is used to fill all the gaps between the bolts, the precast plugs, and the precast slab pockets, while tightening of a nut at the top of the connectors secures the plugs in place before grout hardening. 23 push-out tests and one full-scale composite beam test were conducted to fully illustrate why the novel structural details of the LNSC and FBSC result in superior shear load-slip displacement behaviour compared to conventional welded studs. The tests also served to assess the repeatability of the connector behavior and to quantify the effects of the bolt diameter, concrete plug strength, and bolt pretension. Simple design equations to predict the shear resistance of the connectors are proposed.

8.2 Conclusions

Based on the results presented in the research, and within the specific boundaries of the experimental work and parameters studied, the following conclusions are drawn:

- The LNSC and FBSC allow rapid bridge disassembly and easy, time-efficient replacement of any deteriorating structural component (i.e. precast deck panel, shear connector, and steel beam). Their use can result in significant reduction of the life cycle direct and indirect socio-economic costs related to maintenance, repair, or replacement of precast steel-concrete composite bridges.
- The LNSC and FBSC achieve high levels of accelerated construction by taking full advantage of pre-fabrication. Fabrication of all structural components is carried out in the shop and only the final assembly between the precast slab and the steel beam is carried out on site. Moreover, the latter does not involve working underneath the bridge deck.

- The LNSC and FBSC as compared to welded studs have very high shear resistance and stiffness, and therefore, result in reduction of the required number of shear connectors and slab pockets in comparison to welded studs or previously proposed bolted shear connectors. The characteristic shear resistance and stiffness of the LNSC for an M16 bolt were found equal to 171 kN and 100 kN/mm, respectively. The characteristic shear resistance and stiffness of the FBSC for an M16 bolt were found equal to 161 kN and 104 kN/mm, respectively.
- The LNSC and FBSC as compared to welded studs have large slip capacity (up to 14.0 and 16 mm, respectively) that can be exploited to partial interaction design of very long composite beams (>20 m) with the goal of reducing construction cost.
- The LNSC and FBSC have superior stiffness and strength against slab uplift in comparison to welded studs, e.g. at shear load equal to 80% of the shear resistance, the uplift displacement is less than 4% of the corresponding slip displacement.
- The shear load-slip displacement behavior of the LNSC and FBSC shows repeatability and negligible scatter. Among three identical push-out tests, the maximum deviations of any individual test from the average was less than 8%. Such deviation in the case of welded studs shear can reach values up to +/- 30%.
- Increasing the plug concrete strength from C50 to C96 was found to have negligible effect on shear resistance (9% increase) and slip capacity (5% decrease) of the LNSC.
- Increasing the bolt preload in the FBSC by 40% was found to increase the frictional resistance by 29%.
- The proposed design equations for LNSC and FBSC, were evaluated against test results from specimens with different bolt diameters, plug concrete strengths, and preloads and were found to predict the shear resistance of the LNSC and FBSC with maximum absolute deviation less than 8% and 5%, respectively.
- The shear resistance of the LNSC and FBSC could be approximately considered equal to 1.1 times the bolt tensile resistance for preliminary design purposes.
- The FBSC was used successfully in a full-scale precast composite beam under sagging moment by allowing the beam to reach its partial plastic moment capacity without premature fracture (like slab splitting) using only 80% of its slip capacity
- The composite beam reached 97% of partial plastic capacity at slip displacement equal to 6 mm and vertical deflection equal to *L*/78.
- Using the FBSC, a partial shear connection of 70% degree was developed at 93% of full plastic capacity.

- The maximum deflection, bending moment, and slip in the composite beam were *L/*31, 110% of partial plastic bending, and 80% of slip capacity, respectively. FBSC achieved a very ductile behaviour without any premature failure.
- The composite beam behaved linearly up to 55% of the maximum moment, and the deflection prediction using the elastic theory was reliable.
- Full interaction was developed using the FBSC, i.e. the composite beam had reached 40% of partial plastic design without any slip.
- The structural performance of FBSC used in 70% partial connection composite beam ensures full-interaction between the concrete slab and steel beam until exceeding the SLS deflection limit by 30%.
- No cracks were observed in the concrete slab until 73% of partial capacity, while the compression strains exceeded the elastic limit at 89% of partial capacity.
- The steel beam behaved linearly elastic until 71% of partial capacity when the bottom flange exceeded the elastic limit with only 11% of slip capacity. The mid-depth of section did not exceed the tensile elastic limit until 98% of partial capacity with 39% of slip capacity. The top flange remained elastic throughout the beam test.
- The elastic neutral axis was located in the web and shifted upward as the moment increased, while the plastic neutral axis was located inside the top flange.
- The strain profile of the composite section had linear distribution at 56% of partial capacity.
- Shear lag was observed in the width of the concrete slab where the strain at the edges were about 0.6-0.7 of that at the centre.
- The slab separation in the composite beam test was negligible, e.g. at maximum moment, the separation was less than 0.2 mm.
- The bolt tensile force was constant until a maximum slip of 2 mm and a deflection of *L/*170, and reached 80% of the preload at a slip equal to 4 mm and deflection equal to *L/*85. Further slip did not result in considerable changes in the tensile force.

8.3 Recommendations for further research

The following recommendations can be suggested for further research:

- The fatigue shear resistance of FBSC and LNSC need to be evaluated with pushout tests.
- Pullout tests should be conducted to evaluate the slab separation resistance of the LNSC and FBSC.

- Precast composite beam tests for LNSC and FBSC with different beam lengths, especially for long beams with partial shear connection.
- Composite beam tests with LNSC and FBSC under negative (hogging) bending moment.
- Extending the parametric studies in this thesis (bolt diameter, plug strength, and bolt preload) by including more parameters or doing more tests.
- Develop numerical FEM models for the LNSC and FBSC to optimize their structural design and extend the parametric studies.
- Composite beam tests with longitudinal joints between the concrete panels, and evaluation of the role of LNSC and FBSC on the disassembly procedure.

References

ASCE. (2014). “Report card for America’s infrastructure - Bridges.” Retrieved from: http://www.infrastructurereportcard.org/a/#p/bridges/conditions-and-capacity. (23 October 2016).

Ataei, A., Bradford, M. A. (2014). “FE modelling of sustainable semi-rigid flush end plate composite joints with deconstructable bolted shear connectors.” International Conference on Composite Construction in Steel and Concrete, ASCE, Australia.

Ataei, A., Bradford, M. A., Liu, X. (2016). “Experimental study of composite beams having a precast geopolymer concrete slab and deconstructable bolted shear connectors.” Engineering Structures, 114, 1–13.

Badie, S.S., Tadros, M.K. (2008). “Full-Depth Precast Concrete Bridge Deck Panel Systems.” Transportation research board, Washington, D. C., USA.

Bickford, H. J. (1995). *An Introduction to the design and behaviour of bolted joints.* 3rd ed., Marcel Dekker, Inc., New York, USA.

Biswas, M. (1986). “On modular full depth bridge deck rehabilitation.” J. Trans. Eng. (ASCE) 112, 1, 105-120.

Bradford, M.A., and Pi, Y.-L. (2012). “Computational Modelling of Deconstructable Composite Steel-Concrete Beams.” Proceedings of the Eleventh International Conference on Computational Structures Technology, Civil-Comp Press, Stirlingshire, Scotland.

BSI (British Standards Institution). (1970). “Specification for wheels for agricultural machinery, implements and trailers, Part 3: Nuts.” BS 3486-3, London. UK.

BSI (British Standards Institution). (1976). “Specifications for Building sands from natural sources.” BS 1199, London. UK.

BSI (British Standards Institution). (1979). “Steel, concrete and composite bridges, Part 5: Code of practice for design of composite bridges.” BS 5400-5, London. UK.

BSI (British Standards Institution). (1994). “Draft for Development: Eurocode 4: Design of composite steel and concrete structures, Part 1-1: General rules and rules for buildings.” BS EN 1994-1-1, London. UK.

BSI (British Standards Institution). (2004a). “Eurocode 4: Design of composite steel and concrete structures, Part 1-1: General rules and rules for buildings.” BS EN 1994-1-1, London. UK.

BSI (British Standards Institution). (2004b). “Eurocode 2: Design of concrete structures, Part 1-1: General rules and rules for buildings.” BS EN 1992-1-1, London. UK.

BSI (British Standards Institution). (2005a). “Eurocode 4: Design of composite steel and concrete structures, Part 1-2: General rules and rules for Bridges.” BS EN 1994-2, London. UK.

BSI (British Standards Institution). (2005b). “Eurocode 3: Design of steel structures, Part 1-1: General rules and rules for buildings.” BS EN 1994-1-1, London. UK.

BSI (British Standards Institution). (2005c). “High-strength structural bolting assemblies for preloading, Part 3: System HR, Hexagon bolt and nut assemblies.” BS EN 14399-3, London. UK.

BSI (British Standards Institution). (2005d). “High-strength structural bolting assemblies for preloading, Part 6: Part 5: Plain chamfered washers.” BS EN 14399-6, London. UK.

BSI (British Standards Institution). (2005e). “Eurocode 3: Design of steel structures, Part 1-8: Design of joints.” BS EN 1993-1-8, London, UK.

BSI (British Standards Institution). (2005f). “Steel, concrete and composite bridges, Part 5: Code of practice for the design of composite bridges.” BS 5400-5, London, UK.

BSI (British Standards Institution). (2006). “Eurocode 3 - Design of steel structures - Part 2: Steel Bridges.” BS EN 1993-2, London, UK.

BSI (British Standards Institution). (2009a). “High-strength structural bolting assemblies for preloading, Part 9: System HR or HV – Direct tension indicators for bolt and nut assemblies.” BS EN 14399-9, London. UK.

BSI (British Standards Institution). (2009b). “Metallic materials — Tensile testing, Part 1: Method of test at ambient temperature.” BS EN ISO 6892-1, London. UK.

BSI (British Standards Institution). (2009c). “Testing hardened concrete - Part 3: Compressive strength of test specimens.” BS EN 12390-3, London, UK.

BSI (British Standards Institution). (2009d). “Testing hardened concrete - Part 6: Tensile splitting strength of test specimens.” BS EN 12390-6, London, UK.

BSI (British Standards Institution). (2012). “Aerospace series - Rings retaining, radial mounting, steel, phosphated.” BS EN 3386, London. UK.

BSI (British Standards Institution). (2016). “Draft BS ENISO 15612 Specification and qualification of welding procedures for metallic materials - Qualification by adoption of a standard welding procedure specification.” Draft BS ENISO 15612, London, UK.

Chen, Y-T., Zhao, Y., West, J.S., Walbridge S. (2014). “Behavior of steel–precast composite girders with through-bolt shear connectors under static loading.” Journal of Constructional Steel Research, 103, 168–178.

Chesson, E., Jr., Faustino, N. L., Munse, W.H. (1965). “High-Strength Bolts Subjected to Tension and Shear.” Journal of the Structural Division, ASCE 1965;91(St5).

CSI (Computers & Structures, Inc.). (2015). “Composite Beam Design Manual Eurocode 4-2004 For ETABS® 2016.” Berkeley, California, USA.

Dai, X., Lam, D., and Saveri, E. (2015). "Effect of Concrete Strength and Stud Collar Size to Shear Capacity of Demountable Shear Connectors." J. Struct. Eng., 10.1061/(ASCE)ST.1943-541X.0001267, 04015025.

Dallam, L.N. (1968), “High Strength Bolt Shear Connectors – Pushout Tests” ACI Journal, 65(9), 767 -769.

Dallam, L.N., Harpster, J.L. (1968). “Composite beam tests with high-strength bolt shear connectors.” Report 68-3, Missouri State Highway Department, USA.

Davison, B., Owens, G. W. (2012). *Steel Designers’ Manual.* 7th ed., The Steel Construction Institute, John Wiley & Sons, Ltd, West Sussex, UK.

Dedic, D. J., and Klaiber, F. W. (1984). “High Strength Bolts as Shear Connectors in Rehabilitation Work.” Concrete International, July, pp. 41-46.

Deng, Y., Phares, B. M., Dang, H., and Dahlberg, J. M. (2016). “Impact of Concrete Deck Removal on Horizontal Shear Capacity of Shear Connections.” J. Bridge Eng., 21(3): 04015059.

El-lobody, E. A. (2002). “Finite Element Modeling of shear connection for steel-concrete composite girders,” PhD. Dissertation, Civil Engineering Department - School of Engineering, University of Leeds.

El-lobody, E. A. (2014). Finite Element Analysis and Design of Steel and Steel-Concrete Composite Bridges. Elsevier Inc., Oxford, UK.

Hallmark, R. (2012). “Prefabricated Composite Bridges – a Study of Dry Joints.” Licentiate thesis, Department of Civil, Mining and Natural Resources Engineering, Lulea University of technology, Sweden.

Hanswille, G. (2011). “Composite bridges in Germany. State of the art.” International Workshop on Eurocode 4-2 Composite Bridges, Stockholm, Sweden, March 2011

Heistermann, C. (2012). “Behaviour of Pretensioned Bolts in Friction Connections, Towards the Use of Higher Strength Steels in Wind Towers.” PhD. Thesis, Luleå University of Technology.

Henderson, I.E.J., Zhu, X.Q., Uy, B., Mirza, O. (2015a). “Dynamic behaviour of steel-concrete composite beams with different types of shear connectors. Part I: Experimental study.” Engineering Structures, 103, 298-307.

Henderson, I.E.J., Zhu, X.Q., Uy, B., Mirza, O. (2015b). “Dynamic behaviour of steel-concrete composite beams with different types of shear connectors. Part II: Modelling and comparison” Engineering Structures, 103, 308-317.

Hendy, C. R., and Johnson, R. P. (2006). Designers’ Guide to EN 1994-2 Eurocode 4: Design of composite steel and concrete structures. Part 2: General rules and rules for bridges. Thomas Telford Ltd., UK.

Johnson, R. P. (1967). *Structural Concrete*. McGraw-Hill Publishing company limited, Berkshire, UK, p.32.

Johnson, R. P. (1981). “Loss of Interaction in Short-span Composite Beams and Plates.” Journal of Constructional Steel Research, 1(2), p.11.

Johnson, R. P. (2004). Composite Structures of Steel and Concrete: Volume 1: Beams, Slabs, Columns, and Frames for Buildings. 3rd edition, Blackwell scientific publications, Oxford, UK, p. 32.

Johnson, R. P. (2012). Designers' Guide to Eurocode 4: Design of Composite Steel and Concrete Structures. 2nd edition, EN 1994-1-1, Thomas Telford Ltd.

Johnson, R. P., and Buckby, R. J. (1986). *Composite structures of steel and concrete: Volume 2: Bridges*. 2nd edition, Collins Professional and Technical Books, London, UK.

Johnson, R. P., and May, I. M. (1975). "Partial-interaction design of composite beams." The Structural Engineer, 53 (8), 305-311.

Johnson, R. P., and Yuan, H. (1998a). "Existing rules and new tests for stud shear connectors in troughs of profiled sheeting." Proceedings of the Institution of Civil Engineers-Structures and Buildings, 128 (3). pp. 244-251.

Johnson, R. P., and Yuan, H. (1998b). "Models and design rules for stud shear connectors in troughs of profiled sheeting." Proceedings of the Institution of Civil Engineers-Structures and Buildings, 128 (3). pp. 252-263.

Kulak, G. L., Fisher, J. W., and Struik, J. H. A. (2001). *Guide to Design Criteria for Bolted and Riveted Joints*, 2nd edition, AISC, Chicago, USA.

Kwon, G., Engelhardt, M.D., Klinger, R.E. (2010). "Behavior of post-installed shear connectors under static and fatigue loading." Journal of Constructional Steel Research, 66, 532–41.

Kwon, G., Engelhardt, M.D., Klingner, R.E. (2011). "Experimental Behavior of Bridge Beams Retrofitted with Postinstalled Shear Connectors." Journal of Bridge Engineering, 10.1061/(ASCE)BE.1943-5592.0000184, pp. 536-545.

Lam, D., and Saveri, E. (2012). "Shear capacity of demountable shear connectors." 10th International Conference on Advances in Steel Concrete Composite and Hybrid Structures, Singapore.

Lam, D., Dai, X., and Saveri, E. (2013). "Behaviour of Demountable Shear Connectors in Steel-Concrete Composite Beams." International Conference on Composite Construction in Steel and Concrete VII, ASCE, pp. 618-631.

Liang, Q. Q. (2015). *Analysis and Design of Steel and Composite Structures*. CRC Press, Taylor & Francis Group, NW, USA. P.254.

Lathrop, J. A. (1928). "Roof and Floor Construction." United State Patent Office, Patent No. 1688723, USA.

Lee, M.S.S., and Bradford, M.A. (2013). “Sustainable composite beams with deconstructable bolted shear connectors.” Research and Applications in Structural Engineering, Mechanics and Computation, Taylor & Francis Group, London.

Liu, X., Bradford, M.A., and Lee, M.S.S. (2014). “Behavior of High-Strength Friction-Grip Bolted Shear Connectors in Sustainable Composite Beams.” J. Struct. Eng., 10.1061/(ASCE)ST.1943-541X.0001090, 04014149.

Long, A. E., Basheer, P. A. M., Taylor, S. E., Rankin, B. G. I., and Kirkpatrick, J. (2008). “Sustainable bridge construction through innovative advances.” Proceedings of the Institution of Civil Engineers - Bridge Engineering, Vol. 161, Issue 4, pp. 183-188.

Marshall, W.T., Nelson, H.M., Banerjee, H.K. (1971). “An experimental study of the use of high strength friction grip bolts as shear connectors in composite beams.” The Structural Engineer, 49(4), p.175.

Mirza, O., Uy, B., and Patel, N. (2010). “Behaviour and Strength of Shear Connectors Ultilising Blind Bolting.” Proceedings of the 4th international conference on steel and composite structures, Sydney, pp. 791-796.

Molenstra, N. J. (1990). “Ultimate strength of composite beams.” PhD. Thesis, School of Engineering, University of Warwick, Coventry, UK. P.161.

Mottram, J. T., and Johnson, R. P. (1990). “Push tests on studs welded through profiled steel sheeting.” The Structural Engineer, Vol. 68, No. 10, p.190.

Moynihan, M.C., Allwood, J.M. (2014). “Viability and performance of demountable composite connectors.” Journal of Constructional Steel Research, 88, 47-56.

Nah, H., Lee, H., Kim, K., Kim, J., and Kim, W. (2010). “Evaluating Relaxation of High-strength Bolts by Parameters on Slip Faying Surfaces of Bolted Connections.” International Journal of Steel Structures, Vol 10, No 3, pp. 295-303.

Oehlers, D.J. (1980). “Stud shear connectors for composite beams.” PhD thesis, School of Engineering, University of Warwick, Coventry.

Oehlers, D. J. (1989). “Splitting Induced by Shear Connectors in Composite Beams.” ASCE, J. Struct. Eng., Vol. 115, No. 2, pp. 341-362.

Oehlers, D.J., Bradford, M.A. (1995). *Composite steel and concrete structural members: fundamental behavior*, Elsevier Science Ltd, Oxford.

Oehlers, D.J., and Bradford, M.A. (1999). *Elementary behavior of composite steel & concrete structural members*, Butterworth-Heinemann, Oxford, pp.84-94.

Oehlers, D.J., and Coughlan, C.G. (1986). "The shear stiffness of stud shear connections in composite beams." Journal of Constructional Steel Research, 6, 273-284.

Oehlers, D. J., Johnson, R. P. (1987). "The strength of stud shear connections in composite beams." The Structural Engineer, Volume 65, No. 2I. pp.44-48.

Oehlers, D. J., Seracino, R., and Yeo, M. F. (2000). "Effect of friction on shear connection in composite bridge beams." ASCE, J. Bridge Eng., 5(2): 91-98.

Oehlers, D. J., Sved, G. (1995). "Composite beams with limited-slip-capacity shear connectors." J. Struct. Eng., Volume 121, No.6. pp. 932-938.

PANTURA (2011). "Needs for maintenance and refurbishment of bridges in urban environments." Retrieved from (http://www.pantura-project.eu/Downloads/D5.3.pdf) (23 October 2016).

Pathirana, S. W., Uy, B., Mirza, O., and Zhu, X. (2013). "Numerical Study on the Behaviour of Composite Steel-Concrete Beams Utilising Innovative Blind Bolts." Composite Construction in Steel and Concrete VII, ASCE, pp.676-686.

Pathirana, S. W., Uy, B., Mirza, O., and Zhu, X. (2015). "Strengthening of existing composite steel-concrete beams utilizing bolted shear connectors and welded studs." Journal of Constructional Steel Research, 114, 417-430.

Pathirana, S. W., Uy, B., Mirza, O., and Zhu, X. (2016a). "Bolted and welded connectors for the rehabilitation of composite beams." Journal of Constructional Steel Research, 125, pp. 61–73.

Pathirana, S. W., Uy, B., Mirza, O., and Zhu, X. (2016b). "Flexural behaviour of composite steel-concrete utilizing blind bolt shear connectors" Engineering Structures, 114, 181-194.

Pavlović, M. (2013). "Resistance of Bolted Shear Connectors in Refabricated Steel-Concrete Composite Decks." PhD. Thesis, University of Belgrade, Faculty of Civil Engineering, Belgrade.

Pavlović, M., Markovic, Z., Veljkovic, M., and Budevac, D. (2013). “Bolted shear connectors vs. headed studs behavior in push-out tests.” J. Constr. Steel Res., 88, 134–149.

Ramey, G. E., and Oliver, R. S. (1998). “Rapid Rehabilitation Replacement of Bridge Decks.” Alabama Department of Transportation, Research Project 930-376.

Ranković, S., and Drenić, D. (2002). “Static strength of the shear connectors in steel-concrete composite beams, regulations and research analysis.” Architecture and Civil Engineering, Vol. 2, No. 4, pp. 251 – 259.

Rehman, N., Lam, D., Dai, X., and Ashour, A. F. (2016). “Experimental study on demountable shear connectors in composite slabs with profiled decking.”

Rowe, M., Bradford, M. A. (2013). “Partial Shear Interaction in Deconstructable Steel-Concrete Composite Beams with Bolted Shear Connectors.” Design, Fabrication and Economy of Metal Structures, International Conference Proceedings 2013, Miskolc, Hungary, pp 585-590.

SCI (2016). “Shear connection in composite bridge beams.” Retrieved from http://www.steelconstruction.info/Shear_connection_in_composite_bridge_beams. (23 October 2016).

Spremić, M., Marković, Z., Veljković, M., Budjevac, D. (2013). “Push–out experiments of headed shear studs in group arrangements.” Advanced Steel Construction an International Journal, 9(2),170–91.

Steeve, B. E. and Wingate, R. J. (2012). “Aerospace Threaded Fastener Strength in Combined Shear and Tension Loading.” NASA/TM—2012–217454.

Suwaed, A., Karavasilis, T., and Zivanovic, S. (2016). “Steel-Concrete Composite Structure.” International WIPO Patent No. WO2016/135512A1, Geneva, Switzerland.

Tadros, M. K., and Baishya, M. C. (1998). “Rapid replacement of bridge decks.” NCHRP Rep. 407, Transportation Research Board, Washington, DC.

Teychenné, D. C., Franklin, R. E., and Erntroy, H. C. (1997). *Design of normal concrete mixes*. 2nd edition, Building Research Establishment Ltd, Watford, UK.

Vayas, I., and Iliopoulos, A. (2014). *Design of steel-concrete composite bridges to Eurocodes*. CRC Press, Taylor & Francis Group, Boca Raton, USA, p.490.

Wallaert, J. J. and Fisher, J. W. (1965). "Shear strength of high-strength bolts." Fritz Laboratory Reports. Paper 1822, Lehigh University, Pennsylvania.

Xue, W., Ding, M., Wang, H., and Luo, Z. (2008). “Static Behavior and Theoretical Model of Stud Shear Connectors.” Journal of Bridge Engineering (ASCE), Vol. 13, No. 6, November 1, 2008, pp.623-634, p.626.

Yam, L. C. P. (1981). *Design of Composite Steel-Concrete Structures*. Surrey University Press, London, p.75.

Yuan, H. (1996). “The resistances of stud shear connectors with profiled sheeting.” PhD. Thesis, School of Engineering, University of Warwick, Coventry, UK.

Appendix A: Patent No. WO2016/135512A1

(12) INTERNATIONAL APPLICATION PUBLISHED UNDER THE PATENT COOPERATION TREATY (PCT)

(19) World Intellectual Property Organization
International Bureau

(43) International Publication Date
1 September 2016 (01.09.2016)

WIPO | PCT

(10) International Publication Number
WO 2016/135512 A1

(51) International Patent Classification:
E04B 5/10 (2006.01) *E04B 5/23* (2006.01)
E04B 5/04 (2006.01)

(21) International Application Number:
PCT/GB2016/050515

(22) International Filing Date:
29 February 2016 (29.02.2016)

(25) Filing Language: English

(26) Publication Language: English

(30) Priority Data:
1503410.1 27 February 2015 (27.02.2015) GB

(71) Applicant: **THE UNIVERSITY OF WARWICK** [GB/GB]; University House, Coventry, Warwickshire CV4 8UW (GB).

(72) Inventors: **SUWAED, Ahmed**; c/o The University of Warwick, University House, Coventry, Warwickshire CV4 8UW (GB). **KARAVASILIS, Theodore**; c/o The University of Warwick, University House, Coventry, Warwickshire CV4 8UW (GB). **ZIVANOVIC, Stana**; c/o The University of Warwick, University House, Coventry, Warwickshire CV4 8UW (GB).

(74) Agents: **PIOTROWICZ, Pawel** et al.; Venner Shipley LLP, Byron House, Cambridge Business Park, Cowley Road, Cambridge, Cambridgeshire CB4 0WZ (GB).

(81) Designated States *(unless otherwise indicated, for every kind of national protection available)*: AE, AG, AL, AM, AO, AT, AU, AZ, BA, BB, BG, BH, BN, BR, BW, BY, BZ, CA, CH, CL, CN, CO, CR, CU, CZ, DE, DK, DM, DO, DZ, EC, EE, EG, ES, FI, GB, GD, GE, GH, GM, GT, HN, HR, HU, ID, IL, IN, IR, IS, JP, KE, KG, KN, KP, KR, KZ, LA, LC, LK, LR, LS, LU, LY, MA, MD, ME, MG, MK, MN, MW, MX, MY, MZ, NA, NG, NI, NO, NZ, OM, PA, PE, PG, PH, PL, PT, QA, RO, RS, RU, RW, SA, SC, SD, SE, SG, SK, SL, SM, ST, SV, SY, TH, TJ, TM, TN, TR, TT, TZ, UA, UG, US, UZ, VC, VN, ZA, ZM, ZW.

(84) Designated States *(unless otherwise indicated, for every kind of regional protection available)*: ARIPO (BW, GH, GM, KE, LR, LS, MW, MZ, NA, RW, SD, SL, ST, SZ, TZ, UG, ZM, ZW), Eurasian (AM, AZ, BY, KG, KZ, RU, TJ, TM), European (AL, AT, BE, BG, CH, CY, CZ, DE, DK, EE, ES, FI, FR, GB, GR, HR, HU, IE, IS, IT, LT, LU,

[Continued on next page]

(54) Title: STEEL-CONCRETE COMPOSITE STRUCTURE

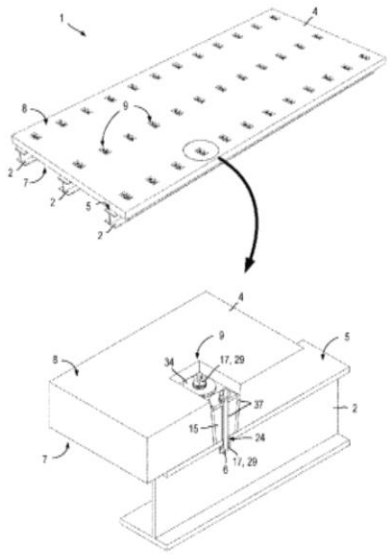

Fig. 2

(57) Abstract: A steel-concrete composite structure (1) is described. The steel-concrete composite structure comprises a steel member (2) having an upper surface (5) and a plurality of shear connector elements (6) upstanding from the upper surface and a concrete slab (4) having upper and lower surfaces (7, 8). The slab is supported on its lower surface by the upper surface of the steel member. The slab comprises a plurality of through holes (9) between the upper and lower surfaces, each through hole tapering towards the lower surface so as to form an inverted frustally-shaped seating surface (10). The concrete slab is configured and positioned with respect to the steel member such that at least one shear connector element projects into each through hole. The steel-concrete composite structure comprises a plurality of removable inverted frustoconical plugs (15), each plug having top and bottom surfaces (18, 19; Fig. 6) and an inverted frustoconically-shaped plugging surface (20; Fig. 6). Each plug has at least one through hole (16) between the top and bottom surfaces. At least one plug (15) is seated in a corresponding through hole (9) of the concrete slab. Each plug is configured such that at least one of the least one shear connector elements (6) projecting into the corresponding through hole (9) is received by a corresponding though hole (16) of the plug. The structure also comprises a plurality of fasteners (17, 29), each fastener coupled to a corresponding shear connector element and arranged to discourage removal of a plug (15) from a through hole (9) of the concrete slab.

WO 2016/135512 A1

LV, MC, MK, MT, NL, NO, PL, PT, RO, RS, SE, SI, SK, SM, TR), OAPI (BF, BJ, CF, CG, CI, CM, GA, GN, GQ, GW, KM, ML, MR, NE, SN, TD, TG).

Published:

— *with international search report (Art. 21(3))*

Steel-concrete composite structure

Field of the invention

The present invention relates to a steel-concrete composite structure, such as a steel-concrete composite bridge, and a shear connector assembly for use in a steel-concrete composite structure.

Background

It can be desirable to use prefabricated, pre-cast steel-concrete composite bridges to build a bridge easily and quickly, particularly in remote areas or other areas where ready-mix concrete is not readily available. Portable steel-concrete composite bridges can be particularly useful in the aftermath of natural disasters, such as earthquakes or flooding, to replace damaged or destroyed infrastructure.

In a typical prefabrication method, concrete panels are usually connected to the steel girders using welded shear studs encapsulated in grouted pockets using epoxy mortar. However, waiting for grouting to harden can slow construction. Furthermore, once a bridge is constructed, it can difficult to repair or replace damaged or worn concrete bridge decks or welded studs.

For these reasons, there has been interest in providing replaceable shear connectors. In general, there are two approaches. The first approach is to use bolts which are embedded inside the concrete slab. Reference is made to L.N. Dallam: "High Strength Bolts Shear Connectors—Push out Tests", American Concrete Institute Journal Proceedings, number 9, pages 767 to 769 (1968), D.J. Dedic and W.F. Klaiber: "High-Strength Bolts as Shear Connectors in Rehabilitation Work", Concrete International, volume 6, issue 7, pages 41 to 46 (1984), G. Kwon et al.: "Behavior of post-installed shear connectors under static and fatigue loading", Journal of Constructional Steel Research, volume 66, issue 4, pages 532 to 541 (2010), D. Lam and E. Saveri: "Shear Capacity of Demountable Shear Connectors", Proceedings of the 10th International Conference on Advances in Steel Concrete Composite and Hybrid Structures (2012), M. Pavlovic et al.: "Bolted shear connectors vs. headed studs behaviour in push-out tests", Journal of Constructional Steel Research, volume 88, pages 134 to 149 (2013), and M.C. Moynihan and J.M. Allwood: "Viability and performance of demountable composite connectors", Journal of Constructional Steel Research, volume 99, pages 47 to 56 (2014).

The second approach is to use bolts threaded through the hardened concrete slab. Reference is made to K. Sattlar: "Betrachtungen Uber Die Verwendung Hochzugfester Schrauben Bel Stahltrager-Verbundkonstruktionen", (Considerations on the Use of High-Tensile Bolts in Composite Concrete and Steel Girder Structures), Preliminary Publication, Sixth Congress, IABSE, 1960, pages 333 to 349 (1960), W.T. Marshall et al.: "An Experimental Study of the Use of High Strength Friction Grip Bolts as Shear Connectors in Composite Beams", The Structural Engineer, volume 49, issue 4, pages 171 to 178 (1971), D.J. Dedic and W.F. Klaiber: "High-Strength Bolts as Shear Connectors in Rehabilitation Work", Concrete International, volume 6, issue 7, pages 41 to 46 (1984), G. Kwon et al.: "Behavior of post-installed shear connectors under static and fatigue loading", Journal of Constructional Steel Research, volume 66, issue 4, pages 532 to 541 (2010), and S.S.M. Lee and M.A. Bradford: "Sustainable composite beams with deconstructable bolted shear connectors", Proceedings of the Fifth International Conference on Structural Engineering, Mechanics and Computation, pages 1373 to 1378 (2013). However, none of these approaches have been widely adopted due to one or more reasons.

For example, there can be very little tolerance and great precision can be required in order to align pre-embedded bolts and/or pre-formed bolt holes during construction. Often such precision cannot be practically achieved in situations in which a pre-fabricated bridge might be erected, such as in remote areas or after a natural disaster.

Furthermore, in modern structural engineering, there is a drive towards achieving sustainable structures. One way to achieve sustainability is to use recyclable materials and to reduce waste. Steel beams can be reused or recycled. However, this requires th steel beams to be separated from the steel-concrete composite slab.

Summary

The present invention seeks to provide an improved steel-concrete composite structure which can be assembled easily and quickly by removing the need for fully grouted pockets and increasing the allowable tolerance for placement of steel and concrete components. The present invention also seeks to provide an improved steel-concrete composite structure which can improve sustainability of steel-concrete constructions by making it easier to separate and re-use steel components.

According to a first aspect of the invention there is provided a steel-concrete composite structure. The steel-concrete composite structure comprises a steel member having an upper surface and a plurality of shear connector elements (such as bolts) upstanding from the upper surface and a concrete slab having upper and lower surfaces. The slab is supported on its lower surface by the upper surface of the steel member. The slab comprises a plurality of through holes between the upper and lower surfaces, each through hole tapering towards the lower surface so as to form an inverted frustally-shaped seating surface. The concrete slab is configured and positioned with respect to the steel member such that at least one shear connector element projects into each through hole. The steel-concrete composite structure also comprises a plurality of removable inverted frustoconical plugs, each plug having top and bottom surfaces and an inverted frustoconically-shaped plugging surface, each plug having at least one through hole between the top and bottom surfaces. At least one plug is seated in a corresponding through hole of the concrete slab and each plug is configured such that at least one of the least one shear connector elements projecting into the corresponding through hole is received by a corresponding though hole of the plug. The steel-concrete composite structure comprises a plurality of fasteners (such as nuts), each fastener coupled to a corresponding shear connector element and arranged to discourage or prevent removal of a plug from a through hole of the concrete slab.

The steel-concrete composite structure can be assembled easily and quickly since the steel members, concrete slab and plugs can be prefabricated off site and the concrete slab can be easily aligned with the steel members. Furthermore, the plugs can be removed by simply undoing or breaking the fasteners thereby allowing the steel members and the slab to be cleanly separated. This can make it easier to recover and re-use steel components.

The concrete slab may comprise a concrete grade between C8/10 and C100/115. The concrete slab may comprise C25/30 grade concrete. The concrete slab may be reinforced with any one of steel rebar, short steel fibres, fibre meshes and/or fibre reinforced polymer composites. The plugs may comprise a concrete grade between C8/10 and C100/115. The plugs may comprise C60/75 grade concrete. The plugs may be unreinforced. The plugs may be reinforced with any one of steel rebar, short steel fibres, fibre meshes and/or fibre reinforced polymer composites.

Each through hole of the concrete slab may be configured to form an inverted frustoconically-shaped seating surface and each plug is seated in a corresponding one of the through holes of the concrete slab. Each plug may contain at least two through holes, and each plug may receive at least two shear connector elements into the respective through holes.

Each through hole of the concrete slab may be configured to form an inverted rectangular-based frustopyramidally-shaped seating surface and at least one plug may be seated in a corresponding one of the through holes of the concrete slab. At least two plugs may be seated in a corresponding one of the through holes of the concrete slab.

Each plugging surface may be coated with a layer of de-bonding material. The de-bonding material may be wax.

Thus, the replaceability of the plugs and/or of the shear connector elements may be improved by including layers of de-bonding material to facilitate removal of the plugs and/or any regions of filling material.

A filling material may be disposed around the one or more plugs in the through hole of the concrete slab. The filling material may be cement based or epoxy based.

Thus, the mechanical performance of the steel-concrete composite structure may be improved. The construction time may be improved relative to welded studs in a fully grouted pocket because the total volume of filling material is relatively reduced, thereby reducing the time taken for the filling material to set and/or cure.

The shear connector elements may be removably attachable to the steel member. The shear connector elements may comprise bolts. Each fastener may comprise a nut which is received by a threaded portion of the corresponding shear connector element.

The fasteners and the sheer connector element may be arranged to urge each plug against the upper surface of the steel member.

Thus, a frictional force is generated which opposes shear between the steel member and the concrete slab, which may improve the mechanical performance of the steel-concrete composite structure because the frictional force must be overcome before commencement of sliding.

Where the shear connector elements are bolts, the bolts may received by through holes in the steel member. Each opening of the through holes in the upper surface of the steel member may comprise a countersunk seat. The steel-concrete composite structure may further comprise additional filling material disposed in the countersunk seat and around the bolt.

Thus, the mechanical performance of a steel-concrete composite structure may be improved by preventing or restricting lateral slip of the shear connector element with respect to the steel member. This can have the effect of constraining the shear connector element to deform with a double plastic hinge in response to shear loading.

Where the shear connector elements are bolts, the bolts may be received by through holes in the steel member. Each opening of the through holes in the upper surface of the steel member may comprise a seat configured to receive a bolt head or a nut. The portion of each bolt passing through the steel member is tensioned by a nut threaded over the bolt and tightened into the seat. The seat configured to receive a bolt head or a nut may be countersunk and the nut may be a cone nut configured to by received into the countersunk seat. The seat configured to receive a bolt head or a nut may be countersunk to an angle of 60 degrees.

Thus, the mechanical performance of a steel-concrete composite structure may be improved by preventing or restricting lateral slip of the shear connector element with

respect to the steel member. This can have the effect of constraining the shear connector element to deform with a double plastic hinge in response to shear loading.

One or more intermediate layers may be provided between the concrete slab and the steel member. The intermediate layer(s) may comprise a metal based material. The intermediate layer(s) may comprise a ceramic based material. The intermediate layer(s) may comprise a wood based material. The intermediate layer(s) may comprise a polymer based material such as a rubber or an elastomer.

One or more fibre reinforced elastomeric elements may be disposed around the one or more plugs in the through hole of the concrete slab. The fibre reinforced elastomeric elements may comprise fibre reinforced rubber. The fibre reinforced elastomeric elements may be shaped to form a frustoconical or frustopyramidal shell. The fibre reinforced elastomeric elements may comprise a block of fibre reinforced rubber including one or more through holes to receive one or more shear connector elements and corresponding plugs. A fibre reinforced elastomeric element may be bonded to the inverted frustoconically-shaped plugging surface of a plug. The fibre reinforced elastomeric elements may be configured such that a hoop stress generated in the elastomeric element in response to a plug being urged against the upper surface of the steel member secures the steel member to the concrete slab.

Thus, the elastomeric elements may provide damping for dynamic loadings of the steel-concrete composite structure.

The steel-concrete composite structure may be a bridge.

According to a second aspect of the invention there is provided a removable plug for use in a steel-concrete composite structure. The removable plug comprises an inverted frustoconical body having top and bottom surfaces and an inverted frustoconically-shaped plugging surface and at least one through hole between the top and bottom surfaces. The removable plug may comprise two, three, four, five or at least six through holes. The through holes of the removable plug may be disposed in a regular polygonal arrangement.

According to a third aspect of the invention there is provided a method of building a steel-concrete composite structure comprising a steel member having an upper surface,

a plurality of shear connector elements; a concrete slab having upper and lower surfaces, the slab comprising a plurality of through holes between the upper and lower surfaces, each through hole tapering towards the lower surface so as to form an inverted frustally-shaped seating surface, a plurality of removable inverted frustoconical plugs, each plug having top and bottom surfaces and an inverted frustoconically-shaped plugging surface, each plug having at least one through hole between the top and bottom surfaces, and a plurality of fasteners. The method comprises coupling the plurality of shear connector elements to the steel member such that the shear connector elements are upstanding from the upper surface, positioning the slab so that it is supported on its lower surface by the upper surface of the steel member and arranged such that at least one shear connector element projects into each through hole, positioning the plurality of plugs such that each plug is seated in a corresponding through hole of the concrete slab and wherein each plug is positioned such that at least one of the least one shear connector elements projecting into the corresponding through hole is received by a corresponding though hole of the plug, and coupling each of the fasteners to a corresponding shear connector element so as to discourage removal of a plug from a through hole of the concrete slab.

A filling material may be disposed around the one or more plugs in the through hole of the concrete slab. Each through hole may be filed with a quantity of filling material before the corresponding plug is emplaced into the through hole, so that the filling material flows around and inside the plug.

Brief Description of the Drawings

Certain embodiments of the present invention will now be described, by way of example, with reference to the accompanying drawings in which:

Figure 1 is a perspective view of a steel-concrete composite structure;

Figure 2 is a cut-away view of a portion of the shear connector assembly included in the steel-concrete composite structure shown in Figure 1;

Figure 3 is a perspective view of a through hole included in a steel-concrete composite structure shown in Figure 1;

Figure 4 is a cross-sectional view of a through hole shown in Figure 3 along a line labelled A-A;

Figure 5 is a cross-sectional view of a through hole shown in Figure 3 along a line labelled B-B;

Figure 6 is a perspective view of a removable frustoconical plug included in a steel-concrete composite structure shown in Figure 1;

Figure 7 is a plan view of a portion of a steel member and a fastener included in a steel-concrete composite structure shown in Figure 1;

Figure 8 is a cross sectional view of a first shear connecter assembly for use in a steel-concrete composite structure shown in Figure 1;

Figure 9 is a cross sectional view of a second shear connecter assembly for use in a steel-concrete composite structure shown in Figure 1;

Figure 10 is a cross sectional view of a third shear connecter assembly for use in a steel-concrete composite structure shown in Figure 1;

Figures 11A to 11E illustrate a method of constructing a steel-concrete composite structure shown in Figure 1;

Figure 12 is a cross sectional view of a test steel-concrete structure;

Figure 13 is a graph comparing the measured loading behaviour of a test structure shown in Figure 12 with a theoretical comparative example; and

Figure 14 is an exploded perspective view of a second steel-concrete composite structure.

Detailed Description of Certain Embodiments

In the following description, like parts are denoted by like reference numerals.

Referring to Figure 1, a steel-concrete composite structure 1 in the form of a beam bridge is shown. The bridge 1 includes rows of elongate steel members 2 supporting a

deck 3 comprising concrete slabs 4. Under load, the steel members 2 are under tension, while the concrete slabs 4 are under compression.

Referring to Figure 2, each steel member 2 takes the form of an I-beam and has a respective upper surface 5. Shear connector elements 6 extend upwardly from the upper surface 5. In this case, the shear connector elements 6 comprise bolts.

Each concrete slab 4 has respective upper and lower surfaces 7, 8. Each slab 4 is supported on its lower surface 7 by the upper surfaces 5 of three steel members 2. In this case, the concrete slab 4 comprises C30/37 concrete, having a compressive strength of 37 MPa and reinforced with steel rebar reinforcements (not shown).

Referring also to Figures 3, 4 and 5, each slab 4 has through holes 9 between the upper and lower surfaces 7, 8. In this case, the through holes 9 are pre-formed into the concrete slab 4 at the time of casting. Each through hole 9 tapers towards the lower surface 7 so as to form an inverted frustally-shaped seating surface 10. In this case, the inverted frustally-shaped seating surface 10 has the shape of a frustum of a rectangular pyramid. The through hole 9 has a width W_1 on the upper surface 8 of the slab 4 and a width W_2 on the lower surface 7 of the slab 4. The through hole 9 has a length L_1 on the upper surface 8 of the slab 4 and a length L_2 on the lower surface of the slab 4.

The through holes 9 are arranged in a line running along the slab 4, aligned with an underlying steel member 2. Thus, at least one shear connector element 6 projects into each through hole 9. In this case, two shear connector elements 6 project into each through hole 9. However, as will be explained in more detail, only one shear connector element 6 or at least three shear connector elements 6 may project into each through hole 9.

At least one inverted frustoconical plug 15 is seated in each through hole 9 of the slab 4. Each plug 15 is positioned such that a shear connector element 6 projecting into the corresponding through hole 9 is received by a corresponding though hole 16 (Figure 6) of the plug 15. In this case, the plugs 15 comprise C60/75 concrete, so that the concrete comprising the plugs 15 is stronger than the concrete comprising the slab 4. Each plug 15 is secured within the corresponding through hole 9 of the slab 4 by a corresponding fastener 17 which is arranged to discourage removal of that plug 15 from the

corresponding through hole 9. In this case, the fastener 17 is a bolt threaded over an end of the shear connector element 6.

Securing the slab 4 to the steel members 2 using the plugs 15 helps to improve the replaceability and/or reusability of a steel-concrete composite structure 1, because the plugs 15 may be removed and replaced by decoupling the fasteners 17. Employing an inverted frustally-shaped seating surface 10 in combination with the frustoconical plugs 15 can increase the tolerance for the placement of the shear connector elements 6 on the steel members 2 and the through holes 9 in the slab 4, thereby reducing the complexity and/or cost of manufacturing and constructing pre-fabricated steel-concrete composite structures 1.

Referring also to Figure 6, each plug 15 has a top surface 18, a bottom surface 19 and an inverted frustoconically-shaped plugging surface 20. Each plug 15 has at least one through hole 16 between the top and bottom surfaces 18, 19. In this case, each plug 15 has a single, centrally positioned through hole 16. The top surface 18 has a top diameter D_1, and the bottom surface 19 has a bottom diameter D_2 which is smaller than the top diameter D_1. The plug has a height H, which in this case is less than a thickness of the slab 4. In this case, the slope angle of the plugging surface 20 is about 5 degrees.

In this case, the length L_1 of each through hole 9 on the upper surface 8 of the slab 4 is at least twice the top diameter D_1 of the plugs 15, such that two plugs 15 may be placed in each through hole 9 side by side, each plug 15 receiving one of the two shear connector elements 7 which project into the corresponding through hole 9.

Referring also to Figure 7, in this case each shear connector 6 may be received by a through hole 24 formed through a portion of a steel member 2. The through hole 24 has an upper opening 24a in the upper surface 5 of the steel member 2 and a lower opening 24b in a lower surface 25 of the steel member 2. In this case, the lower surface 25 is provided by the underside of the steel I-beam flange which contacts the slab 4. The upper opening 24a is countersunk at a first countersinking angle 26a. As shall be described in detail hereinafter, the upper opening 24a may serve as a seat for a fastener 17. In this case, the first countersinking angle 26a is 60 degrees. In this case, the fastener 17 may be a conical nut 27 (Figure 9). Alternatively, instead of providing a seat for a fastener, the upper opening 24a may be filled with filling material 37 (Figure 8)

which acts to enhance a dowel action which opposes slip between the steel member 2 and the slab 4.

The opening of the lower through hole 24b in a lower surface 25 of a portion of a steel member 2 may optionally comprise a seat for a fastener 17. When the lower opening 24b of the through hole 24 is to provide a seat, it may be countersunk at a second countersinking angle 26b. The lower opening 24b may receive a chamfered nut (not shown) having a chamfering angle which matches the second countersinking angle 26b. In this case, the second countersinking angle 26b is 30 degrees. The outer diameter of the countersinking of the lower opening 24b may be greater than or equal to the chamfered nut diameter. Where a countersunk upper opening 24a is used, the lower opening 24b need not also be countersunk. However, both of the upper and lower openings 24a, 24b may be countersunk in some steel-concrete composite structures 1.

Employing a seat for the shear connector element 6 can improve the mechanical performance of a steel-concrete composite structure 1 by preventing or restricting lateral slip of the shear connector element 6 with respect to the steel member 2. This can have the effect of constraining the shear connector element 6 to deform with a double plastic hinge from the upper surface in response to shear loading.

Referring to Figure 8, a first shear connector assembly 30 includes a shear connector element 6 received through a through hole 24 in the steel member 2 and protruding into the through hole 9 of the concrete slab 4. The through hole 24 includes an upper countersunk opening 24a. Optionally, the through hole 24 may also include a lower countersunk opening 24b. In this case, the lower opening 24b is not countersunk. Th shear connecter element is received by the through hole 16 of the plug 15. The plug 15 is positioned within the through hole 9 of the concrete slab 4, with the bottom surface 19 in contact with the upper surface 5 of the steel member 2. In this case, the shear connector element 6 is an M16 steel bolt. The shear connector element 6 includes an upper threaded portion 31 which protrudes above the height H of the plug 15, and a lower threaded portion 32 which protrudes below the lower surface 25 of the steel member 2. A central portion of the shear connector element 6 may be unthreaded in order to increase the cross sectional area of the shear connector element 6 in the plane in which the shear connector element 6 will be subjected to the greatest shear stress.

A nut 29 is received over the lower threaded portion 32 and tightened against the steel member 2. Optionally, one or more washers 35 may separate the nut 29 and the steel member 2. In this case, the steel member 2 includes a lower opening 24b which is not countersunk. Alternatively, the lower opening 24b may be countersunk and receive a chamfered nut (not shown) having a chamfering angle which matches the second countersinking angle 26b.

A retaining washer 34 (also referred to as a "plate" or "repair" washer) having a relatively large difference between its inner and outer circumferences is received over the upper threaded portion 31, and secured against the top surface 18 of the plug 15 by a nut 29. One or more washers 35 may space the retaining washer 34 from the nut 29.

There may be a gap 36 between the inverted frustally-shaped seating surface 10 of the slab 4 and the frustoconically shaped plugging surface 20 of the plug 15. In this case, the gap 36 is approximately 5 mm at the point of closest approach between the plugging surface 20 and the seating surface 10. The gap 36 may be filled by a region of filling material 37. In this case, the filling material 37 is a concrete grout.

There may be a residual gap between the shear connector element 6 and the interior surface of the through hole 16 of the plug 15. In this case, the residual gap is also filled with the filling material 37. The residual gap need not be entirely filled with filling material 37, and is preferably at least half filled. The replaceability of the plug 15 is preferably maintained by making the length of the upper and lower threaded portions 31, 32 just long enough to receive the respective fasteners 17, but not long enough that the threaded portions 31, 32 contact the filling material 37.

Filling the gap 36 with filling material 37 helps to improve the mechanical performance of the steel-concrete composite structure 1. The construction time can be improved relative to welded studs in a fully grouted pocket, because the total volume of filling material 37 used is relatively reduced, thereby reducing the time taken to apply the filling material. When the filling material needs to dry, the time taken for the filling material 37 to set may also be reduced by reducing the volume.

The volume of filling material 37 in the residual gap around the shear connector 6 extends down into the upper countersunk opening 24a, producing a locking mechanism which can be effective in preventing or restricting lateral slip. This can have the effect

of constraining the shear connector element 6 to deform with a double plastic hinge in response to shear loading, relatively increasing the energy absorbed for a given deflection.

Additionally, in this case, the nuts 29 are tightened such that the bottom surface 19 of the plug 15 is urged against the upper surface 5 of the steel member 2, producing a frictional force which opposes shear between the steel member 2 and the slab 4. This helps improve the mechanical performance of the steel-concrete composite structure 1 because the frictional force must be overcome before commencement of sliding and transfer of loading to the dowel action of the filling material 37 and shear connectors 6.

Referring to Figure 9, a second shear connector assembly 39 is substantially the same as the first shear connector assembly 30, except that the shear connector 7 is additionally secured by a middle fastener 40. The middle fastener 40 is received over the portion of the lower threaded portion 32 of the shear connector 6 which extends above the upper surface 5 of the steel member 2. In this case, the middle fastener 40 is a cone nut 27 which is threaded over the shear connector 6 and tightened against the upper surface 5 of the steel member 2. Optionally, one or more cone washers (not shown) may space the middle fastener 40 from the steel member 2.

In this case, the cone nut 27 providing the middle fastener 40 is chamfered to an angle which matches the first countersinking angle 26a of the upper opening 24a in the steel member 2. This helps the middle fastener 40 to cooperate with the upper opening 24a to provide a locking mechanism. In this case, a portion of the internal threading of the cone nut 27 extending from the flat end of the cone nut 27 is removed. This allows the unthreaded portion of the shear connector element 6 to be partially received inside the cone nut 27. This can help to maintain the replaceability of the plug as described hereinbefore, and may also help to ensure that plastic failure of the shear connector element 6 does not initiate in the lower threaded portion 32. In this case, the middle fastener 40, 27 is received onto the shear connector element 6 before the shear connecter element 6 is received through the through hole 24. In this case, the opening of the through hole 16 in the bottom surface 19 of the plug 15 includes a widened end portion 41 forming a seat which receives and fits over the middle fastener 40.

Using a middle fastener 40 can improve the mechanical performance of a steel-concrete composite structure 1. In particular, the cooperation of the cone nut 27 with the

countersunk upper opening 24a produces a locking mechanism which acts to prevent or restrict lateral slip. This can have the effect of constraining the shear connector element 6 to deform with a double plastic hinge in response to shear loading, relatively increasing the energy absorbed for a given deflection.

Additionally, the middle fastener has an increased contact area compared to the shear connector element 6, which can reduce the peak stress in the filling material 37 and plug 15, thereby reducing the risk of local crushing.

Concrete slabs 4 and shear connector assemblies 30, 39 according to the present invention can be easier to repair or replace than structures using conventional welded studs and grouted pockets. In particular, the concrete slab(s) 4 may be replaced if they have become worn or damaged. Where there is access beneath the slab(s) 4, fasteners 17 below the lower surface 25 of the steel member(s) 2 may be removed and the slab(s) 4 uplifted, including the shear connectors 6, plugs 15 and filling material 37. Alternatively, or if there is not access beneath the slab(s) 4, the fasteners 17 above the plugs 15 may be remove and the slab(s) 4 may be uplifted including the plugs 15 and filling material 37, leaving the shear connectors 6 in place.

Additional, the plugs 15 themselves may be replaced if they have become worn or damaged by removing the fasteners 17, extracting an old/worn plug 15 and replacing it with a new plug 15. The shear connectors 6 may additionally be replaced if they become worn, damaged or corroded.

If regions of filling material 37 have been used to fill gaps 36, then the replaceability of the plugs 15 can be maintained by selecting a filling material 37 which is relatively easier to remove than the concrete comprising the plugs 15 and the slab 4. For example, a material such as cement mortar which may be readily chipped or broken away. Additionally, as described hereinbefore, the length of the upper and lower threaded portions 31, 32 may be controlled so that filling material 37 in not in contact with the threaded portions 31, 32.

Referring to Figure 10, a third shear connector assembly 42 is the same as either the first or the second shear connector assemblies 30, 39, except that one or both of the inverted frustally-shaped seating surface 10 of the concrete slab 4 and/or the frustoconically shaped plugging surface 20 of the plug 15 are separated from the filling

material 37 by one or more layers of a de-bonding material 43. In this case, the de-bonding material 43 comprises wax. In this case, the thickness of the layers of de-bonding material 43 is relatively small compared to that of the filling material 37. For example, the layers of de-bonding material 43 may be less than 1 mm, less than 0.5 mm or less than 0.1 mm.

Including one or more layers of de-bonding material 43 helps to improve the replaceability of the plugs 15 and/or of the shear connector elements 6 by facilitating removal of the plugs 15 and/or any regions of filling material 37.

A method of constructing the second steel-concrete composite structure 1 shall be described.

Referring to Figure 11A, a first stage of constructing a portion of a steel-concrete composite structure 1 is shown. Through holes 24 are provided in the steel member 2 at the locations which are to receive the shear connector elements 6. The upper openings 24a in the upper surface 5 of the steel member 2 are countersunk. Optionally, the lower openings 24b may also be countersunk.

Referring also to Figure 11B, an intermediate stage of constructing a portion of a steel-concrete composite structure 1 is shown. Shear connector elements 6 are received into the steel member 2. Shear connector elements 6 may be temporarily secured in position using suitable means such as, for example, wire warped tightly around the bolt (not shown) or locking washers (not shown). In this case, shear connector elements 6 are provided upstanding from the upper surface 5 of the steel member 2 in groups of two shear connectors 6. Alternatively, shear connector elements 6 may be provided upstanding from the upper surface 5 of the steel member 2 in groups of one, two, three, four, five, six or more shear connector elements 7. Where the steel members 2 are I-beams, shear connector elements 6 are preferably provided in groups including an even number of shear connectors elements 6, with the same number disposed either side of the midline of the upper surface 5.

Referring also to Figure 11C, an intermediate stage of constructing a portion of a steel-concrete composite structure 1 is shown. The slab 4 is placed with the lower surface 7 of the slab 4 supported by the upper surface 5 of the steel members 2. The slab 4 is positioned such that each group of shear connector elements 6 is aligned with and

received into a corresponding through hole 9 in the slab 4. In this case, each through hole 9 receives a pair of two shear connector elements 6. Alternatively, more or fewer than two shear connector elements 6 may be received into each through hole 9.

Referring also to Figure 11D, an intermediate stage of constructing a portion of a steel-concrete composite structure 1 is shown. Plugs 15 are placed into each through hole 9 of the slab 4, such that each shear connector element 6 which protrudes into that through hole 9 is received into a corresponding through hole 16 of a plug 15. In this case, two plugs 15 are placed in each through hole 9, each plug 15 receiving one of the two shear connector elements 6 which protrude into the through hole 9. Alternatively, when more or fewer than two shear connector elements 6 protrude into each through hole, each shear connector elements 6 may be received by one of a corresponding number of plugs 15. If required, a gap 36 between the inverted frustally-shaped seating surface 10 formed by the through hole 9 in the slab 4 and the frustoconically shaped plugging surface or surfaces 20 of the plug or plugs 15 may be filled with a filling material 37. Where the gap 36 is filled with a filling material 37, filling material 37 may be poured into the through hole 9 to a certain depth first, with the plugs 15 inserted subsequently. This can help to reduce the incidence of trapped air pockets and ensure even filling of the gap 36 and the residual gaps around each shear connector 6.

Referring also to Figure 11E, a portion of a completed steel-concrete composite structure 1 is shown. The upper ends of the shear connecting elements 6 protrude past the top surfaces 18 of the plugs 15. Fasteners 17 are applied to the upper ends of the shear connecting elements 6 to prevent or discourage the removal of the corresponding plugs 15 from the through holes 9 of the slab 4. In this case, the plugs 15 are secured using retaining washers 34, one or more washers 35 and nuts 29. In this case, the nuts 29 are tightened to secure the plugs 15 against the upper surface 5 of the steel member 2.

Referring to Figure 12, a test steel-concrete structure 44 includes a pair of slabs 4 which are each coupled to a steel member 2 using a shear connector assembly 30. The test structure 44 shown in Figure 12 includes examples of the first shear connector assembly 30, however it will be apparent that either of the second or third shear connector assemblies 39, 42 may be used instead. The test structure 44 may be suitable for conducting full scale push out tests to Eurocode 4 standards.

In this case, the steel member is an I-beam having first and second flanges 45, 46. In this case, the pair of slabs 4 includes a first test slab 47 coupled to the first flange 45 and a second test slab 48 coupled to the second flange 46. The steel member 2 and the first and second test slabs 47, 48 are orientated vertically with respect to a floor 49, upon which the slabs 47, 48 are supported. An upper end portion of the steel member 2 extends above the first and second slabs 47, 48, and a lower end portion of the steel member 2 is suspended above the floor 49. In this case, each of the first and second slabs 47, 48 includes one rectangular frustopyramidal through hole 9, with the long sides L_1, L_2 orientated horizontally. In this case, each through hole 9 receives two shear connector elements 6, and two plugs 15 arranged alongside each other.

A test load 50 is applied to the upper end portion of the steel member 2. The loading configuration of the test structure 44 applies a shear load between the steel member 2 and each of the first and second test slabs 4. The shear loading of the first and second test slabs 47, 48 can be substantially symmetric. Sensors (not shown) record the displacements of the first and second test slabs 47, 48 with respect to the steel member 2. Other sensors (not shown) may record the load and displacement of each individual shear connector element 6. Other sensors (not shown) may record additional information such as, for example, the size of any gaps which open up between the steel member 2 and the first and second test slabs 47, 48 during loading.

Referring to Figure 13, the measured mechanical shear behaviour 51 of an example of the test structure 44 is compared to the theoretical behaviour 52 of a comparative example comprising the same number of shear connecting elements which are welded studs of equivalent diameter, embedded into a concrete slab. The theoretical values 52 were calculated using a model proposed by Xue et al: "Static Behavior and Theoretical Model of Stud Shear Connectors", Journal of Bridge Engineering, ASCE, November/ December, page 623.

The experimental data shown in Figure 13 is measured for a test structure 44 having the following dimensions. The top diameter D_1 of the plugs 15 was 90 mm, the bottom diameter D_2 was 70 mm and the height H was 115 mm. The width W_1 of the through hole 9 on the upper surface 8 of the slab 4 was 116 mm, the width W_2 on the lower surface 7 was 90 mm, the length L_1 on the upper surface 8 was 216 mm, the length L_2 on the lower surface 7 was 190 mm and the thickness of the slab 4 was 150 mm. The slab 4 comprised concrete with a compressive strength of 37.22 MPa and a tensile

strength of 3.67 MPa, and was reinforced with steel according to EC4-1-1 recommendations. EC4-1-1 recommendations include reinforcement which are 10mm diameter ribbed bars, providing 180 mm spacing for vertical bars and 150 mm for transverse bars. The minimum concrete cover was 15 mm. Two middle bars were eliminated in the test due to presence of the slab through hole 9. The plugs 15 comprised concrete having a compressive strength of 73.87 MPa and a tensile strength of 3.708 MPa, and the plugs 15 did not include reinforcements.

The shear connecting elements 6 were grade 8.8 M16 bolts received by through holes 24 in the steel member 2. The upper opening 24a of the through hole 24 was countersunk to an first countersinking angle 26a of 60 degrees and the lower opening 24b was not countersunk. The M16 bolt steel had an elastic modulus of 204.43 GPa, a yield strength 824.76 MPa, an ultimate strength 946.47 MPa and a fracture strength of 703.32 MPa. The upper and lower threaded portions 31, 32 of the shear connector elements 6 extended for 25 mm from either end, leaving a 150 mm long portion unthreaded through the middle.

A third shear connector assembly 42 without a middle fastener 40 was produced, and a gap 36 between the inverted frustally-shaped seating surface 10 formed by the through hole 9 in the slab 4 and the plugging surfaces 20 of the plugs 15 was filled with a filling material 37 comprising a concrete grout with a compressive strength of 48.4 MPa. The concrete grout contained a 1:1 ratio of cement : fine sand, with a water/cement ratio of 0.5. The cement was Quickcem cement from Hanson company. %1.2 of cement weight, TamCem 60 superplasterizer, was also used. One layer of wax was used as the de-bonding material 43.

The test applied shear loading between the steel member 2 and the first and second tes slab 47, 48 and lasted for approximately two and a half hours. The test was conducted under displacement control with a loading rate of approximately 0.1 to 0.2 mm per minute.

The experimental loading curve 51 for the test structure 44 shows improved mechanica performance when compared to theoretical values 52 for welded studs of equivalent diameter embedded into a slab.

The ultimate load and corresponding shear displacement on each shear connector element 6 for the test structure 44 are provided along with comparative examples in Table 1 below. All values correspond to shear connector elements in the form of steel M16 bolts.

Table 1

	Year	Ultimate load per M16 bolt / kN	Shear displacement at ultimate load / mm
Example test structure 44	2015	186	17.4
Lee and Bradford *ibid.*	2013	153	31.5
Dallam *ibid.*	1968	122	5.4
Marshall *et al. ibid.*	1971	122	~8
Pavlovic *et al. ibid.*	2013	90	5.5
Lam and Saveri *ibid.*	2012	75	8.8

The loading performance of the example test structure 44 is believed to be due to one or more factors. Without wishing to be bound by theory, application of a pre-load to the plugs 15 produces a frictional force between the bottom surfaces 19 of the plugs 15 and the upper surface 5 of the steel member 2. Such a frictional force must be overcome before the slab 4 and the steel member 2 begin to slip relative to one another, which can improve the loading performance by delaying slip until a larger load is reached.

At higher loads, shearing is resisted by a combination of the frictional force and a dowel action of the shear connector elements 6 and the plugs 15. Using relatively high strength concrete for the plugs 15 helps to produce an effective dowel action by increasing the loading required to initiate local crushing of the plug 15 material by the shear connector elements 6.

Receiving the shear connector elements 6 through the steel member 2 using a countersunk upper opening 24a can help to constrain the shear connector elements 6 to deform with a double plastic hinge, which can increasing the energy absorbed. Additionally, the peak stresses on the slab 4 can be reduced, because the plugs 15 have an increased bearing surface area compared to the shear connecter elements 6 alone. This can help to prevent cracking and/or crushing of the concrete slab 4.

Second steel-concrete composite structure 53

Referring to Figure 14, a second steel-concrete composite structure 53 is shown. The second steel-concrete composite structure 53 is the same as the steel-concrete composite structure 1, except for the second through holes 54 in the slab 4 and the second frustoconical plugs 55. Each second through hole 54 tapers towards the lower surface 7 of the slab 4 so as to form a second inverted frustally-shaped seating surface 56. In this case, the second inverted frustally-shaped seating surface 56 has a frustoconical shape. In this case, four shear connector elements 6 are disposed in a square arrangement and received into each of the second through holes 54.

Each of the second plugs 55 has a top surface 18, a bottom surface 19 and a second inverted frustoconically-shaped plugging surface 57. In this case, each second plug 55 has four through holes 16 between the top and bottom surfaces 18, 19, disposed in a square arrangement. Each of the second plugs 55 is positioned in a corresponding second through hole 54 such that the four shear connector elements 6 are received by the corresponding through holes 16 of one of the second plugs 55.

Securing each of the second frustoconical plugs 55 with more than one shear connecting element 6 received into each second plug 55 can reduce the shearing load or each individual shear connecting element 6.

Although the second steel-concrete composite structure 53 has been described with four shear connector elements 6 received into each second through hole 54, different numbers of shear connector elements may be used. For example, one, two, three or more than four shear connector elements 6 may be used instead, corresponding to a second plug 55 including one, two, three or more than four through holes 16. Although the second steel-concrete composite structure 53 has been described with the shear connector elements 6 disposed in a square arrangement, the shear connector elements 6 may be disposed differently and need not be arranged in a regular shape. The second steel concrete composite structure 53 is not restricted to frustoconical second through holes 54 receiving frustoconical second plugs 55. For example, the second through holes 54 and second plugs 55 may each have the shape of a frustum of a pyramid with any polygonal shaped base or a frustum of an oval based cone.

Modifications

It will be appreciated that many modifications may be made to the embodiments hereinbefore described.

For example, steel-concrete composite structures 1, 53 have been described as bridges. However, a steel-concrete composite structure can take other form such as, for example, a building structure comprising a steel frame of a building and a concrete slab forming part of a floor.

Steel concrete composite structures 1, 53 have been described with three steel members 2 supporting a concrete slab 4. However, fewer or more steel members 2 may be used to support a slab 4. Furthermore, a slab 4 need not be provided as a single piece, and a steel-concrete composite structure 1, 53 may include more than one slab 4 supported by the steel members 2.

Steel concrete composite structures 1, 53 have been described with steel members 2 directly supporting a concrete slab 4. However, the steel members 2 need not directly support the slab 4, and one or more intermediate layers (not shown) may be provided between the concrete slab 4 and the steel members 2. The intermediate layer(s) may comprise a metal based material. The intermediate layer(s) may comprise a ceramic based material. The intermediate layer(s) may comprise a wood based material. The intermediate layer(s) may comprise a polymer based material such as a rubber or an elastomer.

The steel-concrete composite structures 1 need not be restricted to slabs 4 including rectangular frustopyramidal through holes 9 which receive two shear connecting elements 6 and two corresponding plugs 15. Alternatively, the steel composite structure 1 may use include through holes 9 which are frustoconical or a frustum of a pyramid with a base of any polygonal shape. Additionally or alternatively, each through hole 9 may receive only one, or at least three shear connecting elements 6, each of which may be received by a corresponding plug 15. Additionally or alternatively, each plug 15 may include more than one through hole 16 and receive more than one shear connector element 6.

The inverted frustally-shaped seating surfaces 10, 56 and the frustoconically shaped plugging surfaces 20, 57 may be smooth. This can improve the replaceability of the

plugs 15, 55 by making them easier to remove. The seating surfaces 10, 56 and plugging surfaces 20, 57 may be made smooth without substantially affecting the loading performance of a steel-concrete composite structure 1, 53 because the shape of the seating surfaces 10, 56 and plugging surfaces 20, 57 acts to urge the concrete slab 4 against the steel members 2.

The through holes 9, 54 have been described as being pre-formed into the slab 4 at the time of casting. However, the through holes 9, 54 may alternatively be formed in situ at the time of constructing/assembling the steel-concrete composites structure 1, 53.

The plugs 15, 55 have been described as being urged against the steel members 2 by pressure exerted by the fasteners 17. However, the fasteners 17 need not be tightened and may simply prevent the plugs 15, 55 from being removed. In such a case, the fasteners 17 may be lock nuts or a pair of nuts 29 may be tightened against each other.

The shear connector elements 6 have been described as removable bolts. However, the shear connector elements 6 need not be bolts, and may alternatively be studs, pins or dowels. The shear connector elements 6 have been described as being removeably coupled to the steel members 2. However, the shear connector elements 6 may be irremovably coupled to the steel members 2, for example, by welding or brazing. The fasteners 17 need not be nuts 27, 29, and other types of fastener may be used. For example, the fastener 17 may be a pin or wire inserted through an end of the shear connector element 6 which protrudes above the top surface 18 of a plug 15, 55, such that the shear connector element 6 is prevented or discouraged from being withdrawn from the through hole 16 of the plug 15, 55.

The slab 4 has been described as comprising C25/30 concrete having a compressive strength of 30 MPa. However, other grades of concrete may be used for the slab 4, such as, for example, any concrete grade between C8/10 and C100/115, dependent upon the expected loading of a steel-concrete composite structure 1, 53. The concrete slab 4 has been described as being reinforced with steel rebar. However, other types of concrete reinforcement may be used such as, for example, short steel fibres, fibre meshes, fibre reinforced polymer composites or any other type of concrete reinforcement which would be suitable for the expected loading of a steel-concrete composite structure 1, 53.

The plugs 15, 55 have been described as comprising C60/75 concrete having a compressive strength of 75 MPa. However, other grades of concrete may be used for the plugs 15, 55 such as, for example, any concrete grade between C8/10 and C100/115 dependent upon the expected preloading of shear connector elements 6 and the required dowel action. The plugs 15, 55 may be reinforced using steel rebar or other types of concrete reinforcement such as, for example, short steel fibres, fibre meshes, fibre reinforced polymer composites or any other type of concrete reinforcement which would be suitable for the intended loading.

The height H of the plugs 15, 55 has been described as being less than the thickness of the slab 4. However, in particular where a further top surface (not shown) is to be laid overlying the upper surface 8 of the slab 4, the height H of the plugs 15, 55 may be equal to or exceed the thickness of the concrete slab 4.

The slope angle of the inverted frustoconically shaped plugging surfaces 20, 57 has been described as being about 5 degrees. However, the slope angle of the frustoconically shaped plugging surfaces 20, 57 may be less than 5 degrees, between 5 and 10 degrees, up to 15 degrees or more than 15 degrees. Larger slope angles may provide a larger force urging the concrete slab 4 against the steel member 2 in response to shear loading. Larger slope angles may increase the axial loading of the shear connector elements 6, which can reduce shear strength.

An upper openings 24a of a through hole 24 in a steel member 2 which receives a shear connector element 6 have been described as being countersunk to form a seat, and a lower opening 24b has been described as optionally countersunk to form a seat. However, other types of seat may be used such as, for example, a square seat to receive a carriage bolt or a cylindrical seat into which a nut 29 may be tightened using a socket wrench. The upper opening 24a of a through hole 24 has been described as being countersunk to an first countersinking angle 26a of 60 degrees and a lower opening 24b of a through hole 24 has been described as being optionally countersunk to an second countersinking angle 26b of 30 degrees. However, the first and second countersinking angles 26a, 26b need not be restricted to these values and may instead be, for example, less than 15 degrees, less than 30 degrees, less than 45 degrees, less than 60 degrees or more than 60 degrees.

The gap 36 has been described as being approximately 5 mm across. However, the gap 36 may be larger, for example between 5 to 10 mm or more than 10 mm. Alternatively, the gap 36 may be smaller, for example, the gap may be substantially eliminated if sufficiently precise placement and alignment of the shear connector elements 6 and the concrete slab 4 is possible. The filling material 37 has been described as a concrete grout and may be, for example, cement or epoxy based. Grouts used are preferable durable and display minimal shrinkage on setting and over time.

The gap 36 may be filled by pre-filling each through hole 9, 54 with a quantity of filling material 37 before emplacing the corresponding plug 15, 55 into the through hole 9, 54, so that the filling material 37 flows around and inside the plug 15, 55. Alternatively, the gap 36 may be filled after the plug 15, 55 has been secured by a fastener or fasteners 17. If the filling material 37 is low viscosity before it sets, sealant (not shown) such as, for example, silicone rubber sealant, may be applied around the perimeter of the opening of the through hole 9, 54 on the lower surface 7 of the slab 4 to prevent the filling material 37 from penetrating between the lower surface 7 of the concrete slab 4 and the upper surface 5 of the steel member 2.

The de-bonding material 43 has been described as wax. However, other types of de-bonding material 43 may be used such as, for example, chemical release agents used to treat the surfaces 10, 20, 56, 57 such that they do not bond to the filling material 37. Alternatively, the plugs 15, 55 may be placed within a frustoconical shell (not shown) comprising, for example, polymeric material, so that the frustoconically shaped plugging surfaces 20, 57 do not directly contact the filling material 37.

The gap 36 has been described as being filled with filling material 37 which is concrete grout. However, the filling material may be replaced by high strength fibre reinforced elastomeric elements (not shown). For example, a sheet of fibre reinforced rubber shaped into a frustoconical or frustopyramidal shell, or a block of fibre reinforced rubber including through holes to received the plugs 15, 55. Such elastomeric elements may be inserted into the through holes 9 of the slab such that, when plugs 15, 55 are inserted and fasteners tightened, the resulting hoop stress secures the steel member 2 to the slab 4. When elastomeric elements are used, they may be bonded to either of the plugging surfaces 20, 57 or the seating surfaces 10. When elastomeric elements are used, either of the plugging surfaces 20, 57 or the seating surfaces 10 may be oiled to

assist during insertion. Using elastomeric elements may provide damping for dynamic loadings.

Claims

1. A steel-concrete composite structure comprising:

a steel member having an upper surface and a plurality of shear connector elements upstanding from the upper surface;

a concrete slab having upper and lower surfaces, the slab supported on its lower surface by the upper surface of the steel member, the slab comprising a plurality of through holes between the upper and lower surfaces, each through hole tapering towards the lower surface so as to form an inverted frustally-shaped seating surface, the concrete slab configured and positioned with respect to the steel member such that at least one shear connector element projects into each through hole;

a plurality of removable inverted frustoconical plugs, each plug having top and bottom surfaces and an inverted frustoconically-shaped plugging surface, each plug having at least one through hole between the top and bottom surfaces, wherein at least one plug is seated in a corresponding through hole of the concrete slab and wherein each plug is configured such that at least one of the least one shear connector elements projecting into the corresponding through hole is received by a corresponding though hole of the plug; and

a plurality of fasteners, each fastener coupled to a corresponding shear connector element and arranged to discourage removal of a plug from a through hole of the concrete slab.

2. A steel-concrete composite structure according to claim 1, wherein each through hole of the concrete slab is configured to form an inverted frustoconically-shaped seating surface and each plug is seated in a corresponding one of the through holes of the concrete slab.

3. A steel-concrete composite structure according to claim 1, wherein each through hole of the concrete slab is configured to form an inverted rectangular-based frustopyramidally-shaped seating surface and at least one plug is seated in a corresponding one of the through holes of the concrete slab.

4. A steel-concrete composite structure according to any preceding claim, wherein at least two plugs are seated in a corresponding one of the through holes of the concrete slab.

5. A steel-concrete composite structure according to any preceding claim, wherein each plugging surface is coated with a layer of de-bonding material.

6. A steel-concrete composite structure according to any preceding claim, further comprising a filling material disposed around the one or more plugs in the through hole of the concrete slab.

7. A steel-concrete composite structure according to any preceding claim, wherein the shear connector elements are removably attachable to the steel member.

8. A steel-concrete composite structure according to any preceding claim, wherein the shear connector elements comprise bolts.

9. A steel-concrete composite structure according to any preceding claim, wherein each fastener comprises a nut which is received by a threaded portion of the corresponding shear connector element.

10. A steel-concrete composite according to claim 9, wherein the fasteners and the sheet connector element are arranged to urge each plug against the upper surface of the steel member.

11. A steel concrete composite structure according to any one of claims 8 to 10, wherein the shear connector elements are received by through holes in the steel member and each opening of the through holes in the upper surface of the steel member comprises a countersunk seat;

further comprising additional filling material disposed in the countersunk seat and around the shear connector elements.

12. A steel-concrete composite according to any one of claims 8 to 10, wherein the shear connector elements are received by through holes in the steel member and each opening of the through holes in the upper surface of the steel member comprises a seat configured to receive a bolt head or a nut; and

wherein the portion of each shear connector elements passing through the steel member is tensioned by a nut threaded over the shear connector elements and tightened into the seat.

13. A bridge comprising a steel-concrete composite structure according to any preceding claim.

14. A removable plug for use in a steel-concrete composite structure according to any preceding claim, comprising:

an inverted frustoconical body having top and bottom surfaces and an inverted frustoconically-shaped plugging surface; and

at least one through hole between the top and bottom surfaces.

15. A method of building a steel-concrete composite structure comprising a steel member having an upper surface; a plurality of shear connector elements; a concrete slab having upper and lower surfaces, the slab comprising a plurality of through holes between the upper and lower surfaces, each through hole tapering towards the lower surface so as to form an inverted frustally-shaped seating surface; a plurality of removable inverted frustoconical plugs, each plug having top and bottom surfaces and an inverted frustoconically-shaped plugging surface, each plug having at least one through hole between the top and bottom surfaces; and a plurality of fasteners, the method comprising:

coupling the plurality of shear connector elements to the steel member such that the shear connector elements are upstanding from the upper surface;

positioning the slab so that it is supported on its lower surface by the upper surface of the steel member and arranged such that at least one shear connector element projects into each through hole;

positioning the plurality of plugs such that each plug is seated in a corresponding through hole of the concrete slab and wherein each plug is positioned such that at least one of the least one shear connector elements projecting into the corresponding through hole is received by a corresponding though hole of the plug; and

coupling each of the fasteners to a corresponding shear connector element so as to discourage removal of a plug from a through hole of the concrete slab.

1/13

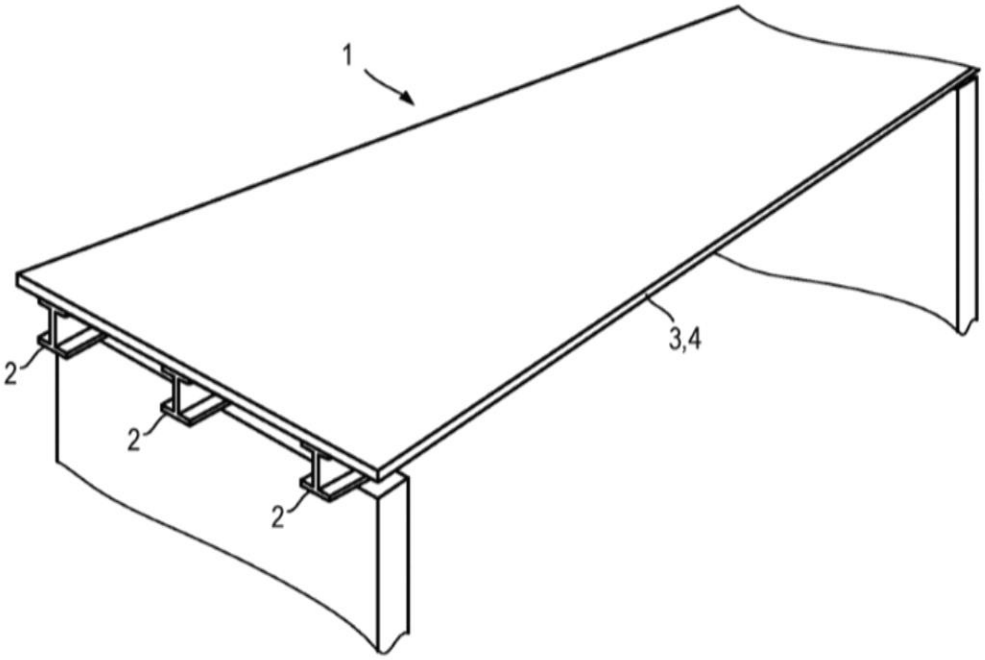

Fig. 1

2/13

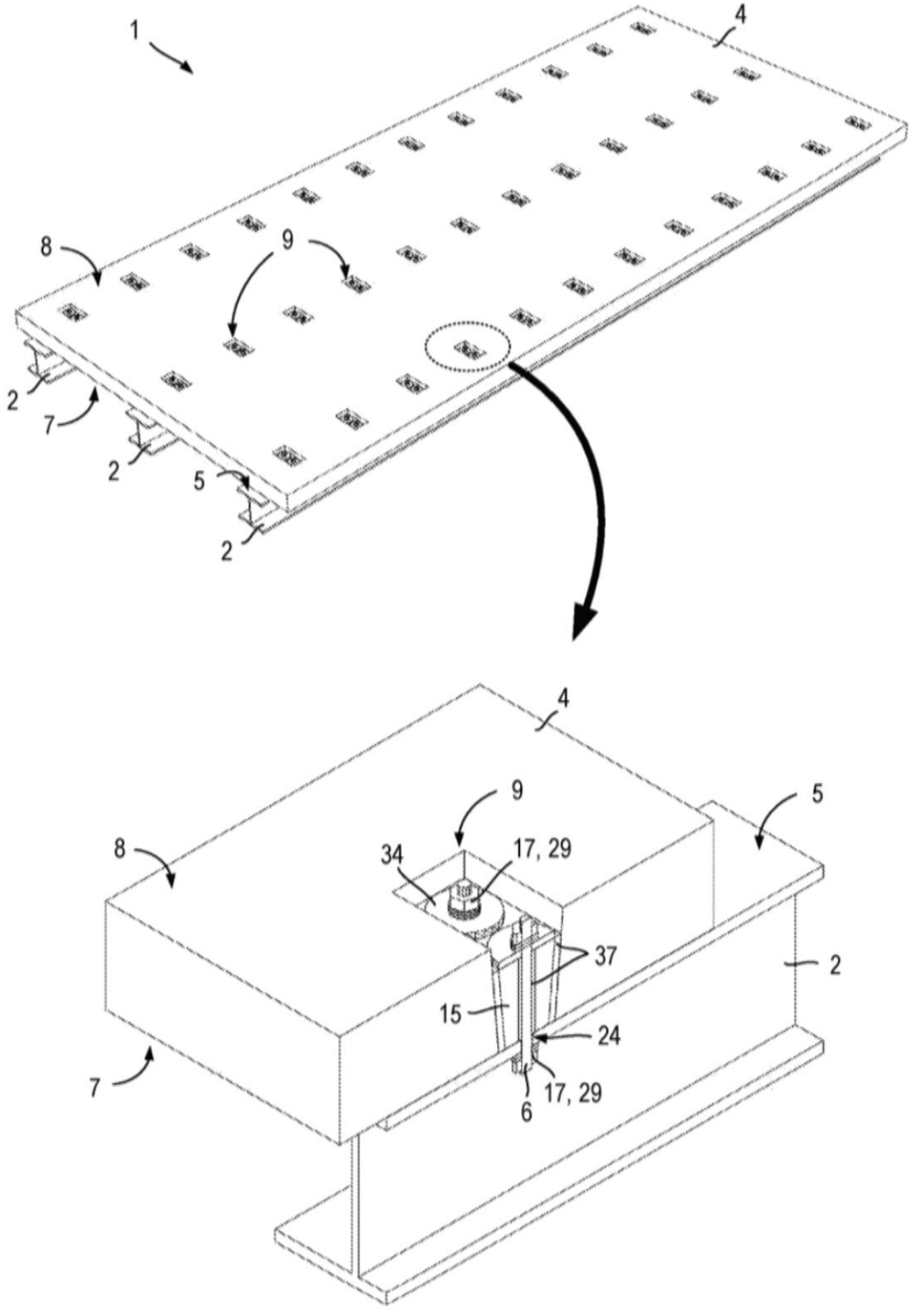

Fig. 2

3/13

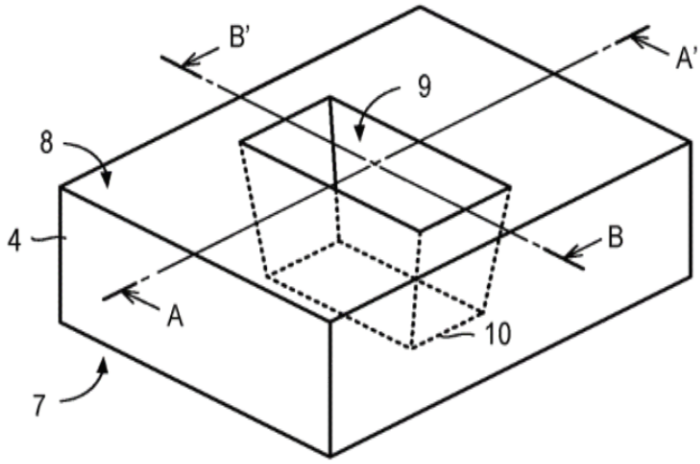

Fig. 3

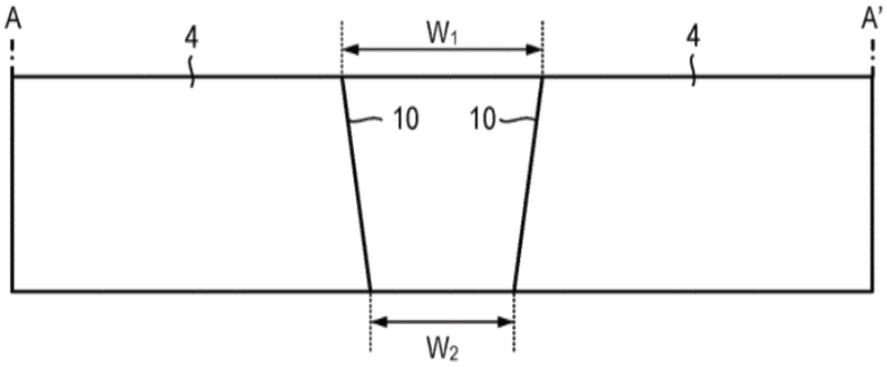

Fig. 4

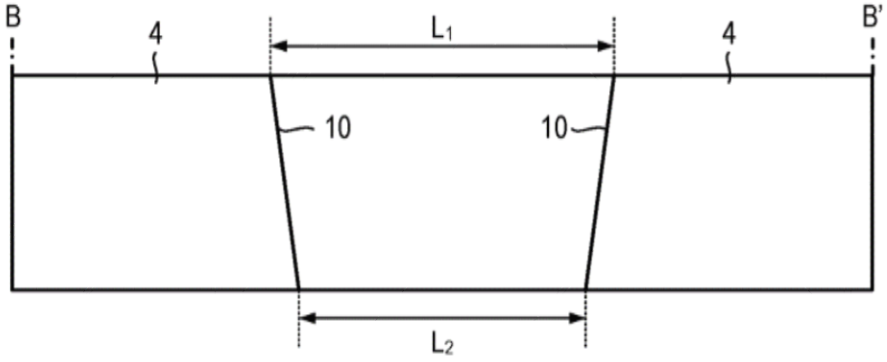

Fig. 5

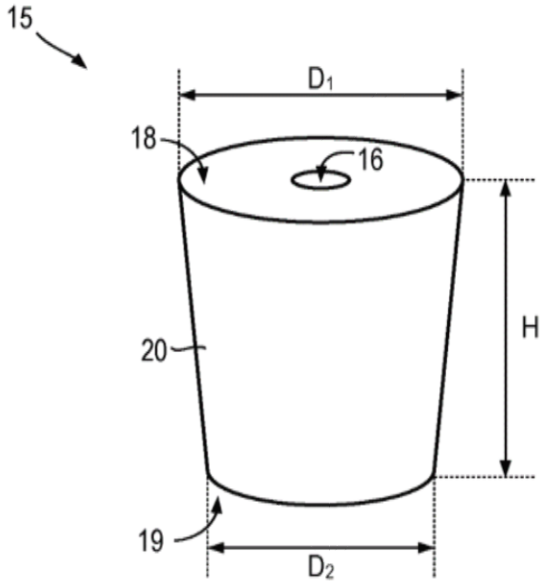

Fig. 6

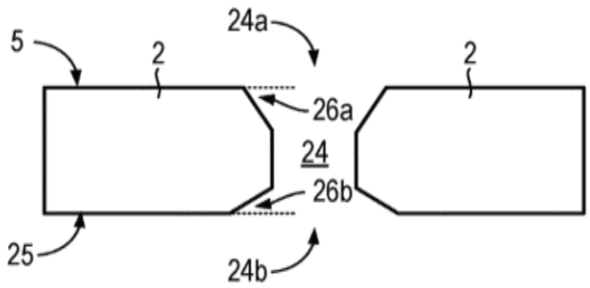

Fig. 7

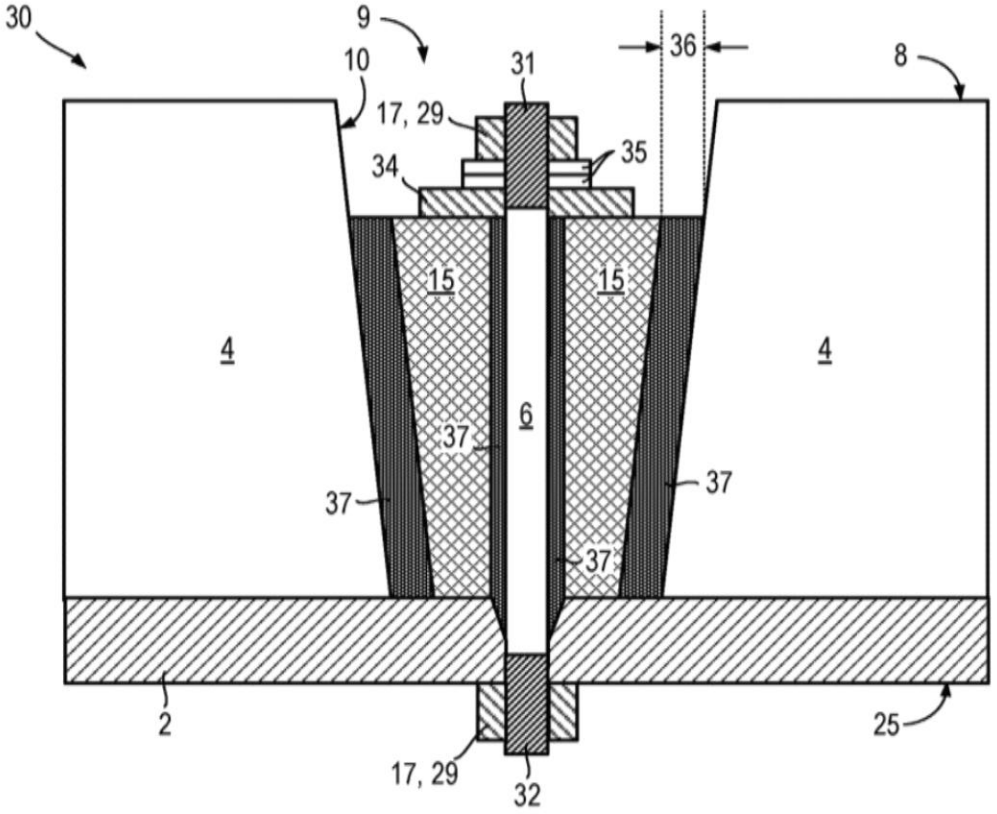

Fig. 8

6/13

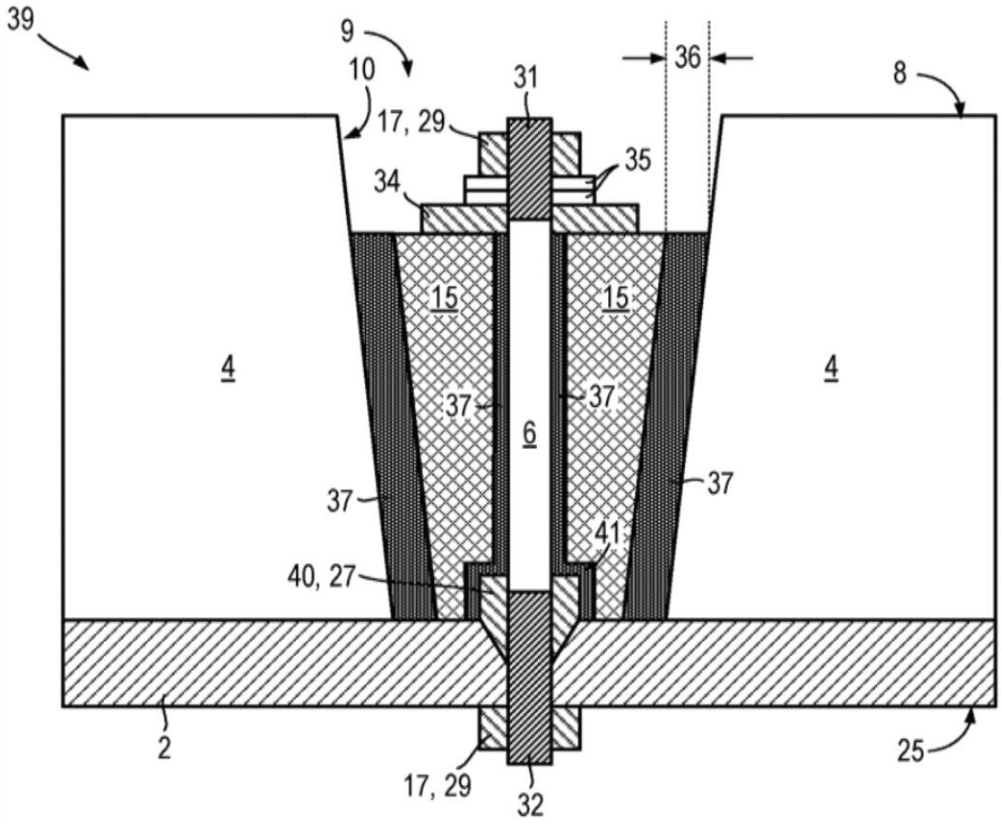

Fig. 9

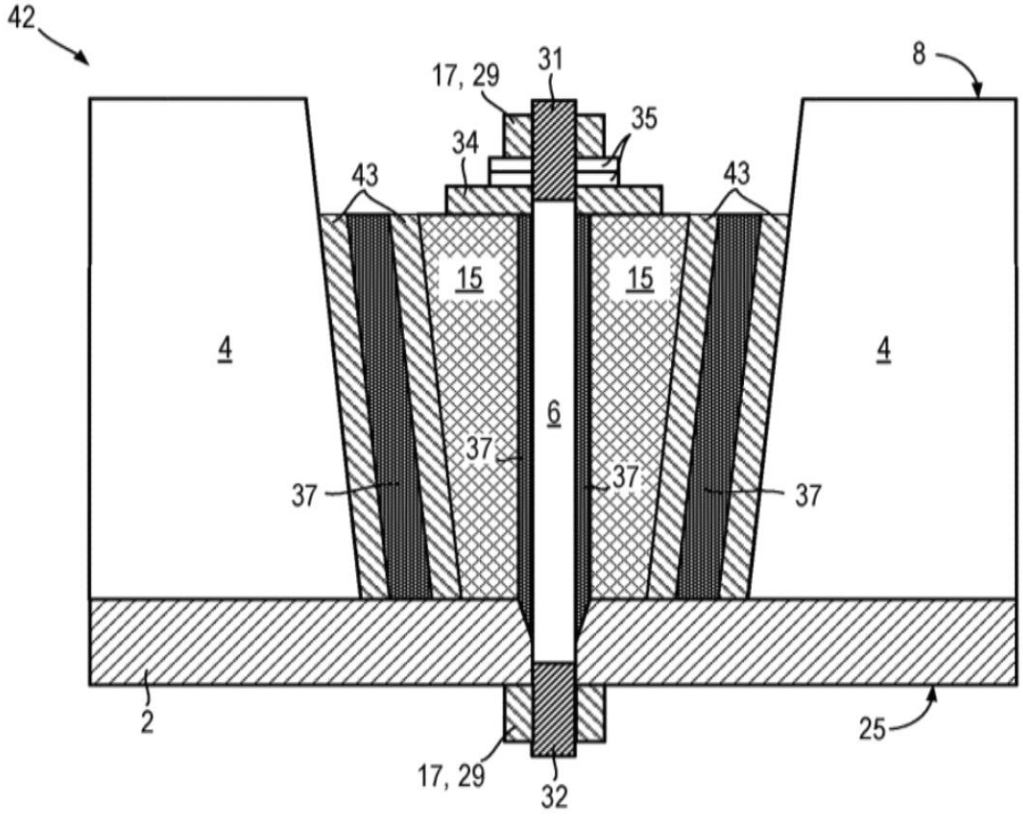

Fig. 10

8/13

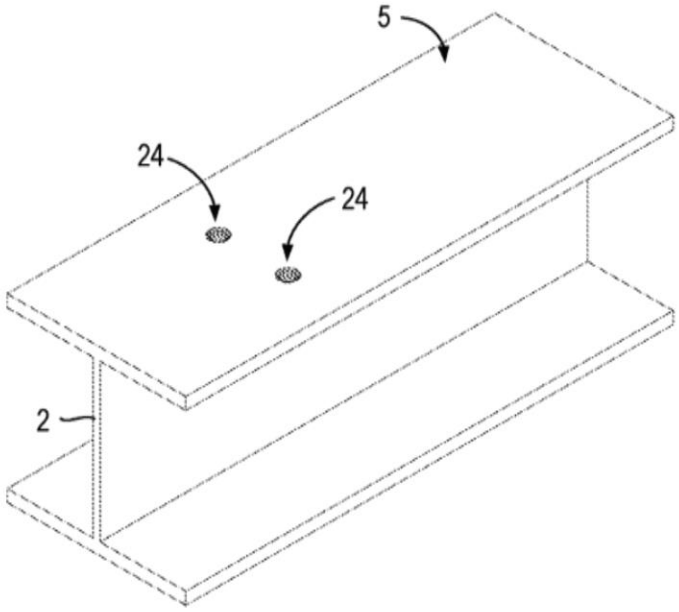

Fig. 11A

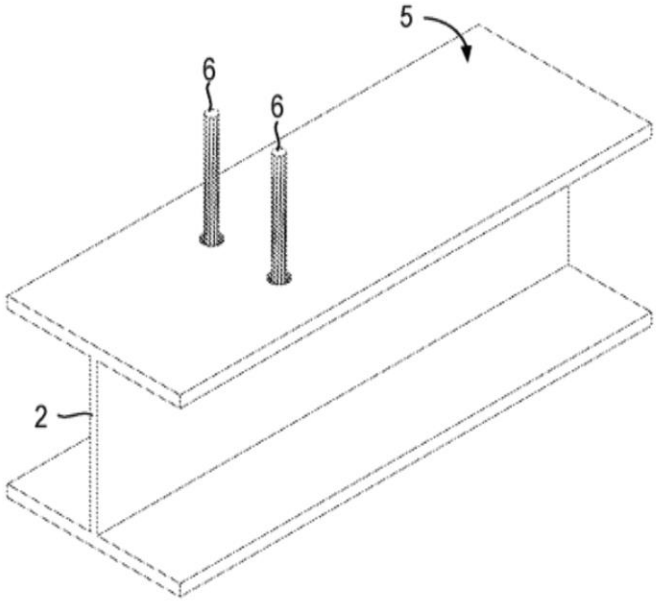

Fig. 11B

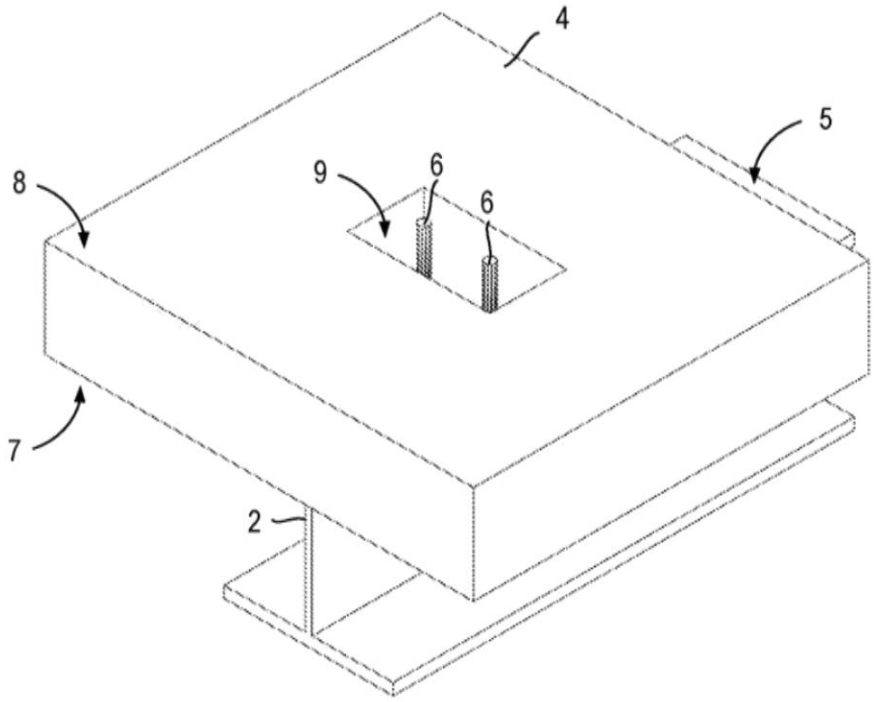

Fig. 11C

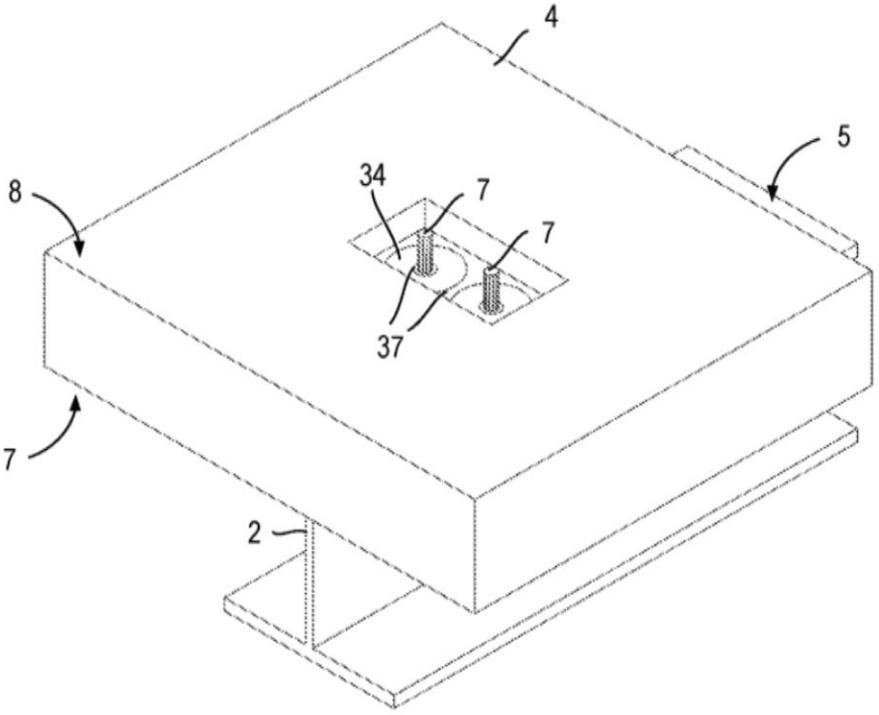

Fig. 11D

10/13

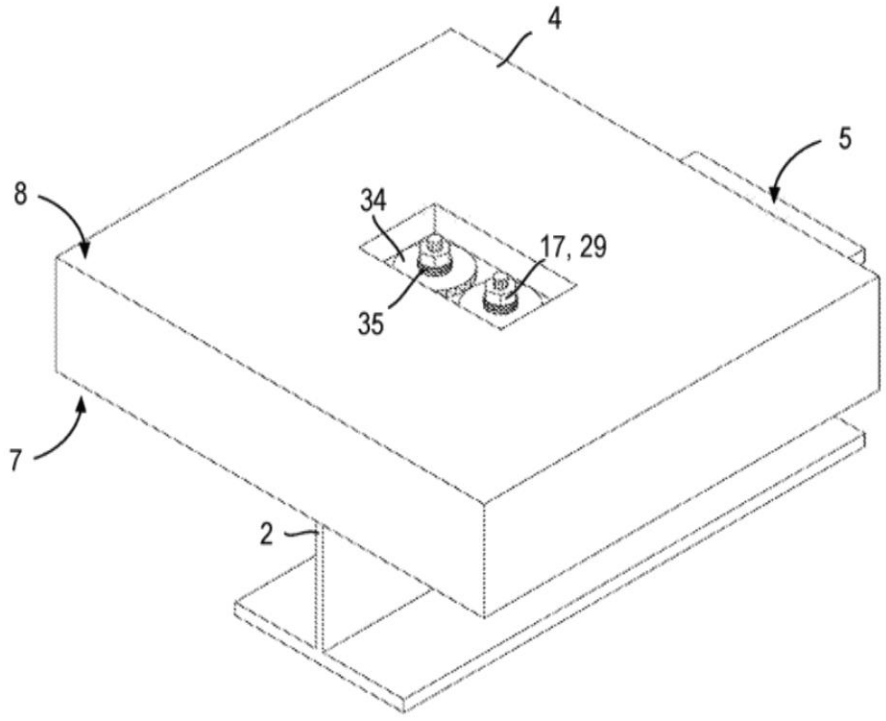

Fig. 11E

11/13

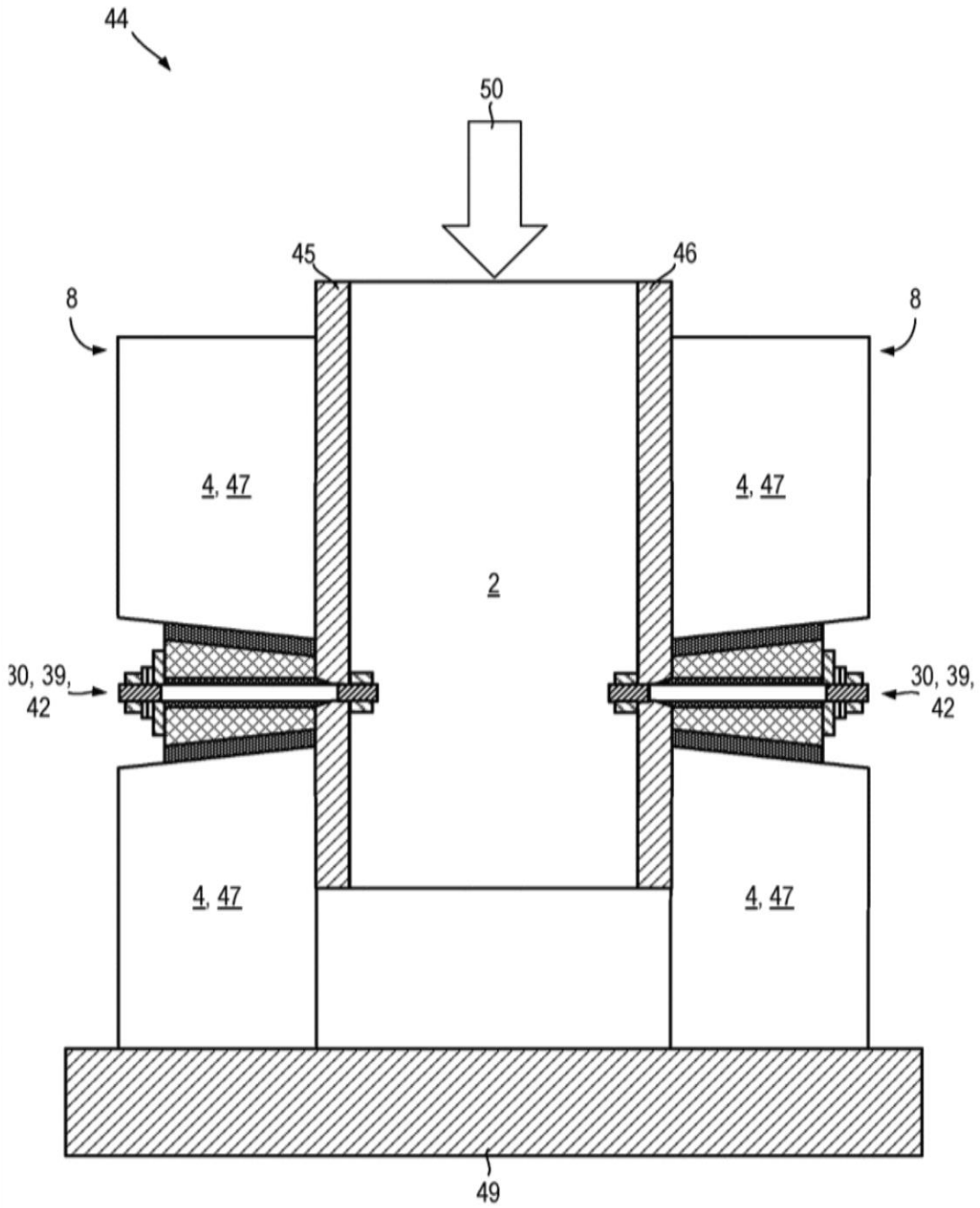

Fig. 12

12/13

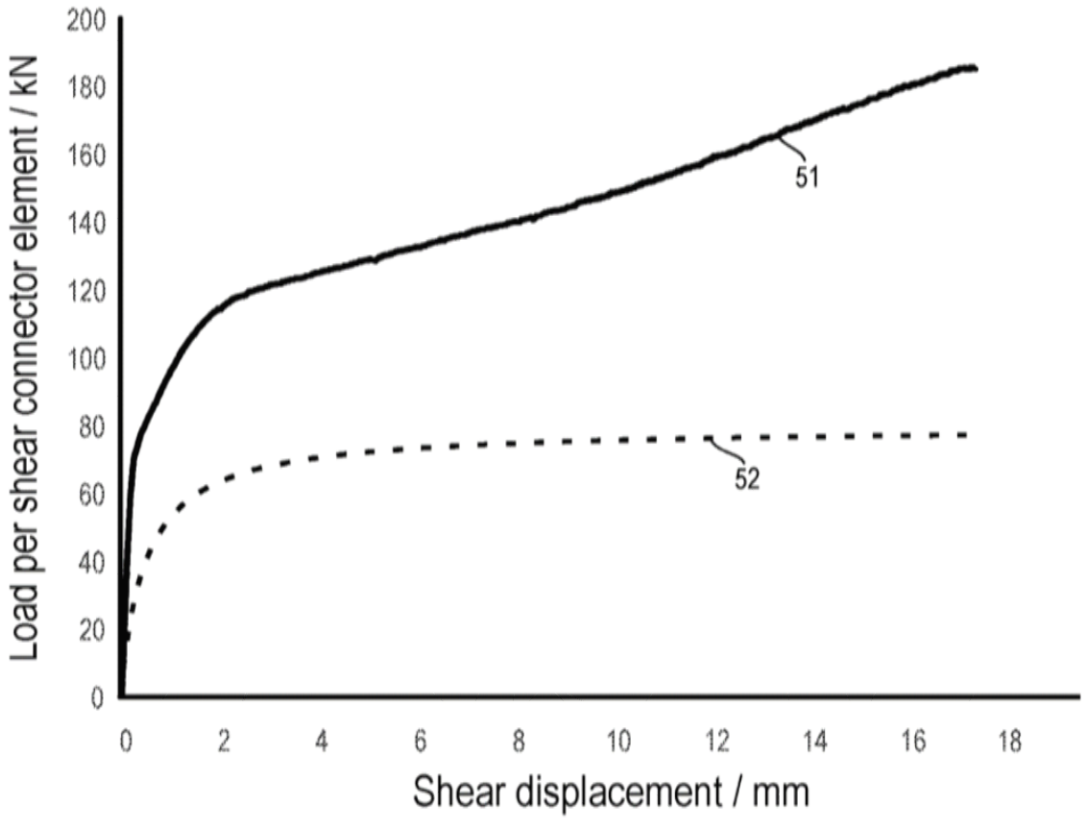
Load per shear connector element / kN
200
180
160
140
120
100
80
60
40
20
0
0
2
4
6
8
10
12
14
16
18
Shear displacement / mm
51
52

Fig. 13

13/13

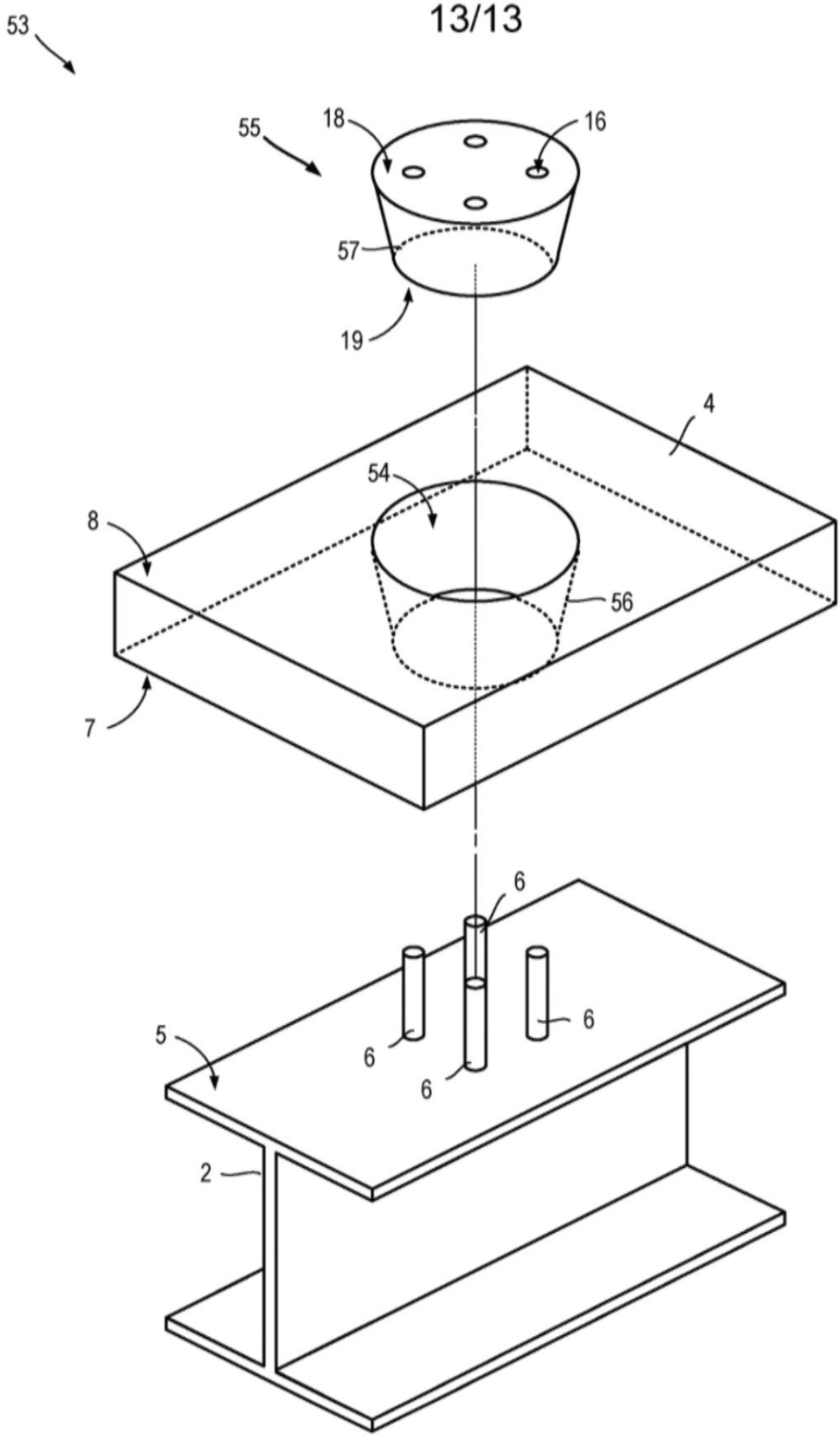

Fig. 14